STUDY OF SELECTED WATER MANAGEMENT STRATEGIES FOR PROTON EXCHANGE MEMBRANE FUEL CELLS

by

Mauricio Blanco

B.A.Sc., University of British Columbia, 2004

A THESIS SUBMITTED IN PARTIAL FULFILLMENT OF THE REQUIREMENTS FOR THE DEGREE OF

DOCTOR OF PHILOSOPHY

in

THE FACULTY OF GRADUATE STUDIES

(Chemical and Biological Engineering)

THE UNIVERSITY OF BRITISH COLUMBIA
(Vancouver)

August 2011

ABSTRACT

Proton exchange membrane fuel cells (PEMFC) are a promising energy conversion alternative for a number of applications including automotive, small power generation, and micro applications. However, many issues, such as poor water management and voltage instability, still have to be addressed in order to remove technical barriers to commercialization. In this work, water management issues in PEM fuel cells were investigated in detail with the purpose of developing approaches to reduce the negative effect of liquid water inside the fuel cell.

The performance of the PEM fuel cell deteriorates when operated at low humidity to dry conditions. It was demonstrated that the use of perforated sheets as water barrier layers improved the operational life of the fuel cell significantly (>3x) compared to a fuel cell with no additional layers. These sheets increase the water content in the cathode catalyst layer and membrane, via back-diffusion to the anode. In addition, these perforated sheets were also used as a diagnostic tool in order to further investigate the role of cathode and anode MPLs. It was shown that the cathode MPL decreases the water saturation in the catalyst layer and improves water removal via the cathode GDL. It was also shown that the anode MPL plays a role in reducing voltage stability at high flow rates and flooding conditions. Perforated sheets were further explored for use as an engineered gas diffusion layer. This type of approach has the advantage that it can be tailored to specific parameters and conditions.

Finally, a new flow field design, used on the cathode side, in which the active area can be modified, is presented and proven to improve the cell voltage and power stability at low power levels. This method increases the effective flow rate inside the flow field by decreasing the active area, resulting in the removal of liquid water and improving the gas diffusion to the cathode catalyst layer. This novel design can also be used to improve cell-to-cell water and gas distribution in fuel cell stacks.

PREFACE

In Chapter 1, the literature review section regarding “Gas Diffusion Layers” (Section 1.4.2) was prepared by M. Blanco under the supervision of Dr. David Wilkinson. Part of this section was published as a book chapter: M. Blanco, D.P. Wilkinson. Diffusion Layers, in D.P. Wilkinson, J.J. Zhang, J.W. Fergus, R. Hui and X. Li (Eds.), Proton Exchange Membrane Fuel Cells: Materials Properties and Performance, Green Chemistry and Chemical Engineering Series, CRC Press, Boca Raton, FL, Chapter 4, 2009.

In Chapter 1, the literature review section regarding “Water Mitigation Strategies” (Section 1.4.1.2) was prepared by M. Blanco under the supervision of Dr. David Wilkinson. A version of this section was published as a section of a journal article: R. Anderson, L. Zhang, Y. Ding, M. Blanco, X. Bi, D.P. Wilkinson. A critical review of two-phase flow in gas flow channels of proton exchange membrane fuel cells. Journal of Power Sources 2010;195: 4531-53.

A version of Chapter 3 has been published: M. Blanco, D.P. Wilkinson, H. Wang. Application of water barrier layers in a proton exchange membrane fuel cell for improved water management at low humidity conditions. International Journal of Hydrogen Energy 2011;36:3635-48. I conducted all the design and testing, analyzed the results and wrote the manuscript under D.P. Wilkinson’s guidance. H. Wang assisted with advice.

A version of Chapter 4 has been submitted for publication: Blanco M, Wilkinson DP, Wang H. Experimental investigation of the effect of cathode and anode microporous layers in a proton exchange membrane fuel cell. I conducted all the design, testing, analysis of the results, and writing of the manuscript under D.P. Wilkinson’s guidance. H. Wang assisted with ideas and proof reading.

Parts of Chapter 5 has been published: Blanco M, Wilkinson DP, Wang H, Liu SZS. Engineered gas diffusion layers for proton exchange membrane fuel cells. ECS Transactions 2009;25:1507-18. In addition, sections of this work have been

submitted for publication: Blanco M, Wilkinson DP, Wang H. Engineered perforated sheets as gas diffusion layers for proton exchange membrane fuel cells. I conducted all the design, testing, analysis of the results, and writing of the manuscripts under D.P. Wilkinson's guidance. H. Wang assisted with ideas for the manuscript.

Chapter 6 is based on work conducted with the National Research Council – Institute for Fuel Cell Innovations (NRC-IFCI). A version of this work has been published in:

- Wilkinson DP, Blanco M, Zhao H, Wu J, Wang H. Dynamic flow field for fuel cells. Electrochemistry and Solid State Letters 2007;10:B155-60.
- Blanco M, Wilkinson DP, Yan G, Zhao H, Wang H. Flow control in a fuel cell flow field for improved performance and reliability. ECS Transactions 2006;1:355-66.
- Wilkinson DP, Rahbari R, Zimmerman J, Blanco M. Flow control apparatus and method of fuel cell flow field. US2008248365, WO02005121917, CA2569859.

I assisted J. Zimmerman with the design of the flow field plates and conducted all the testing for the single cell fuel cell by myself. The tests with the fuel cell stack were performed by J. Wu, H. Zhao, and myself. I analyzed all the data and wrote the manuscript under the supervision of Dr. David Wilkinson. H. Wang assisted with advice.

TABLE OF CONTENTS

LIST OF TABLES

LIST OF FIGURES

LIST OF ABBREVIATIONS

AFC	Alkaline fuel cell
AWR	Anode water removal
BD	Back diffusion
CC	Carbon cloth
CCL	Cathode catalyst layer
CCM	Catalyst coated membrane
CFP	Carbon fiber paper
CL	Catalyst layer
DI	De-ionized
DM	Diffusion media
DMFC	Direct methanol fuel cell
DMS	Dimethyl silicon
EOD	Electroosmotic drag
FEP	Fluoroethylenepropylene
FF	Flow field
GDL	Gas diffusion layer
HFR	High frequency resistance
HHV	Higher heating value
HOR	Hydrogen oxidation reaction
LHV	Lower heating value
MCFC	Molten carbonate fuel cell
MEA	Membrane electrode assembly
MEMS	Microelectromechanical systems
MPL	Microporous layer
OA	Open area
OCV	Open circuit voltage
ORR	Oxygen reduction reaction
PAFC	Phosphoric acid fuel cell
PAN	Polyacrylonitrile
PEM	Proton exchange membrane
PEMFC	Proton exchange membrane fuel cell

PS	Perforated sheet
PTFE	Polytetrafluoroethylene
PTL	Porous transport layer
SDS	Sodium dodecyl sulphate
SEM	Scanning electron microscope
SOFC	Solid oxide fuel cell
RH	Relative humidity
WCO	Water crossover
WML	Water management layer

LIST OF SYMBOLS

A	Active area (m^2)
a	Cross-sectional area (m^2)
$a_{product,\,j}$	Activity of the product species j
$a_{reactant,\,j}$	Activity of the reactant species j
b_a	Anodic Tafel slope (V)
b_c	Cathodic Tafel slope (V)
$C_{b,\,j}$	Bulk concentration of species j (mol cm^{-3})
C_d	Channel depth – perforated sheets (mm)
C_w	Channel width – perforated sheets (mm)
D_H	Hydraulic diameter (m)
D_{H_2O}	Water diffusion coefficient in the membrane ($m^2\ s^{-1}$)
D_j	Diffusion coefficient of species j ($cm^2\ s^{-1}$)
d_p	Diameter perforations – perforated sheets (mm)
E	Potential (V)
E^o	Potential at standard conditions (V)
E_c^o	Cathode potential at standard conditions (V)
E_a^o	Anode potential at standard conditions (V)
E_e	Equilibrium potential (V)
$E_{e,T}$	Equilibrium potential with a temperature correction (V)
$E_{e,P}$	Equilibrium potential with a pressure correction (V)
E_{OCV}	Open circuit potential (V)
F	Faraday's constant (96,485 C mol^{-1})
f	Friction factor
$f_{laminar}$	Friction factor for laminar flow
$f_{turbulent}$	Friction factor for turbulent flow
G	Gibb's free energy (J mol^{-1})
H	Enthalpy of reaction (J mol^{-1})

H_f	Heat of formation (J mol^{-1})
i	Current density (mA cm^{-2})
i_a	Anodic current density (mA cm^{-2})
i_c	Cathodic current density (mA cm^{-2})
i_o	Exchange current density (mA cm^{-2})
$i_{o,a}$	Anodic exchange current density (mA cm^{-2})
$i_{o,c}$	Cathodic exchange current density (mA cm^{-2})
i_L	Limiting current density (mA cm^{-2})
$i_{L,a}$	Anodic limiting current density (mA cm^{-2})
$i_{L,c}$	Cathodic limiting current density (mA cm^{-2})
$k_{m,j}$	Mass transfer coefficient of species j (cm s^{-1})
k	Permeability of porous media (m^2)
k_p	Membrane hydraulic permeability (m^2)
L	Channel length (m)
m_{Air}	Molar flow rate of air (mol s^{-1})
$m_{H_2O,vap}$	Molar flow rate of water vapor (mol s^{-1})
n	Number of electrons per molecule
n_a	Number of electrons transferred in the cathodic reaction
n_c	Number of electrons transferred in the cathodic reaction
ΔN_g	Change of gaseous moles between products and reactants (mol)
$N_{H_2O,air,in}$	Molar flux of water vapor at the inlet of air stream (mol s^{-1} m^{-2})
$N_{H_2O,BD}$	Molar flux of water vapor at the due to back diffusion (mol s^{-1} m^{-2})
$N_{H_2O,drag}$	Molar flux of water vapor due to drag (mol s^{-1} m^{-2})
$N_{H_2O,H_2,in}$	Molar flux of water vapor at the inlet ofH_2 stream (mol s^{-1} m^{-2})
$N_{H_2O,hyd}$	Molar flux of water vapor due to hydraulic permeation (mol s^{-1} m^{-2})
$N_{H_2O,r}$	Molar flux of water vapor due to reaction (mol s^{-1} m^{-2})
P	Pressure (kPa abs)
P_a	Pressure anode (kPa abs)

P_c	Pressure cathode (kPa abs)
P^o	Standard state pressure (kPa abs)
P_1	Pressure at state 1 (kPa abs)
P_2	Pressure at state 2 (kPa abs)
P_{Air}	Partial pressure of air (kPa abs)
$P_{C,total}$	Total pressure in the cathode gas stream (kPa abs)
$P_{H_2O,vap}$	Partial pressure of the water vapor (kPa abs)
P_{vs}	Water vapor saturation pressure (kPa abs)
ΔP	Pressure drop (kPa abs)
ΔP_{total}	Total pressure drop in a flow field (kPa abs)
ΔP_{inlet}	Pressure drop at the inlet of the flow field (kPa abs)
ΔP_{outlet}	Pressure drop at the outlet of the flow field (kPa abs)
$\Delta P_{diffusion}$	Diffusion pressure drop through the GDL (kPa abs)
p_j	Partial pressure of gaseous species j (kPa abs)
p	Perimeter (m)
R	Ideal gas constant (J mol^{-1} K^{-1})
Re	Reynold's number
R_{total}	Total area-specific cell resistance (Ω cm^2)
S	Entropy (J mol^{-1} K^{-1})
T	Temperature (K)
T_{dp}	Dew point temperature (K or ℃)
T_{cell}	Cell Temperature (K or ℃)
T_{gas}	Gas temperature (K or ℃)
t	Thickness – perforated sheets (mm)
t_{max}	Maximum time that the fuel cell can hold a specific current (hr)
u_s	Superficial velocity (m s^{-1})
ΔV_g	Volume change for gaseous components inside fuel cell cell (m^3)
W_C	Water collected in the reservoir over a period of time (g min^{-1})

$W_{Cathode}$	Total cathode water transport rate (g min^{-1})
W_{el}	Electrical work (J mol^{-1})
W_{in}	Water in the humidified air (g min^{-1})
W_{vap}	Water vapor in the exhaust air (g min^{-1})
x	Determined portion of the channel length (m)

Greek

α	Exchange transfer coefficient
δ	Diffusion boundary layer thickness (cm)
γ_j	Activity coefficient of gaseous species j
η	Thermodynamic efficiency
η_{act}	Activation overpotential (V)
$\eta_{act,a}$	Anodic activation overpotential (V)
$\eta_{act,c}$	Cathodic activation overpotential (V)
η_{conc}	Concentration overpotential (V)
$\eta_{conc,a}$	Anodic concentration overpotential (V)
$\eta_{conc,c}$	Cathodic concentration overpotential (V)
η_{ohm}	Ohmic overpotential (V)
λ	Membrane hydration
λ_{air}	Stoichiometric coefficient for air
λ_{H_2}	Stoichiometric coefficient for hydrogen
λ_p	Stoichiometric coefficient of the product species j
λ_r	Stoichiometric coefficient of the reactant species j
$\lambda_{a,j}$	Stoichiometric coefficient for species *j* in the anode
$\lambda_{c,j}$	Stoichiometric coefficient for species *j* in the cathode
μ	Fluid viscosity (kg m^{-1} s^{-1})
ν	Average flow velocity (m s^{-1})
ξ	Electroosmotic drag coefficient

ρ	Fluid density (kg m^{-3})
τ	Membrane thickness (m)
φ_a	Relative humidity anode
φ_c	Relative humidity cathode
χ_j	Mole fraction of the gaseous species j

ACKNOWLEDGEMENTS

With this thesis, a major part of both my personal and professional life is completed. I would not have been able to accomplish this without the help and support of many people.

I am heartily thankful to my supervisor, Dr. David Wilkinson, for his unconditional support and encouragement throughout this project. His continuous advice allowed me to undertake what sometimes seemed like an impossible project to complete. I am deeply grateful for the opportunity he gave me 5 years ago and I will always cherish his advice and friendship.

My appreciation also goes out to my committee members Dr. Fariborz Taghipour, Dr. Brian Wetton, Dr. Xiaotao Bi, and especially to Dr. Haijiang Wang who has always been on hand ready to help.

Many thanks go to Dr. Walter Mérida, who through his undergraduate course put that seed of curiosity in me regarding fuel cells and clean energy technologies.

My gratitude also goes to everyone in my research group at UBC, especially to Dr. Alfred, Omar, Ryan and Bruce, not just for their advice and the numerous discussions that we had, but especially for their friendship. I would like to acknowledge Dr. Arman Bonakdarpour, Dr. Alfred, and Ryan for going over my thesis and giving me positive criticism. I would also like to thank everyone at the NRC-IFCI, particularly the MEA group and Dr. Titichai Navessin, the Unit Fuel Cell group, and Jonathan Martin for their help and support.

Special thanks go to my family for their unconditional support during my life. My mom and my dad have always been there for me, and there are no words that could thank them enough for their love and guidance. I would also like to thank my brothers, not just for being the best brothers anyone could ask for, but for their continuous help and friendship. Los quiero mucho!

During the hard times of this long journey, one person always kept cheering me up and giving me energy: my lovely wife – Mariana. This accomplishment is as much yours as it is mine and from the bottom of my heart, I want to thank you for your absolute love and support during this stage of my life.

Y para seguir con la tradición: Fuerza Canejo, Estudie y Triunfe!

Dedicado a mi amada esposa, padres y hermanos

Dedicated to my lovely wife, parents and brothers

1 INTRODUCTION[1]

1.1 A brief history and background of fuel cell technology

Fuel cells are electrochemical devices that convert chemical energy stored in the form of fuel and oxidant into electrical energy. The principles behind fuel cells were first mentioned by Schoenbein in 1838 [1], and then demonstrated by William Grove in 1839 with his "gaseous voltaic battery" [2,3]. This "battery" used hydrogen and oxygen as the reactants, platinum metal as the electrodes, and sulphuric acid as the electrolyte. Chen [4] describes in great detail, and in chronological order the specifics of fuel cell development from the early stages. In the late 1930s, an engineer named Francis Bacon began working on fuel cells and by 1959 his research group was able to demonstrate a 6 kW hydrogen fuel cell that used an alkaline electrolyte (KOH) [4]. In the 1960s, fuel cells based on Bacon's designs were developed and built by Pratt and Whitney. These cells were extensively used by the U.S. Space Program, especially during the Gemini Program for the Apollo spacecrafts [5]. However, the high cost of materials and short lifetime of these fuel cells prevented their wider application.

In the past thirty years, research in fuel cells has increased significantly because a great number of applications have been identified as feasible markets. These include transportation (e.g., automobiles, buses, scooters, bicycles, locomotives, boats, underwater vehicles), distributed power generation, onsite cogeneration power, back-up power, portable power, space, airplanes, and material handling [5,6]. Therefore, various types of fuel cells have been investigated for a wide variety of applications. Usually, fuel cells are classified by their electrolyte and operating temperatures. Table 1.1 lists some of the most typical fuel cells and their main applications.

---

[1] Sections of these chapter were published in:
Blanco M, Wilkinson DP. Diffusion Layers. In: Wilkinson DP, Zhang JJ, Fergus JW, Hui R, Li X, editors. Proton Exchange Membrane Fuel Cells: Materials Properties and Performance, Green Chemistry and Chemical Engineering Series, CRC Press, Boca Raton, FL; 2009, Chapter 4, p. 191-303.
Anderson R, Zhang L, Ding Y, Blanco M, Bi X, Wilkinson DP. A critical review of two-phase flow in gas flow channels of proton exchange membrane fuel cells. Journal of Power Sources 2010;195:4531-53.

Table 1.1 – List of most common types of fuel cells.

Fuel Cell Type	Fuel	Oxidant	Electrolyte	Temp. [°C]	Application
Alkaline Fuel Cell (AFC)	H_2	O_2	Potassium hydroxide, KOH	65–220	Spacecraft
PEM Fuel Cell (PEMFC)	H_2	O_2, Air	Proton exchange membrane	25–80	Automotive, small-scale stationary power, portable
Phosphoric Acid Fuel Cell (PAFC)	Natural gas, bio gas, H_2	O_2, Air	Phosphoric acid H_2PO_4	150–205	Stationary power
Direct Methanol Fuel Cell (DMFC)	CH_3OH	O_2, Air	Proton exchange membrane	50–130	Portable
Molten Carbonate Fuel Cell (MCFC)	Natural gas, biogas, coal gas, H_2	O_2, Air	Mixture of alkali carbonates retained in ceramic matrix of $LiAlO_2$	600–660	Stationary power
Solid Oxide Fuel Cell (SOFC)	Natural gas, biogas, coal gas, H_2, CO	O_2, Air	Oxygen ions conducting ceramic	500–1,000	Stationary power, auxiliary power

1.2 Proton exchange membrane fuel cells

Proton exchange membrane fuel cells (PEMFC) are generally considered to be the closest to wide scale commercialization and are being considered for a number of applications including automotive, small power generation, and micro applications. Figure 1.1 shows a schematic of a typical PEMFC.

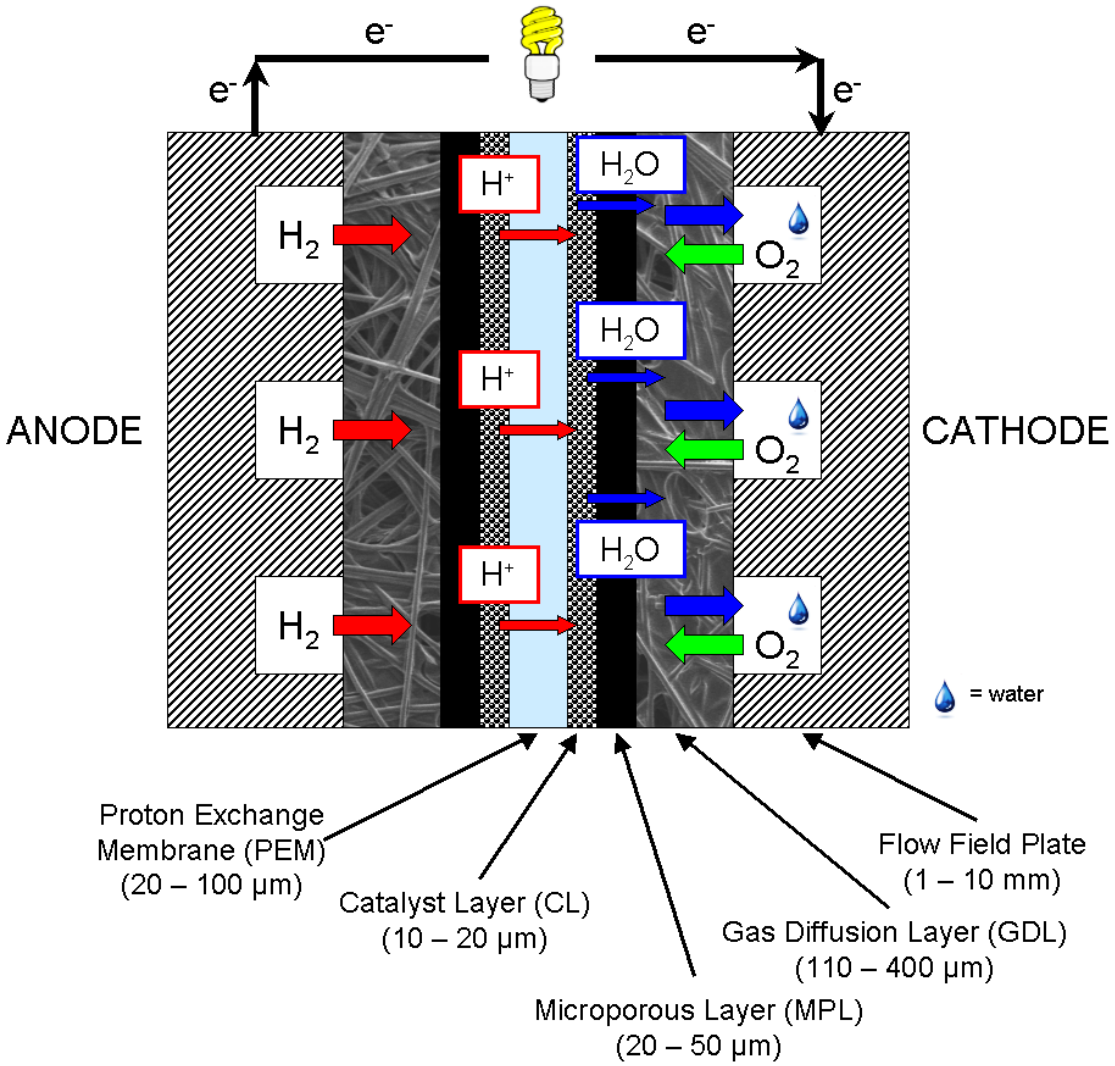

Figure 1.1 – Schematic cross sectional view of a Proton Exchange Membrane Fuel Cell (not to scale).

In a PEM fuel cell, hydrogen fuel enters the anode flow field (FF) plate, which is usually made from graphite or stainless steel, and flows through the channels towards the gas diffusion layer (GDL). The anode GDL, usually made out of carbon fiber paper or carbon cloth, helps the gas to diffuse evenly through this material towards the anode catalyst layer (CL). A microporous layer (MPL) could be located between the GDL and CL in order to improve water management, to decrease contact resistance between the GDL and CL, and to give mechanical support to the CL. At the anode catalyst layer, which consists of carbon supported platinum (Pt) nano particles, the hydrogen oxidation reaction occurs. Equation (1.1) shows the oxidation reaction of hydrogen which occurs at the anode:

$$H_2 \rightarrow 2H^+ + 2e^-,\ E^o = 0.00V \quad (1.1)$$

The electrons flow from the anode through an external circuit towards the cathode side. The hydrated protons (H_3O^+) diffuse through the proton exchange membrane (e.g., a perfluorosulfonic acid polymer) and reach the cathode catalyst layer. The polymeric membrane is kept hydrated to allow sufficient proton conductivity. At the cathode side, oxygen (usually in air) enters the flow field plate and flows through the GDL and MPL towards the cathode CL. In this layer, the oxygen reduction reaction (ORR) occurs and water is produced. Most of the water that is produced is then forced out of the CL, towards the cathode GDL and the flow field channels. Some water that is produced diffuses to the anode. Equation (1.2) shows the half-cell reaction corresponding to the cathode side, ORR:

$$\frac{1}{2}O_2 + 2H^+ + 2e^- \rightarrow H_2O,\ E^o = 1.23V \quad (1.2)$$

Combining Equations (1.1) and (1.2), we obtain the overall fuel cell reaction:

$$\frac{1}{2}O_2 + H_2 \rightarrow H_2O,\ E^o = 1.23V \quad (1.3)$$

The assembly constituted by the anode GDL (and MPL), anode CL, membrane, cathode CL, cathode GDL (and MPL) is referred to as the membrane electrode assembly (MEA). There are two standard ways of preparing an MEA; the first way is to impregnate or spray both anode and cathode catalyst layers on the corresponding GDL surfaces. In the second way, both catalyst layers are sprayed directly onto the membrane, thus forming a catalyst coated membrane (CCM). In order to improve the proton conductivity in the cathode CL, ionomer particles (Nafion®) are also added to this layer. In addition, in order for the membrane to transport the protons easily, it has to be fully hydrated, thus both hydrogen and oxygen gases are usually humidified before they enter the fuel cell.

Although there has been tremendous development in PEMFCs in the past two decades, many issues still have to be addressed before they can be commercialized on a wide scale. Water management issues, dehydration, flooding, and poor fuel and oxidant distribution in the gas diffusion layer (GDL) and flow field channels are just some of the issues that researchers have been trying to undertake by improving the membrane electrode assembly (MEA) and flow field design. The water issues are usually caused by the accumulation of liquid water in the MEA, which blocks areas and paths preventing oxygen gas access. Dehydration problems are common when the cell runs at high gas flow rates, affecting the proton conductivity in the membrane. Dry gases and dry operating conditions also have a direct impact on the dehydration of the MEA.

In addition, the following are some of the technology gaps that still have to be dealt with in order for PEMFCs and other fuel cells to be feasible and viable for different applications:

- Lack of reliability and durability of fuel cell components such as the membrane, GDL, catalyst, etc. More work is necessary to fully understand early and long-term failure modes.
- Material degradation issues of catalysts, catalyst supports, membrane, flow fields, seals, etc.
- Costs can be a factor of 1.2 to 5 times too high at larger volumes.
- Operational flexibility regarding sub-zero operation, high temperature operation, start-up and duty cycles, etc.
- Technology simplification and integration of key components, like GDLs and flow field plates.
- Fuel production and infrastructure, fuel energy density and fuel storage.
- Water management and reactant distribution within the fuel cell.

1.3 Basic operational principles of PEM fuel cells

1.3.1 Thermodynamic and electrochemical aspects

From a thermodynamic point of view, the maximum electrical work that can be produced by the fuel cell reaction (see Equation (1.3)) is related to the free-energy change (available energy in an isothermal process) of the reaction at a constant pressure and temperature. This energy is also known as the Gibbs free energy, ΔG (J mol^{-1}):

$$W_{el} = -\Delta G \tag{1.4}$$

where W_{el} is the electrical work (J mol^{-1}). It is important to note that the overall fuel cell reaction is spontaneous and is thermodynamically favourable because the change in the free energy of the reaction is negative. The electrical work can also be defined as:

$$W_{el} = nFE \tag{1.5}$$

where n is the number of electrons per molecule, F is the Faraday's constant (96,485 C mol^{-1}), and E is the potential (V). Combining equations (1.4) and (1.5), the potential can be written as:

$$E = \frac{-\Delta G}{nF} \tag{1.6}$$

The value for the potential will change depending on the operating conditions. The standard potential, E^o, is defined as the potential at standard conditions: 298 K, 101.3 kPa (1 atm), and an activity of 1 for all reactants and products. In a fuel cell, the standard cell potential is the difference between the cathode and anode half-cell potentials:

$$E^o = E_c^o - E_a^o \tag{1.7}$$

The previous equations are based on standard conditions; but, both temperature and pressure can affect equation (1.6), and their effects must be considered. The

effect of temperature change in the potential, at constant pressure, can be expressed as:

$$\left(\frac{\partial E_e}{\partial T}\right)_P = -\frac{1}{nF}\left(\frac{\partial \Delta G}{\partial T}\right)_P = \frac{\Delta S}{nF} \tag{1.8}$$

where E_e is the equilibrium potential (V) at operating conditions rather than at standard conditions, and ΔS is the entropy (J mol^{-1} K^{-1}). In PEM fuel cells, the entropy does not change significantly at typical operating temperature ranges, thus equation (1.8) can be approximated as:

$$E_{e,T} = E^o + \frac{\Delta S}{nF}(T - 298) \tag{1.9}$$

where $E_{e,T}$ is the equilibrium potential (V) with a temperature correction, and T is the operating temperature (K).

The effect of pressure change on the potential, at constant temperature, can be expressed as:

$$\left(\frac{\partial E_e}{\partial P}\right)_T = -\frac{1}{nF}\left(\frac{\partial \Delta G}{\partial P}\right)_T \tag{1.10}$$

From the Maxwell equations [7]:

$$\left(\frac{\partial \Delta G}{\partial P}\right) = \Delta V_g \therefore \left(\frac{\partial E_e}{\partial P}\right) = -\frac{\Delta V_g}{nF} \tag{1.11}$$

where ΔV_g is the volume change for gaseous components inside the cell (m^3) (assuming ideal gas behaviour), thus:

$$\Delta V_g = \frac{\Delta N_g RT}{P} \tag{1.12}$$

where ΔN_g is the change of gaseous moles between the products and the reactants (mol), R is the ideal gas constant (J mol^{-1} K^{-1}), T is the operating temperature.

Substituting equation (1.12) into equation (1.11) and integrating between P_1 and P_2, results in the following equation:

$$E_{e,P_2} = E^o - \frac{\Delta N_g RT}{nF} ln\left(\frac{P_2}{P_1}\right) \tag{1.13}$$

where $E_{e,P}$ is the equilibrium potential (V) with a pressure correction at P_2, P_1 is 101.3 kPa, and P_2 is the operating pressure (kPa).

The gaseous concentration of the reactants and products can also affect the cell potential. The first step for this correction is to analyze how the Gibbs free energy changes with reactant concentrations:

$$\Delta G = \Delta G^o + RTln\left(\frac{\prod_j a_{product,\,j}^{\lambda_p}}{\prod_j a_{reactant,\,j}^{\lambda_r}}\right) \tag{1.14}$$

where $a_{product,\,j}$ is the activity of the product species j (reduced species), $a_{reactant,\,j}$ is the activity of the reactant species j (oxidized species), λ_p is the stoichiometric coefficient of the product species j, and λ_r is the stoichiometric coefficient of the reactant species j. Now, combining this equation with the previous relationship shown in equation (1.6), the effect of product and reactant concentrations (activities) on the cell potential, also referred to the Nernst equation, can be obtained:

$$E_e = E^o - \frac{RT}{nF} ln\left(\frac{\prod_j a_{product,\,j}^{\lambda_p}}{\prod_j a_{reactant,\,j}^{\lambda_r}}\right) \tag{1.15}$$

It is important to note that activity is a measure of the effective concentration of a species. It is a dimensionless quantity, is difficult to measure and depends on its chemical nature. For an ideal gas, activity is simply a ratio of its partial pressure and the pressure in its standard state, then, $a_j = p_j\left(P^o\right)^{-1}$, where p_j is the partial pressure (in kPa) of gaseous species *j* and P^o is the standard state pressure (100

kPa) [7,8]. In ideal gases, $p_j = \chi_j P$, where χ_j is the mole fraction of the gaseous species *j*, and P is the total pressure (kPa). For non-ideal gases, the activity is then $a_j = \gamma_j p_i \left(P^o\right)^{-1}$, where γ_j is the activity coefficient of gaseous species *j* [7,8]. For a dilute (ideal) solution, the activity can be assumed to be equivalent to the molar concentration of the species divided by the standard-state molar concentration (both concentrations in mol cm^{-3}). For non-ideal solutions, the activity coefficient (γ_j) is then used along the ratio between the concentrations explained above. For pure components (e.g., liquid water) the activity is equal to 1.

1.3.2 Theoretical fuel cell efficiency

The efficiency of an energy conversion device is usually defined as the ratio between useful energy output and energy input. Thus, the efficiency of a fuel cell is defined as:

$$\eta = \frac{\Delta G}{\Delta H} = 1 - \frac{T\Delta S}{\Delta H} \tag{1.16}$$

where, η is the thermodynamic efficiency and ΔH is the change in enthalpy of the reaction (J mol^{-1}), which corresponds to the difference between the heats of formation, ΔH_f, of products and reactants. Combining this expression with equation (1.6) gives:

$$\eta = -\frac{nE_e F}{\Delta H} \tag{1.17}$$

The physical state of the products is very important when calculating the overall efficiency of the reaction. For example, when water is the product, the heat of formation for liquid and vapor water is substantially different. If the product is liquid water, then the higher heating value (HHV) (286,020 J mol^{-1}) is used. On the other hand, if the product is water vapor, then the lower heating values (LHV) (241,980 J mol^{-1}) is used. The difference between these two heating values is the molar latent heat for condensation.

1.3.3 Fuel cell potential losses

In an operational fuel cell, the ideal (or theoretical) cell potential is equal to the equilibrium potential, E_e, and it has a value of 1.23 V at standard conditions. However, in operating fuel cells, a number of phenomena lead to voltage losses. These losses are also referred to as polarization losses. The performance of a fuel cell is typically reported in the form of a polarization curve (see Figure 1.2), in which the cell potential (V) is plotted versus current density, i (mA cm^{-2}). There are four main voltage losses: (i) fuel crossover, (ii) activation losses, (iii) ohmic losses, and (iv) mass transport losses. E_{OCV} is the open circuit cell voltage at a current density value of 0 mA cm^{-2}.

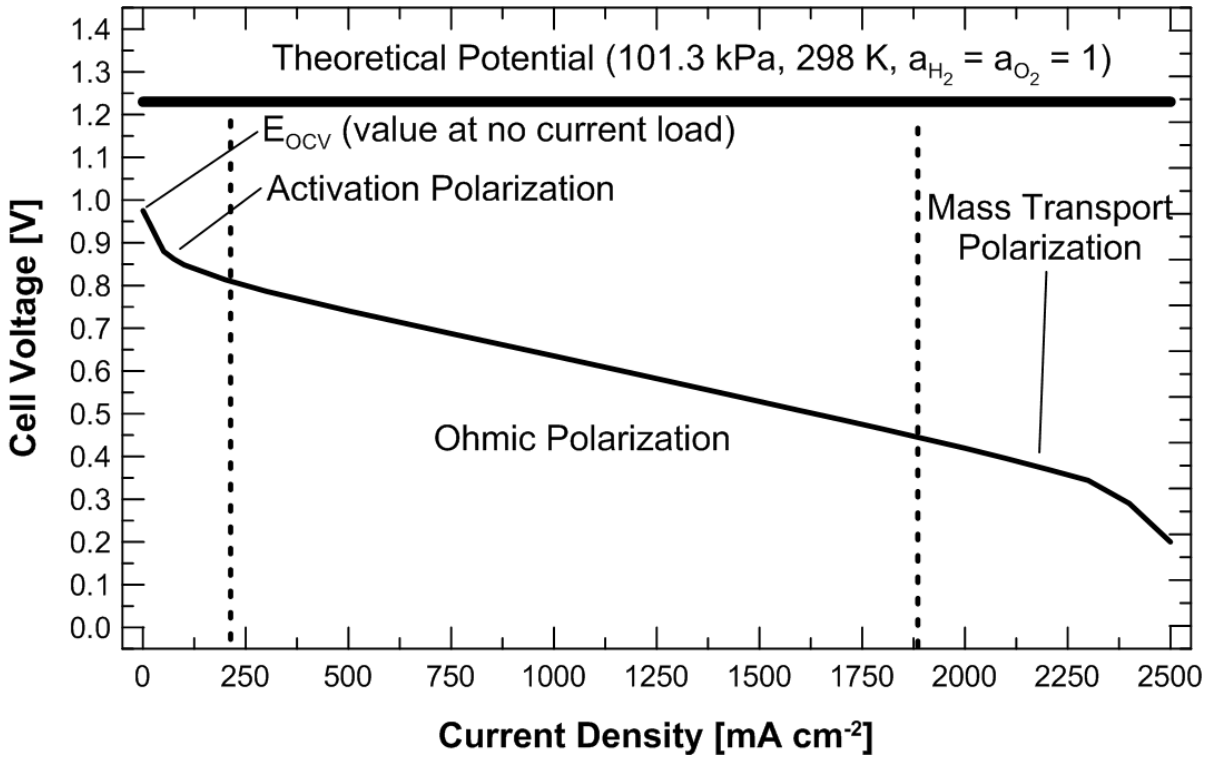

Figure 1.2 – A typical polarization curve for a PEM fuel cell. For this curve the fuel cell was a single cell (49 cm^2) and the gases, cell, and dew point temperatures were at 75 °C. The pressure for both inlet reactant gases was 206.8 kPag (approx. 30 psig), and the air/hydrogen stoichiometry ratio was 2.0/1.5. The catalyst coated membrane (CCM) was a Primea® 5510 membrane (0.4 mg Pt cm^{-2} on each side) and the anode and cathode gas diffusion layers (GDL) were SGL 25BC GDLs.

1.3.3.1 Fuel crossover and internal currents

The first loss is related to the mixed potential due to the fuel crossover from the anode to the cathode through the electrolyte (membrane). Thus, the fuel reacts directly with the oxygen because the Pt catalyst of the cathode is active for H_2 oxidation as well. In addition, this loss can also occur when small currents can cross the electrode gap even though the ionic conductor is ideally an insulator. These losses are the reason that causes the open circuit voltage (OCV), E_{OCV}, to decrease from the theoretical value because the H_2 and O_2 activities are lowered now [8]. In typical PEM fuel cells, open circuit voltages are around 0.97 and 1.10 when air or oxygen are used as oxidants, respectively.

1.3.3.2 Activation losses

These losses are related to the kinetics of the reactions that take place on the surface of the anode and cathode electrodes (at the cathode this loss is more severe). Thus, a proportion of the voltage generated is lost in driving the chemical reaction that transfers the electrons to or from the electrode. This energy (or voltage) loss can be reduced with increasing the temperature and pressure. The overall activation overpotential or polarization loss, η_{act} (V), can be estimated with the following equation:

$$\eta_{act} = \frac{RT}{\alpha nF} ln\left(\frac{i}{i_o}\right) \tag{1.18}$$

where, α is the exchange transfer coefficient which ranges between 0–1 (0.5 for the hydrogen electrode and 0.1–0.5 for the oxygen electrode [8]), i is the total current density (mA cm^{-2}), and i_o is the exchange current density (mA cm^{-2}), which is the rate at which the reaction proceeds at equilibrium; thus, a large value of this exchange current density represents a more active catalyst and results in a lower activation loss. It is important to note that the oxygen reduction reaction (ORR) activation losses are generally responsible for up to 70% of the potential losses in a hydrogen fuel cell (for a cell operating at 0.6 V) [5]. Typical values of the exchange

current density for the ORR are ~10^{-7} mA cm^{-2}, compared to values of ~1 mA cm^{-2} for the hydrogen oxidation reaction (HOR) [8].

The expression for the activation overpotential for the anode and cathode sides, respectively, can be also expressed with the help of the Tafel equation, thus:

$$\eta_{act,a} = b_a log\left(\frac{i_a}{i_{o,a}}\right) \tag{1.19}$$

$$\eta_{act,c} = -b_c log\left(\frac{i_c}{i_{o,c}}\right) \tag{1.20}$$

where b_a and b_c are the Tafel slopes for the anode and cathode, $i_{o,a}$ and $i_{o,c}$ are the exchange current densities for both anode and cathode, and i_a and i_c are the anodic and cathodic current densities. The Tafel slopes are defined as:

$$b = 2.3\frac{RT}{\alpha F} \tag{1.21}$$

Please note that equations 1.19 and 1.20 are the same as equation 1.18 but modified to reflect the individual anode and cathode reactions.

1.3.3.3 Ohmic losses

As the current density increases, the ohmic losses (second region in the polarization curve) also become a loss factor. The voltage drop caused by this loss is related to the resistance of the flow of electrons through the electrodes, flow field plates, and current collectors. This loss also includes the resistance to the flow of ions through the electrolyte (membrane). These losses can be expressed by Ohm's Law:

$$\eta_{ohm} = iR_{total} \tag{1.22}$$

where i is the total current density (mA cm^{-2}) and R_{total} is the total area-specific cell resistance (Ω cm^2). Usually the total resistance is the sum of the ionic (i.e., electrolyte), electronic and contact resistances. The electronic resistance is

negligible due to the electronic conductivities of the materials used for most components (e.g., graphite, metals, etc.). The ionic resistance increases if the membrane is contaminated or dehydrated.

1.3.3.4 Mass transport losses

At high current densities, mass-transport losses (or concentration losses) become increasingly important. These losses are due to the reactants' inability to reach the electrocatalytic sites on the surface of the electrodes. Usually, transport losses for oxygen are more important than H_2 because of the flooding of the cathode by liquid water. At high current densities, more water is produced in the catalyst layer. If the reactant gases do not diffuse fast enough to the catalyst layer then the current density decreases. Thus, these mass transport losses limit the maximum current density that a cell can provide. Mass transport or concentration overpotential, η_{conc}, can be expressed as:

$$\eta_{conc} = \frac{RT}{nF}\sum_j ln\left(1-\frac{i}{i_{L,j}}\right) \tag{1.23}$$

$$i_{L,j} = -\frac{nF}{\lambda_j}\frac{D_j}{\delta}C_{b,j} = \frac{nF}{\lambda_j}k_{m,j}C_{b,j} \tag{1.24}$$

where $i_{L,j}$ is the limiting current density of species j (mA cm^{-2}), λ_j is the stoichiometric coefficient for species j, D_j is the diffusion coefficient of species j (cm^2 s^{-1}), δ is the diffusion boundary layer thickness (cm), $C_{b,j}$ is the bulk concentration of species j (mol cm^{-3}), and $k_{m,j}$ is the mass transfer coefficient of species j (cm s^{-1}). The overall mass transport loss can be attributed to the anode and cathode sides:

$$\eta_{conc,a} = \frac{RT}{n_aF}\sum_j \lambda_{a,j} ln\left(1-\frac{i_a}{i_{L,a,j}}\right) \tag{1.25}$$

$$\eta_{conc,c} = \frac{RT}{n_cF}\sum_j \lambda_{c,j} ln\left(1-\frac{i_c}{i_{L,c,j}}\right) \tag{1.26}$$

where n_a and n_c are the number of electrons transferred in the anodic and cathodic reactions, respectively. $\lambda_{a,j}$ and $\lambda_{c,j}$ are the stoichiometric coefficients for species *j* in the anode and cathode, and $i_{L,a,j}$ and $i_{L,c,j}$ are the limiting current densities for species *j* in the anode and cathode, respectively.

Overall, PEM fuel cell performance depends on the kinetics of the HOR and ORR, membrane hydration, contact resistances within the materials used, O_2 transport, and H_2O content and transport inside the cell. Therefore, efficient fuel cell operation and performance involves improved rates of the reactions, transport of reactant gases, and correct water balance for the membrane.

1.4 Literature review

1.4.1 Water management in PEM fuel cells

As mentioned previously, water management is one of the most important issues for PEM fuel cells. Water flooding and drying inside the cell are two of the main performance concerns that exist when water management is not satisfactory. More research is required in order to reduce (or eliminate) the impact of such issues and hence improve the overall performance of the fuel cell system [9-11].

1.4.1.1 Water transport inside fuel cells

Water transport inside PEM fuel cells is a complex interplay of various processes in different parts of the cell. Figure 1.3 illustrates some of the most important water transport processes inside a fuel cell.

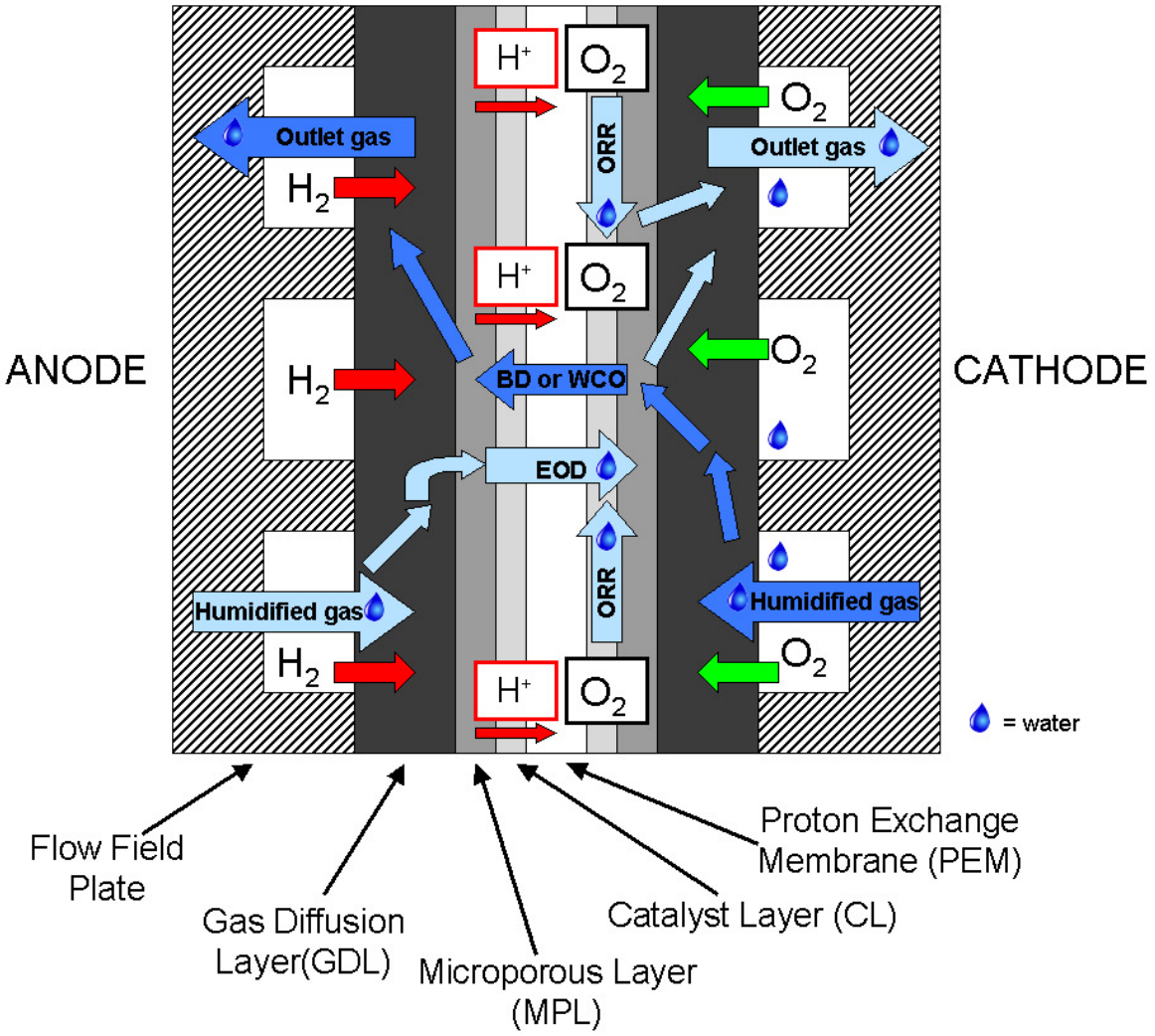

Figure 1.3 – Simplified schematic of the water transport within a PEM fuel cell (not to scale). BD and WCO refer to back diffusion and water crossover, respectively. EOD stands for electroosmotic drag. The outlet gases in the cathode and anode side are water vapor and unused oxygen and hydrogen, respectively.

The first source of water originates from the feed reactant gases that are normally humidified, thus, the molar fluxes of water vapor in the fuel (hydrogen) and oxidant (air) inlet streams are defined as:

$$N_{H_2O,H_2,in} = \frac{\lambda_{H_2}}{2F} \frac{\varphi_a P_{vs(T_{a,in})}}{P_a - \varphi_a P_{vs(T_{a,in})}} i \tag{1.27}$$

$$N_{H_2O,air,in} = \frac{\lambda_{air}}{4F} \frac{\varphi_c P_{vs(T_{c,in})}}{P_c - \varphi_c P_{vs(T_{c,in})}} i \tag{1.28}$$

where $N_{H_2O,H_2,in}$ and $N_{H_2O,air,in}$ are the molar fluxes of water vapor at the inlet of the fuel and oxidant streams (mol s^{-1} m^{-2}), λ_{H_2} and λ_{air} are the hydrogen and air stoichiometric coefficients, φ_a and φ_c are the relative humidities for the anode and cathode sides, $P_{vs(T_{a,in})}$ and $P_{vs(T_{c,in})}$ are the water vapor saturation pressures at the inlet temperatures of the anode and cathode sides (kPa), and P_a and P_c are the total pressures at the anode and cathode sides (kPa).

In addition, at the cathode side, water is produced at the catalyst layer by the oxygen reduction reaction (ORR), thus the molar water flux due to the ORR reaction can be described as (mol s^{-1} m^{-2}):

$$N_{H_2O,r} = \frac{i}{2F} \tag{1.29}$$

The water transport inside the membrane is a complex process since there are a number of different mechanisms that determine the water transport. One mechanism is the electroosmotic drag (EOD), which is the phenomenon in which water is dragged from the anode to the cathode by protons moving through the electrolyte (membrane). The molar flux of water due to electroosmotic drag (in mol s^{-1} m^{-2}) is:

$$N_{H_2O,drag} = \xi(\lambda)\frac{i}{F} \tag{1.30}$$

where $\xi(\lambda)$ is the electroosmotic drag coefficient defined as the number of water molecules per proton and is a function of the membrane hydration, λ. The water generated by the reaction in the cathode catalyst layer, equation (1.29), and the electroosmotic drag create a large concentration gradient across the membrane [5]. Thus, some molar flux of water diffuses from the cathode to the anode (i.e., back diffusion (BD) or water crossover (WCO)). The rate of water diffusion in the membrane (in mol s^{-1} m^{-2}) is:

$$N_{H_2O,BD} = D_{H_2O}(\lambda)\frac{\Delta c_{H_2O}}{\Delta z} \tag{1.31}$$

where $D_{H_2O}(\lambda)$ is the water diffusion coefficient (m^2 s^{-1}) in the membrane at the membrane hydration of λ, and $\Delta c_{H_2O} / \Delta z$ is the water concentration gradient (mol m^{-3}) along the z-direction (through the membrane) (m^{-1}). In addition to diffusion due to concentration gradients, water can also be hydraulically pushed from one side of the membrane to the other if there is a pressure gradient large enough between the cathode and the anode. The molar flux of water due to this hydraulic permeation (in mol s^{-1} m^{-2}) is given essentially by Darcy's law and can be defined as:

$$N_{H_2O,hyd} = \frac{k_p}{\mu} c_{H_2O} \left(\frac{P_c - P_a}{\tau} \right) \tag{1.32}$$

where k_p is the membrane hydraulic permeability (m^2), μ is the dynamic viscosity of water (kg m^{-1} s^{-1}), P_c and P_a are the cathode and anode pressures (kPa), and τ is the membrane thickness (in the z-direction).

In general, the transport of water located at the GDL, MPL, and catalyst layer is governed mainly by diffusion (for vapor) and Darcy's flow through capillary pressure (for liquid). In the flow field channels, there is a significant flow of gases that moves the water (and other species) in the direction of flow by means of convection [5,6,12].

In the case of the gas species, the main transport mechanism inside the GDL and MPL is through diffusion. In the catalyst layers, it has been shown that the gas transport is governed by Knudsen diffusion, which is independent of the total pressure [13]. It is important to note that not all the specifics of the transport mechanisms in each fuel cell component are yet understood completely, thus, there is still a great deal of work on these areas.

1.4.1.2 Water flooding mitigation strategies

Water in the PEM fuel cell is an unavoidable product of the electrochemical reaction and the presence of local oversaturated water vapor. Therefore, mitigation of negative water effects, as part of the overall water management, will always be an issue for PEM fuel cells. Even if steps are taken to avoid severe flooding in active

fuel cells, consideration must be given to the increased parasitic power loss associated with implementing water mitigation strategies. Parasitic losses are the waste energy taken from the fuel cell in order to enhance the fuel cell's ability to create more energy (e.g., air compressor). The main purpose of these strategies is to maintain a water balance inside the cell and to reduce the negative effects associated with two-phase flow inside the flow field channels, the gas diffusion layers (GDLs), and the catalyst layers (CL). Some of the methods used to improve water management are based on simply modifying the operating conditions of the fuel cell, which in part depend on the targeted application. The different components of a fuel cell system can also be individually designed in order to mitigate the overall water management issues. In addition, the use of extra systems or components (e.g., external valves, acoustic woofers, electroosmotic pumps, etc.) has been developed to improve the cell's performance by solving durability issues related to poor water management. However, many water management approaches lead to increased parastitic loads, system volume and complexity, so continued study into new methodologies is still essential.

1.4.1.2.1 Operating conditions

Modifying the operating conditions in fuel cell systems is a common water issue mitigation strategy. A key goal for the PEMFC is to keep all of the water in the vapor state but close to saturation to prevent membrane dehydration. Some of the operating conditions that determine the water accumulation (or water dehydration) inside a fuel cell are gas flow rates, pressures, temperatures, relative humidities, and specific current loads at which the fuel cell is running.

Usually, gas flow rates are based on stoichiometry, which is defined as the ratio between the actual gas flow rate used and the minimum stoichiometric amount of gas flow rate required for the reactions to occur. Since most of the water is accumulated on the cathode side of the fuel cell, much attention has been paid to the effect of high air/oxygen flow rates for the removal of water. When pure oxygen is used, the required stoichiometry is typically between 1.2 and 1.5, and when air is used the stoichiometry is 2.0 or higher [5]. Higher gas flow rates increase the cell

performance, but also increase the total parasitic losses since the air compressor would consume more power [14]. Although the performance of the cell improves with higher air stoichiometries, excessively high flow rates dry the membrane and the overall voltage decreases significantly. Natarajan and Nguyen [15] demonstrated that high flow rates affect the local current densities and ohmic resistances of the membrane, especially near the inlet of the cathode flow field channel because of increased membrane dehydration.

High gas flow rates, especially on the cathode side, can also be used to purge accumulated liquid water inside the channels, the GDL, and the catalyst layer. This purging step is especially important when the fuel cell is operated at freezing temperatures. Thus, dry gases are used for both reactant streams during the shutdown procedure in order to eliminate most of the liquid water [16-18]. In some cases, anode purging is not necessary since the amount of water is small, thus, improving fuel efficiency [16]. The timing of the gas purging method is an important parameter. If the stack is purged right after cell operation (prior to system shutdown), then there is a high probability that a large amount of liquid water will remain inside the cell after purging. On the other hand, if the cell is allowed to cool to room temperature (25 °C), a greater amount of liquid water will condense and the dry gas can remove it more effectively. Also important is the purge duration period. The resistance of the membrane can increase significantly after the water near the membrane is evaporated. Ideally, purging is not performed for extensive periods of time (longer than 100 seconds) because a dry membrane (high membrane resistance) will have a direct impact on the current that the stack will be able to achieve during a cold startup. Normally, gas purging is performed for no longer than a minute [16,19].

One other parameter that can have a direct impact on the stack's performance after purging is the humidity of the purging gas. Dry gases, air or N_2 for cathode and H_2 or N_2 for anode, are normally used for this procedure, but they can increase the membrane resistance very rapidly, which would affect the cell performance for the next start. Introducing humidity to the purging gas can reduce the degradation of the membrane without significantly affecting the removal of water from the cell [20]. The

use of humidity in the purging step becomes even more important after a number of freeze/thaw cycles in order to avoid overall cumulative performance degradation [21,22]. For more information on purging and its influence with respect to cold starts, the reader is referred to the following references [23-26].

The pressure of the gases, the pressure drop within the flow field plates, and the pressure difference between the anode and cathode can be varied in order to improve water removal inside PEM fuel cells. Pressurizing gases not only improves fuel cell performance but it also allows for better water management [5]. Pressure drop within the flow field plates is a key factor when designing cells with improved water removal capabilities. This depends on the choice of flow field design. Details about flow field designs and their pressure drops are given in Section 1.4.1.2.3.

Ballard Power Systems proposed and demonstrated a method called anode water removal [27-29] in which the water concentration profile or gradient of the proton exchange membrane is modified in order to increase the back diffusion rate of water from the cathode to the anode. Thus, the water at the cathode catalyst layer diffuses through the membrane and is removed via the anode reactant gas stream. One way of creating the water concentration gradient is by using high flow rates of hydrogen at the anode while reducing the outlet anode pressure substantially. The high flow rates decrease the water concentration on the anode side, which creates a water concentration gradient in the membrane between the anode and cathode sides. Thus, the water back diffusion rate of water from the cathode towards the anode increases, reducing the amount of water on the cathode side. More details regarding this method are explained in Chapter 2 (Section 2.1.5).

The temperature of the fuel cell has a great impact on the overall cell performance and on the liquid water accumulation inside the flow field channels. At low temperatures (less than 50 °C [30]), more liquid water accumulates in the channels. This leads to a blockage of airflow and decreases the cell's performance due to the lack of oxygen reaching active sites in the catalyst layer. Once the temperature is increased (e.g., 75 °C), the amount of liquid water in the channels is reduced since the capacity for water to stay in vapor state is greater at high temperatures than at

low temperatures [30]. Therefore, the flow channels are substantially less blocked with water and the cell's performance improves. Figure 1.4 shows how the water accumulation decreases when the cell temperature is increased at the same current density. At 75 °C, it can be observed that the flow field channels do not have water accumulation and just one channel has water droplets. In addition, when the cell temperature is increased the cathode pressure drop decreases since there is less liquid water present in the gas diffusion layers and the flow channels [31]. Chuang et al. [32] observed that even slight changes of the cell temperature (76 → 80 ◦C) are enough to decrease the amount of liquid water accumulated in the channels and in the GDLs, especially at high current densities. For example, at 76 °C the water content, measured using a neutron imaging technique, was 350 mg compared to 317 mg of water when the cell temperature was 80 °C.

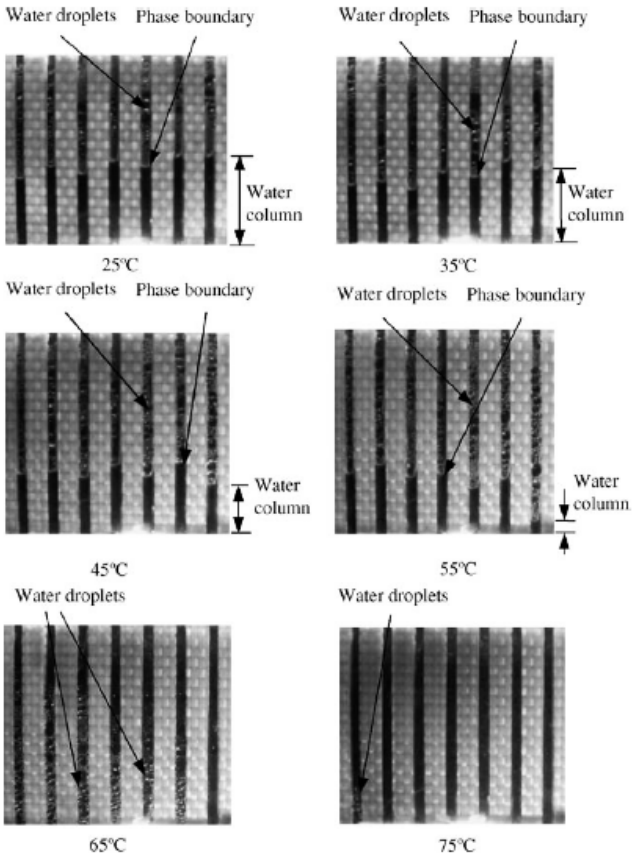

Figure 1.4 – Effect of cell temperature on cathode water build-up in parallel channels. The fuel cell used was a 5 cm^2 transparent single cell with 1 mm thick stainless steel cathode plate (0.8 mm wide channels machined all the way through) and a plexiglass cathode end plate in order to observe the flow field channels. The MEA was composed of a Nafion® 1135 membrane sandwiched between two carbon fiber papers (not specified). Both anode and cathode catalyst layers had a Pt loading of 0.4 mg cm^{-2}. The cell was operated at atmospheric pressure, an oxygen flow rate of 30 ml min^{-1} and a hydrogen flow rate of 50 ml min^{-1}, and a constant current density of 400 mA cm^{-2}. The gases were not humidified. (Reprinted from Liu et al. [30] with permission from Elsevier).

Higher temperatures also decrease the surface tension and viscosity of liquid water, facilitating more convective water removal in the flow channels [31]. Increasing the temperature between the cathode inlet and outlet to establish a thermal gradient has been shown to be an effective method for water management [33]. This can be accomplished through the use of a coolant flow field that can create such temperature gradients. In addition, temperature gradients can be controlled inside fuel cell stacks in order to improve fuel cell startup from freezing temperatures. In general, the use of temperature gradients in order to control the water migration from one side of the membrane to the other, also referred to as thermo-osmosis, is of critical importance in the reduction of overall water issues [34,35].

The relative humidity of the gases is another important operating condition that can be varied to mitigate water flooding and two-phase flow inside fuel cells. Bernardi [36] discussed how the water balance in fuel cells is more sensitive to changes in the relative humidities at the inlet of the air stream than at the inlet of the fuel side, leading most studies to deal with the relative humidity of the cathode side. Büchi and Srinivasan [37] performed tests with dry gases and showed the performance of the cell was around 60% lower compared to the same cell with humidified gases (at 500 mA cm^{-2}). This performance loss was attributed to the increase of the membrane's resistance due to dehydration (and reduced liquid content in the channels and MEA). In addition, long exposure to dry (no humidification) conditions has a direct impact on the fuel cell's overall performance, thus, compromising the durability of the fuel cell [5]. In general, the ideal relative humidity for a fuel cell system has to be determined after consideration of the flow field design, the MEA materials, and the application for which the fuel cell system will be used. For example, if the GDL does not have enough porosity it may not remove water efficiently at higher water production rates. However, at dry conditions, this may be favorable since the water accumulated in the GDL can keep the membrane humidified.

Figure 1.5 shows an example of a single fuel cell with and without humidified gases. It is evident that at high current densities (greater than 1200 mA cm^{-2}) the membrane is likely dehydrated, causing the cell performance to quickly deteriorate. Although for the midrange current densities the cell with dry gases performs similarly to the case with humidified gases, it is important to note that after prolonged hours of operation a number of failures are encountered, which are likely associated with the dry gases (i.e., dehydration due to lack of water content in the fuel cell). In general, there should be an appropriate water balance inside the fuel cell, and the ideal humidity for a specific fuel cell design and operating condition(s) should be set to achieve such a balance.

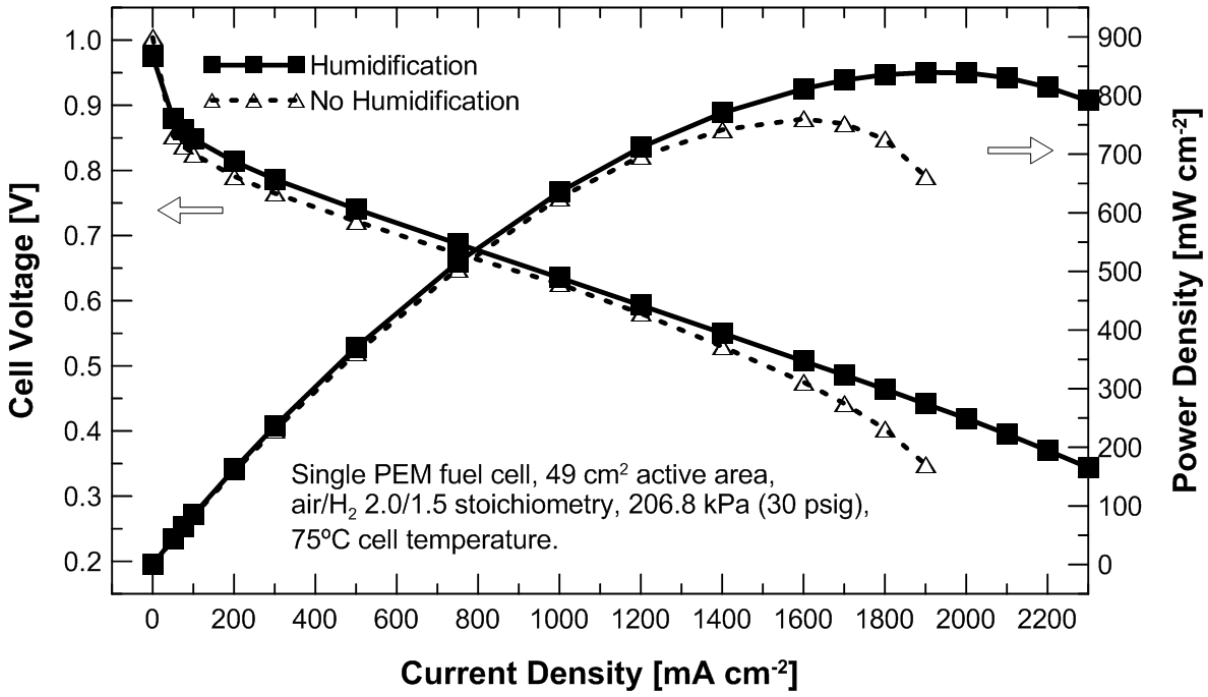

Figure 1.5 – Performance comparison for a fuel cell with fully humidified reactant gases (100% RH) and no humidified reactant gases. The MEA was composed of a Gore 5510 Primea Series membrane (0.4 mg Pt cm^{-2} on each side), SGL 25 BC GDLs for both the anode and cathode sides. The active area was 49 cm^2 [38].

1.4.1.2.2 Membrane electrode assembly design

Modification of the proton exchange membrane, the catalyst layers, and the gas diffusion layers are all valid approaches to improve the overall water management inside fuel cell stacks. It is important to note that one main concept, which can be implemented in any fuel cell component, is based on creating non-uniformity and in-plane gradients in the fuel cell structure in order to improve the overall performance of the cell [39]. These gradients along the MEA's surface (or between components) can change the electrochemical activity or modify the water transport along the whole cell. As discussed, by creating pressure and/or temperature gradients along the GDLs and the flow field channels (between the inlet and the outlet points of the gas streams) the accumulation of water and subsequent water removal can be significantly improved. Many other parameters can be manipulated non-uniformly such as hydrophobicity (PTFE content) and porosity.

Membrane and catalyst layers

The use of thin membrane materials improves the back diffusion rates of water from the cathode side towards the anode side. However, due to mechanical strength issues the membrane cannot be too thin because pinholes can be formed rapidly and the membrane can dry out faster. Membranes between 25 and 40 μm in thickness are recommended for most fuel cell applications [40].

One approach to reduce water accumulation inside the fuel cell is to use membranes with porous fiber wicks, as proposed by Watanabe et al. [41]. In this method, twisted threads of porous polyester fibers are placed (and hot pressed) between two Nafion® 117 sheets in order to supply water directly to the membranes. The MEA will be fully humidified, thus eliminating the need for humidifying the fuel and oxidant gases. Watanabe et al. also found that reducing the amount of porous fibers can modify the amount of water supplied through the wicks depending on the current density and fuel cell application.

Catalyst layer structure can also be modified in order to reduce the effect of flooding by improving the gas and liquid water transport [40,42,43]. Nguyen et al. [42] proposed a catalyst layer structure that separates transport channels for gas and liquid phases. The structure has a number of ionic (Nafion®) and electronic (carbon with catalyst) interconnected paths for proton and electron transport. The ionic film must be thick enough to avoid ionic resistance but thin enough to facilitate gas transport. The best Nafion® to carbon weight ratio found was found to be 1:1. This structure also has hydrophobic particles (PTFE) filling parts of the empty spaces between the ionic and electronic networks. Thus, the voids near the ionic film (hydrophilic) help liquid transport and the voids near the PTFE particles help the gas transport. Watanabe et al. [44,45] developed thin self-humidifying membranes that have highly dispersed nanocrystallites of Pt and oxides (such as TiO_2 or SiO_2). The Pt particles along with the oxides allow the reaction of H_2 and O_2, while keeping the product water at the hygroscopic oxide sites.

Gas diffusion layers

Gas diffusion layers used in PEM fuel cells are normally treated with an agent such as PTFE or fluoroethylenepropylene (FEP) to increase hydrophobicity. For cathode GDLs, this coating is vital since most of the water produced and accumulated inside the cell exits through the cathode side. For the anode GDL, this coating is not as critical but still important when dealing with back diffusion of water and to give more structural strength to the GDL. Another strategy for improving the water transport inside fuel cells is to use a thin microporous layer (MPL) on the surface of the GDL that faces the catalyst layer and the membrane. This layer is made with carbon black particles and PTFE (i.e., for hydrophobicity), and is usually deposited only on top of one of the surfaces of the GDLs, forming a double-layer diffusion layer. Microporous layers are now commonly used to improve the overall performance and voltage stability of fuel cells [46]. More details regarding treatments normally used on GDLs for water management purposes (including MPLs) are discussed in Section 1.4.2.

Diffusion and water barriers

Normally in fuel cells, any type of layer that acts as a barrier (either for gas or liquid) is avoided since it reduces the gas accessibility to the catalytic sites and increases the liquid water accumulation inside the cell. However, for specific conditions (e.g., low humidity) having these barriers may actually be beneficial. Graftech International produces laminated graphitic foils with perforations that can be used in fuel cell applications. They claim that these foils can be used as gas diffusion barriers in order to improve water hydration inside the cell at dry conditions [47]. However, no data are available in the literature that demonstrates their claim. In direct methanol fuel cells (DMFC), the use of liquid barriers on the anode side has been employed in order to reduce fuel crossover to the cathode side. In fact, Lam [48] was able to demonstrate a significant fuel crossover reduction, around 73%, when using perforated graphitic foils as barrier layers.

1.4.1.2.3 Flow field design and configuration

The flow field channels should distribute the reactant gases over the electrode surfaces as uniformly as possible in order to utilize the active catalyst efficiently.

These channels also have to collect and remove the product water in order to minimize flooding effects of liquid water. The fixed channel geometries and fixed active areas of flow fields determine the reactant flow characteristics over the operating range of the fuel cell. The most common flow field designs currently in use are parallel (straight) channels, serpentine, and interdigitated [6,49-51] (see Figure 1.6). The parallel design is comprised of a number of straight channels connected to common inlet and outlet headers. One issue associated with this design is that water tends to accumulate in the channels and the pressure drop is too low to remove the water [6,49]. This issue leads to the maldistribution of the reactant gases in the flow field, causing reactant starvation in some channels and an excess of reactants in other channels (i.e., the full active area is not utilized). In order to improve this type of flow field design, the Ballard automotive fuel cell (Mk900) was designed with longer parallel channels (i.e., an exaggerated aspect ratio), to increase pressure drop and to reduce the maldistribution issues [52].

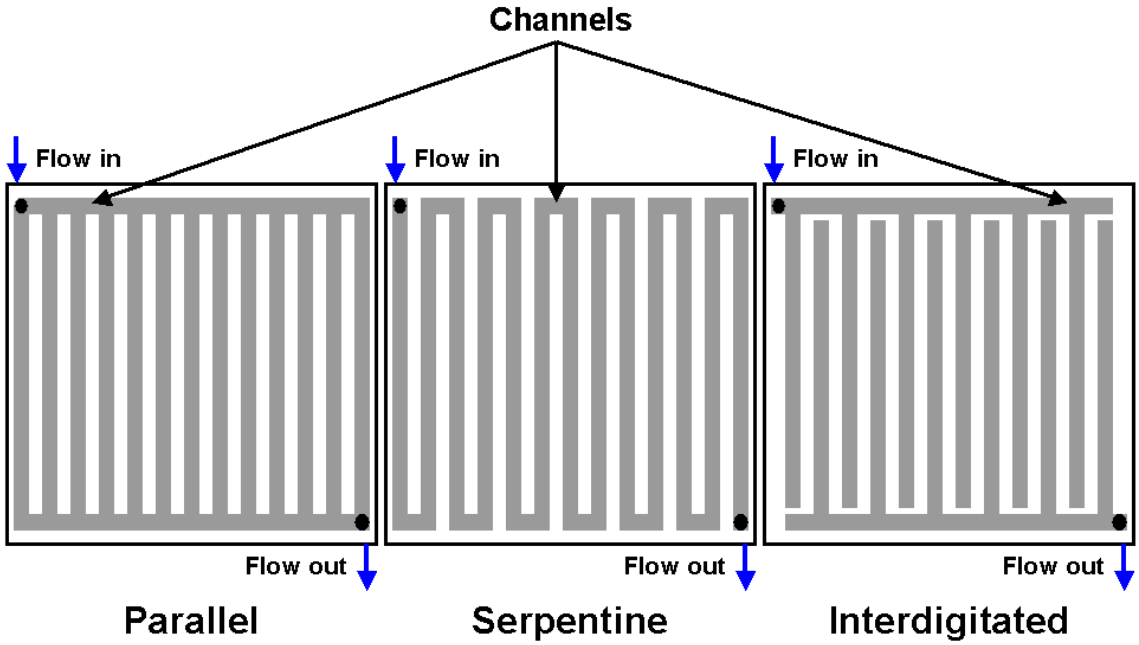

Figure 1.6 – Schematics of the three most common flow field designs.

In general, the pressure drop for continuous straight channel flow field can be calculated using Darcy-Weisbach equation [53] as follows:

$$\Delta P = \frac{fL\rho v^2}{2D_H} \tag{1.33}$$

where f is the friction factor, v is the average flow velocity (m s^{-1}), D_H is the hydraulic diameter (m), L is the channel length (m), and ρ is the fluid density (kg m^{-3}). The hydraulic diameter is related to the channel's cross-sectional area, a, and perimeter, p, ($D_H = \frac{4a}{p}$). The friction factor can be considered to be a combination of laminar and turbulent terms given by [50]:

$$f = f_{laminar} + f_{turbulent} = \frac{64}{Re} + f_{turbulent} = \frac{64\mu}{\rho v D_H} + f_{turbulent} \tag{1.34}$$

where Re is the Reynold's number and μ is the fluid viscosity (kg m^{-1} s^{-1}). Substitution of this expression into Darcy-Wesibach equation gives the following overall expression for pressure drop in the flow field channel:

$$\Delta P = \frac{32\mu L v}{D_H^{\,2}} + \frac{f_{turbulent} L\rho v^2}{2D_H} \tag{1.35}$$

The flow velocity v is related to the reactant stoichiometry by

$$v_{air} \approx \left(\frac{RT}{P}\right)\left(\frac{\lambda_{air} iA}{4F}\right)\frac{60}{0.21} \approx \frac{60(22.4)\lambda_{air} iA}{(0.21)4F} \approx 0.0166\lambda_{air} iA \text{ in slpm} \tag{1.36a}$$

$$v_{H_2} \approx \left(\frac{RT}{P}\right)\left(\frac{60\lambda_{H_2} iA}{2F}\right) \approx \frac{60(22.4)\lambda_{H_2} iA}{2F} \approx 0.0070\lambda_{H_2} iA \text{ in slpm} \tag{1.36b}$$

where λ_{air} and λ_{H_2} are the stoichiometric coefficients (inverse of utilization) of the respective reactants, i is the current density (A cm^{-2}), and A is the cell active area (cm^2). These approximations are at standard conditions.

Serpentine flow fields have one or more continuous channels connected to an inlet and outlet header and typically follow a path with several bends (see Figure 1.6). These flow fields generally have longer channel lengths and a greater pressure drop along the channels due to the bends, which facilitates water removal. Multiple serpentine channels are used for large active areas in order to avoid excessively

high pressure drops [50]. Li et al. [54] presented a method for designing serpentine flow fields based on an appropriate flow channel pressure drop so that all of the liquid water is evaporated and removed from the cell through the flow fields. However, it is important to note that the cells designed through this method exhibited inferior performance (600 mA cm^{-2} at 0.6 V) compared to similar serpentine flow fields found in the literature (≥ 1000 mA cm^{-2} at 0.6 V).

For interdigitated (or discontinuous) flow fields, there are a number of parallel discontinuous channels (i.e., the channels are discontinuous from the inlet header to the outlet header) (see Figure 1.6). The reactant gases are forced to flow through the porous electrodes (or GDL) in order to reach the channels connected to the outlet manifolds. Since the gases are forced along a short path through the GDL and catalyst layer, the liquid water is removed more efficiently, resulting in better performance at higher current densities. However, these flow fields do not remove the water located at the inlet of the channels properly, and the voltage stability at low current densities is very poor [51]. In general, this flow field type is most suitable for high current densities, but it increases the parasitic losses due to the larger pressure drops. Equation (1.35) alone does not provide an accurate measure of pressure drops in interdigitated channels because additional pressure drops caused by the diffusion of the reactant gases through the gas diffusion layer from one channel to another are not represented. For an interdigitated flow field the total pressure drop would be given by the sum of each pressure drop contribution,

$$\Delta P_{total} = \Delta P_{inlet} + \Delta P_{outlet} + \Delta P_{diffusion} \tag{1.37}$$

where ΔP_{inlet} is the pressure drop at the inlet (kPa), ΔP_{outlet} is the pressure drop at the outlet (kPa), and $\Delta P_{diffusion}$ is the diffusion pressure drop (kPa) through the GDL. Perry's Chemical Engineers Handbook [55] gives the diffusion pressure drop as:

$$\Delta P_{diffusion} = -\frac{u_s L \mu}{k} \tag{1.38}$$

where u_s is the superficial velocity (m s^{-1}), L is the channel's length (m), and k is the permeability of the media (m^2).

In addition to these pressure drops, for the interdigitated flow field the change in pressure over the length of the channel can be assumed to be constant, i.e.

$$\frac{dP}{dL} = const \tag{1.39}$$

Using equations (1.35) and (1.39) we have:

$$dP = \left[\frac{32\mu V(x)}{D_H(x)^2} + \frac{f_{turbulent}\rho V(x)^2}{2D_H(x)} \right] dL \tag{1.40}$$

where x is a determined portion of the channel length (m). Now, with equations (1.38) and (1.40), the overall pressure drop in an interdigitated flow field can be expressed as:

$$\Delta P_{total} = 2\int_0^L \left[\frac{32\mu V(x)}{D_H{}^2} + \frac{f_{turbulent}\rho V(x)^2}{2D_H} \right] dL - \frac{VL\mu}{k} \tag{1.41}$$

Another key factor regarding flow fields channels of a fuel cell is the direction in which the flow fields (coolant included) are placed, since it also has an influence on the overall water management and performance of the cell. Depending on the application, it may be desirable for the coolest region of the coolant channels to coincide with the area in which the oxygen concentration in the cathode channels is the highest and where there is the least amount of water in the cell. Wilkinson et al. [33] used this approach to create a thermal gradient across the cathode electrode in order to keep the product water in the vapor phase (see Section 1.4.1.2.1). They also operated a fuel cell with dry gases by using the cathode and coolant flow field in co-flow and the anode in counter-flow. Similarly, cross-flow operation between the fuel and the oxidant channels may be preferred to co-flow or counter-flow configurations. Figure 1.7 shows the schematics of some flow field configuration examples. In Figure 1.8, it can be observed how the performance of a single cell fuel cell changes depending on the configurations of the anode and cathode flow fields. For this specific cell design, the cross-flow arrangement resulted in the best

performance, approximately 5 to 10% better than the other two arrangements, at current densities higher than 1000 mA cm^{-2}.

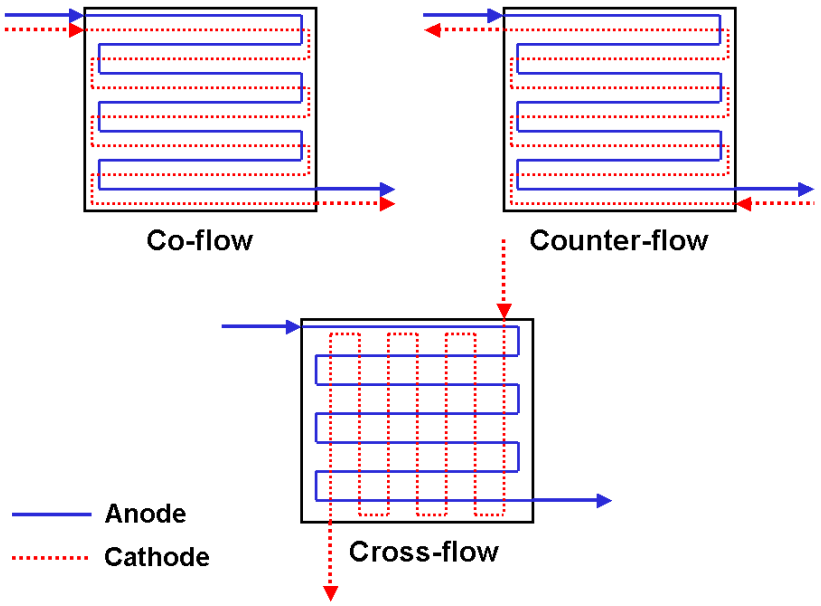

Figure 1.7 – Examples of different anode and cathode flow field arrangements.

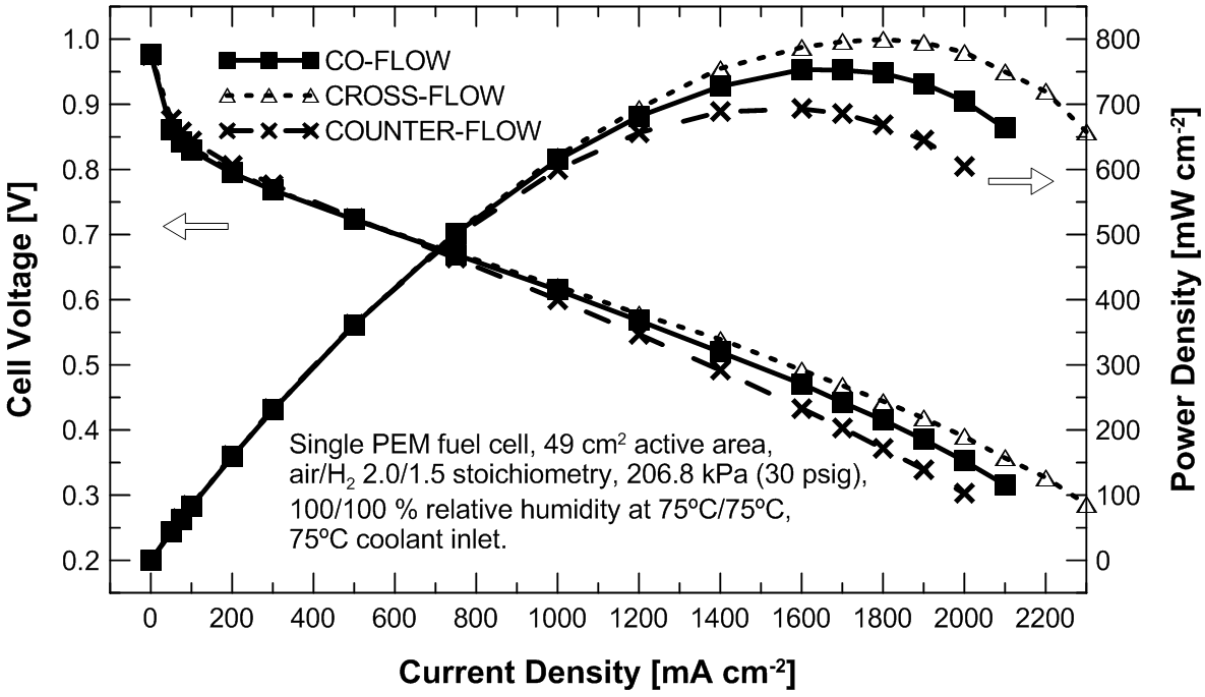

Figure 1.8 – Performance comparison between co-flow, cross-flow and counter-flow configurations between the anode and cathode flow fields. The MEA was composed of a Gore 5510 Primea Series membrane (0.4 mg Pt cm^{-2} on each side), SGL 25 DC GDL for the anode and SGL 25 BC GDL for the cathode. The anode and cathode flow field plates had single-path serpentine flow fields. The active area was 49 cm^2 [38].

The cross-sectional shape of the flow field channels also plays a key role in effective water removal. For example, Trabold et al. [56,57] demonstrated how triangular shaped flow field channels can have designated localized water collection regions. The water then accumulates away from the gas diffusion layer, which allows more gas to reach the catalyst layer. In addition, the cross-section of the channels can be designed to change gradually along the length of the channel, modifying the pressure drop and gas distribution along the active area [58]. Johnson et al. [59] developed a differential pressure flow field for water removal by changing the shape of the flow field channels with respect to each other.

The flow field channels can also be modified with respect to their hydrophilicity. Hydrophilic channels may improve the transport of gases to the reactant sites by facilitating the water transport in the edges and surfaces of the channels [60]. However, very hydrophilic channels result in greater pressure drops due to liquid water blockage. The wetting capabilities of the channels can be modified by using different cross-sectional geometries and/or by altering the surface characteristics of the flow field plate materials [61].

The use of porous plates (e.g., porous graphite, porous metals, etc.) with standard flow fields has improved water management in fuel cells, especially when dealing with dry conditions and gases at ambient pressures [62]. United Technologies Company (UTC) developed a fuel cell stack with porous flow field plates in which the pores are filled with liquid water [63-66]. These plates have coolant flow fields filled with water on one side and gas flow channels on the other that are in contact with the MEA. Since the plates are gas impermeable, the gas does not diffuse through the pores towards the coolant channels. The water accumulated in the gas channels is wicked towards the coolant side since the gas streams are at higher pressure than the coolant streams. Thus, issues related to water accumulation in the flow field channels are reduced significantly. Miachon and Aldebert [67] also used a porous plate to improve water management by forcing the gases to pass through porous carbon blocks situated between non-porous graphite plates in order to reach the GDL instead of flowing through channels.

Another way of modifying the flow field channels to reduce the accumulation of water in the GDL and in the flow channels is through the use of absorbent wicking materials. Examples of these materials include polyvinyl alcohol sponges, absorbent cotton cloth, and absorbent cotton paper [68-71]. These materials can be located near the inlet and outlet areas of the flow fields in order to absorb excess water and to humidify the dry gases that enter the channels. This approach would then potentially eliminate the need for a humidification system.

1.4.1.2.4 Use of additional systems

There have been a number of proposed add-on systems that attempt to improve overall fuel cell stack performance without increasing the parasitic energy demand significantly. Nguyen et al. [72-74] presented a system that used sequential exhaust or purging of individual cells in a stack as a liquid water management strategy. This system used a device (electromechanical valves or rotating device located outside the stack) that allowed each cell in the stack to exhaust separately from the other cells. Thus, each cell was guaranteed to receive adequate gas flow without water accumulation. One important issue with this concept is the added complexity to the system due to the addition of extra valves. Matsumoto et al. [75] proposed a fuel cell stack that changed the flow field of the cathode plates by changing the external port arrangement with valves depending on the power that the cell was delivering (e.g., parallel flow field at high power levels and serpentine flow field at low power levels). Hensel et al. [76,77] have proposed another system in which a stack was designed to facilitate control of fuel, air and cooling water to each cell. The delivery system for this stack used micro-valves located outside the stack to manipulate the fuel flows to each cell. It is claimed that these micro-valves are being developed so they can potentially be implemented inside the internal manifold of the stack.

Researchers at Stanford University have developed a PEM fuel cell integrated with an electroosmotic pump to improve the water management of the cells at different conditions [78-82]. In their latest design, a porous carbon plate with parallel flow field channels was connected to a small electroosmotic pump placed outside the fuel cell.

The hydrophilic porous plate acts as a wick and absorbs water from the flow channels and the GDL until the region is saturated. At this point, the pump is used to remove the remaining water from the cell. Between the plate and the pump, there is a polyvinyl alcohol filter that connects both components and filters out any particles that may damage the pump (see Figure 1.9). It is claimed that this system consumes just 1% of the overall fuel cell power at low current loads and only up to 0.5% at medium to high current densities. These tests were performed with single cell fuel cells, and the implementation of such a system into an actual fuel cell stack has not been demonstrated. The addition of an electroosmotic pump does not only just increase the overall complexity and size of a fuel cell stack, but it can also impose a negative effect on the overall reliability of the system.

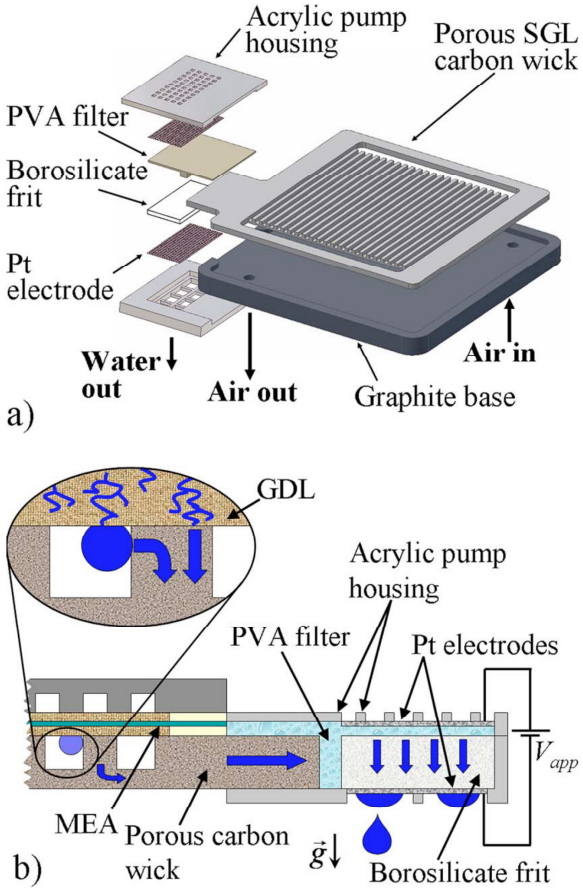

Figure 1.9 – (a) Schematic of a porous plate with an external electroosmotic pump used in fuel cells and (b) detailed view of the water path with the porous plate and electroosmotic pump (Reprinted from Litster et al. [81] with permission from The Electrochemical Society).

Acoustic woofers are another method in which additional systems are incorporated into fuel cells in order to generate pulsating flows. This has resulted in the improvement of water management and of fuel cell overall performance [83]. However, the overall fuel cell efficiency is slightly decreased, between 2 to 3%, due to the use of the woofer. Vibration and acoustic methods have also been considered as possible approaches for the removal of excess product water in PEM fuel cell stacks [84,85]. This method would use waves (flexural, acoustic, or surface waves) to remove the water droplets inside the fuel cell. However, these methods are still in the theoretical and modeling stages, and no practical experiments have been reported.

1.4.2 Gas diffusion layers

The gas diffusion layer (GDL) is usually made out of carbon fiber paper (CFP) or carbon cloth (CC) and is a vital component of the MEA and fuel cell since it provides the following functions and properties:

- To evenly distribute the reactant gases from the flow field channels to the catalyst layer. For this, GDLs have to be porous enough so all the gases flow without major problems.
- To remove the water produced and accumulated in the catalyst layers towards the flow field channels. The GDL must have large enough pores so that the condensed water can leave the catalyst layer, MPL and GDL without blocking any pores that may affect the transport of reactant gases.
- To provide mechanical support to the catalyst layer and the membrane in order for these two components not to be affected by the pressure that the landings or ribs of the flow field plate put on them. Therefore, the GDL has to be made out of a material that does not deform substantially after long hours of operation so that it is still able to provide mechanical support.
- To conduct electron flow from the bipolar plates to the catalyst layer and vice versa with low resistance between them. In order for the GDL to be able to do this successfully, it has to be made of a material that is a good electron conductor.

- To transfer the heat produced from the catalyst layer to the bipolar plates in order to keep the cell at the desired temperature of operation. Thus, the GDL should be made out of a material that has a high level of thermal conductivity so the removal of heat is as efficient as possible.

In this thesis, gas diffusion layers will be considered as the porous media that help the transport of the reactant fluids and products from one surface to another. In addition, the MPL will be defined as the additional layer or layers (made out of carbon black and water repellent particles) located between the CL and the GDL. It is important to note that although “microporous layer” and “gas diffusion layer” are the common names for these components, as well as the ones used in this thesis, there are a number of different names that can be found in the literature. For example, when both the catalyst layer and the GDL are mentioned as one component, then the name “diffusion electrode” is commonly used. Since the GDL is of a porous nature, it has also been called the “diffusion media” (DM) or “porous transport layer” (PTL). Sometimes the GDL is also referred to as the component formed by an MPL and a backing layer. The MPL has also been called the “water management layer” (WML) because one of its main purposes is to improve the water removal inside the fuel cell. In this thesis these components will be referred to as the MPL and GDL because these names are widely used in the fuel cell industry.

1.4.2.1 Different types of gas diffusion layers

There are a number of different materials that have been considered as potential candidates to be used as gas diffusion layers in PEM fuel cells. The two materials that have been used the most so far in fuel cell research and products are carbon fiber papers (CFPs) and carbon cloths (CCs), also known as carbon woven fabrics. Both materials are made from carbon fibers. Although these materials have been quite popular for fuel cells, they have a number of drawbacks, particularly with respect to their design and model complexity, that have led to the study of other possible materials.

1.4.2.1.1 Carbon fiber paper

Carbon fiber papers are made of carbon polyacrylonitrile (PAN) fibers, which are cut into small pieces then coated with water and a binder (e.g., polyvinyl alcohol). After rolling the material inside an oven, it is impregnated with a resin (e.g., phenolic resin) [86]. Figure 1.10 shows SEM (scanning electron microscope) micrographs of a carbon fiber paper with and without a hydrophobic coating. As seen in Figure 1.10d, some of the pores of the CFP can be partially blocked if too much coating is used. For more information and details regarding the fabrication processes of carbon fiber papers please refer to [87-89].

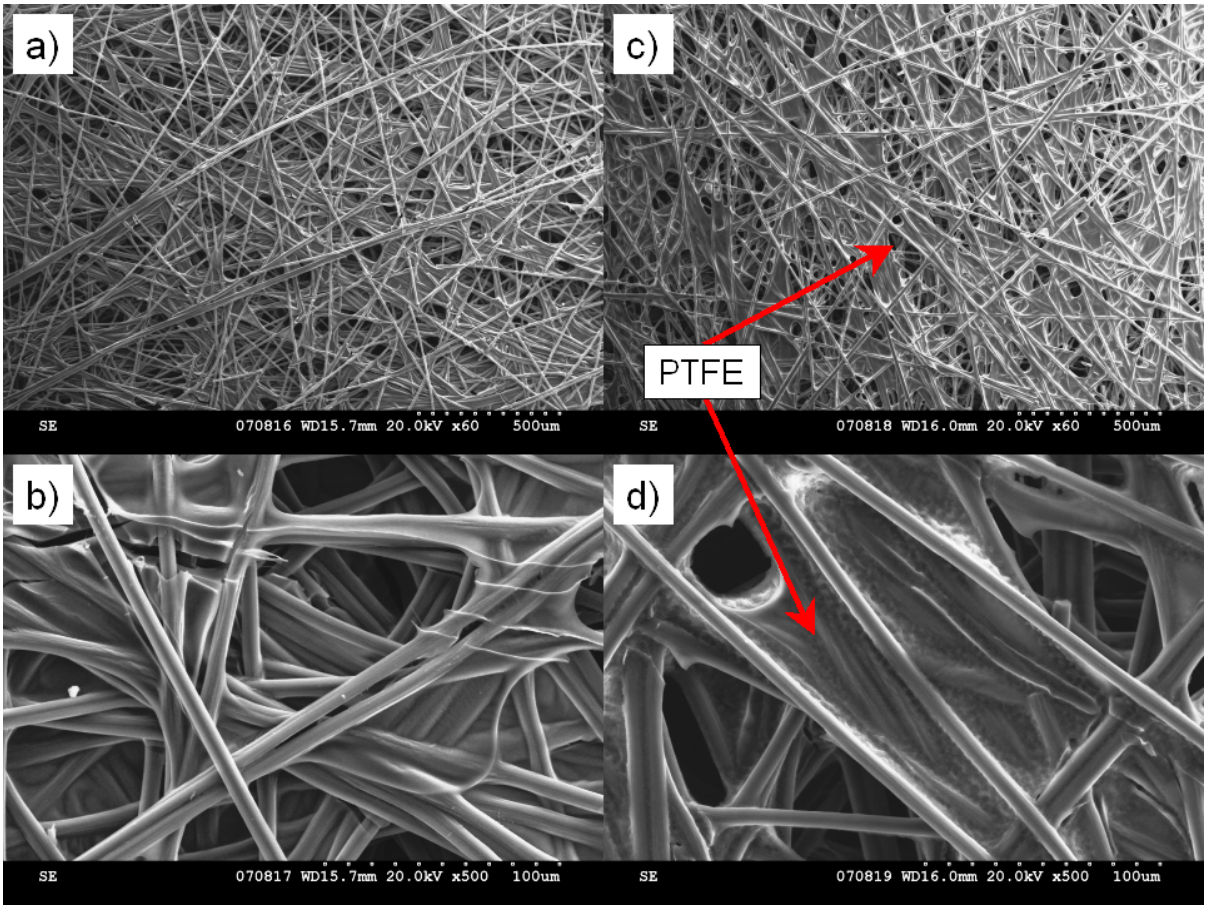

Figure 1.10 – Scanning electron microscope (SEM) micrographs of typical carbon fiber paper sheets used in fuel cells: (a) Toray TGPH-060 carbon fiber paper (CFP) with no PTFE (reference bar indicates 500 μm); (b) close-up view of the TGPH-060 CFP with no PTFE (reference bar indicates 100 μm); (c) Toray TGPH-060 CFP with 20% PTFE (reference bar indicates 500 μm); (d) close-up view of the TGPH-060 CFP with 20% PTFE (reference bar indicates 100 μm). PTFE stands for polytetrafluoroethylene.

1.4.2.1.2 Carbon fiber cloth

Along with CFPs, carbon cloths (CC) have also been widely used materials for gas diffusion layers in fuel cells. The majority of these fabrics are made from PAN fibers that are twisted together in rolls. These rolls then go through a process of weaving or knitting until the cloths are formed [86]. Instead of using a resin to hold these materials together, their woven structure provides the mechanical strength and integrity needed. Figure 1.11 shows SEM micrographs of a typical carbon cloth material used in fuel cells with and without hydrophobic coating, in which it can be observed that the CCs have a much more organized structured than CFPs.

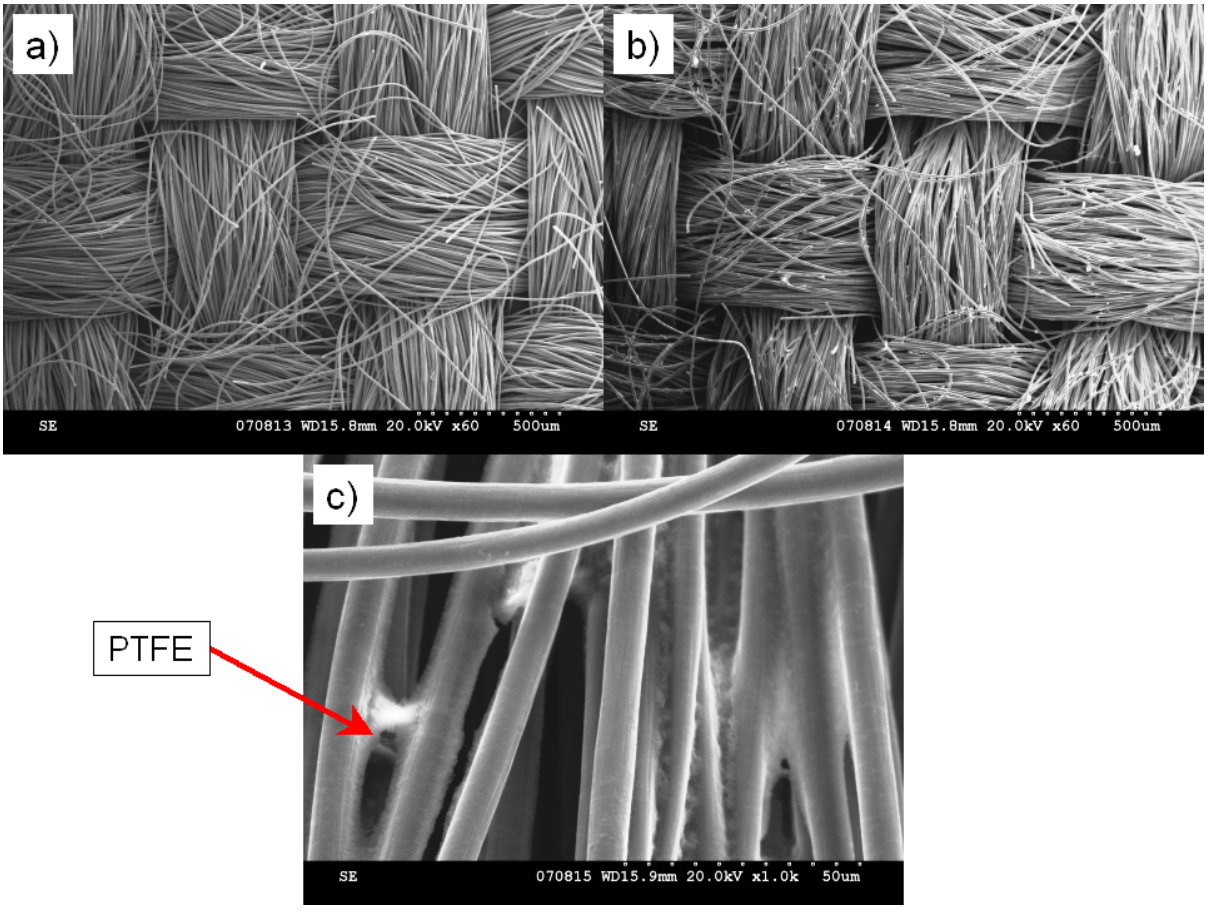

Figure 1.11 – Scanning electron microscope (SEM) micrographs of typical carbon fiber cloths used in fuel cells: (a) E-Tek Carbon Cloth "A" with no PTFE (reference bar indicates 500 µm); (b) E-Tek Carbon Cloth "A" with 20% PTFE (reference bar indicates 500 µm); (c) close-up view of the E-Tek Carbon Cltoh "A" with 20% PTFE (reference bar indicates 50 µm).

1.4.2.1.3 Metal gas diffusion layers

Due to their high electrical and thermal conductivity, materials made out of metal have been considered for fuel cells. Only a very small amount of work has been presented on the use of metal materials as gas diffusion layers in the PEM fuel cell because most of the research has been focused on using metal plates as bipolar plates [90] and current collectors. The GDLs have to be thin and porous, and have high thermal and electrical conductivities. They also have to be strong enough to be able to support the catalyst layers and the membrane. In addition, the fibers of these metal materials cannot puncture the thin proton electrolyte membrane.

Of the most common GDL materials, carbon fiber papers are widely known for being mechanically weak since their microstructure is destroyed when excessive compression forces are applied to them (i.e., when compressing a fuel cell). This destruction of the materials affects the porosity, which has a direct impact on gas and liquid transport mechanisms within the GDL and the fuel cell [91]. Carbon cloths have better mechanical strength due to their lack of compressibility. Compression forces on GDLs can also affect the overall electrical conductivity of the cell. Thus, metal meshes (e.g., expanded metals or screens), perforated sheets, felts, and foams have all been considered as possible GDLs to overcome some of the conventional GDL limitations.

<u>Metal meshes</u>

In electrochemical systems, metal meshes have been widely used as the backing layers for catalyst layers (or electrodes) [92-95] and as separators [96]. In fuel cells where an aqueous electrolyte is employed, metal screens or sheets have been used as the diffusion layers with catalyst layers coated on them [97]. In direct liquid fuel cells, such as the direct methanol fuel cell (DMFC), there has been research with metal meshes as diffusion layers in order to replace the typically used CFP and CC diffusion layers since they are considered not suitable for the transport and release of carbon dioxide gas from the anode side of the cell [98]. Shao et al. [99] used a Titanium mesh as the GDL for the cathode (air) side, which was coated on both sides with carbon black (Vulcan XC-72) and PTFE (i.e., with microporous layers on each side). It was shown that this novel cathode GDL performed similar to

conventional CFP GDLs under comparable conditions. Similar metal sheets have also been used as GDLs in the cathode of PEMFCs. Wilkinson et al. [100,101] presented the idea of using fluid distribution layers made out of metal meshes with electrically conductive fillers inside the holes of the meshes. A very similar idea was also presented by Hamada et al. [102].

In most of these studies, the meshes used were expanded metals that are readily available since they are used in many industries. Expanded metals are usually made with a precision die that slits and stretches the material in a single operation. The material is then passed through a set of rollers in order to obtain the desired thickness [103]. Figure 1.12 shows pictures of an expanded metal mesh similar to those used as GDLs in fuel cells.

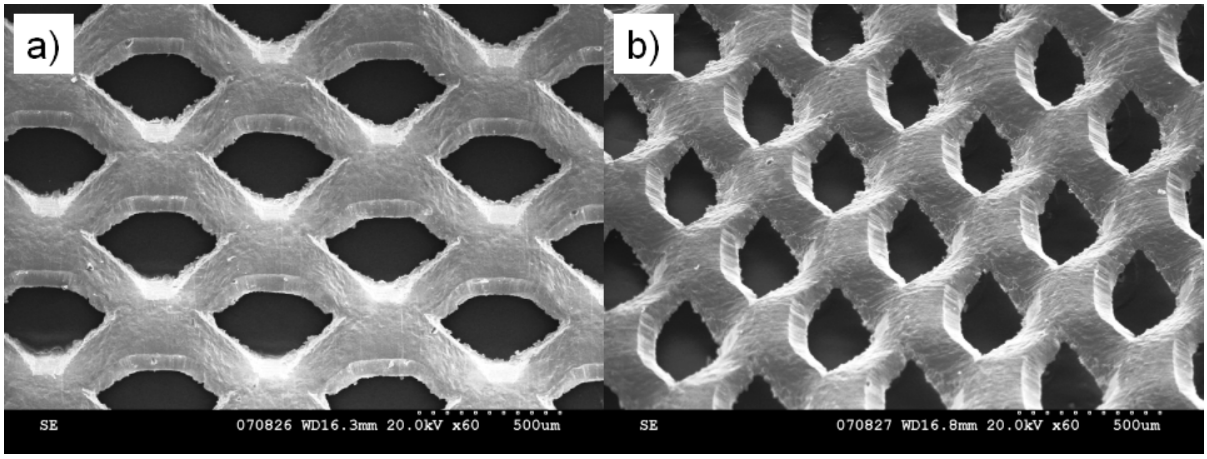

Figure 1.12 – Scanning electron microscope (SEM) micrographs of a typical stainless steel expanded metal (reference bars indicate 500 μm): (a) Picture taken with material sitting flat; (b) Picture taken with the material tilted at 45˚.

Sintered metals

Sintered metals have also been considered as possible GDLs given that these materials exhibit great mechanical strength and electrical conductivity. Hottinen et al. [104,105] used titanium sintered meshes as GDLs on the cathode side of a PEMFC since the porosity of these Ti metal sheets does not reduce when in compression. It was demonstrated that in order for the cell to achieve at least 90% of baseline performance, the sintered meshes had to be coated with platinum. However, the results showed that a cell with CFP (SIGRACET GDL10-BB) as the GDL still

performed slightly better (especially at high current densities) than the cell with the Pt-coated sintered Ti mesh. Cisar et al. [106] presented another example in which a GDL consisting of sintered metal fibers was used on the cathode side of a PEMFC. These fibers were unified or bonded to the flow field plate (made out of metal) before assembly in order to combine the two components into one.

Micromachined meshes

Micromachining has also been used to fabricate perforated metal meshes as GDLs in micro fuel cells. Fushinobu et al. [107] developed thin, perforated Ti films/sheets using micro fabrication technology (see Figure 1.13). However, the performance of the PEMFC using these GDLs was substantially lower compared to a cell with CFP as a GDL. Wan et al. [108] published a study in which a thin Ti substrate with micro-flow channels machined on it was used in a micro-PEMFC. This Ti sheet was also used as the cathode current collector, flow field plate, and GDL. Acceptable performance (approx. 0.6 V at 300 mA cm^{-2}) was achieved with these components when they were coated on both sides with a microporous layer.

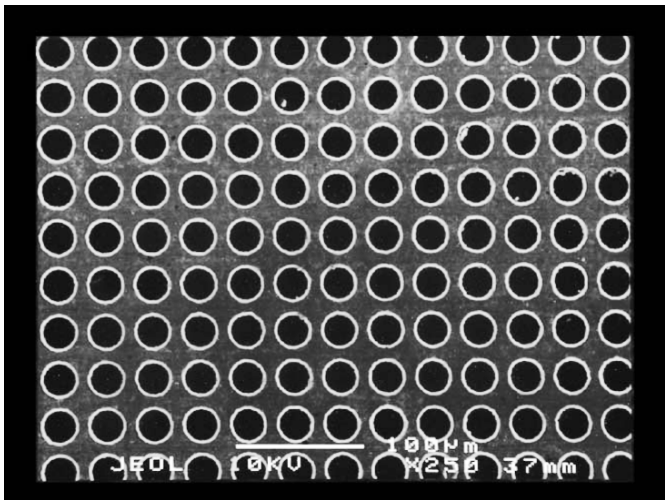

Figure 1.13 – Scanning electron microscope (SEM) image of a Ti gas diffusion layer with 25 μm diameter holes (reference bar indicates 100 μm). (Reprinted from Fushinobu et al. [107] with permission from Elsevier).

Zhang et al. [109,110] also used micro fabrication techniques in order to develop a thin perforated copper foil and use it as a cathode GDL in a 10 cm^2 PEMFC. In addition to the metal GDL, an “enhancement” layer was used that consisted of a

porous material located between the perforated copper foil and the flow field plate (CFP was used in this study). This layer improved the overall short-term performance and water management of the cell. However, the authors did not discuss any possible long-term issues related to contamination of the membrane due to the use of a copper GDL.

Lee et al. [111,112] developed thin perforated stainless steel sheets to be used as GDLs on the cathode side of a micro-PEMFC. The micro holes (50 μm in diameter) in the stainless steel sheet were fabricated by lithography and wet etching. Unfortunately, no performance data of these GDLs were presented.

Metal foams

Metal foams have been used in the past in the development of flow field plates. For example, Gamburzev et al. [113] used Ni foams as both a GDL and a flow field plate with an MPL layer on one of its surfaces. They observed that such a design had high contact resistance between the nickel foam and the MPL and also increased gas diffusion resistance due to the required MPL thickness. In another study, Fly et al. [114] designed a fuel cell stack in which the gas distribution layers were made out of metal foams (open cell foams). In addition, more than one foam (with different porosity) could be sandwiched together in order to form a GDL with variable porosity. However, no experimental data were presented to demonstrate the advantages of using these GDLs.

1.4.2.1.4 Engineered gas diffusion layers

One of the main issues with the CFPs and CCs used as the gas diffusion layers is the non-controlled variation in porosity (and other localized properties); for example, the porosity characteristics between carbon papers are not repeatable [115]. These materials are hard to improve since only average pore sizes and volume densities can be measured and most of the development has been based on empirical parameters (see Figures 1.10 and 1.11). In addition, water management and mass transport limitations, which are some of the major issues for the fuel cell, could be improved considerably if the GDLs can be carefully designed, taking into account all

their parameters [107]. Ideally, GDLs should be designed based on the specific fuel cell application, taking into account the necessary porosity (i.e., open area), improved gas diffusion and distribution, water removal capability, etc. Therefore, engineered materials in which the porosity and perforations used for liquid and gas transport are specifically designed in order to achieve the desired performance have started to be considered as possible GDLs. It is important to note that CC materials are more ordered and property controlled than CFPs; thus, they could be considered as partially engineered GDLs. In addition, some of the studies explained earlier regarding the use of micromachined metal GDLs are also considered as engineered GDLs.

Perforated non-porous materials

One of the first fuel cell designs that used these types of engineered materials was presented by Wilkinson et al. [100]. They presented the idea of using a fluid impermeable sheet material (e.g., graphitic foil) as GDLs for both the anode and the cathode. The sheets had perforations in the regions corresponding to the active area of the cell, and were filled with electrically conductive filler or with catalyst, thus, increasing the overall active zone (ideal for liquid fuel cells).

Later, the same group presented a similar design of this perforated material in which more advanced ideas related to the development of the perforations were introduced (see Figure 1.14) [101]. They showed that the perforations could increase in size in a graded or banded manner or their area density could change also in a graded or banded manner (see Figures 1.14a-1.14d). Also, the perforations could have different cross sectional shapes, for example, straight, tapered, or any other combination (see Figure 1.14e); they could also be connected to each other in different ways with passages or grooves, similar to flow fields (see Figure 1.14f). Other types of materials such as expanded metals, metal screens, and perforated metal sheets were also considered. Integrating both the GDL and the flow field plate into one component, and thus reducing the overall size and cost of the cell even further, was also explained in detail. All of these designs can also be tailored in order to improve the overall gas permeability of the specific GDL and reduce the mass transport limitations within the cell [101]. To the best knowledge of the author, there

are limited published results or published experimental data that demonstrate how these engineered GDLs perform as gas diffusion layers.

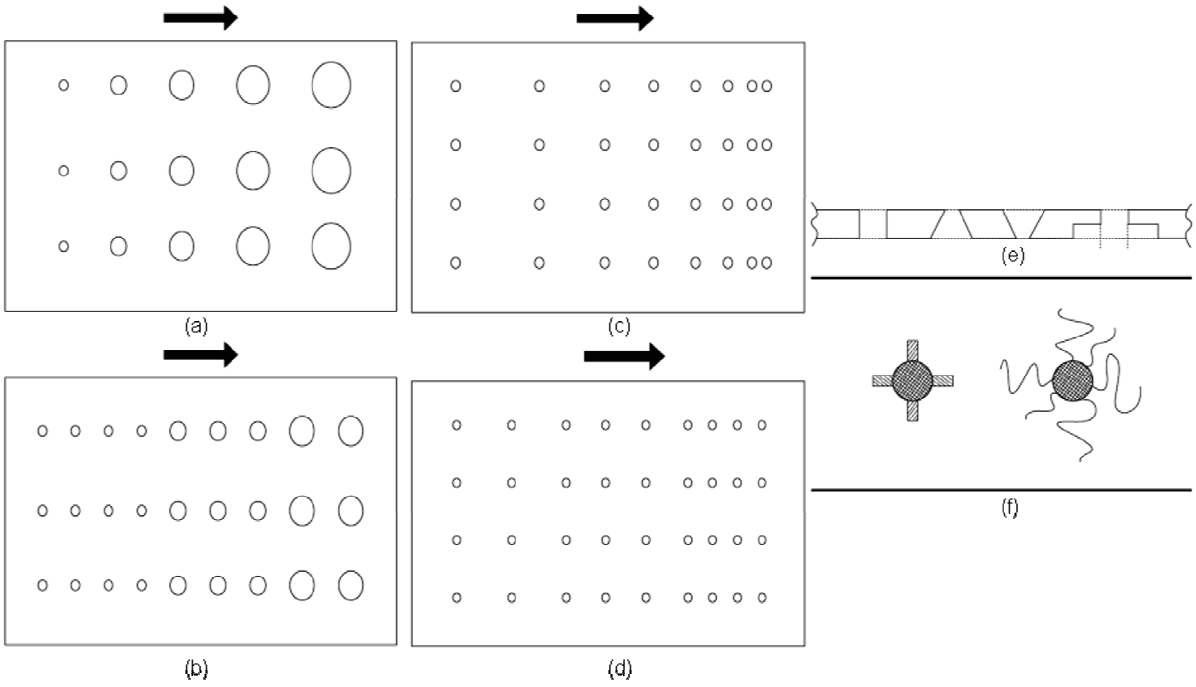

Figure 1.14 – Perforated pores: (a) different sizes in graded manner; (b) different sizes in banded manner; (c) different density of perforations in a graded manner; (d) different density of perforations in a banded manner; (e) perforations with different cross-sections; (f) plane view of perforations with extra passages/grooves [101].

Mercuri [116] of Graftech Inc. developed graphitic sheet materials made out of compressed expanded graphite particles. In general, these materials consist of a monolithic graphitic structure that is flexible, conformable, electrically and thermally conductive, and is not deformed easily when compressed. In order to be used as gas diffusion layers in electrochemical cells, the sheets or foils were perforated by mechanical impact. This process was performed with a pressing roller, which had protrusion elements that were forced through one side of the graphite sheet. Similar to the earlier work of Wilkinson et al. [100,101], the perforations could also be designed using different sizes, shapes and placements in order to improve gas diffusion and reduce water flooding in fuel cells [117]. In addition, these materials can also be made hydrophobic (waterproof), the perforations can be filled with catalyst (important in liquid fuel cells), and the overall electrical and thermal conductivity can be enhanced [118-120]. Figure 1.15 shows pictures of some

expanded graphite foils fabricated by Graftech Inc. with 2,500 tips per square inch (Figure 1.15a) and 1,200 tips per square inch (Figure 1.15b).

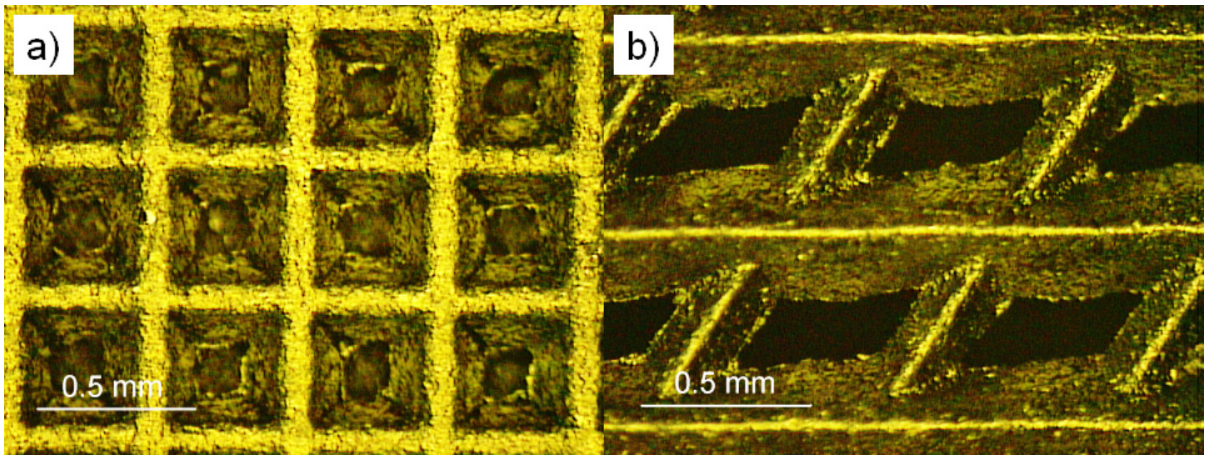

Figure 1.15 – Grafcell® flexible graphite diffusion layers by Graftech Inc. with 21% open area (reference bar indicates 0.5 mm): (a) 2,500 tips per square inch, (b) 1,200 tips per square inch.

Few experimental data have been published regarding these types of diffusion layers. Yazici [121] presented a study in which the graphitic foils (Graftech Inc.) were used as cathode gas diffusion layers in direct methanol fuel cells. These foils had a 2,500 tpi (tips per square inch) and 15% open area. When compared to a CC (ELAT with MPL), this GDL did 5 to 10% better, especially at dry conditions. Once the cell temperature was increased from room temperature to 80˚C, there was no clear difference between the CC and the graphitic foil GDL. In another study, a perforated graphitic foil was used with an MPL on top of one of its surfaces as the cathode GDL in a cylindrical PEMFC [122,123]. Recently, Gurau et al. [124] tested a number of different Graftech expanded graphite sheet materials, called Grafcell®, as cathode gas diffusion layers. It was demonstrated that the best performing GDLs had high open area and low hole density. However, the tests were performed at reactant stoichiometric ratios for both cathode and anode sides of 5.0 and 3.0, respectively. These ratios are unrealistic and significantly greater than those typically used by the fuel cell industry, which are around 2.0 for the cathode and 1.5 for the anode [5]. In addition, none of the details regarding the exact open areas, exact amount of perforations/holes and specific characteristics of the holes (size, shape, etc.) are given.

Zhou et al. [125,126] investigated the use of perforated materials as cathode GDLs in PEMFCs through modelling (no experimental results were reported). However, the group's model results were produced based only on conservation of mass and momentum (i.e., energy and electrochemical equations were not considered). This model studied only how different shapes of perforations affected the liquid water removal through the GDL. It was concluded that the GDL with trapezoidal-shape perforations with the smaller area facing the flow field channels enhanced water removal inside the MEA. However, neither experiments nor performance-based data were published.

In Section 1.4.2.1.3, it was mentioned that Zhang et al. [109,110] developed a technique to micro-machine a thin metal film prepared from copper. This material had a number of perforations that followed a predetermined pattern and such a design can be changed fairly easily by just changing one of the masks that were used in the fabrication process. Lee et al. [127] used a silicon substrate and machined micro-perforations and micro-channels on it using MEMS (micro-electro-mechanical systems) techniques in order to use it as the cathode diffusion layer and flow field channel plate in a micro-PEMFC.

Perforated porous materials

Modifying existing carbon fiber papers in order to improve gas and liquid water transport through the use of perforations and grooves can also be considered as part of an engineered GDL approach. Johnson et al. [128] and Wilkinson et al. [39] used pierced and grooved GDLs in order to improve the liquid water transport inside the GDL and the MEA. The location of these modifications is highly dependent on the operating conditions and design of the fuel cell. For example, at fully humidified conditions more perforations should be located near the outlet of the cathode flow field channels in order to enhance water removal. In fact, most of the water issues are usually near the outlet of the flow field plate; hence these grooves and perforations were located mostly around these areas.

Gerteisen et al. [129] used a Nd:YAG laser to make 80 µm diameter holes in a CFP. The location of these holes aligned with the serpentine flow field channel of the cathode plate. Although the active area was fairly small (1 cm^2), the MEA with the perforations presented less liquid water accumulation and oxygen transport limitations, which resulted in better water management and overall fuel cell performance. Recently, the same research group presented a similar study in which a 6-cell fuel cell stack (30.87 cm^2 active area) with perforations (or water transport channels) in the cathode GDLs (around 950 holes in each CFP) was tested at various operating conditions [130]. The perforations were placed 1 mm apart from each other and were aligned to the serpentine flow field of the cathode plate. It was observed that in comparison with a stack with normal CFPs, the perforations improved the water transport from the CL towards the FF plates. In addition, the modified stack presented a lower overpotential and higher stability in the high current density range. However, the size of the holes, distance between the holes, and location of the holes were not analyzed. In addition, this approach under dry conditions deteriorated cell performance because of the increased water removal and membrane dehydration.

Manahan et al. [131] used a ytterbium fiber laser to make 300 µm perforations in different CFPs with MPLs. They analyzed these GDLs in order to understand the effects of tailored internal structure of the CFP on the performance and transport characteristics of PEMFCs. Their results suggested that proper tailoring of the fuel cell GDL (e.g., perforation size, geometry, and location) has significant potential to reduce liquid water accumulation and improve the fuel cell performance.

Nishida et al. [132,133] used small grooves (200 µm wide) in a CFP in three different locations in a 5 cm^2 fuel cell. These grooves helped with the removal of liquid water, thus stabilizing the voltage output of the cell and reducing the water issues inside the GDL. However, no other sizes and shapes of grooves were analyzed, nor were other operating conditions investigated. Through a mathematical model, Lee et al. [134] analyzed the use of engineered pore paths (vertical and horizontal) in common CFPs in order to separate liquid transport paths from the gas-diffusion paths in order to improve PEMFC performance. It was concluded that using a combination of

vertical and horizontal engineered paths could reduce the average liquid saturation levels in typical CFP GDLs.

In general, there is only a limited amount of available data and published literature demonstrating these concepts regarding rationalized and engineered gas diffusion layers. It is evident that there is a need to study in more detail engineered GDLs that can improve fuel cell performance, especially at extreme operating conditions, and that can facilitate the modeling process and predictive capability due to their simplified nature.

1.4.2.1.5 Other materials

Other materials studied as gas diffusion layers can be found in the literature. Chen-Yang et al. [135] made GDLs for PEMFCs from carbon black and un-sintered PTFE, comprising PTFE powder resin in a colloidal dispersion. The fuel cell performance of this novel GDL was shown to be 0.25 V less (at 400 mA cm^{-2}) than the case with the CFP as GDL. However, because the manufacturing of these carbon black/PTFE GDLs is inexpensive, they can still be considered as potential candidates.

Gas diffusion layers have been developed that combine more than one type of material within them. For example, Koschany [136] proposed the use of layered GDLs made out of two materials, each with different gas permeabilities and manufactured one on top of the other. Normally, the materials with the lowest permeability were made either out of expanded graphite or metal, and the other materials were made out of carbon fibers. Another example of combining more than one material is the one published by Voss et al. [137], in which a new material called POLYMET® is described. This is a composite polymer with a porous three-dimensional polymeric structure metallized with a surface coating of different types of metals and alloys. The end result is a woven/felt-based material that can be used as a GDL in fuel cells and that helps to reduce the internal resistance of a PEMFC with a membrane. Campbell et al. [138] developed gas diffusion layers made out of glass fiber webs filled with carbon and PTFE particles. The same research group

later designed special GDLs made with different carbons claiming to improve the overall fluid diffusion towards the catalyst layer [139].

1.4.2.1.6 Performance comparison of different gas diffusion layers

Most of the studies in which the performances of more than one GDL are compared deal with CFP and CC GDLs. Publications in which other GDL materials are compared to conventional designs are scarce (please refer to Sections 1.4.2.1.3, 1.4.2.1.4 and 1.4.2.1.5). Therefore, performance comparison between conventional GDL materials (CFPs and CCs) will be emphasized in this section. Table 1.2 summarizes the most important studies that investigated the performance differences between carbon cloths and carbon fiber papers as cathode GDLs.

Ralph et al. [140] compared a CC (Zoltek PWB-3) and CFP (Toray TGP-090) as cathode GDLs, using a Ballard Mk 5 single PEMFC hardware at 100% relative humidity (RH) at 80 °C. It was observed that the carbon cloth demonstrated a distinct advantage over the CFP at current densities greater than 600 mA cm^{-2}, while at lower current densities both GDLs performed similarly. It was claimed that this was because the CC material enhanced mass transport properties and improved the water management within the cell due to its porosity and hydrophobicity.

Spernjak et al. [141] used a transparent fuel cell (the end plate was made out of polycarbonate) to visualize the water accumulation inside the flow field channels with different GDL materials. It was observed that at humidified conditions the CC (untreated – no PTFE – AvCarbon TM 1071 HCB) was able to perform and remove the water better than CFP (untreated – no PTFE – TGP-H-60). In fact, it was concluded that water was trapped inside the GDL when the CFP was used, resulting in the flooding of the catalyst layer. However, the performance of these two materials was not compared when they were coated with PTFE and additional MPLs.

Similar results were also reported by Moreira et al. [142] after testing a small single cell also with both CFP and CC as the GDLs. However, the difference between the performances of each GDL was not as large; in fact, the CFP did better at lower

current densities (due to lower ohmic losses). The difference in observation may be caused by the fact that these tests were performed with dry gases (i.e., no humidification) and at a lower cell temperature of 25°C. Williams et al. [143,144] performed an extensive analysis with different materials as GDLs over a wide range of humidity conditions. The CFP GDL (with an MPL) showed greater performance at low relative humidity conditions, while the more hydrophobic CC (E-TEK CC with MPL) was superior at saturated inlet conditions. Antolini et al. [145] had similar observations and experimental results.

Table 1.2 – Summary of the main studies comparing carbon cloth and carbon fiber paper as cathode GDLs.

Authors	Carbon Fiber Paper	Carbon Cloth	Observations
Ralph et al. [140]	TGP-090 (No PTFE content specified)	Panex PWB-3 (No PTFE content specified)	CC performs better at current densities greater than 600 mA cm^{-2}. At 1300 mA cm^{-2} the FC with a CC GDL had a voltage of ~0.57 V, compared to a voltage of ~0.35 V for the case with a CFP GDL
Spernjak et al. [141]	TGP-060 (0 wt% PTFE)	AvCarbon TM 1071 HCB (0 wt% PTFE)	It was observed with a transparent fuel cell that the CC removed more water than the CFP at fully humidified conditions.
Moreira et al. [142]	EC-TP1-060 ElectroChem. (30 wt% PTFE)	EC-CC1-060 ElectroChem. (30 wt% PTFE)	For dry gases (no humidification) and a cell temperature of 25 °C, CFP had better performance at low current densities due to less ohmic losses. CC had better performance at current densities greater than 500 mA cm^{-2}.
Williams et al. [143,144]	TGP-120 (No PTFE content specified) with MPL (13 wt% PTFE)	E-TEK V.2.11 (no PTFE content specified) with MPL	CFP had better performance at dry conditions (no humidification) than the CC since the ohmic resistance of CFP was between 10 to 30% lower than the CC. The CC showed better performance at saturated inlet conditions due to greater hydrophobicity.
Akyalçin et al. [146]	SGL Carbon 10BB (30 wt% PTFE)	Electrochem CC (30 wt% PTFE)	CC has a coarse fiber network that leads to the catalyst particles entering deeply into the CC, thus, causing high ohmic resistance due to poor contact with the CL.
Wilkinson et al. [39,128]	TGP-090 (20 wt% PTFE) with MPL (20 wt% PTFE)	Details not specified	Grooved CFP and half-CFP/half-CC as cathode GDLs presented the best performance at 100% RH. Grooved CFP improved water removal capability.

Through mathematical modeling based on experimental results, Wang et al. [147] were able to conclude that, at high humidity conditions, CC performs better than CFP because of the highly tortuous structure of the CFP, which leads to an increase in mass transport limitations under these conditions. In addition, the detachment of water droplets from the CFP smooth surface is difficult, thus increasing the amount of water film blocking the pores. On the other hand, at dry conditions, the CFP is able to retain water within the MEA and maintain the necessary hydration for the membrane.

Akyalçin et al. [146] were able to draw similar conclusions experimentally. They also concluded that CFP performs better at dry conditions since CC has a highly coarse fiber network, which leads to the active catalyst particles entering the pores of the CC, thus causing high ohmic resistance due to low contact with the CL. However, it is important to note that Frey et al. [148] stated that the carbon cloth, which is more flexible with a structure that does not change during pressing, had better electrical contact with the CL. On the other hand, due to its smooth surface, the CFP had less impact on the electrode surface, creating an inferior electrical contact with the CL.

In order to improve the performance of fuel cells, Wilkinson et al. [39,128] compared typical CFP cathode GDLs with modified GDLs (from CFP or CC) that improved the mass transport at high current densities (> 1000 mA cm^{-2}). Figure 1.16 shows the different GDLs that were used in order to improve the cell's performance. The grooves and perforations in the carbon fiber papers were located near the outlet region of the active area in order to increase the porosity and improve the water and oxygen transport (see Section 1.4.2.1.4). It can be seen that the grooved CFP enhances the water removal capability of the cell, thus, improving the oxygen transport and overall cell performance. Similar strategies can be implemented with other types of GDLs, such as metallic or engineered GDLs.

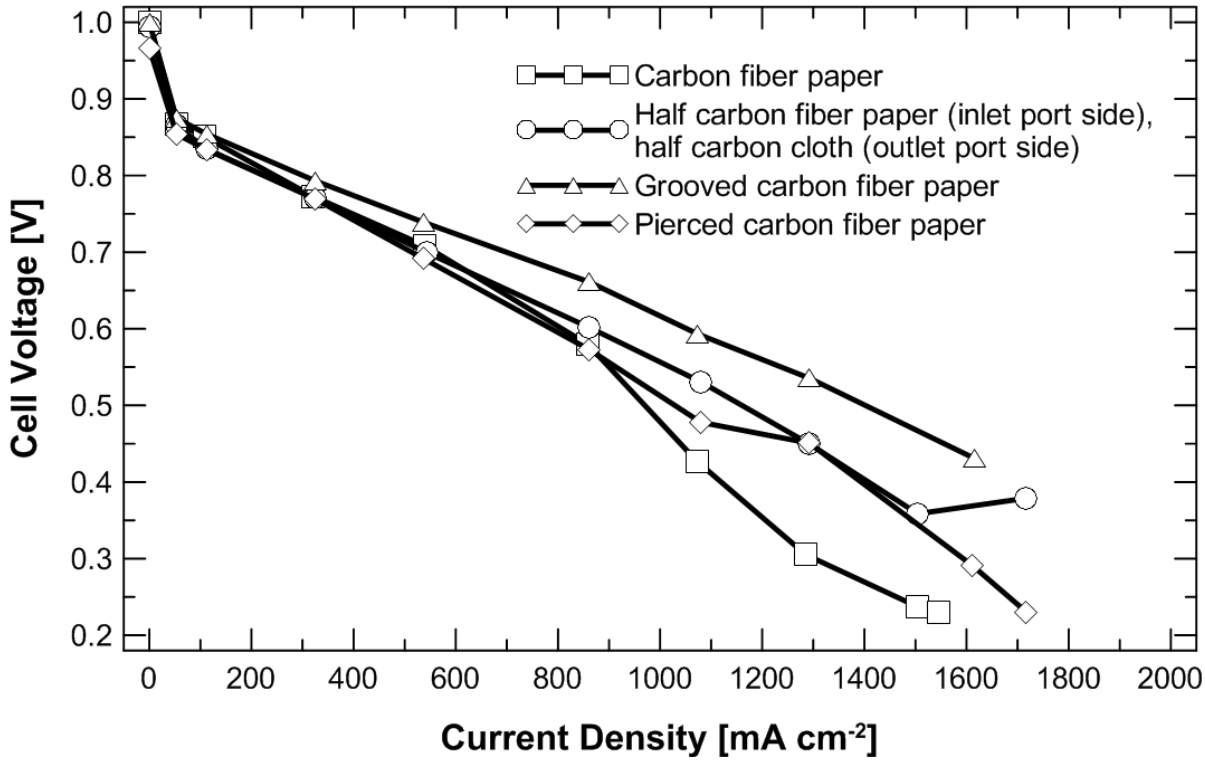

Figure 1.16 – Polarization curves showing the effect of modified diffusion layers (air/H_2, 2/1.5 stoichiometry, 3.1/3.1 bara, 100/100% relative humidity, 80°C). (Modified from Wilkinson et al. [39] with permission from Elsevier).

Most of these mentioned studies concentrated on the cathode side of the PEMFC because it has been shown that the difference between materials on the anode side does not represent a major performance loss due to flooding at high- or low-humidity conditions [149]. Therefore, the type of GDL used on the anode side does not result in major performance differences over a wide range of operating conditions.

1.4.2.2 Surface treatments and coatings

After the diffusion materials are fabricated, a number of post-treatments and coatings are still necessary in order to tailor the final properties of these materials based on the specific fuel cell application and the associated operating conditions. The following sections explain in detail the different treatments that are normally used on gas diffusion layers for fuel cells. Brief examples showing how these treatments change the performance of the GDLs will also be discussed.

1.4.2.2.1 Hydrophobic treatments

Gas diffusion layers used in PEMFCs are normally treated with a hydrophobic agent such as polytetrafluoroethylene (PTFE) or fluoroethylenepropylene (FEP). The most typical method is to dip the material into a solution of PTFE and then sinter it. This treatment increases the hydrophobicity of the materials since most of the CFPs and CCs are not hydrophobic enough after fabrication. An important goal for coating the GDL with these agents is to coat the whole material (including the fibers), rather than just the top surface of the sheet. For cathode GDLs, this coating is extremely important because most of the water produced and accumulated inside the cell exits through the cathode side. For the anode GDL, this coating is not as critical but still important (especially when dealing with back diffusion of water) and it can provide some structural strength to the GDL.

The most common loadings of PTFE and FEP are from 5 to 30 wt% PTFE. Park et al. [150] concluded that high levels of PTFE content (> 30 wt%) decreased the gas permeability and porosity of CFPs (TGP-H-060 and TGP-H-090). They also showed that a CFP (TGP-H-060) with 15 wt% PTFE had the best performance with relatively dry conditions compared to a thicker paper with the same hydrophobic content.

Lin et al. [43] did an extensive study on the effect of the PTFE content on the performance of Toray and SGL Carbon Sigracet® carbon fiber papers. It was observed that increasing the hydrophobicity of the GDL enhanced both the gas and water transport when the fuel cell operated with high levels of humidity. However, excessive amounts of PTFE reduced the amount of hydrophilic pores, thus deteriorating the water flow out of the catalyst layer and the GDL. Velayutam et al. [151] used carbon fiber papers (Avcarb P50) with different PTFE contents (from 7 to 30 wt%) and with a microporous layer (MPL) having 20 wt% PTFE (the hydrophobic content of the MPL was not changed). It was observed that when the cell was operated at 55°C and ambient pressure conditions, the GDL with 23 wt% PTFE performed very well in both the low and high current density regions (see Figure 1.17). In addition, it was shown that the performance of the GDLs improves at first when increasing the content of PTFE but once a maximum point is reached the performance decreases rapidly.

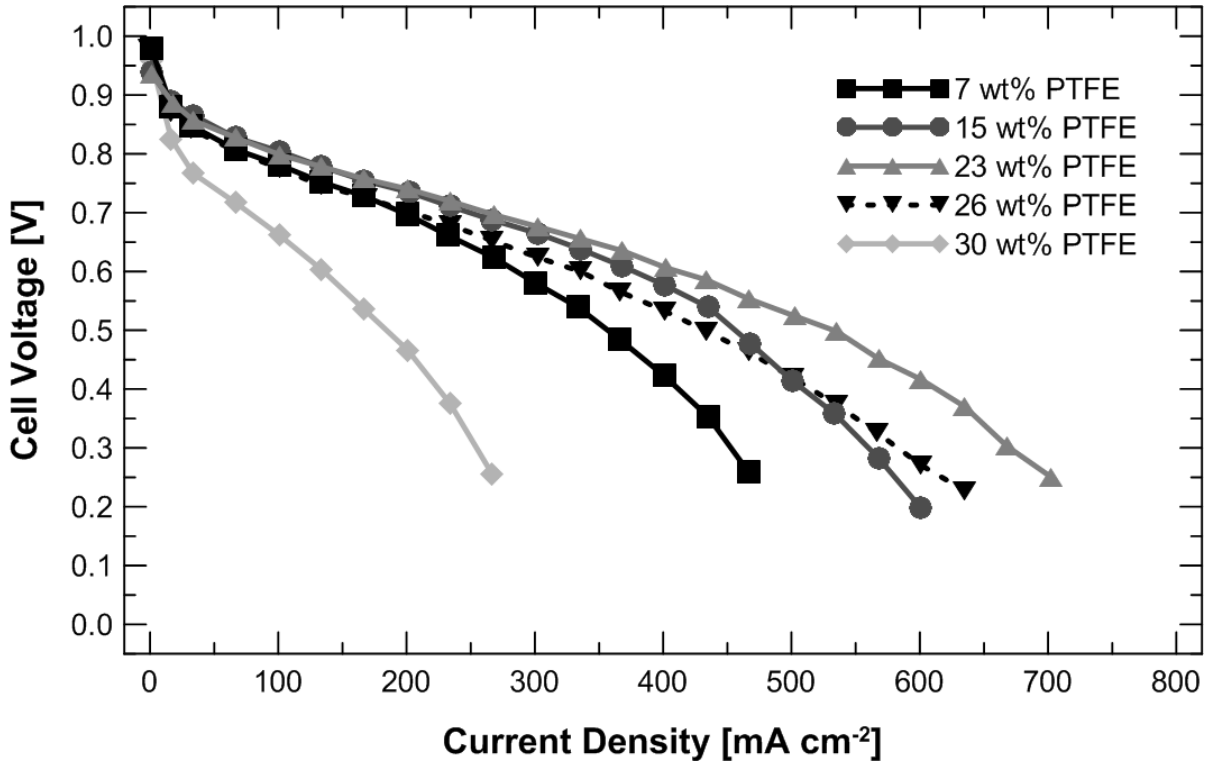

Figure 1.17 – Effect of PTFE in the GDL of PEM fuel cells. Operating Conditions: fuel cell temperature of 55ºC; anode and cathode dew point temperatures of 65/40ºC; hydrogen and air stoichiometries of 1.5/2.5; ambient pressure for air and hydrogen; serpentine flow field for anode and cathode. Anode GDL was an AvCarb P50 CFP (PTFE content not specified); cathode GDL was an AvCarb P50 CFP. Electrodes were fabricated using 20% Pt/C. Anode catalyst loading of 0.25 mg Pt cm^{-2} and 0.5 mg cm^{-2} of Nafion® (5% solution); cathode catalyst loading of 0.50 mg Pt cm^{-2} and 1.0 mg cm^{-2} of Nafion® (5% solution). Type of membrane not specified (Modified from Velayutam et al. [151] with permission from John Wiley & Sons, Inc.).

Tüber et al. [152] used a transparent PEM fuel cell in order to visualize the water accumulation inside the flow field channels and on the surface of different GDLs while operating the fuel cell at room temperature. In the case of the hydrophobic CFP (TGP-H-090 with 25 wt% PTFE), it was observed that the water appeared randomly distributed along the flow channels. The water produced at the cathode side seemed unable to penetrate the CFP until enough pressure was generated and then small droplets were formed on the surface of the GDL. Similar observations where presented by Spernjak et al. [141], who also developed a transparent fuel cell to visualize the different behavior of treated and untreated GDLs. This transparent cell indicated that with treated GDLs the water produced at the cathode side emerges as droplets on the surface of the material over the entire visible area. With

the untreated GDLs, water preferred to be in contact with the side walls of the channels, and the water formed films and slugs near the channel walls. This behavior caused greater water management issues and lower gas transport towards the active areas.

The PTFE content in a GDL also affects thermal conductivity. Usually, the thermal conductivity decreases with increasing PTFE percentage in the GDL [153]. However, the electrical conductivity of these materials stays relatively constant at various PTFE loadings because the structure of the carbon fibers that are part of the overall paper do not change with the addition of the PTFE [154].

Although in most cases it is necessary to have an even coat of the hydrophobic layer within the gas diffusion layer, sometimes it is desirable to have different regions within the surfaces that are more (or less) hydrophobic than others in order to create gradients within the active area [39]. Mathias et al. [86] developed a PTFE-gradient process in which the PTFE-coated GDLs are placed over a vacuum fixture. Then, the outer substrate surface (the one away from the draw) undergoes a grinding step while still exposed to the vacuum draw. The grinding produces a PTFE dust that is pulled through the substrate by the vacuum draw, creating high and low hydrophobic particle density regions within the GDL.

1.4.2.2.2 Hydrophilic treatments

Although, hydrophilic properties in GDLs may also be desired when dealing with specific conditions (such as dry conditions), the amount of work found in the literature regarding these treatments in GDLs is very limited.

Tüber et al. [152] used a transparent fuel cell at 30ºC in order to visualize both hydrophobic and hydrophilic gas diffusion layers. They discussed the idea of hydrophilizing a CFP with sodium dodecyl sulphate (SDS) to absorb and distribute the product water inside the GDL, thus preventing the water clogging of gas channels. A fuel cell was operated at a constant voltage of 0.5 V with three different GDLs: a standard, hydrophobic and hydrophilic CFP. It was observed that in all

three cases the current density decreased at the beginning of the tests; however, the hydrophilic GDL outperformed the others because the current drop was not as sudden as with the two hydrophobic GDLs. This result was attributed to the homogenous distribution of water inside the GDL as a result of the hydrophilic coating.

Campbell et al. [155] found that the catalyst utilization in the electrode and fuel cell performance could be improved by making the carbon-supported catalyst hydrophilic. This was done by treating the carbon-supported catalyst with a suitable acid such as nitric acid in order to introduce surface oxide groups on the carbon. In principle, this same approach could be applied to the carbon components of the GDL and MPL. Jung et al. [156] added SiO_2 particles, which are hydrophilic, to the catalyst layer of both the anode and cathode in order to improve the cell's performance at low relative humidities. This hydrophilic coating could also be applied to the GDL (or MPL) instead.

1.4.2.2.3 Microporous layers

A layer of carbon black and hydrophobic agent (e.g., PTFE) is usually deposited on top of one of the GDL surfaces (forming a diffusion double-layer) as shown in Figure 1.18. As is seen in this figure, the MPL is a dense layer with small pores. In fact, this catalyst backing layer or MPL forms smaller pores than the GDL (20 to 200 nm pores for MPLs [157] and 0.05 to 100 μm pores for typical CFP DLs [158,159]). This layer also acts as another mechanism to reject water, which is critical especially when the fuel cell is operated at high humidity levels [158]. The MPL also provides support for the catalyst layer, which is located either on top of it or on the surface of the proton exchange membrane. The catalyst layer usually consists of either carbon supported catalyst or catalyst black mixed with either PTFE and/or proton conducting ionomer (e.g., Nafion® ionomer). Since the sizes of the pores in a typical GDL are in the range of 0.05 to 100 μm and the average pore size of the catalyst layer is just a few hundred nanometers, the risk of having low electrical contact between both layers is high [157]. MPLs improve the electrical contact and also help to prevent catalyst particle loss and clogging of the GDL pores with catalyst particles

[115,144,160,161]. Various research groups have been able to demonstrate that the best PTFE loading in the MPL is around 20 wt% when operating a fuel cell at fairly high humidity conditions [151,162-165].

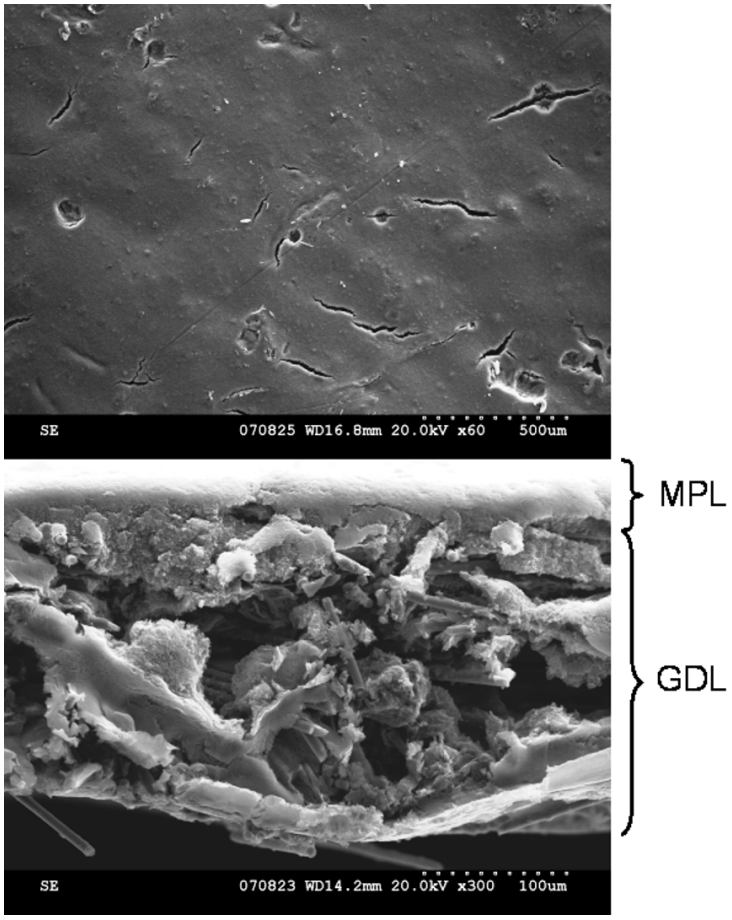

Figure 1.18 – Scanning electron microscope micrographs of SGL Carbon GDL 25 BC (CFP with MPL): (a) Top-view of the MPL (reference bar indicates 500 μm); (b) Cross-section of the GDL with MPL on top (reference bar indicates 100 μm).

The MPL can also be made out of a carbon based polymer porous sheet that is simply placed between the CL and GDL when assembling the fuel cell [157,166-168]. The sheet-based MPL approach is not as common and is not widely used. In fact, in previous years a commercial based MPL film was available (Carbel® MP, W.L. Gore & Associates, Inc.). Shi et al. [166] prepared an MPL sheet using a two-roll-shaft roller to roll a mixture of carbon black and PTFE repeatedly. Once the desired toughness in the film was achieved, it was sintered. This MPL sheet performed well, especially under high humidification conditions.

Microporous layers are now commonly used in order to improve the overall performance of a fuel cell at both fully humidified and low humidity conditions [43,151]. It is believed that they play a key role in the overall water management within the fuel cell. However, it is still unclear exactly how the MPL affects the water transport mechanism inside the GDL and the MEA. Some of the different studies on the effect of cathode MPLs are now discussed.

Passalacqua et al. [169] were able to show that with an MPL the performance of the cell improves substantially. They concluded that the MPL reduced the size of the water droplets, thus enhancing the oxygen diffusion. This layer also prevented the catalyst particles from penetrating into the GDL. Park et al. [150] also concluded that with the addition of an MPL both the water management and electrical conductivity improved.

Similar observations were also presented by Song et al. [170] and Holmstrom et al. [149], especially when investigating the fuel cell's performance at high current densities. GDLs without an MPL on the cathode side lead to major mass transport losses at high humidity conditions due to water flooding. The losses were between 60 to 100 mV at 1000 mA cm^2 [149]. The MPL has also been shown to effectively improve the start-up performance of a PEMFC by suppressing water accumulation at the electrode, which is important especially when dealing with sub-zero conditions [171].

MPLs have also been studied in order to understand how they can affect other aspects of the fuel cell performance. Mirzazadeh et al. [172] used a three-electrode electrochemical cell in order to study the oxygen reduction reaction (ORR) and determine whether this was the main parameter that improved the overall performance of the cell. From the experiments, it was concluded that the use of the MPL improves performance at high current densities, but at low current densities a GDL without MPL shows better performance. Williams et al. [173] observed that a GDL without MPL had a higher limiting current density compared to a GDL with MPL. However, the MPL was considered to still be critical since it improves the

current collection and reduces resistance. None of these studies provide an explanation or mechanism of how the MPL actually helps fuel cell performance.

After testing a number of GDLs with and without MPLs, Lin et al. [43] postulated that the MPL seemed to push more liquid water back to the anode through the membrane. Basically, the small hydrophobic pores in the MPL result in low liquid water permeability and reduce the water transport from the catalyst layer towards the GDL. Therefore, more water accumulated in the CL is forced towards the anode (back-diffusion). This reduces the amount of water that is removed through the cathode GDL, decreases the number of blocked pores within the cathode gas diffusion layer, and improves the overall gas transport from the GDL towards the active zones. One drawback of using the MPL is that the water saturation in the catalyst layer increases and causes more flooding [43].

One contradictory point regarding how the MPL works is related to the water saturation in the catalyst layer of the cathode side. Nam et al. [174] stated that by using a microporous layer near the CL, the water condensed in the GDL cannot enter the CL, thus reducing the overall saturation of the active catalyst zones. This idea was also presented by Pasaogullari et al. [175] in which they concluded that in the presence of an MPL the liquid saturation in the catalyst layer is reduced substantially. Kitahara et al. [176] demonstrated that the MPL reduced water content in the catalyst layer and increased water accumulation inside the GDL area closest to the flow field channels. These concepts contradict those presented earlier since it is not clear whether the liquid saturation does in fact increase in the cathode catalyst layer or not. This may depend directly on the rate at which the water goes back (or is forced) to the anode.

Through neutron radiography imaging, Owejan et al. [177] were able to observe that MEAs that had cathode GDLs with MPLs had better distribution of water over the active area at high current densities. GDLs without MPLs tended to have more water accumulated in one location of the active area (closer to the outlet). One issue with this work was that the water accumulation observed was for the entire MEA and the water quantities were not separated between the anode and cathode sides. Lu et al.

[178] have shown that in GDLs with an MPL the water paths inside the CFP are not interconnected due to the blocking effect of the MPL, which reduces the water saturation inside the GDL and the amount of water breakthrough in the GDL/flow field interface. On the other hand, inside CFPs without MPLs, the water paths are interconnected to each other causing a larger number of water breakthrough points at the GDL/flow field interface, causing flooding in the flow field channels. Similarly, Nam et al. [179] proposed that the MPL reduces the number of liquid water breakthrough paths towards the GDL, which decreases the liquid water saturation in the GDL and enhances the overall oxygen diffusion. In addition, they concluded that the MPL reduces the size and saturation level of interfacial water droplets formed in the catalyst layer, which increases the oxygen diffusion rate into the catalytic sites and enhances the electrochemical reactions.

Through the use of a transparent fuel cell, Spernjak et al. [141] were able to visualize the anode flow field plate (and GDL without MPL) while operating the fuel cell with different CFPs (with and without MPLs) as cathode GDLs. It was observed that liquid water was present in the anode flow field only when an MPL on the cathode side was used. Again, this is an indication that the cathode side creates a pressure barrier that pushes the water towards the anode. These observations agree with the ones presented mathematically by Weber et al. [180]. Although they did not report any experimental work, their two-phase fuel cell model concluded that the MPL acts as a valve that pushes water away form the cathode GDL towards the anode though the membrane. Pasaogullari et al. [181] also presented a two-phase fuel cell model in which the effect of the MPL was studied. They concluded that the water flux towards the anode is enhanced when the following MPL characteristics are used: smaller pore size, lower porosity, larger thickness, and higher hydrophobicity. Kim et al. [182] studied the MPL through electrochemical impedance spectroscopy (EIS) experiments and water transport coefficient measurements. It was concluded that the MPL reduced mass transport losses and increased the oxygen diffusion in the catalyst layer. In addition, the MPL increased the water flux from cathode to anode compared to the case without MPL.

To shed some light on the water transport mechanisms when MPLs are used, Atiyeh et al. [46,183-185] presented an experimental method designed to investigate the net water drag coefficient in order to have a better indication of the amount of water flowing from the cathode to the anode. They observed that the performance of the fuel cell improved when the anode, the cathode, or both, had microporous layers. However, after implementing the water balance measurements, they were not able to observe a significant difference on the net water drag coefficient for a fuel cell with a cathode MPL and an anode without an MPL, compared to a cell without any MPLs. It is important to note that they were able to observe that the MPL does in fact improve the fuel cell performance and cell voltage stability when operating at constant conditions (i.e., the voltage fluctuations are significantly reduced when the cathode GDL has an MPL). The results related to the net water coefficient do not correlate with the observations presented previously, thus, more experimental work is necessary in order to investigate the processes behind how the MPL helps the performance of the fuel cell.

Recently, Owejan et al. [186] performed *in-situ* and *ex-situ* tests in order to elucidate which water transport mechanism (vapor or liquid) dominates inside a fuel cell when MPLs are used. It was observed that thermal and vapor concentration gradients across the GDL are enough to remove product water in the vapor phase, even at high current densities. The MPL liquid water permeability properties were found to have an insignificant effect on mass transport losses because the thermal properties of the GDL had a key role in creating a temperature gradient that pushes the water vapor from the catalyst layer. It was proposed that the MPL acts as a barrier that prevents condensed liquid water, accumulated in the larger pores of the CFP, from diffusing back to the catalyst layer and forming liquid water films. The effects of water crossover from the cathode to the anode side when a cathode MPL is used were not studied.

Figure 1.19 summarizes some of the roles that the MPL plays in order to improve fuel cell performance. Although several studies and theories have emerged in order to explain how the MPL improves fuel cell performance, there are still doubts and

questions on how specifically the MPL changes the gas and water transport mechanisms inside a fuel cell.

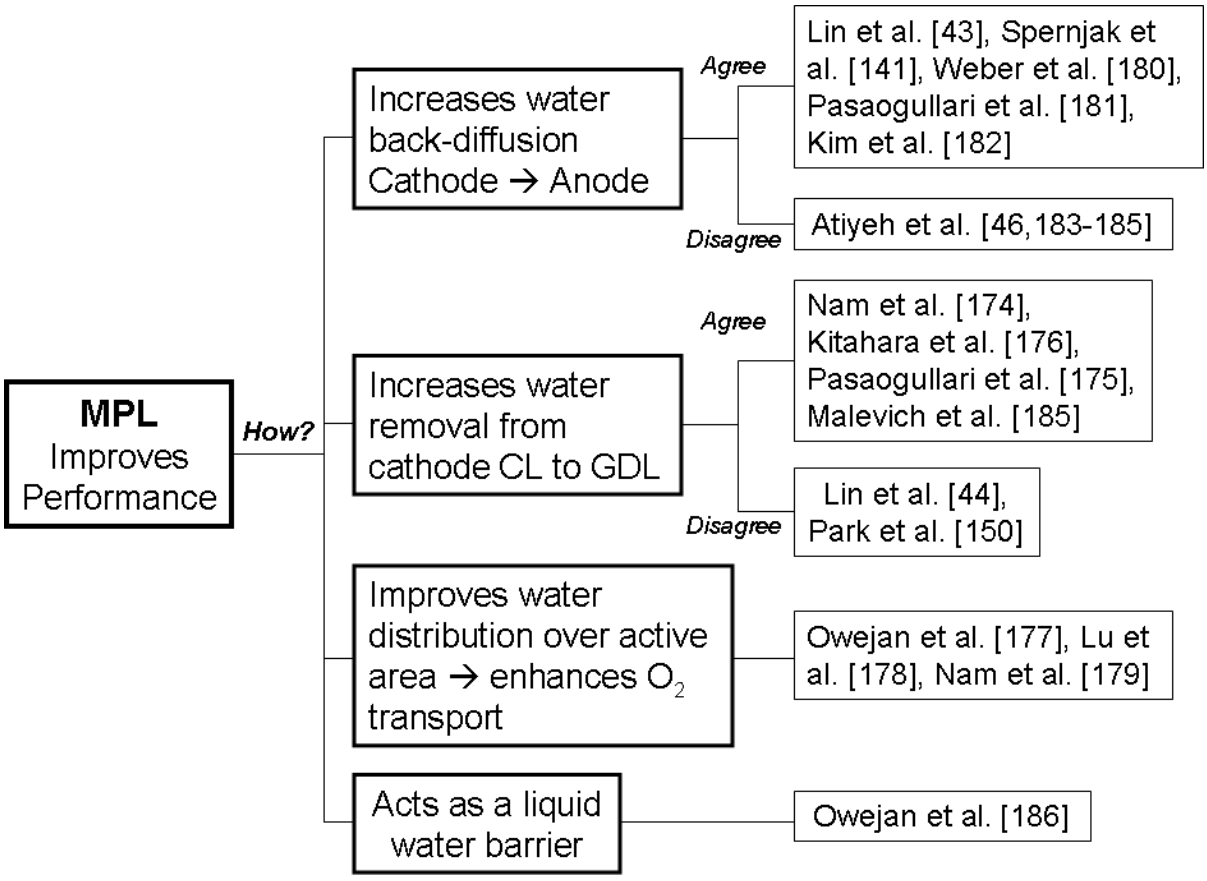

Figure 1.19 – Summary of the different studies regarding the cathode MPL mechanisms to improve fuel cell performance.

All the previous studies discussed the influence of the cathode MPL; however, very limited results can be found in the literature regarding the influence of the anode MPL. Kitahara et al. [187] observed that the small pores in a anode MPL-coated GDL reduce the amount of water transport, resulting in lower PEFC performance. Owejan et al. [186] concluded with polarization data that the influence of the anode MPL in performance was insignificant, however, under dry conditions and high current densities (>2000 mA cm^{-2}) a slight increase in performance was observed without the anode MPL. Similar observations were also given by Kim et al. [182].

1.5 Research objectives and thesis layout

Based on the literature review presented in Sections 1.4.1 and 1.4.2 a number of areas were identified that needed further exploration. The common theme for these areas is water management in PEM fuel cells and how it affects the cell performance. Thus, the goals of this work are to understand in more detail water management related issues in proton exchange membrane fuel cells (PEMFC) and to design methods that can reduce the negative effects of these issues. One specific aspect of this research was the use of perforated sheets as a water barrier layer, a diagnostic tool, and as an engineered gas diffusion layer.

One of the areas chosen as part of this work was fuel cell operation at low to no gas humidification conditions. Ultimately, the need for humidification systems in fuel cell systems should be eliminated in order to simplify the fuel cell system and to reduce operational costs and space. However, there are irreversible losses in fuel cells due to exposure to low humidity to dry conditions (see Section 1.4.1.2.1). Therefore, a component of this research is to investigate the improvement of PEM fuel cell performance and durability with the use of liquid water barrier layers. In order to achieve this, it is necessary to understand how the performance of a PEM fuel cell deteriorates at dry or low humidity conditions and how different water barrier layers affect the performance and durability of the fuel cell. Chapter 3 shows that adding a non-porous material (such as stainless steel) with perforations between the cathode flow field plate and the gas diffusion layer (GDL) improves the water saturation in the cathode GDL and catalyst layer, increases the water content in the anode, and keeps the membrane hydrated.

As discussed in Section 1.4.2.2.3, microporous layers (MPL) have been widely used to improve fuel cell performance and water management capabilities inside fuel cells. However, much is still unknown regarding how the MPL affects both gas and liquid transport mechanisms depending on the operating conditions. Therefore, in this work the gas and liquid interplay inside fuel cells is analyzed and further clarification of the role of the microporous layer on the cathode and anode sides of the fuel cell is given. In order to reach this goal, different experimental approaches were used to study oxygen diffusion resistances and the liquid water effect on mass

transport losses. In addition, perforated sheets were used as a diagnostic tool to understand how the liquid water transport mechanism changes with different GDLs (with and without MPLs). Chapter 4 describes in detail each experimental approach and how the perforated sheets are used as a diagnostic tool since they exacerbate the mass transfer resistance and liquid water blockage inside the cell analogous to the MPL. This approach sheds some light on the complex interaction between gas and liquid transport mechanisms. Conclusions are offered about the role of the cathode MPL along with a simple analysis of the influence of having an anode MPL.

The use of structured or engineered materials in fuel cells, offers the possibility of tailoring their parameters and characteristics to match the needs of specific fuel cell applications and operating conditions (see Section 1.4.2.1.4). In order to look into benefits and issues of using these engineered materials, this work investigates the use of perforated sheets (without the addition of carbon fiber papers or carbon cloths) as gas diffusion layers in PEM fuel cells. Chapter 5 discusses the use of these structured GDLs for different operating conditions. Sheets with different thickness, open area, and in-plane diffusion capabilities are also analyzed. Particular attention is given to the mass transport losses and in-plane diffusion of these engineered GDLs.

The last area of research identified was related to the improvement of voltage stability (and water removal) at low current densities (and power densities). As stated in Section 1.4.1.2.3, a number of flow field designs have been used in the fuel cell industry and one common issue is the ineffective removal of liquid water at low flow rates. Currently, fuel cells are designed around their peak power density; thus, cathode flow channels perform effectively at such conditions. However, these flow fields have issues when flow rates are significantly lower (i.e., at low power). Therefore, it was recognized that it is important to develop a flow field capable of improving voltage stability at low power densities but also with good performance at peak power levels. Chapter 6 describes the design and development of a new approach of changing the flow field active area within a cell with changing operating conditions. Experimental results show that the voltage instability and water management issues that occur in a fuel cell, particularly at low power levels, can be

removed by changing the effective active area inside the fuel cell. This method is also shown to work in a fuel cell stack.

Chapter 7 summarizes the work of this thesis and recommends future studies that can be developed based on the findings and conclusions of this research.

All the *ex-situ* and *in-situ* experimental methods and apparatus used in each of the mentioned chapters are described in Chapter 2. This includes the different materials used in the membrane electrode assembly (MEA), all the fuel cells tested, *ex-situ* experimental setups, and *in-situ* fuel cell testing setups. In addition, all the protocols followed for MEA and fuel cell assembly/testing, and for all the experiments are explained in detail.

Figure 1.20 summarizes the thesis layout and structure.

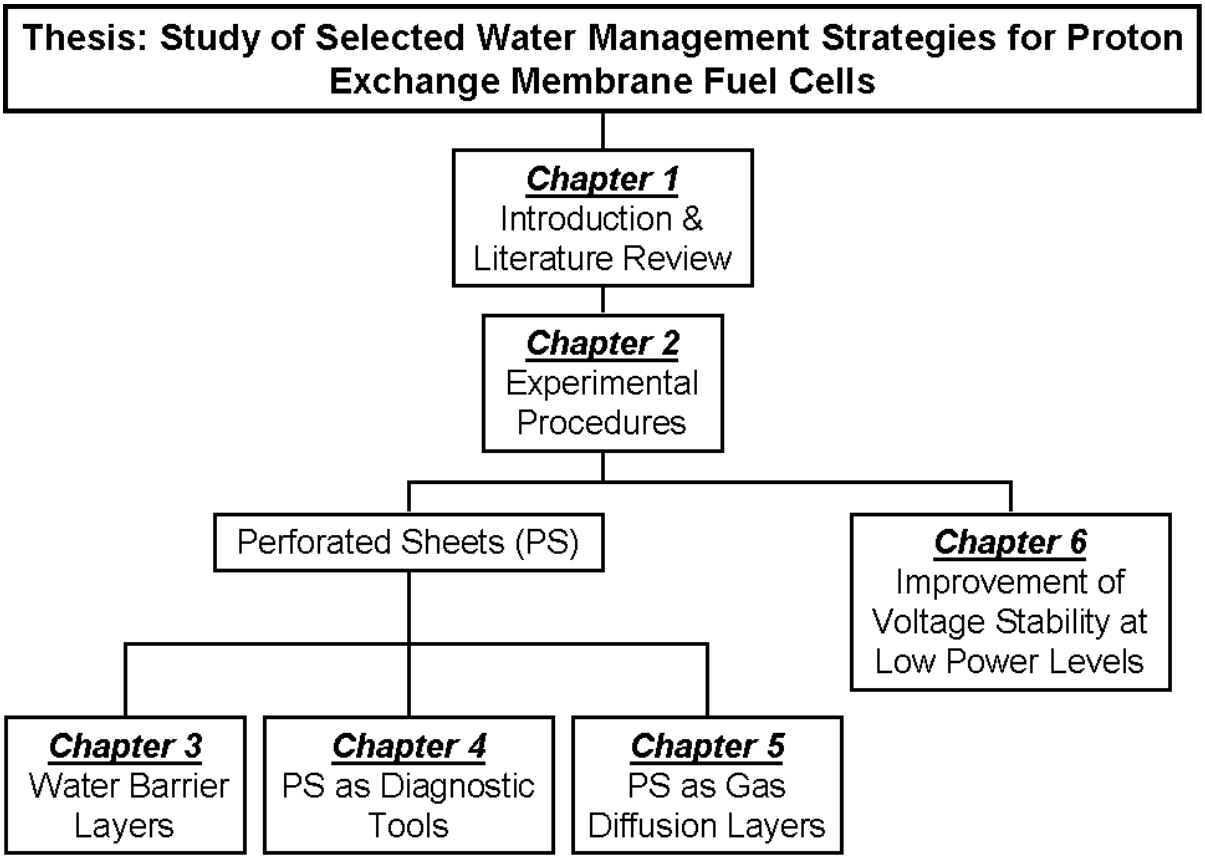

Figure 1.20 – Thesis layout.

2 EXPERIMENTAL PROCEDURES[2]

In order to produce reliable and reproducible data it is critical to follow a strict set of standards and testing protocols. Two types of PEM fuel cell (and corresponding test stations) were used for most of the work presented here; therefore, this chapter is divided into two main sections, each related to the type of fuel cell used. Both sections describe in detail the materials and equipment used for all the performed experiments. In addition, a brief explanation of each experiment (and the subsequent steps followed) is described.

2.1 49 cm^2 fuel cell

The following sections describe in details the 49 cm^2 fuel cell, materials, and equipment used for the work presented in Chapters 3, 4, and 5. The experimental explanations and protocols are also discussed.

2.1.1 Materials

2.1.1.1 Hardware

Figure 2.1 shows a picture of the fuel cell used. The cell used a pneumatic piston, located on top of all the components, for compression in order to distribute the pressure evenly across the cell. Compressed nitrogen gas was used to push the piston. Uniform compression was confirmed with the use of a pressure sensitive film (Pressurex, super-low, Sensor Products Inc.). All the inlet and outlet lines of the reactant gases were connected to the manifold, located at the bottom of the cell. De-ionized (DI) water was used as a coolant in order to maintain the temperature (and heat) of the cell constant. Thermocouples were inserted inside the cell, in the bottom

[2] Sections of this work have been published in:
Blanco M, Wilkinson DP, Wang H. Application of water barrier layers in a proton exchange membrane fuel cell for improved water management at low humidity operating conditions. International Journal of Hydrogen Energy 2011;36:3635-48.
Blanco M, Wilkinson DP, Wang H, Liu SZS. Engineered gas diffusion layers for proton exchange membrane fuel cells. ECS Transactions 2009;25:1507-18.
Blanco M, Wilkinson DP, Yan G, Zhao H, Wang H. Flow control in a fuel cell flow field for improved performance and reliability. ECS Transactions 2006:1:355-66.
Wilkinson DP, Blanco M, Zhao H, Wu J, Wang H. Dynamic flow field for fuel cells. Electrochemistry and Solid State Letters 2007;10:B155-60.

end plate, to monitor the temperature of the reactant gases (inlet and outlet) and coolant DI water (inlet and outlet), as well as the overall temperature of the fuel cell.

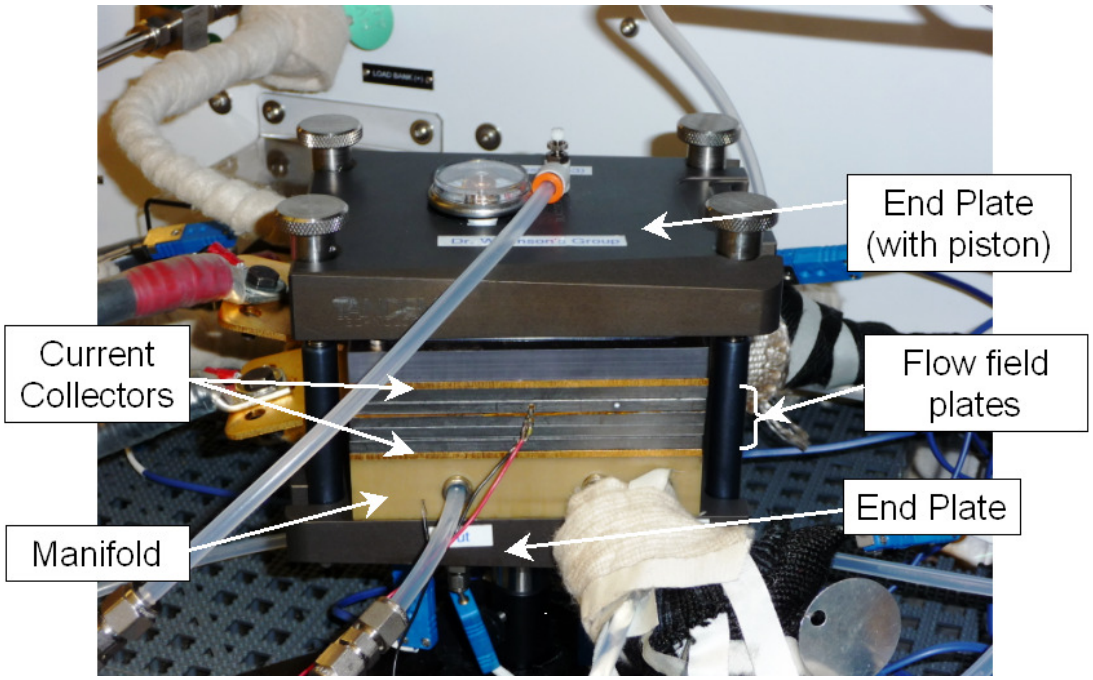

Figure 2.1 – Picture of the 49 cm^2 fuel cell used in fuel cell testing.

For the anode and cathode flow field plates, both had single path serpentine flow fields with an active area of 49 cm^2. These plates were made out of graphite (Tandem Technologies, Vancouver, Canada). Table 2.1 shows the details of both anode and cathode flow field channels. Both flow field plates had Silicone JRTV (Dow Corning) gaskets for sealing. Figure 2.2 shows these two flow field plates.

Table 2.1 – Properties of the anode and cathode flow field channels used in the 49 cm^2 fuel cell.

Properties	Anode Flow Field Plate	Cathode Flow Field Plate
Flow field type	Serpentine	Serpentine
Number of channel paths	1	1
Number of channel bends	27	27
Cross-sectional shape	Trapezoidal	Trapezoidal
Channel width – bottom [mm]	1.00	0.89
Channel width – top [mm]	1.27	1.57
Draft angle[a]	15°	15°
Channel depth [mm]	0.51	1.27
Landing width [mm]	1.17	0.86

[a]Draft angle is the angle that the channel walls make with vertical.

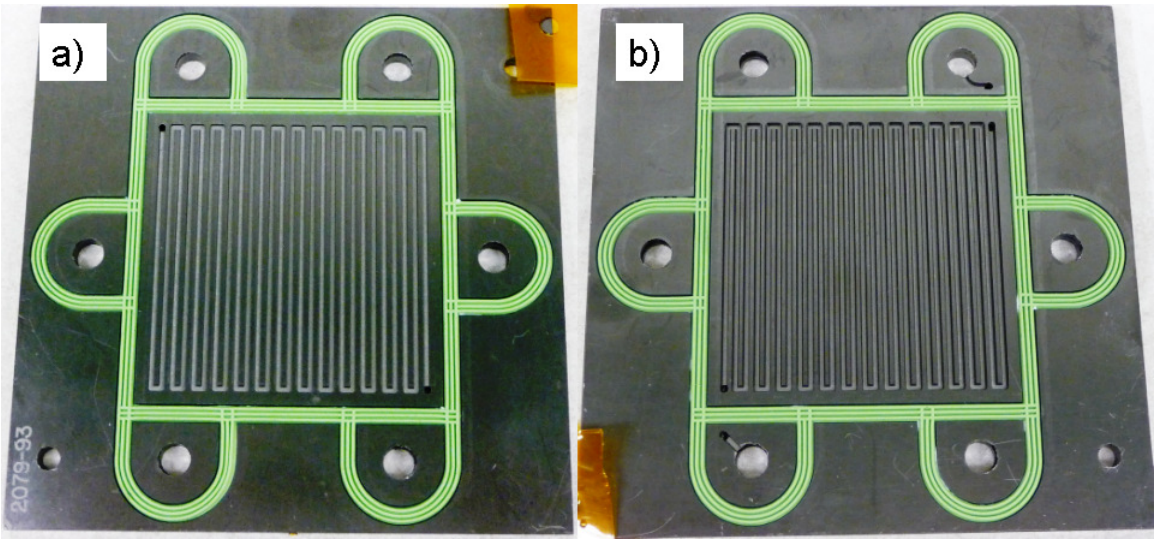

Figure 2.2 – Picture of the (a) anode and (b) cathode serpentine flow field plates (with gaskets) used for fuel cell testing. The active area of the plates is 49 cm^2.

Both flow field channels were used in a co-flow configuration for all of the tests performed, unless specified otherwise. However, this cell is designed in a way that cross- or counter- flow configurations can also be used if necessary. Figure 1.8 compares the performance of the three flow field configurations possible with the single cell hardware used in this work. Co-flow configuration was chosen since it allowed for an easier understanding of the gradient effects over the active area. In addition, this configuration increases dehydration when gases with low humidity are used [188]. This is particularly important for the dry and low humidity gas study described in Chapter 3.

2.1.1.2 Membrane electrode assembly

The membranes used were Primea® 5510 50 µm thick catalyst coated membranes (CCM) from W.L. Gore & Associates with a 0.4 mg cm^{-2} Pt catalyst loading for both the anode and cathode catalyst layers. The thickness of the membrane by itself was approximately 25 µm. Saint-Gobain K250 polyimide films (25 µm thick), with silicon adhesive on one side, were used as sub-gaskets to protect the edges of the membranes. The membrane was cut slightly larger than the active area in order to attach the polyimide films to the CCM and function properly as gaskets. The gas

diffusion layers (GDL) were then aligned to this CCM when assembling the fuel cell. Figure 2.3 shows a picture of a typical membrane electrode assembly with the polyimide films. For more details on how the MEA was assembled please refer to Appendix B.

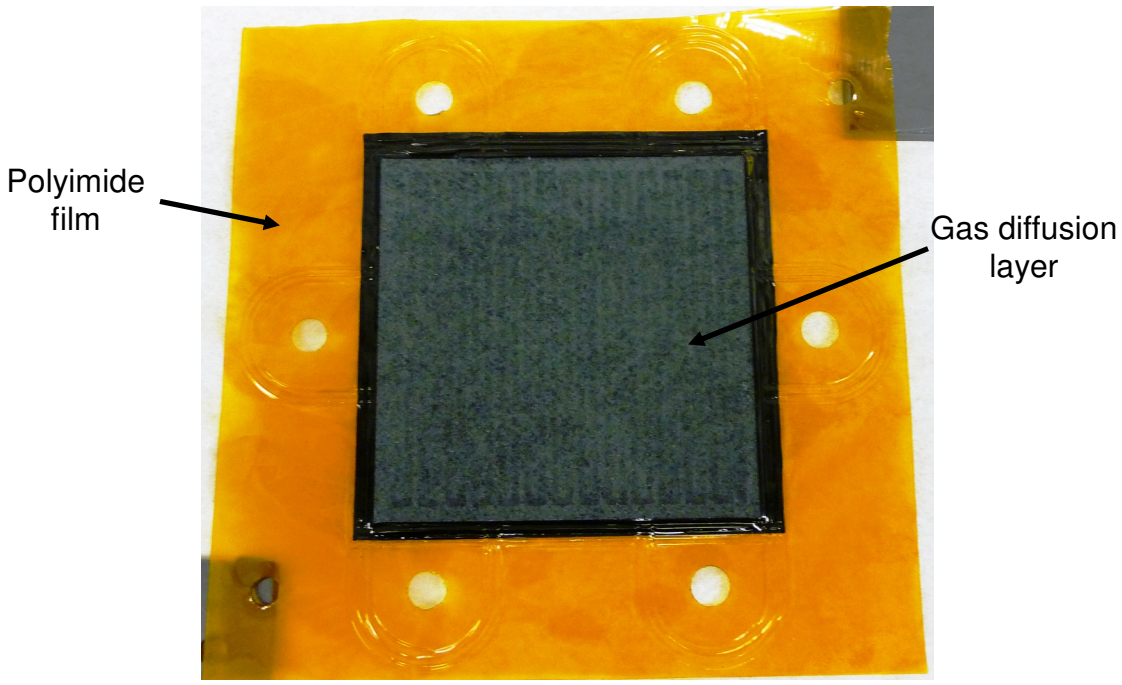

Figure 2.3 – Picture of a typical 49 cm^2 membrane electrode assembly with the polyimide sub-gaskets.

2.1.1.3 Gas diffusion layers

A number of GDLs were used for the different components of this work. Most of the materials tested were carbon fiber papers (CFPs). For the anode side, the GDL that was mainly used was the Sigracet® 25DC GDL from SGL Carbon. Table 2.2 summarizes the details of the materials used as GDLs.

For Chapters 3, 4, and 5, the baseline MEAs used the 25DC and 25BC GDLs for the anode side and cathode sides, respectively. Although the cell performance improved by 14 mV (at 1000 mA cm^{-2}, 75°C for the cell and gases, and 100% relative humidity) when the anode GDL was 25BC, the CFP with higher PTFE content was used in order to limit the water accumulation on this side of the fuel cell. The influence of the microporous layer on the anode side is discussed in Chapter 4.

Table 2.2 – Properties of gas diffusion layers used for fuel cell tests.

Material	Thickness [µm]	Porosity [%]	PTFE Content [wt. %]	Description
Sigracet® 25DC GDL (Anode)	235	80	20	CFP with MPL (23 wt. % PTFE)
Sigracet® 25DA GDL (Anode)	213	86	20	CFP without MPL
Sigracet® 25BC GDL (Anode and Cathode)	235	80	5	CFP with MPL (23 wt. % PTFE)
Sigracet® 25BA GDL (Cathode)	190	88	5	CFP without MPL
Toray® TGPH-030	110	80	20	CFP without MPL

2.1.1.4 Perforated sheets

For Chapters 3, 4, and 5 different perforated metal sheets were used for various purposes. These stainless steel 316L sheets were perforated by VACCO Industries (California, USA) using a photo-etching process. The sheets were not treated with any hydrophobic agent and their initial contact angle before testing was found to be approximately 78°, i.e., hydrophilic especially in their landing areas (i.e., space between holes). Firstly, sheets with different perforation diameters of 10 mm, 1 mm, 0.5 mm and 0.15 mm (and corresponding structured patterns of perforations) were used. Figure 2.4 shows a schematic of typical stainless steel 316L perforated sheets (PS) used. Table 2.3 summarizes the main characteristics of each metal sheet. The open flow field area is the open area of the flow field channels with respect to the perforated sheets i.e., the percentage of area of the flow field that is not blocked by the landing areas of the perforated sheets. It is also important to note that landing width here is the shortest distance between the perforations.

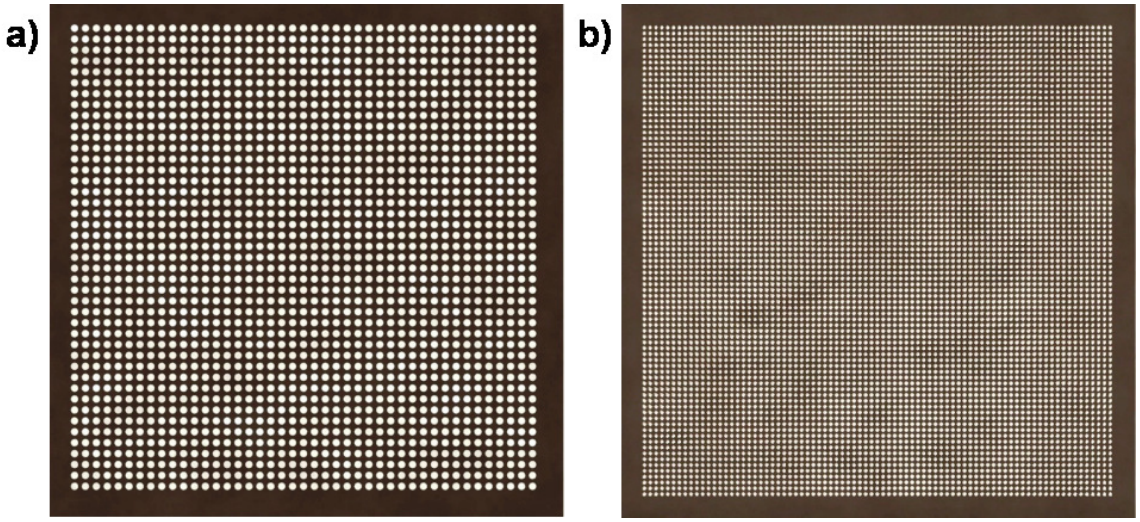

Figure 2.4 – Schematic of stainless steel perforated sheets (70 mm x 70 mm) with (a) 1 mm and (b) 0.5 mm diameter holes.

Table 2.3 – Characteristics of the perforated stainless steel 316L sheets.

Sheet Name	Area of each hole [mm^2]	Thickness [mm]	Landing width [mm]	# of holes per cm^2	Open area [mm^2]	Open flow field area [mm^2][a]
10mm PS	78.53	0.050	1	0.73	67.5	66.4
1mm PS	0.79	0.050	0.5	37.73	34.7	34.5
1mm PS	0.79	0.100	0.5	37.73	34.7	34.5
1mm PS	0.79	0.200	0.5	37.73	34.7	34.5
0.5mm PS	0.20	0.050	0.3	133.89	30.7	30.1
0.15mm PS	0.02	0.050	0.3	423.18	8.8	8.5

[a]Open area of the flow field channels with respect to the perforated sheets

Photo-etching is a simple and cost effective manufacturing process that is widely used in industry. Thus, it was chosen for making the perforations. In addition, the photo-etching process is already well developed and can easily be used for large-scale manufacturing. The spacing or landing between the perforations in each sheet was chosen based on the restrictions posed by the photo-etching manufacturing process and the recommendations give by VACCO in order to not affect the flatness and structural properties of the sheets. In general, the diameter of the perforations has to be 1.3 times the thickness of the materials (1.3t), with a minimum size of 0.15 mm. The landings between the perforations must be at least the same size as the thickness of the metal sheet, with a minimum size of 0.15 mm. However, after inspecting a number of different perforated sheets with perforations larger than 0.5

mm it was noticed that the materials were very weak and got damaged after fuel cell testing due to the small landing widths. Therefore, the landings widths listed in Table 2.3 are those found to give the best structure stability to the sheets, especially after being compressed inside a fuel cell.

Other designs of perforated sheets were used in order to understand how the in-plane diffusion (of gases) could be improved in these sheets. Therefore, small channels were etched on one side of the sheets. These sheets were used in the analyses shown in Chapters 5. Figure 2.5 shows the schematic for one perforated metal sheet design with in-plane diffusion capability. Table 2.4 summarizes the characteristics of the different perforated sheets that were designed to study the impact of channels and sheet thickness on the in-plane diffusion. The photo-etching process used restricts the depth of the channels to be at least half the thickness of the material (0.5t), if the material is 0.05 mm thick. If the thickness of the sheet is greater than 0.05 mm, then the channel depth has to be less or equal to 1.3 times the thickness of the sheet (1.3t). It is important to note that sheets with smaller channels (<0.15 mm) interconnecting the perforations were not possible to fabricate with the manufacturing method used. In fact, the dimensions shown in Table 2.4 represent the limit of the manufacturing capabilities of this photo-etching process.

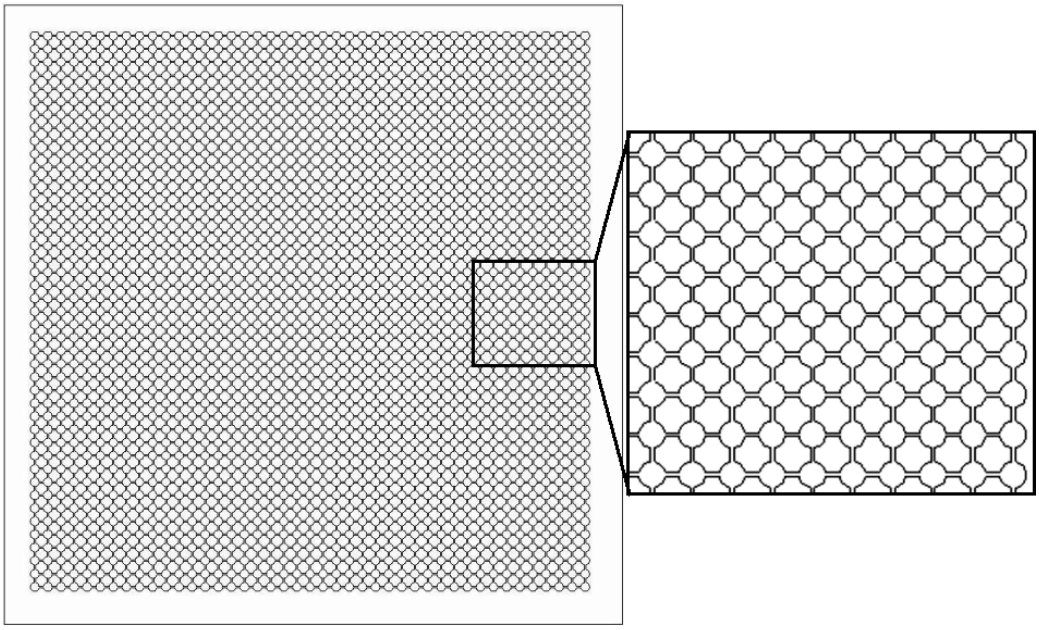

Figure 2.5 – Schematic of a perforated sheet (1 mm diameter holes and 0.05 mm thick) with 0.15 mm width channels etched in one side of the sheet. The channels were 0.025 mm deep.

Table 2.4 – Characteristics of metal perforated sheets with different thicknesses and channel widths. These channels were etched on just one side of the sheets. All these sheets had 1 mm diameter holes. Note that the names of these sheets match those shown in Table 5.1.

Sheet Name	Thickness [mm]	Landing width [mm]	Channel width [mm]	Channel depth [mm]
PS-B	0.050	0.5	0.15	0.025
PS-C	0.050	0.5	0.50	0.025
PS-D	0.050	0.5	1.00	0.025
PS-F	0.100	0.5	0.50	0.050
PS-G	0.100	0.5	0.50	0.075
PS-H	0.100	0.5	1.00	0.050
PS-I	0.100	0.5	1.00	0.075
PS-K	0.200	0.5	0.50	0.100
PS-L	0.200	0.5	0.50	0.150
PS-M	0.200	0.5	1.00	0.100
PS-N	0.200	0.5	1.00	0.150

2.1.2 2 kW Hydrogenics fuel cell station

All the experiments presented in Chapters 3, 4, and 5 were performed with a 2 kW Hydrogenics fuel cell test station (Hydrogenics Test Systems, now Greenlight Innovations). Figure 2.6 shows the fuel cell station with a single cell fuel cell. This station controlled the flow rates, inlet pressures, humidity, and temperature of the

reactant gases. Temperature thermocouples were used to measure the temperature values of the fuel cell, reactant gases inlet and outlet lines, and coolant inlet and outlet lines. The test station also controlled the DI water flow rate and temperature used to cool/heat the fuel cell. An integrated load bank was used to control and monitor the electrical load to the cell. The data was acquired by the HyWARE II software at a rate of one data point per second. This software was also used to create scripts (with the HyAL™ automation language) in order to perform automated tests.

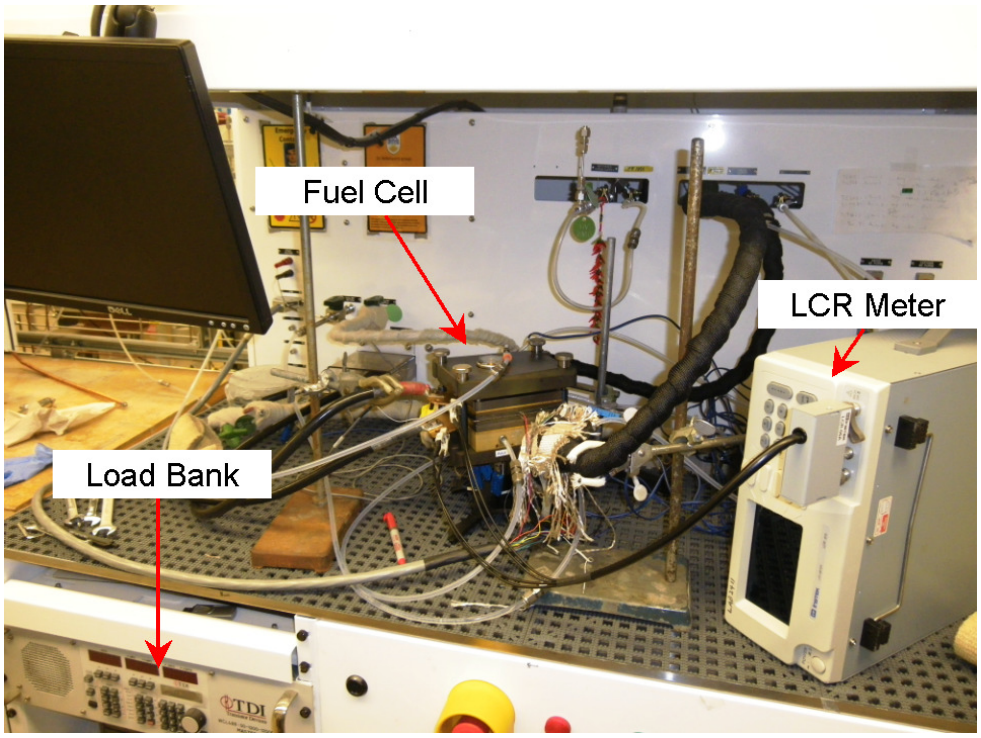

Figure 2.6 – Picture of the 2 kW Hydrogenics fuel cell station and testing set-up.

2.1.3 Polarization measurements

A series of testing protocols were developed to create a standard test method, which was used throughout the project in order to produce good quality fuel cell test data in a reliable and safe manner. In addition, these protocols also allowed baseline performance to be established for commercially available materials (e.g., CCM, GDLs, etc.). For more details on all the test protocols explained in this section please refer to Appendix C.

2.1.3.1 Leak testing and membrane conditioning

An important step prior to polarization measurements was to leak check the fuel cell. One way to do this was by connecting the assembled fuel cell, with the MEA already placed inside the cell, to the test station and flow gases at specific flow rates with no back pressure. These gases were then pressurized slowly making sure that the gas pressure did not decrease and stayed within 1 kPa of the set value. Similarly, the cell could also be submerged into a water tank in order to observe any bubble formation around the cell. This last method is not as effective when finding internal leaks within the cell. This leak test can be performed with N_2 for both cathode and anode sides, or with air and H_2, respectively.

Once it was confirmed that the cell did not have a leak, the next step was to condition the membrane in order for it to get humidified and work properly. This step is also referred to as cell break-in or the MEA start-up procedure. There are different ways of performing this step since each membrane manufacturer recommends specific procedures that enhance their membranes performance. The procedure followed here, was found to give the best results for the specific membranes used. Firstly, the gas flow rates for both reactant gases were set to a minimum flow rate corresponding to 500 mA cm^{-2} (with an air/hydrogen stoichiometry of 2.0/1.5). The gases were then pressurized stepwise until the desired back-pressure was reached. At this point, a small current load was applied ensuring that the cell voltage was maintained above 0.5 V (e.g., current density of 500 mA cm^{-2} or less). The cell, gas, and dew point temperatures were then increased step-wise (i.e., 3 to 4 steps) until the determined set-points were achieved. The cell temperature should always be slightly above (or equal) to the reactant dew point temperature in order to prevent water condensation within the cell. While the station heated the gases, cell, and humidifiers, the current load was increased every 5 to 10 minutes (e.g., 500, 750, 800, and 1000 mA cm^{-2}). Once the desired operating conditions were reached, the fuel cell was operated at a current density in which the cell voltage was approximately 0.6 V (i.e., 1000 mA cm^{-2}). The fuel cell was then operated at these conditions for 6 to 8 hours, or until the variations in the cell voltage were smaller than

±10 mV for at least one hour. Figure 2.7 shows the cell voltage as a function of time during a typical MEA conditioning procedure. This figure also shows in more detail the last hour of this procedure, in which it can be observed that the cell voltage is stable (based on the mentioned standards).

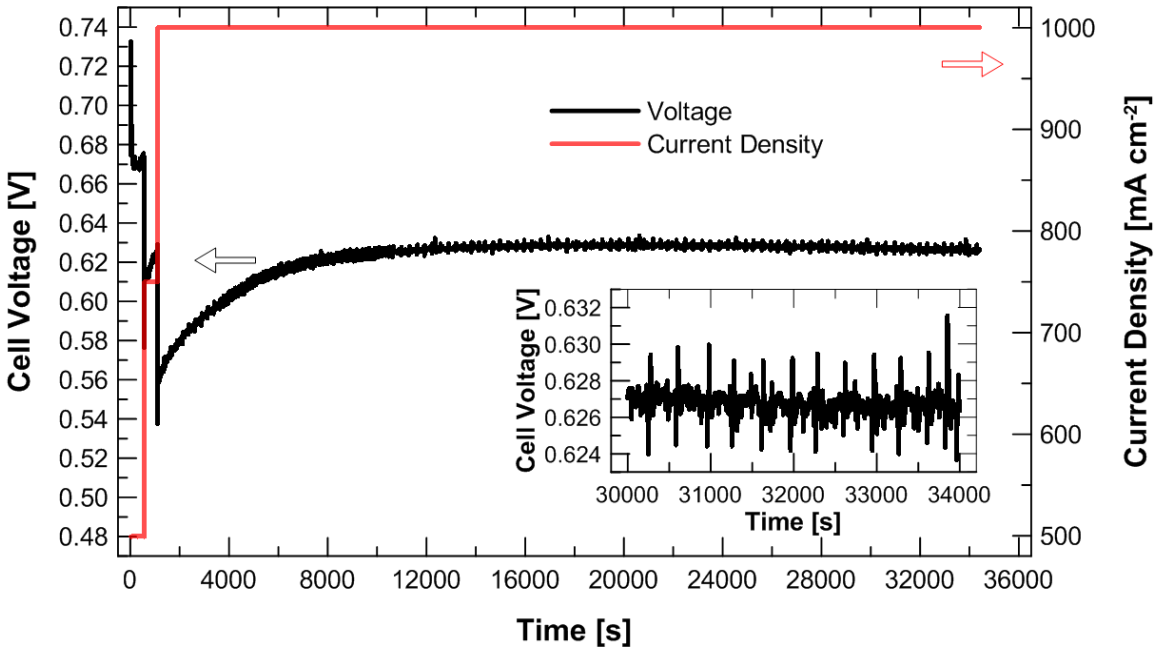

Figure 2.7 – Cell voltage and current density traces for a typical MEA conditioning procedure. For these tests the gases, cell, and dew point temperatures were 75 °C, the pressure for both inlet reactant gases was 206.9 kPag (approx. 30 psig), and the air/hydrogen stoichiometry ratio was 2.0/1.5. The CCM was a Primea® 5510 membrane (0.4 mg Pt cm^{-2} on each side) and the anode and cathode GDLs were SGL 25DC GDL and SGL 25BC GDL, respectively.

In the above procedure, constant current was the preferred method to operate the fuel cell. However, constant voltage could also be employed. In addition, previously used MEAs were re-conditioned by running the fuel cell at a constant current (similar to the one used in the last step of the break-in procedure) until the cell voltage was stable (±10 mV for at least one hour). This re-conditioning procedure was usually shorter than the conditioning of fresh MEAs.

2.1.3.2 Compression pressure tests

An important parameter in fuel cell performance is the compression pressure for the whole cell. It is vital to have good electrical contact between all the components

without damaging them by over-compression. The previous procedures (leak test and MEA conditioning) for the first baseline MEA were performed at a standard cell compression pressure of 100 psi, which was acceptable for the tests. However, this value did not necessarily represent the optimized compression pressure. Thus, the optimized compression pressure was determined when the fuel cell was operated at standard conditions and a constant current density of 1000 mA cm^{-2}. Once all the conditions were reached the compression pressure was increased gradually until a peak cell voltage was achieved, corresponding to the ideal compression pressure. Figure 2.8 shows an example of this procedure.

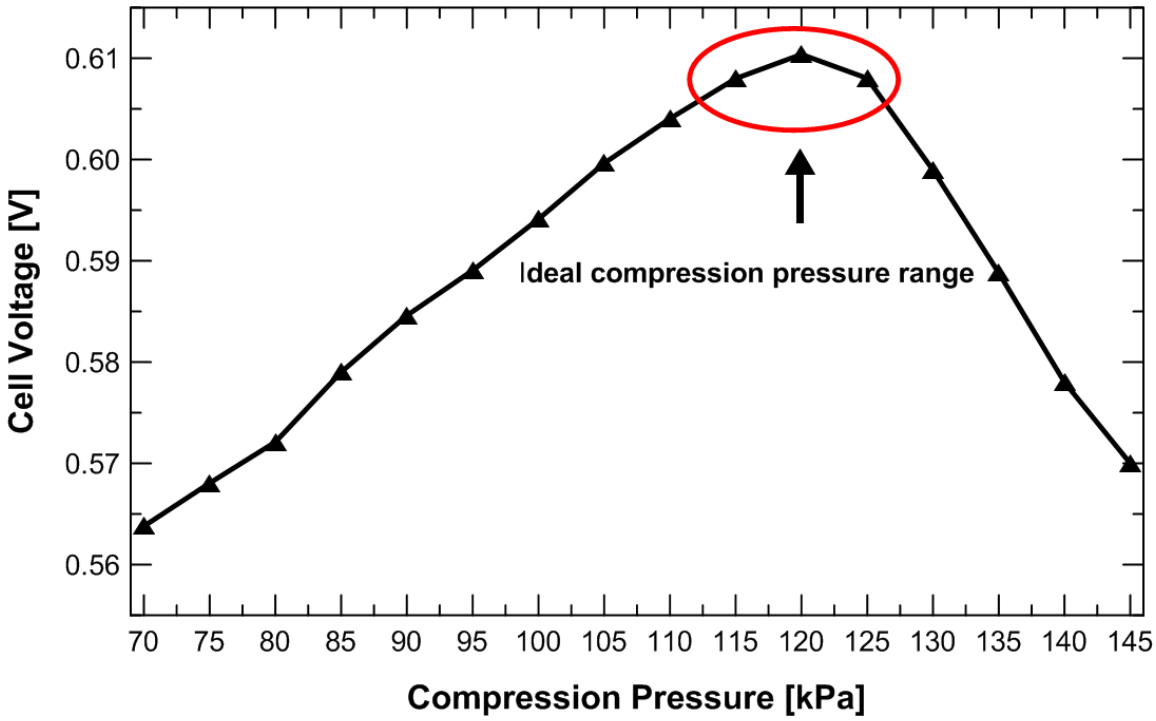

Figure 2.8 – Cell voltage versus compression pressure. For these tests the gases, cell, and dew point temperatures were 75 °C, the pressure for both inlet reactant gases was 206.9 kPag (approx. 30 psig), and the air/hydrogen stoichiometry ratio was 2.0/1.5. The CCM was a Primea® 5510 membrane (0.4 mg Pt cm^{-2} on each side) and the anode and cathode GDLs were SGL 25DC GDL and SGL 25BC GDL, respectively.

In addition to the previous procedures, a pressure sensitive film (Pressurex, super-low, Sensor Products Inc.) was used to confirm uniform compression between the anode and cathode plates.

2.1.3.3 Polarization curve protocol

Following a strict protocol is important when performing polarization curves in order to be able to collect reliable and repeatable data. The final protocol used for this work was based on the reports by the US Fuel Cell Council and US Department of Energy [189,190]. A number of different steps were performed in order to find the most reliable curves. In general, the first step was to reach the set points for the desired operating conditions. Once this was completed, the fuel cell was held for 15 minutes at each desired current density, starting from low to high current densities. The number of points in a polarization curve depends on the areas that are being investigated. For example, a greater number of points should be tested in the low current density region in order to study the electrode kinetics of the reactions. More points can be tested in the middle-range of the current density if ohmic losses are important. Similarly, more weight can be given to the higher current densities if analysis of mass transport losses (and limiting current) is desired. In most of the studies presented here the emphasis was given to the mid- to high current density range.

After the maximum current density was attained (limited by the load bank) in the polarization testing, the fuel cell was tested at six more current densities, in a descending order from high to low current values, for at least 15 minutes at each point. This was performed to compare the hysteresis associated with increasing or decreasing current densities. This was especially important when testing at low humidity conditions since the cell could be degrading. If the difference between the increasing and decreasing cases was less than or equal to 10 mV at a given current value then the polarization curve was completed. The cell voltage recorded at each current measurement was averaged over a time period of at least 3 minutes (one data point per second) corresponding to the steady state condition of the cell.

Figure 2.9 shows a polarization curve that was performed following the above steps. As it can be observed the cell voltage values recorded in for the descending order are higher than those for the ascending order. For this specific polarization curve, the difference between the increasing and decreasing current densities is around 18 to 26 mV, which would make this specific curve not acceptable based on the

standards mentioned above. It is important to note that for certain GDL configurations, especially those with perforated sheets as GDLs, the difference between the increasing and decreasing cases was greater than 10 mV in most cases due to water removal limitations. Therefore, for those specific cases differences lower than 15 to 20 mV were acceptable.

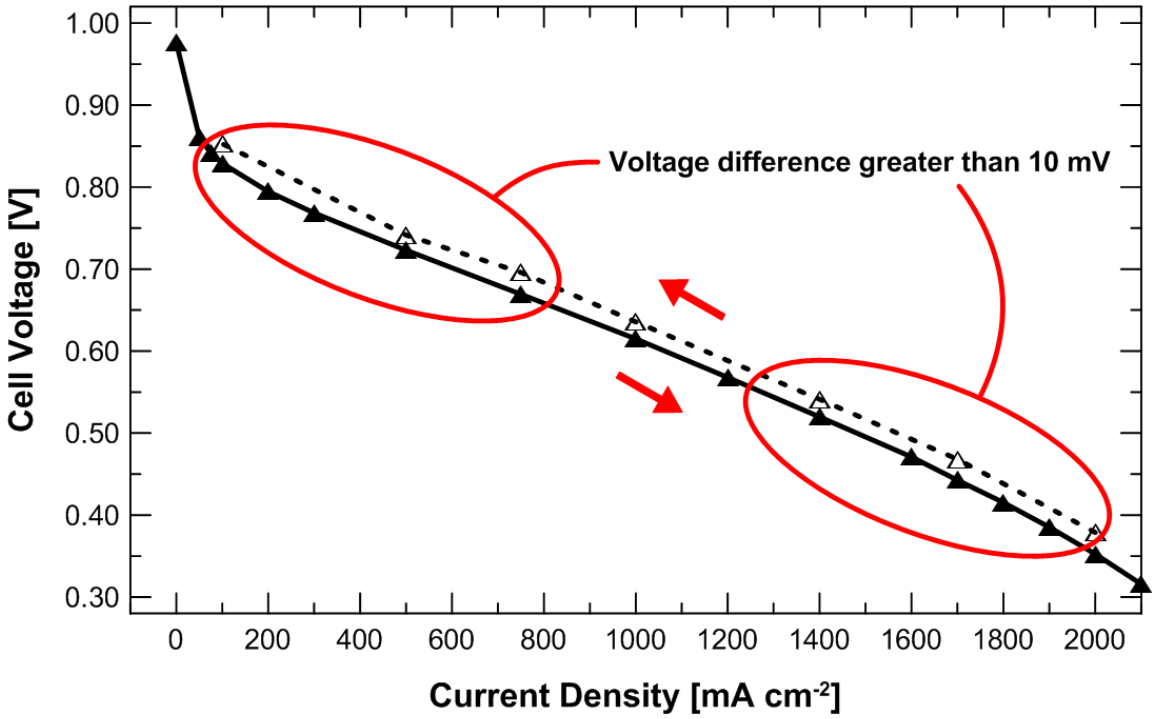

Figure 2.9 – Example of a typical polarization curve. For these tests the gases, cell, and dew point temperatures were 75 ℃, the pressure for both inlet reactant gases was 206.9 kPag (approx. 30 psig), and the air/hydrogen stoichiometry ratio was 2.0/1.5. The CCM was a Primea® 5510 membrane (0.4 mg Pt cm^{-2} on each side) and the anode and cathode GDLs were SGL 25DC GDL and SGL 25BC GDL, respectively.

Ideally, for a polarization curve the conditions at each current density should not be affected by the previous tested current density. For example, the water produced at a specific current load should not affect the conditions for the following point if enough time is allowed to reach steady state. Therefore, gas purging, mainly on the cathode side, is commonly performed in order to remove all the water accumulated inside the cell. This step ensures that voltage measurement at a given current density is not influenced by the state of the cell from the previous measurement. In our studies, it was found that with the baseline MEAs purging was only necessary when the dew point temperature of the gases was greater than the temperature of

the gases (i.e., flooding conditions). However, when other GDL configurations were used (i.e., with the perforated metal sheets) purging was necessary for the flooding and 100% RH (fully humidified) conditions. At low relative humidities (e.g., 25% RH) it was found that purging was not necessary with any GDL configuration since the water accumulated inside the cell did not affect the current density performance significantly.

Three main operating conditions were used for polarization tests: fully humidified (i.e., 100% RH), flooding conditions, and low humidity conditions (i.e., 25% RH). Table 2.5 gives more details for these experimental conditions.

Table 2.5 – Experimental conditions used for polarization testing.

Condition	T_{cell} [°C]	T_{gas} [°C]	T_{dp} [°C]	Inlet Pressure [kPa gauge]	Cathode/Anode Stoichiometric Ratio
Fully Humidified (100% RH)	75	75	75	206.8	2/1.5
Flooding	75	75	95	206.8	2/1.5
Low Humidity (25% RH)	75	75	45.4	206.8	2/1.5

2.1.3.3.1 Error treatment

As stated previously, the cell voltage recorded at each current measurement was averaged over a time period of at least 3 minutes (at steady state conditions). The subsequent standard deviation was calculated for each averaged cell voltage value. Each standard deviation was then used in order to add error bars for all the polarization data shown in this work. Most of the polarization tests shown in Chapters 3, 4, and 5 were performed at least three times in order to obtain repeatable observations. In all the cases, the voltage differences (at specific current densities) between each repetition were within 15 mV, which was considered acceptable. The data shown from these polarization tests is the data corresponding to one of the three repeated tests.

In addition to repeat the tests, in some cases the same tests were repeated 2 to 4 times with completely new MEA materials. This allowed to observe the repeatability between materials of different batches. In addition, this process was especially

important when specific tests showed erratic or unexpected behaviour. In general, if major differences were observed between tests (e.g., voltage differences >30 mV) then more repetitions were performed until a pattern was recognized. Figure 2.10 shows the polarization data of four identical MEAs at fully humidified conditions. For this example, the voltage difference between the four cases was always within ±15 mV at all the current densities.

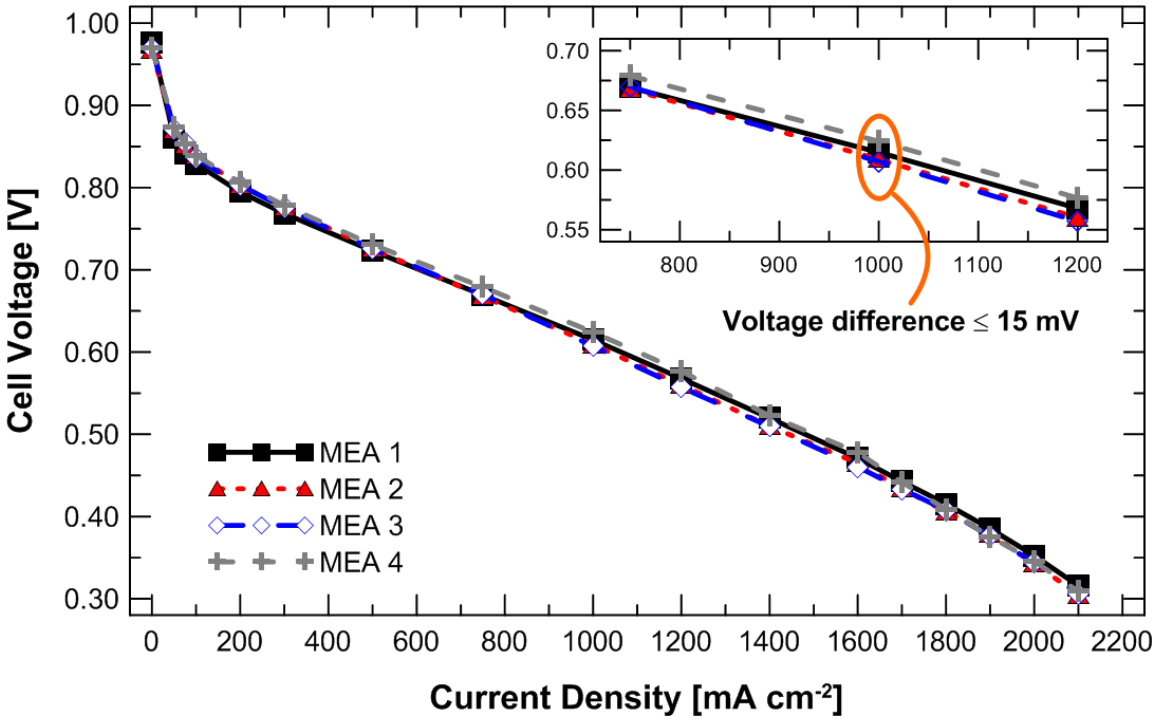

Figure 2.10 – Polarization data of four different tests with identical MEA materials. For these tests the gases, dew point, and cell temperatures were 75 °C, the pressure for both inlet reactant gases was 206.8 kPag, and the air/hydrogen stoichiometry ratio was 2.0/1.5. The cathode and anode GDLs were SGL 25BC (with MPL) and SGL 25DC (with MPL) carbon fiber papers, respectively. Note that error bars are not shown for clarity.

Another method used to observe the reproducibility between the materials used for this project was to compare the membrane conditioning results between MEAs with same configurations. In most cases, the cell voltages were within ±15-20 mV of each other. Figure 2.11 shows an example of the membrane conditioning tests for four different MEAs. All these MEAs had perforated sheets (1 mm diam. holes) and 25BC GDLs in the cathode side. It can be observed that all the MEAs had similar performances (within the error range) during the conditioning test. The inset in

Figure 2.11 shows in more detail the cell voltages for each case in the last hour of the tests.

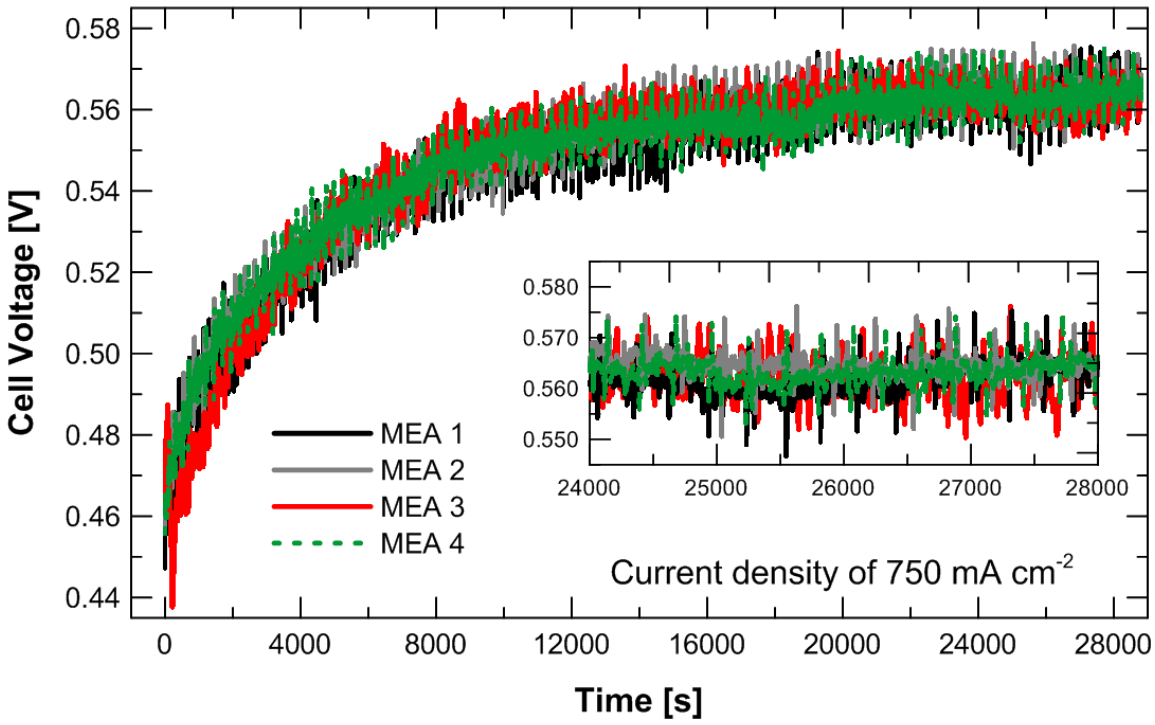

Figure 2.11 – Conditioning of four different MEAs with the same GDL configurations. For these tests the MEAs had a 25BC (with MPL) GDL and a 1 mm perforated sheet in the cathode side. In the anode side a SGL 25DC (with MPL) GDL was used. For all the membrane conditioning tests the gases, dew point, and cell temperatures were 75 °C, the pressure for both inlet reactant gases was 206.8 kPag, and the air/hydrogen stoichiometry ratio was 2.0/1.5. The current density was 750 mA cm^{-2}. The cathode and anode GDLs were SGL 25BC (with MPL) and SGL 25DC (with MPL) carbon fiber papers, respectively.

The pressure drop data shown in Chapters 3 and 4 have error bars corresponding to the standard deviations of the pressure drops recorded in each test.

2.1.3.4 High frequency resistance measurements

For all the polarization measurements, the high frequency resistance (HFR) of the cell was measured at 1 kHz using an LCR meter (GW-Instek LCR-819). The HFR corresponds to the cell resistance and consists predominantly of the membrane ionic resistance, and other residual resistances arising from electronic and contact resistances [191]. The LCR meter can be seen in Figure 2.6. Prior to any testing, the HF resistance of the fuel cell, with different GDLs but without the CCM, was

measured at a cell temperature of 75 °C (see Figure 2.12a). A graphitic foil was placed between the GDLs and flow field plates in order to know the resistance that the fuel cell (and most of the fuel cell materials) have. This test was performed for every single GDL configuration used and presented in this thesis. The resistance obtained from this *ex-situ* test was then subtracted from the HFR value measured when performing fuel cell testing (Figure 2.12b). Thus, the final resistance value represented the resistances of the membrane, catalyst layers, and contact resistances between the GDLs and the catalyst layers as shown in the classical equivalent circuit in Figure 2.13. The term R_{ext} represents the sum of all the resistances due to the graphite plates (flow field, coolant, and blank plates), the current collectors, wires to measure the cell voltage, and cables connected to the load bank. Please note that the circuit shown here, especially the part regarding the membrane and catalyst layers represents just a classical equivalent circuit for these parts. It does not go into more detail regarding the exact (and possibly more precise) circuit representation of these components since it is beyond the scope of this thesis. For more detail on equivalent circuits in fuel cells please refer to [192-194].

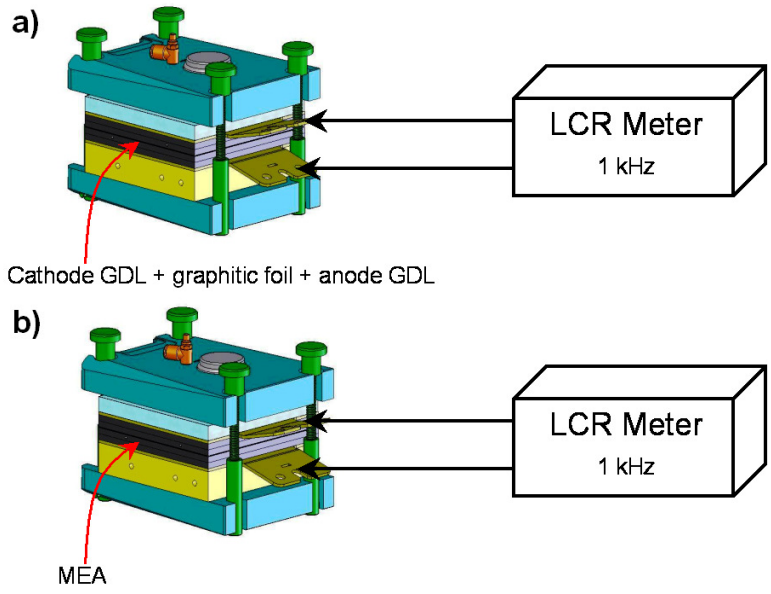

Figure 2.12 – Schematics of the high frequency resistance (HFR) measurements: (a) HFR measurement of the cell with the cathode and anode GDLs and a graphitic foil placed between them; (b) HFR measurement of the fuel cell with an MEA while performing fuel cell testing.

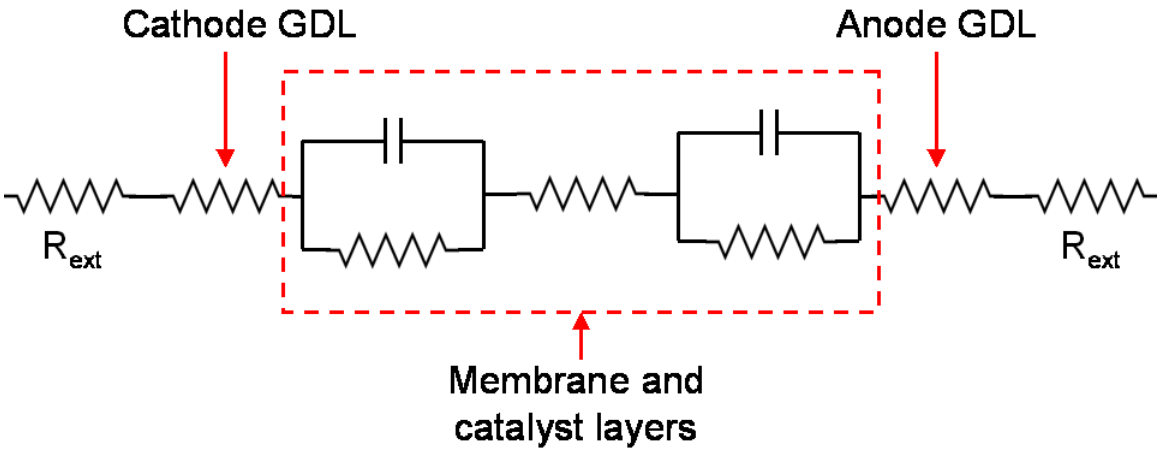

Figure 2.13 – Classic equivalent circuit of the fuel cell. R_{ext} corresponds to the resistances due to the plates, current collectors, and wires of the load bank.

2.1.3.5 Pressure drop analysis

The pressure drop on both the anode and cathode side was also measured since this can be used as an indicator of water flooding given that water accumulation in the MEA and flow field channels can result in larger pressure drops [178,195,196]. However, if the pressure drop for different GDLs is being compared in order to provide an insight into water accumulation inside the channels, it is important to determine how much of the pressure drop is affected by the GDL itself. Therefore, the pressure drops of the different GDL configurations used in this study were also measured with non-active conditions (i.e., no current) and without humidification (i.e., single-phase). At these conditions, for the cathode side, the difference in pressure drops between the 25BA (without MPL) and 25BC (with MPL) GDLs was less than 5% (see Figure 2.14). However, with the active tests (low humidity conditions and assumed two-phase flow) this difference increased to greater than 12% for flow rates higher than 1.64 SLPM (corresponding to 1000 mA cm^{-2}). These results confirm that the pressure drop for different GDL configurations as an indicator of water accumulation in the single fuel cell is a good assumption. Similar observations can be given for all the GDL configurations used in this project. This is especially important for the analysis presented in Chapters 3 and 4. Figure 2.14 also shows the cathode pressure drop when a solid material is used instead of a CFP. As expected, the pressure drop with this solid sheet material (graphitic foil) is greater than when CFPs are used under non-active conditions since with the porous CFP

case the gas has more paths to travel through, thus, reducing the overall pressure drop. However, once the fuel cell is active, the 25BA CFP (without MPL) experiences a greater pressure drop due to water accumulation.

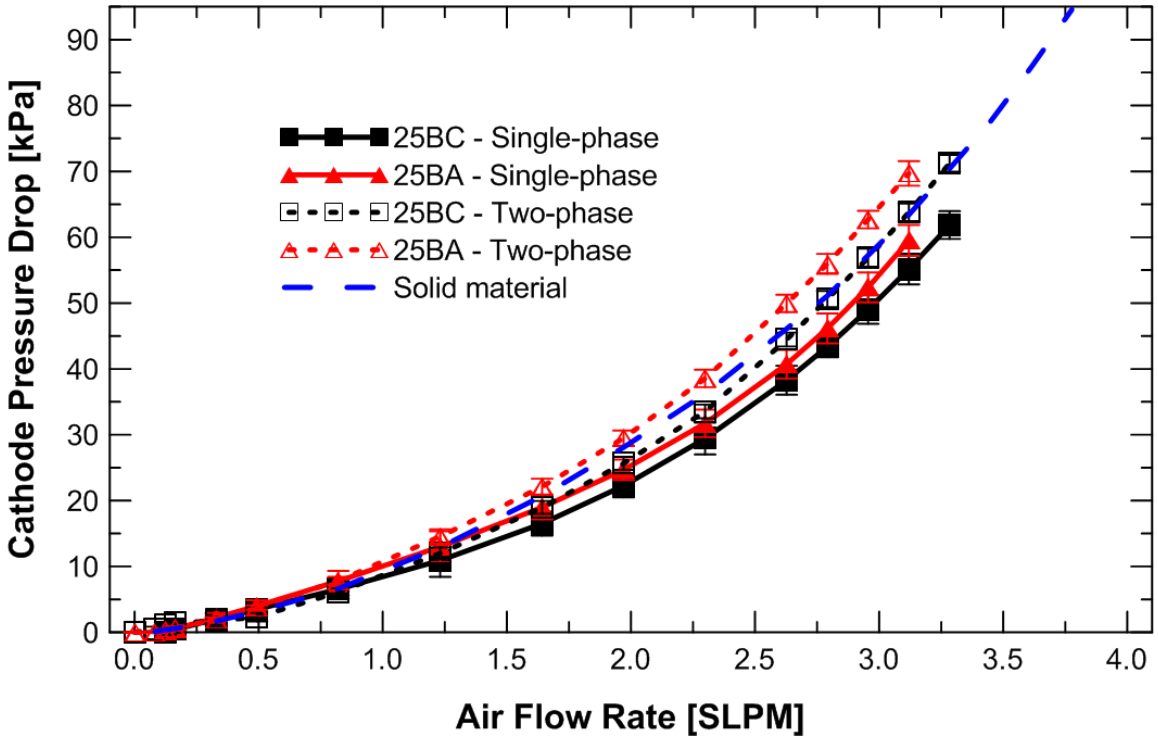

Figure 2.14 – Cathode pressure drop versus air flow rate. The solid symbols represent the single-phase pressure drops (non-active conditions). The open symbols represent the two-phase pressure drops (active conditions at 25% RH). The anode GDL was SGL 25DC for all the cases.

2.1.3.6 Multi-component gas analysis

For a more detailed study of mass transport losses originated by different GDL configurations, multi-component gas analysis was used as a diagnostic tool [197-199]. This technique consists of performing a number of polarization curves with different oxidant mixtures such as pure O_2, air, and heliox (21% O_2 in He). Each polarization curve provides specific information that can describe different aspects of the fuel cell performance and how well it was designed. For instance, pure O_2 and heliox can be used to provide a better understanding of concentration losses and mass transport losses in PEM fuel cell, respectively. The reason for this is that, oxygen diffuses at a higher rate in helium (He) than in nitrogen (N_2) (i.e., in air) since the diffusion coefficient of O_2 in He is 1.3298 cm^2 s^{-1} and the diffusion coefficient of

O_2 in N_2 is 0.1637 cm^2 s^{-1} [197,198]. Thus, the performance of the fuel cell with heliox as the oxidant gas significantly improves the mass transport region of the polarization curve. Prior to calculating the mass transport losses for a specific GDL configuration (voltage difference between the heliox and air curves), the polarization curves were HFR corrected in order to remove the ohmic losses and contact resistances from the final calculated losses. It is important to note that the stoichiometries for the different oxidant gases used were kept equal to 2.0. Figure 2.15 shows an example of polarization curves with different oxidant gases.

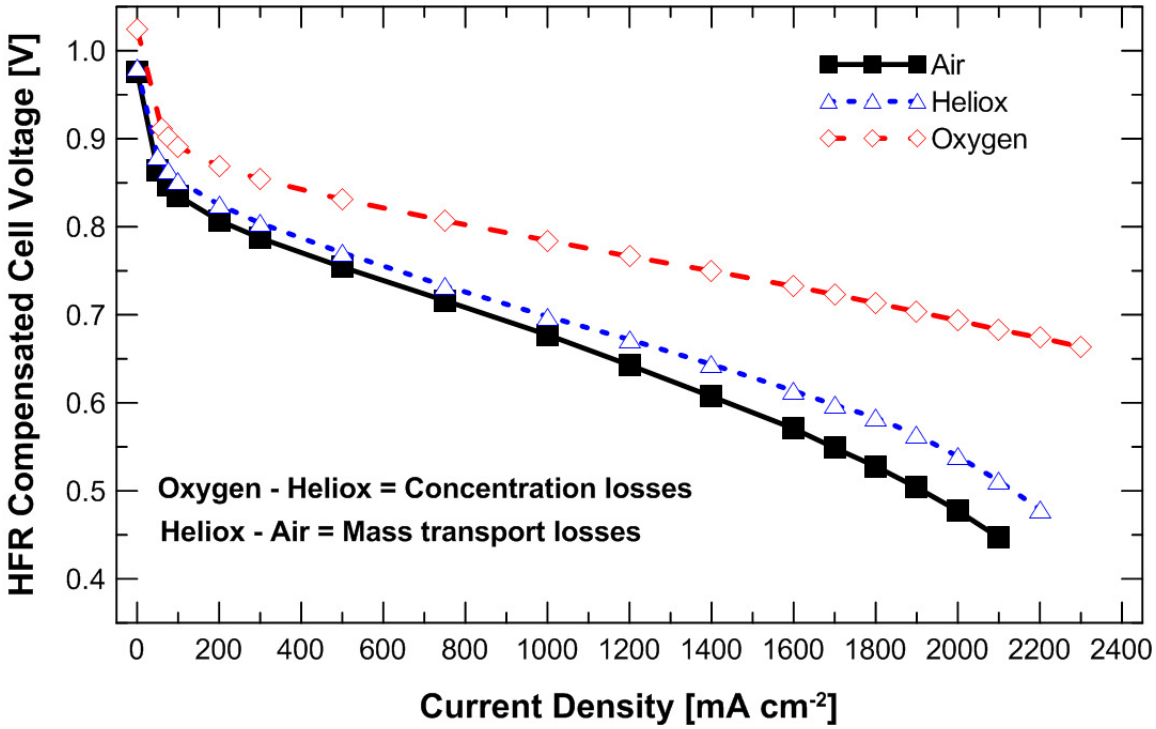

Figure 2.15 – Example of multi-component gas analysis. For these tests the gases, cell, and dew point temperatures were 75 °C, the pressure for both inlet reactant gases was 206.9 kPag (approx. 30 psig), and the oxidant gas/hydrogen stoichiometry ratio was 2.0/1.5. The CCM was a Primea® 5510 membrane (0.4 mg Pt cm^{-2} on each side) and the anode and cathode GDLs were SGL 25DC GDL and SGL 25BC GDL, respectively. The polarization curves are HFR compensated.

2.1.4 Water transport rate tests

In order to understand how the perforated sheets affect the water transport capability of the cathode GDL, the water transport rates of different MEA configurations were estimated using an *ex-situ* experimental technique similar to that presented by Dai et al. [200,201] (see Chapter 3). Figure 2.16 shows a schematic of the experimental

set-up. Briefly, humidified air (at 75 ℃ and 25% RH) was fed to the cathode flow field plate, and deionized (DI) water was fed to the anode and the coolant sides of the cell (at 75 ℃). A Toray® TGPH-060 carbon fibre paper with no water proofing was used on the anode side in order to give mechanical support to the catalyst coated membrane and to keep it fully humidified. On the cathode side, different GDL configurations were used. The air flow rate, corresponding to a specific current density, was kept constant for 1 hour. The water removed from the cell by the air stream was then condensed in a high efficiency, water-cooled condenser and collected into a reservoir. The collected water was then used to calculate the actual water transport rate from the anode side to the cathode side with different cathode configurations. The following equation shows how the final water transport rate was calculated:

$$W_{Cathode} = W_C - W_{in} + W_{vap} \tag{2.1}$$

where $W_{Cathode}$ is the total cathode water transport rate (g min^{-1}); W_C is the water collected in the reservoir over a specific period of time (g min^{-1}); W_{in} is the water in the humidified air (g min^{-1}) and is calculated using the water saturation pressure at the dew point temperature; and W_{vap} is the water vapor in the exhaust air (g min^{-1}) and is calculated using the water saturation pressure at the temperature of the exhaust air (a thermocouple was used for this).

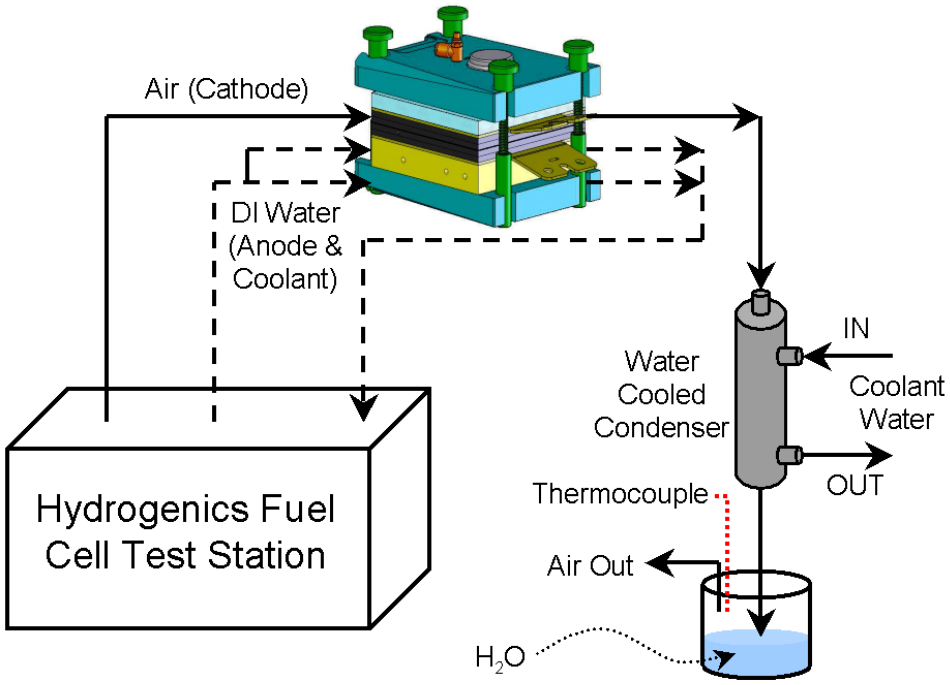

Figure 2.16 – Schematic of the testing set-up used for water transport rate measurements. This is an *ex-situ* experiment with no current load.

2.1.5 Anode water removal method

Another method used to understand mass transport issues inside fuel cells is the anode water removal (AWR) technique [27-29]. Ballard Power Systems first proposed this method in which liquid water accumulated in the cathode can be drawn by a concentration gradient across the membrane to the anode and removed in the fuel stream. This concentration gradient is created by drying the anode side. This method can be used as a diagnostic tool since it can remove water in the cathode without directly affecting other conditions presented in the cathode (e.g., thermal and concentration). Therefore, the effects due to water accumulation in the cathode are reduced or eliminated, thus separating mass transport from other effects. The change of the water concentration gradient in the proton exchange membrane increases the back diffusion rate of water from the cathode to the anode such that water at the cathode catalyst layer diffuses through the membrane and is removed via the anode reactant gas stream. Figure 2.17a shows how the water concentration in a membrane changes when the AWR method is used. Figure 2.17b

shows how the water collected in the anode outlet stream increased with higher hydrogen stoichiometries.

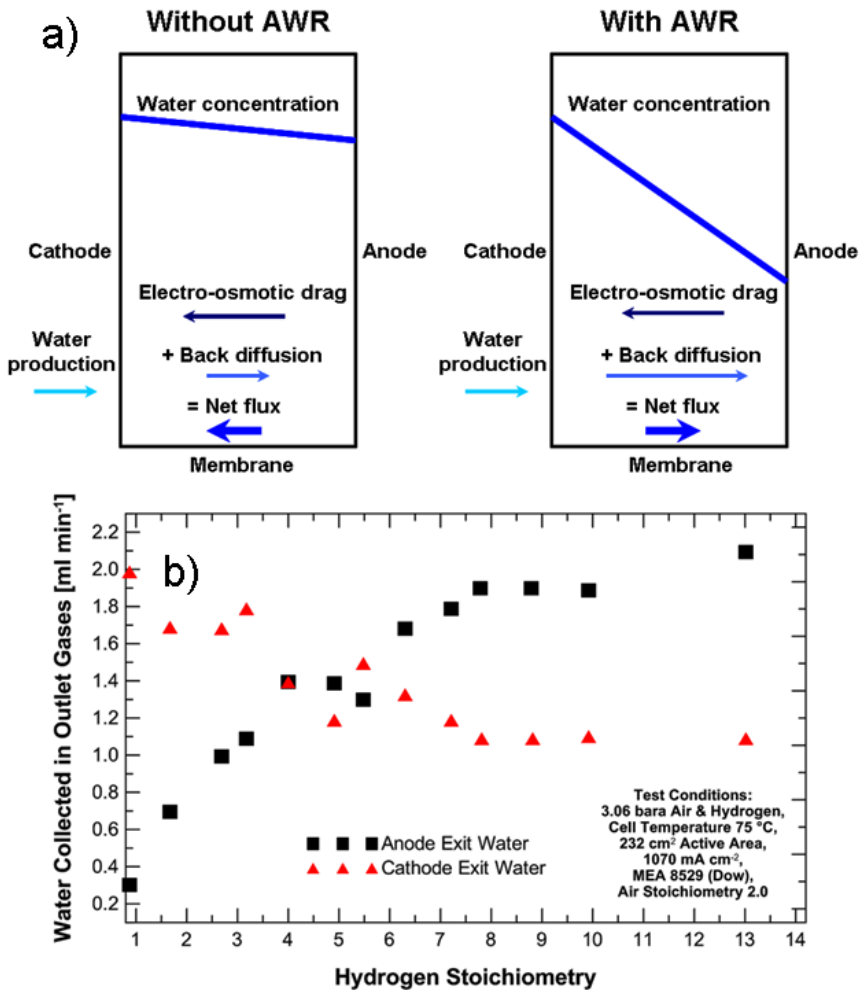

Figure 2.17 (a) Schematic of the water concentration through the membrane when the anode water removal (AWR) method is performed, and (b) water collected in the outlet gases during AWR tests (modified from Voss et al. [28] with permission from Elsevier).

This method can be accomplished by modifying the relative humidity or thermal gradient of the anode side; however, the recommended approach is to create a pressure gradient along the anode flow field channel in order to increase the ability of the fuel stream to carry water vapor [28]. As the pressure of the anode gas stream decreases along the flow channel at high fuel flow rates (high stoichiometries) of the fuel gas, it can carry a larger mole fraction of water vapor. Once the flow rate reaches an optimum level, the water concentration gradient draws the optimum amount of water from the cathode side towards the anode through the membrane

before dehydration becomes an issue. The cell voltage increases with higher fuel flow rates until a peak in performance is reached (Figure 2.18), where the cell's internal resistance increases with high flow rates due to the membrane drying out from too much water removal [28]. This peak in performance corresponds to the removal of water in the cathode catalyst layer. This method allows investigation of the cell and electrode performance potential in the absence of mass transport limitations. Thus, various GDL configurations can be studied and compared since their true performance without mass transport losses can be observed.

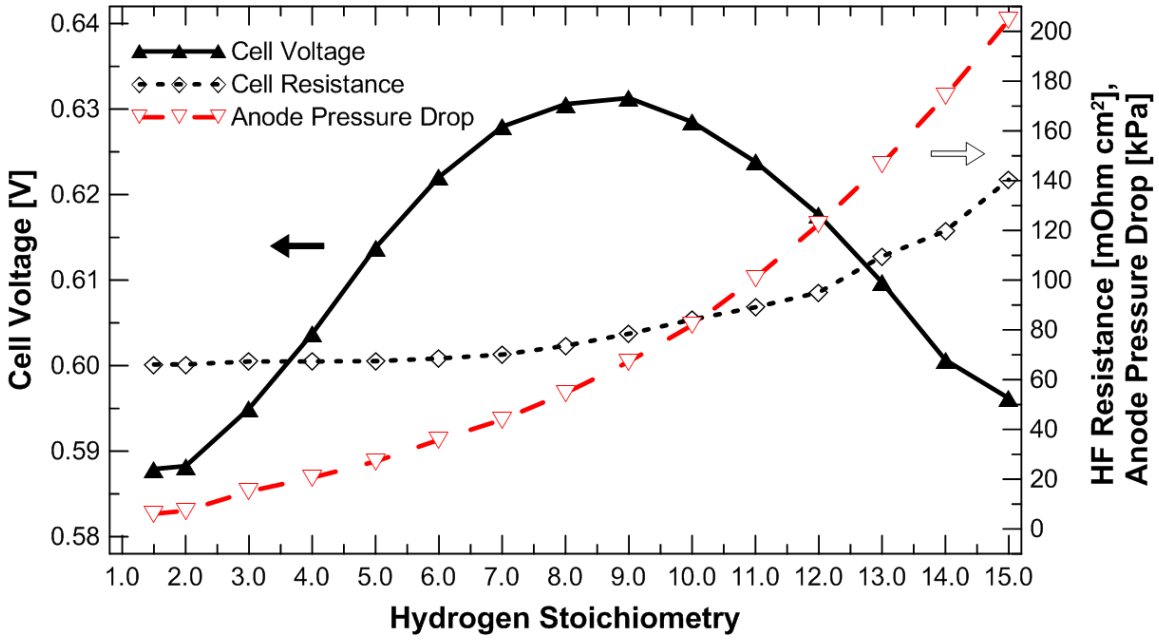

Figure 2.18 – Example of the anode water removal method. For these tests the gases and cell, temperatures were 75 °C, the air was fully humidified (100% RH) and the hydrogen was dry (no humidification), the pressure for both inlet reactant gases was 206.8 kPag (approx. 30 psig), and the air stoichiometry was 2.0. The CCM a Primea® 5510 membrane (0.4 mg Pt cm^{-2} on each side) and the anode and cathode GDLs were SGL 25DC GDL and SGL 25BA GDL, respectively.

The protocol used for these tests was as follows. The cell, gases, and cathode dew point temperatures were 75 °C. The air flow rate was kept constant (stoichiometry of 2.0). For the anode side, the hydrogen gas was dry (no humidification) and its stoichiometry was increased until fuel cell performance peaked and voltage stability was observed at a specific current density. The hydrogen stoichiometry was increased step-wise every 2 minutes, while holding the current density at 1000 mA cm^{-2}. During these tests the cathode side was kept hydrated (100% relative

humidity), thus, the only water inside the cell was that produced in the cathode catalyst layer and that introduced by the oxidant gas.

2.2 Mk 5 Ballard fuel cell

Two Mk5 Ballard fuel cells, single cell and stack, were used for all the tests related to Chapter 6.

2.2.1 Hardware

Figure 2.19 shows a Ballard Mk 5 (Ballard Power Systems) fuel cell stack similar to the ones used for the experiments presented here. Both the single cell and fuel cell stack used an internal humidification system located before the cathode and anode plates. This system consisted of a series of Nafion® membranes located between plates that had flow field channels. One flow field was for DI water and the other for a reactant gas and it was previously determined that the gas was fully humidified after flowing through the plate humidifier. Both the single cell and stack had a pneumatic piston located on top in order to compress the cell evenly. The ideal compression pressure for these fuel cells was 689.5 kPa (100 psia). All the anode flow field plates were standard single-pass serpentine flow fields. The standard cathode flow field plates used for comparison were six-pass serpentine flow fields. All the flow field plates were made out of graphite. Table 2.6 shows the parameters of these flow field plates. Both standard flow field plates are shown in Figure 2.20.

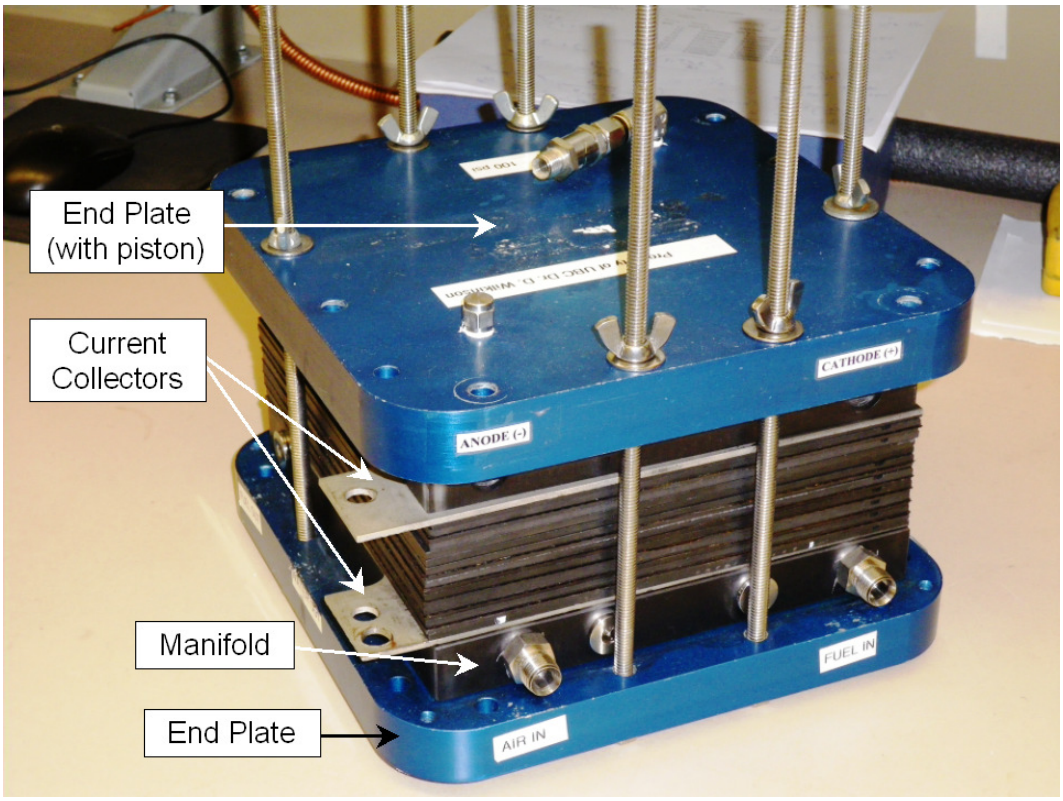

Figure 2.19 – Picture of a Ballard Mk 5 fuel cell stack similar to those used in the tests.

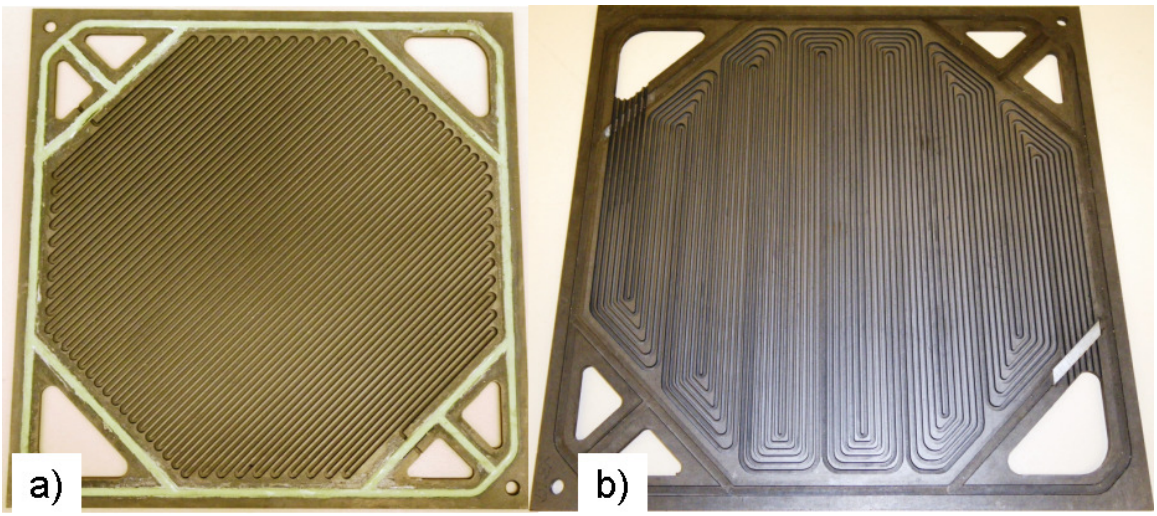

Figure 2.20 – Standard (a) anode and (b) cathode flow field plates for the Mk 5 fuel cells. These plates were made out of graphite. The active area for these plates is 280 cm^2.

The membrane electrode assembly (MEA) used in the Mk 5 fuel cells consisted of a Nafion 115 membrane, and a total Pt catalyst loading of 1.0 mg cm^{-2} (0.7 mg Pt cm^{-2} on the cathode and 0.3 mg Pt cm^{-2} on the anode) with Toray TGP 090 (20 wt. % of PTFE) GDLs for both anode and cathode sides. Both the anode and cathode GDLs

had an MPL with 20 wt% PTFE. No assembly was needed for these MEAs since Ballard Power Systems manufactured them.

Two different special cathode plates with interdigitated and serpentine flow fields were designed and used for the single cell tests. For the fuel cell stack tests just the cathode plates with serpentine flow fields were used.

Table 2.6 – Parameters of the flow field channels used with the Mk5 fuel cell.

Properties	Anode Flow Field	Standard Mk5 Cathode Flow Field	Interdigitated Flow Field	Serpentine Flow Field
Flow field type	Serpentine	Serpentine	Interdigitated	Serpentine
Number of paths	1	6	N/A	6
Cross-sectional shape	Trapezoidal	Trapezoidal	Squared	Squared
Channel width – bottom [mm]	1.28	1.28	0.50	1.50
Channel width – top [mm]	1.59	1.59	0.50	1.50
Draft angle[a]	7°	7°	0°	0°
Channel depth [mm]	1.27	1.27	0.20	1.00
Landing width [mm]	0.40	0.92	0.80	0.80

[a]Draft angle is the angle that the channel walls make with vertical.

2.2.1.1 Cathode interdigitated flow field plate

The active area of the interdigitated cathode flow field (260 cm^2 active area) was divided into six separate sections. Figure 2.21 shows a schematic of this plate with tubing and valves. Table 2.6 shows the specific parameters of this flow field channel. The sections corresponding to valves 1 and 6 each have an area of 38.5 cm^2, the area for each of the sections controlled by valves 2 and 5 is 52.2 cm^2 and, finally, the last two sections (valves 3 and 4) each have an area of 39.4 cm^2. Each section was connected to a valve (closed or opened manually) at the exit of the flow field located outside of the fuel cell. Thus, if a valve was closed the corresponding area in the flow field was also closed forcing the reactant flow to go to the other sections of the cathode.

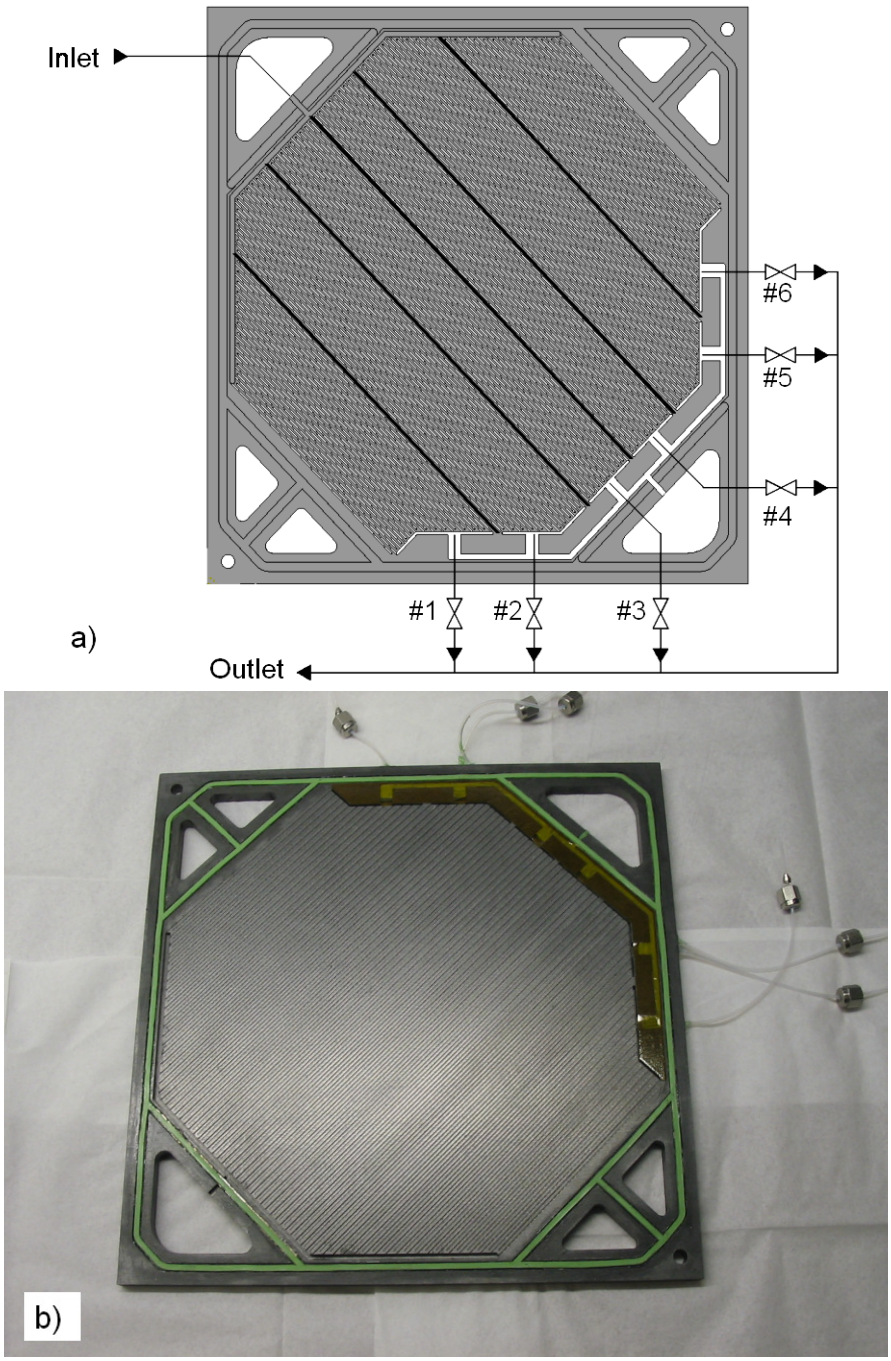

Figure 2.21 – (a) Schematic and (b) picture of the interdigitated cathode plate.

2.2.1.2 Cathode serpentine flow field plate

The serpentine flow field (280 cm^2 active area) was also divided into six separate sections as shown in Figure 2.22. Table 2.6 shows the specific parameters of this flow field channel. The channels of this flow field were designed such that all adjacent channel areas are isobaric in order to prevent gas shorting. The sections

corresponding to valves 1 and 6 each have an area of 46.6 cm^2, the area for each of the sections controlled by valves 2 and 5 is 47.2 cm^2, and the last two sections (valves 3 and 4) each have an area of 46.2 cm^2.

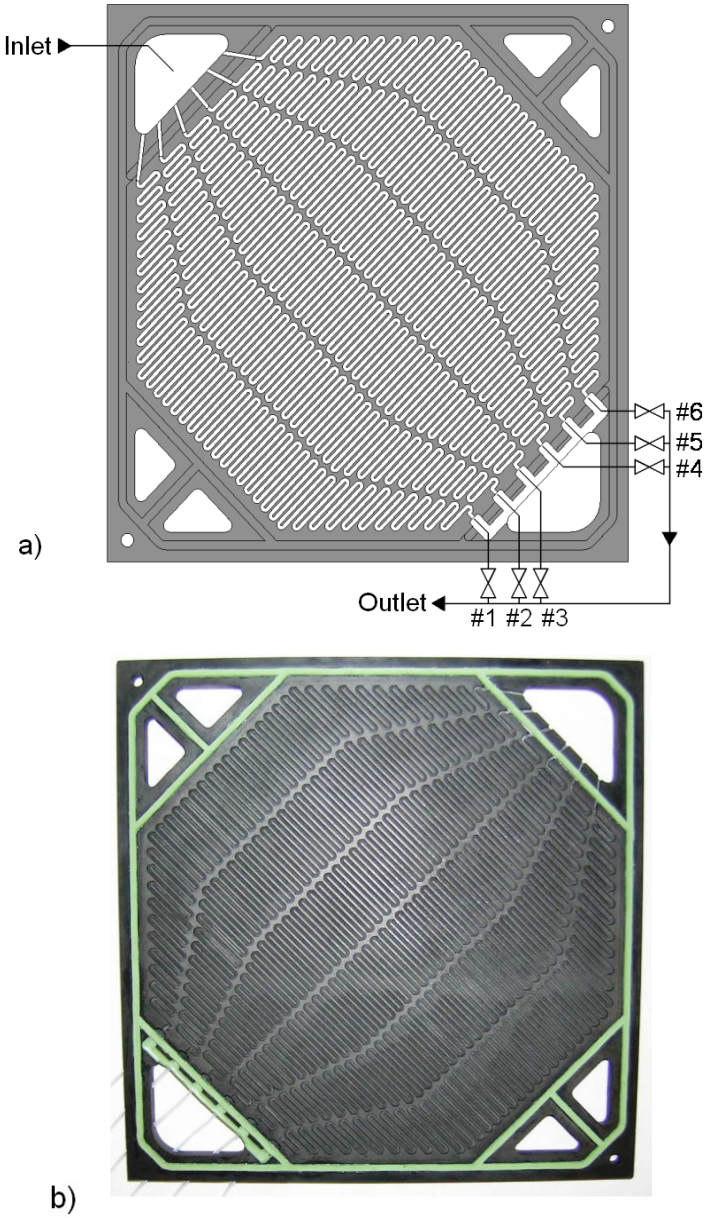

Figure 2.22 – (a) Schematic and (b) picture of serpentine flow field plate.

For the fuel cell stack, Figure 2.23 shows a schematic of how the cells and the external valves were connected. In this case just six valves were used (one for each flow field section) and each section of each cell was connected together to its corresponding valve.

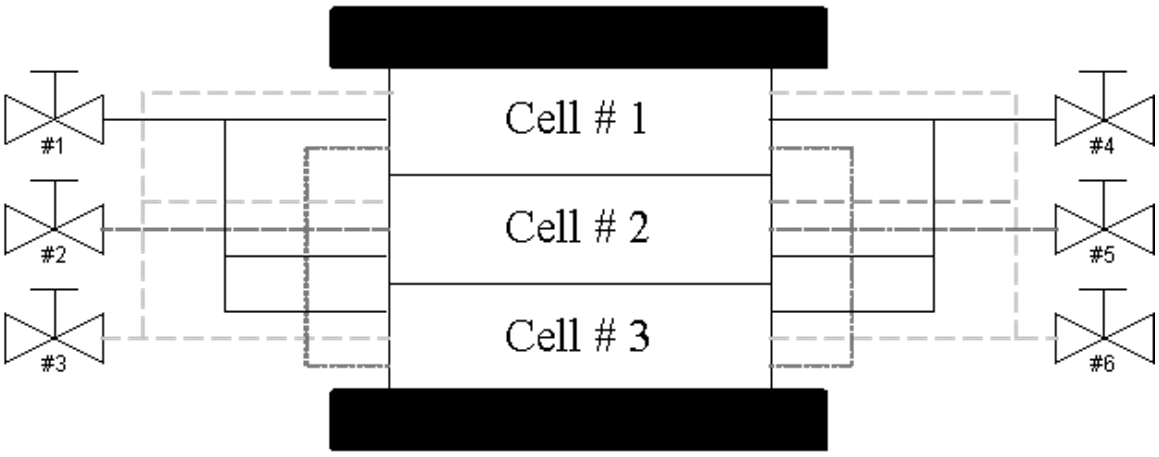

Figure 2.23 – Schematic of the setup of the fuel cell stack with external valves.

2.2.2 1 kW Ballard fuel cell station

All experiments discussed in Chapter 6 were performed using a Ballard 1 kW test station, custom designed and built by Ballard Power Systems (see Figure 2.24). This test station was manually controlled and could provide accurate control of the reactant pressures and gas flow rates for both the fuel and the oxidant gases. It also regulated the temperature of the DI water used as a coolant and as part of the internal humidification system of the fuel cells. The flow rate of the DI water was constant at all times. The cell temperature was characterized by the temperature of the oxidant out stream that was also equivalent to the coolant out temperature. This manual station also had a load bank used to draw current from the cell and a chart recorder for voltage measurements.

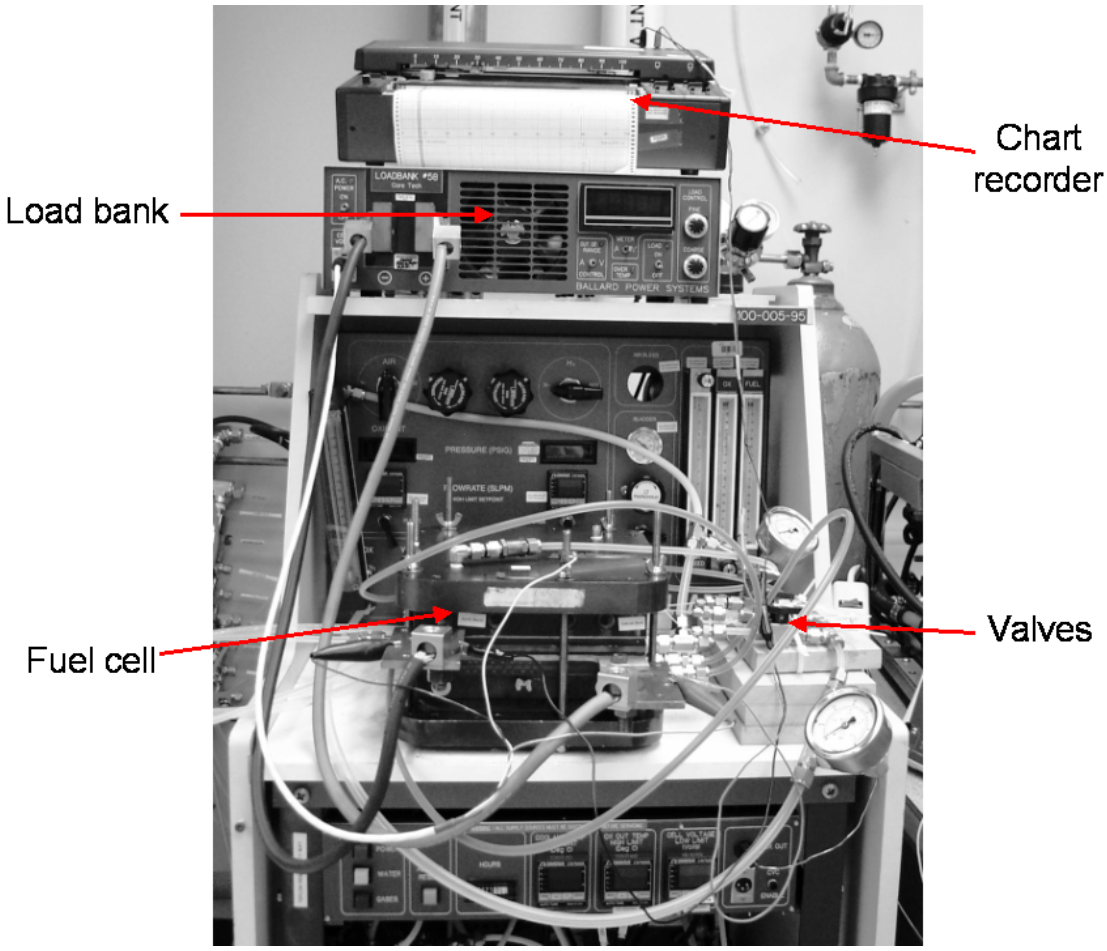

Figure 2.24 – Picture of the Ballard Mk 5 fuel cell station used for fuel cell testing.

2.2.3 Experiments at low gas stoichiometries and low power densities

Most of the experiments performed in Chapter 4 are explained in detail in this section. The fuel cells used for these tests were the Ballard Mk5 cells explained in Section 2.2.1. The fuel cell testing for most of the single cell cases was carried out at 75 ℃, the pressure for both reactant gases was 206.8 kPag (30 psig), the hydrogen stoichiometry was kept constant at 1.5, and the air stoichiometry was varied in the experiments. It is important to note that for the serpentine flow field certain operating conditions had to be modified in order to complete the tests successfully (details of these changes are explained in Section 6.3.3) (e.g., lower air/H_2 stoichiometries). The main experimental test procedure was to run the cell at low power (50–100 mA cm^{-2}, based on the total active area), with an air stoichiometry of 2.0 and with all the valves open. Then, the air stoichiometry was changed to lower values (≤1.5) until either significant performance loss and/or voltage instability was observed. At this

point some active area sections were closed down until performance and/or voltage stability were recovered.

In order to observe that the system shown in Chapter 6 also works in a fuel cell stack, the stack was tested with an overall cell temperature of 60°C, which is lower than the humidification temperature of the reactant gases (75°C). Thus, the gases were saturated and condensation was present in the cell. This resulted in instability of the overall performance of the cell as a result of the water condensation, i.e., flooding. The pressure of both reactant gases was the same as for the single cell testing (30 psig), the hydrogen stoichiometry was kept constant at 1.5, and the air stoichiometry was varied in the experiments. For these tests, once the stack was running and voltage instability was observed, certain sections/areas in each cell of the fuel cell stack were closed in order to observe the influence on the stack's overall performance.

3 APPLICATION OF WATER BARRIER LAYERS FOR IMPROVED DURABILITY AND WATER MANAGEMENT AT LOW HUMIDITY CONDITIONS[3]

3.1 Introduction

Large-scale commercialization of proton exchange membrane fuel cells (PEMFCs) faces a number of challenges including efficiency, cost, reliability, and durability [202-204]. In addition, a number of applications (e.g., portable back-up power, material handling, automotive, etc.) require these fuel cell systems to perform efficiently with restricted space limitations [62,205]. Therefore, it is critical for fuel cell systems to perform at conditions in which additional equipment (i.e., balance of plants) can be significantly reduced. One way of performing this task is to run the system at reduced or zero relative humidity (RH) conditions. This will eliminate the use of humidification systems currently used to humidify the reactant gases in order to maintain the necessary hydration level inside the membrane electrode assembly (MEA) for proton conductivity [206]. These humidification systems not only require heat and water supplies, which decreases the overall power density and efficiency of the system, but also account for a significant fraction of system's volume, weight, and cost. However, removing these systems is challenging because the durability and reliability of the overall fuel cell system are normally adversely affected.

It is a well-known phenomenon that the performance of a typical PEM fuel cell deteriorates when dry gases are used due to the drying of the membrane, which increases the ohmic resistance and reduces the hydrogen proton flux from the anode to the cathode [207]. Long exposure to these harsh conditions has a direct impact on the fuel cell's overall performance, thus, compromising the longevity of the fuel cell. Recently, there have been many research studies investigating the effects of dry conditions on hydrogen fuel cells. It has been shown that with dry feed, irreversible losses due to damage of the membrane and catalyst layers are created

[3] A version of Chapter 3 has been published:
Blanco M, Wilkinson DP, Wang H. Application of water barrier layers in a proton exchange membrane fuel cell for improved water management at low humidity conditions. International Journal of Hydrogen Energy 2011;36:3635-48.

that can potentially reduce the fuel cell stack lifetime expectancy and increase the probability of failure [208-210]. These irreversible losses mainly occur at the cathode side since the cathode humidity has a stronger impact on the membrane's resistance [211]. This indicates that the diffusion of water through the membrane is a dominant process for water transport inside the MEA [212]. In addition, the dehydration rate inside the cell increases significantly with increases in cell and gas temperatures, large flow stoichiometries, and low gas pressures [143,207,213,214]. Another component that is greatly affected with dry gases is the cathode catalyst layer in which the ionic, charge-transfer, and mass-transfer resistances increase when proton transport and humidity levels at the catalytic sites are reduced [205,207].

In order to improve the cell performance at dry conditions different approaches have been proposed. As explained in Section 1.4.1.2.2, self-humidifying proton exchange membranes have been demonstrated and have achieved improved performance with dry gases [44,45]. However, the manufacturing process for these membranes is very complex because they contain Pt or metal-oxide catalyst particles. Addition of Pt in the membrane increases the system's overall cost. Another approach to improve the cell performance and avoid dehydration at dry conditions is to design gas diffusion layers (GDL) with microporous layers (MPL) (or water management layers) with low hydrophobicity [143]. In addition, the MPLs can also be designed with PTFE concentration gradients along the GDL's area in order to change the hydrophobicity of the layer [215]. More details on MPLs are given in Section 1.4.2.2.3.

Self-humidifying can also be achieved through the use of water absorbent wicks that can be located near the inlet and outlet areas of the flow field(s) to facilitate absorption of excess water and to humidify the dry gases that enter the channels eliminating the need for a humidification system [68-71] (see Section 1.4.1.2.3). Some of the wicking materials used are: porous polyester fibers, polyvinyl alcohol sponges, absorbent cotton cloth, absorbent cotton paper, and porous stainless steel sheets. As stated in Section 1.4.1.2.3, porous flow field plates have also been

proposed as mechanisms that improve the self-humidifying capabilities of the cell with dry conditions [62,64,67].

Different flow field designs, mostly for the cathode plate, have been demonstrated as possible solutions for fuel cell operation with dry reactant gases. Qi et al. [216] designed serpentine flow channels with two inlets and two outlets for both the anode and cathode gases. One inlet was located near one of the outlets; thus, the exiting gas stream would humidify the dry gas entering the plate. In general, for fully humidified operation the parallel flow field design is considered to have a number of drawbacks related to flow distribution and water management. However, at dry conditions this design provides better performance and uniform distribution of water activity, ionic conductivity, and current density over the active area [217]. Direction of the flow fields, as shown in Section 1.4.1.2.3, including the coolant channels, of a fuel cell also influences the overall water management and performance of the cell. Wilkinson et al. [33] operated a fuel cell successfully with dry gases by using the cathode and coolant flow field in co-flow and the anode in counter-flow. In addition, a co-flow configuration between the anode and cathode channels has been proven to deteriorate the performance at dry conditions since the water content of the membrane is very low in the inlet region [188].

In this chapter, it is shown that at dry (no humidification) conditions the MPL improves cell durability compared to a GDL without an MPL. However, GDLs with an MPL still have a serious issue when operating at low humidity conditions for long periods of time. Therefore, a method to increase the water accumulation in the cathode GDL and catalyst layers in order to improve the cell durability at low humidity conditions is presented. This is achieved by placing non-porous perforated materials between the cathode flow field channels and the GDL. The impact of perforated sheets on the performance and durability of PEM fuel cells was examined at low humidity conditions and results are presented. GDLs with and without microporous layers (MPL) were used. This analysis is performed using polarization curves, voltage stability data, and measurements of membrane resistance, pressure drop, and water transport rates.

3.2 Experimental

The details of the fuel cell hardware, proton exchange membranes and catalyst layers, and testing equipment used can be found in Sections 2.1.1.1, 2.1.1.2, and 2.1.2, respectively. For this chapter, the anode GDL was a Sigracet® 25DC carbon fiber paper from SGL Carbon. For the cathode side two different GDLs were used: Sigracet® 25BC and 25BA. Section 2.1.1.3 and Table 2.2 give more details regarding these GDLs. The description of the perforated metal sheets used is in Section 2.1.1.4, Figure 2.4, and Table 2.3. All the perforated sheets used in this chapter were 0.05 mm thick.

For the various polarization tests performed, the single fuel cell assembly was compressed to 792.9 kPa (115 psia), the gases were pressurized to 206.8 kPag (30 psig) at the inlet, and the air and hydrogen stoichiometries were kept constant at 2.0 and 1.5, respectively. Every MEA was initially conditioned following the protocol explained in Section 2.1.3.1. For all the polarization performance tests, the temperatures of the gases and the fuel cell were kept constant at 75 °C. The dew point temperature for both gases was kept constant at 45.4 °C, which corresponded to a relative humidity (RH) of 25% (i.e., low humidity conditions). A dew point temperature of 75 °C, which corresponded to 100% RH (i.e., fully humidified conditions), was used just for the tests analyzed in Section 3.3.1. The protocols used for all the polarization measurements are explained in detail in Section 2.1.3. The pressure drop on both the anode and cathode sides was also measured and the details regarding these measurements are found in Section 2.1.3.5.

In order to understand how the perforated sheets affect the water transport capability of the cathode GDL, the water transport rates of different MEA configurations were estimated using an experimental technique explained in Section 2.1.4.

For the durability tests, it was desired to use parameters that would accelerate the deterioration of the fuel cell performance at dry conditions. For these tests we operated the fuel cell at a current density of 1000 mA cm^{-2} because this current has been shown to accelerate degradation [203,218]. In addition, both reactant gases were introduced with no humidification, the cell and gas temperatures were

increased to 75 °C, and the pressure of the gases were lowered to 90 kPag (around 13 psig inlet pressure). Lower pressures and higher temperatures in the flow field channels allow the gas stream to carry more water vapor, thus, drying the cell faster [28,29]. More details regarding how these specific conditions were chosen are provided in Section 3.5. A higher current density could have been used in order to accelerate degradation even further, however, it was desired to keep the resulting cell voltage between 0.3 to 0.6 V since the peak powers for most fuel cell applications are found within these voltage ranges [5].

3.3 Results and discussion

3.3.1 Effect of low humidity conditions on fuel cell performance

In order to compare fuel cell performance at low humidity conditions and how they affect the cell performance, two MEA configurations commonly used in fuel cells were tested (see Figure 3.1a). Two different operating conditions were used: 100% RH and 25% RH. The main difference between the two cathode GDLs is that the 25BA does not have an MPL whereas the 25BC does. The anode GDL used was the same for both cases (i.e., 25DC). At 100% RH, there is a significant voltage difference between the GDLs with and without an MPL, in the current range of 500 to 1800 mA cm^{-2}. This indicates that the presence of an MPL on the cathode side has a major role on managing the water in PEM fuel cells, and increases the cell performance by reducing the liquid-water saturation in the GDL pores and active sites in the catalyst layer, and enhancing oxygen diffusion. At higher flow rates, i.e., current densities higher than 1800 mA cm^{-2}, the performance difference between the two GDLs is no longer detectable. It is conjectured that for the 25BC GDL this is the result of membrane dehydration due to the combination of higher flow rates, because of higher currents, and the use of the MPL to remove the product water. On the other hand, at these high current densities the gas flow rate is high enough for the 25BA GDL to remove sufficient water towards the flow field plates. This opens the path for the gases to diffuse through, and helps maintaining enough water content near the membrane to keep it hydrated.

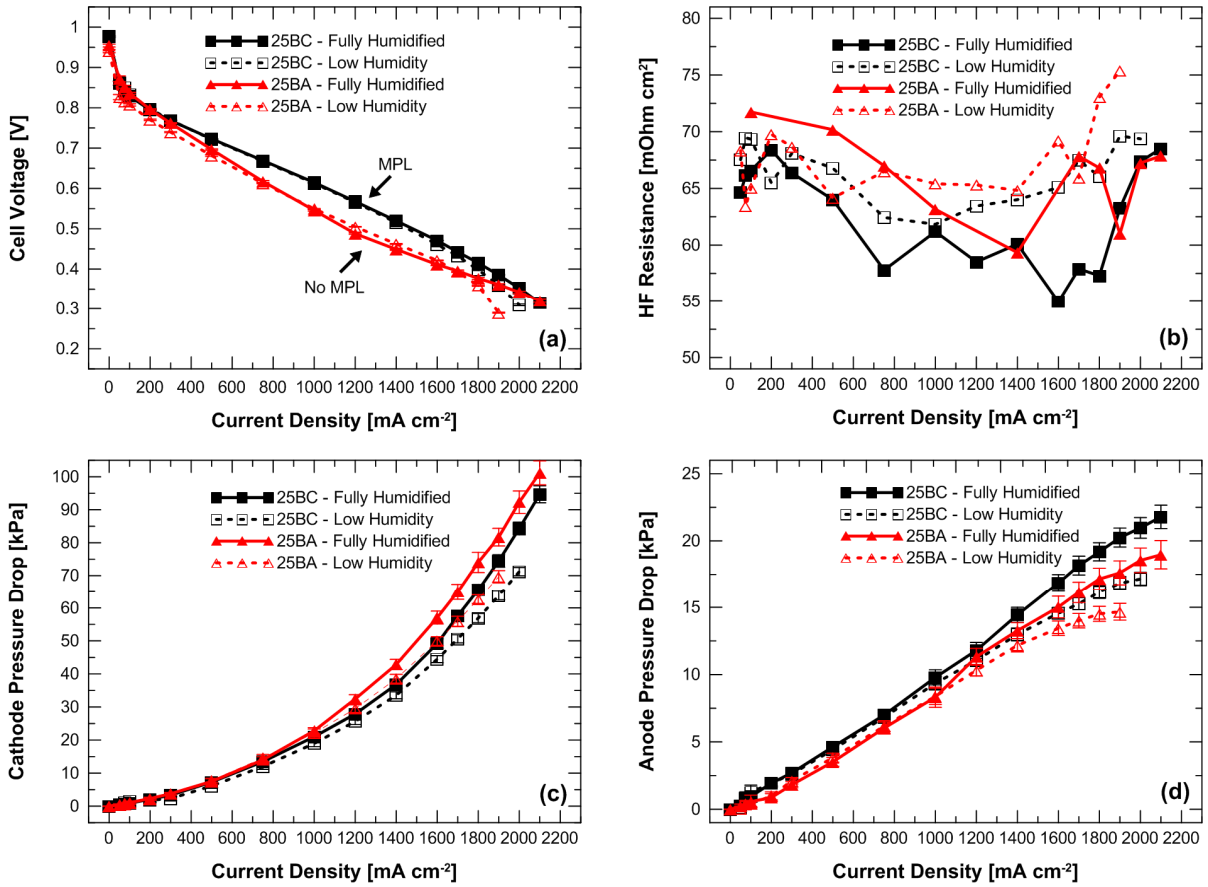

Figure 3.1 – (a) Cell voltage, (b) high frequency resistance, (c) cathode pressure drop, and (d) anode pressure drop versus current density for PEM fuel cells with two different GDLs at fully humidified conditions (100% RH) and low humidity conditions (25% RH). 25BA and 25BC refers to SGL 25BA (GDL without MPL) and SGL 25BC (GDL with MPL), respectively. The anode GDL for all cases was 25DC (with MPL).

At 25% RH, the performance difference between the two GDLs is similar to that in the 100% RH condition, however, at high current densities the GDL without MPL cannot match the performance of GDLs with MPL at low humidity conditions. This indicates that at low humidity conditions the MPL also enhances water distribution between the GDL and the catalytic sites, which allows for the hydration of the membrane. The cell's high frequency resistance data also support these observations (Figure 3.1b). At low humidity conditions (25% RH) and high flow rates, the HFR is lower for the case with MPL than without MPL (68 vs. 76 mOhm cm^2 at 1900 mA cm^{-2}), which indicates that the membrane is more hydrated when the MPL is present.

At current densities higher than 1000 mA cm^{-2}, the cathode pressure drop for the 25BA GDL is greater than that of the 25BC GDL (with an MPL) for both operating conditions (see Figure 3.1c). This could be a sign of less water accumulation in the flow field channels when the 25BC is used. In addition, the anode pressure drop for the 25BC is 13 to 17% (at 100% RH) and 7 to 14% (at 25% RH) greater than that for the 25BA GDL due to the positive impact that the MPL has on the water crossover from the cathode to anode side of the fuel cell (see Figure 3.1d).

For repeatability, the polarization measurements were performed three times. In all the cases, the voltage differences (at specific current densities) between each repetition were within 15 mV, which was considered acceptable. To operate for longer periods at dry or low humidity conditions, it is important for the membrane to stay hydrated as long as possible without affecting the diffusion paths of the reactant gases. Figure 3.2 shows how the fuel cell with 25BA and 25BC cathode GDLs behave when operated at a constant current density of 1000 mA cm^{-2} at dry (no humidification) conditions. As observed, the GDL with MPL allows the fuel cell to operate for a longer period of time. In fact, it appears that the MPL acts as a water barrier layer and this keeps the high frequency resistance low, thus, improving the membrane hydration (see Fig. 3.2b). In the case of the 25BA CFP, the resistance is significantly greater, which indicates membrane and catalyst layer dehydration (see Section 2.1.3.4).

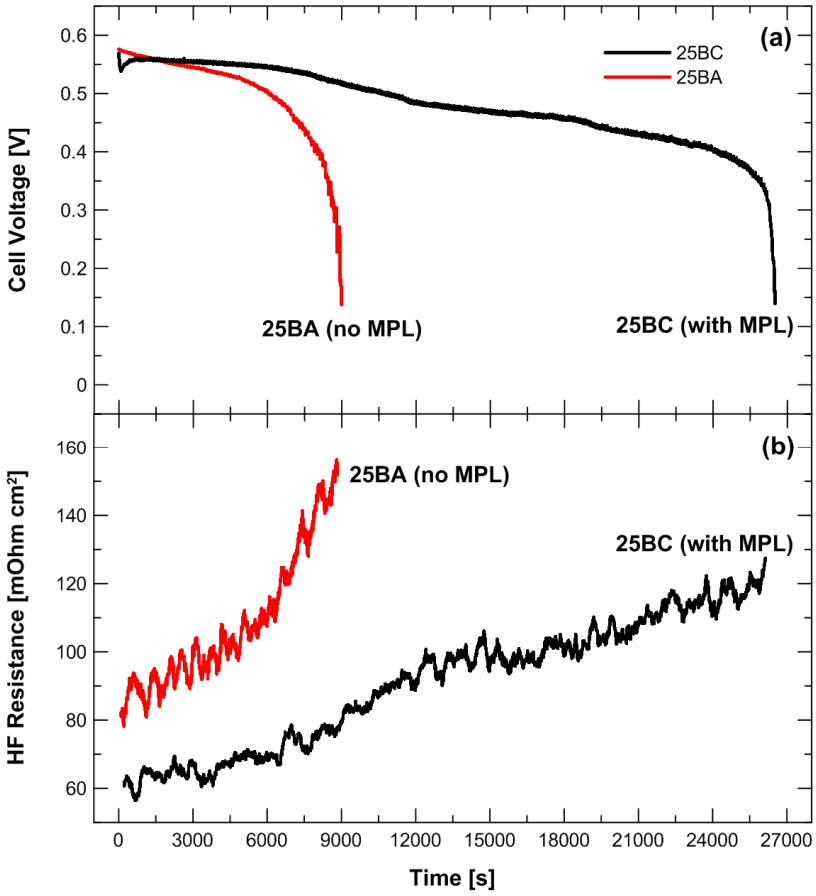

Figure 3.2 – (a) cell voltage and (b) high frequency resistance versus time. For these tests the gases and cell temperatures were 75 °C, the pressure for both inlet reactant gases was 70 kPag (approx. 10 psig), the gases were dry (no humidification), the air/hydrogen stoichiometry ratio was 2.0/1.5, and the cell was kept at a constant current density of 1000 mA cm^{-2}. 25BA and 25BC refers to SGL 25BA (GDL without MPL) and SGL 25BC (GDL with MPL), respectively. The anode GDL for all cases was SGL 25DC (with MPL).

Based on the positive effect that the MPL had on the performance under dry conditions, it was decided to look at a barrier layer approach for water management under dry and low humidity conditions. As explained in Section 1.4.1.2.2, barrier layers have been used in other applications such as direct methanol fuel cells (DMFCs) to reduce transport of species [48,219-221]. This could also be a useful approach for PEM fuel cells. Graftech International claims to produce perforated graphite sheets that can be used as gas diffusion barriers and that could improve water management inside the fuel cell at dry or low humidity conditions [47]. Unfortunately, to the best of the author's knowledge, there are no published results regarding this. We tested a number of perforated graphite sheets from Graftech; however, the results were inconclusive due to the mechanical issues found with

these films. It was found that each graphitic sheet deformed during testing and intruded into the cathode flow field channels. Thus, causing significantly higher cathode pressure drops (40-50% higher than the 25BC CFP case) that affected the gas and liquid transport inside the cell. This caused questionable observations. In addition, these sheets broke very easily after each test and it was nearly impossible to remove them without damaging them when disassembling the fuel cell. A summary of these results and findings are shown in Appendix D.

3.3.2 Effect of perforated sheet arrangement inside the MEA

The effect of the location of the perforated sheets in the MEA as water barriers was examined. The following GDL and perforated sheet (1 mm dia. holes and 0.05 mm thick) configurations were tested at dry conditions (25% RH): (i) perforated sheet next to the flow field (FF) and 25BA next to the CCM (FF/1mmPS/25BA/CCM); (ii) 25BA paper next to the FF and the perforated sheet next to the CCM (FF/25BA/1mmPS/CCM); (iii) perforated sheet next to the FF and 25BC next to the CCM (FF/1mmPS/25BC/CCM); and (iv) 25BC paper next to the FF and the perforated sheet next to the CCM (FF/25BC/1mmPS/CCM).

As shown in Figure 3.3, the location of the perforated sheets inside the MEA is critical, since the performance is significantly lower (cannot reach current densities higher than 600 mA cm^{-2}) when they are placed next to the CCM and the GDL is next to the cathode flow field plate. In addition, the standard deviation of the voltage measurements increases dramatically compared to the other configurations (see Figure 3.3b). This appears to be due to increased water accumulation in the catalyst layers.

The best performance is achieved with the perforated sheet placed between the flow field and the GDL. An interesting point is that with the 25BA CFP (near the CCM) the cell experienced a reproducible slight improvement in performance compared to the case with the 25BC (with MPL) material (near the CCM) at higher current densities. The tests with the 25BA CFP (near the CCM) were repeated 3 times and in each repetition the voltage values (at specific current densities) were within 15 mV of each

other. A possible reason for this is that more water accumulates in the catalyst layer, due to the lower porosity of the perforated sheets coupled with the smaller pore size in the MPL.

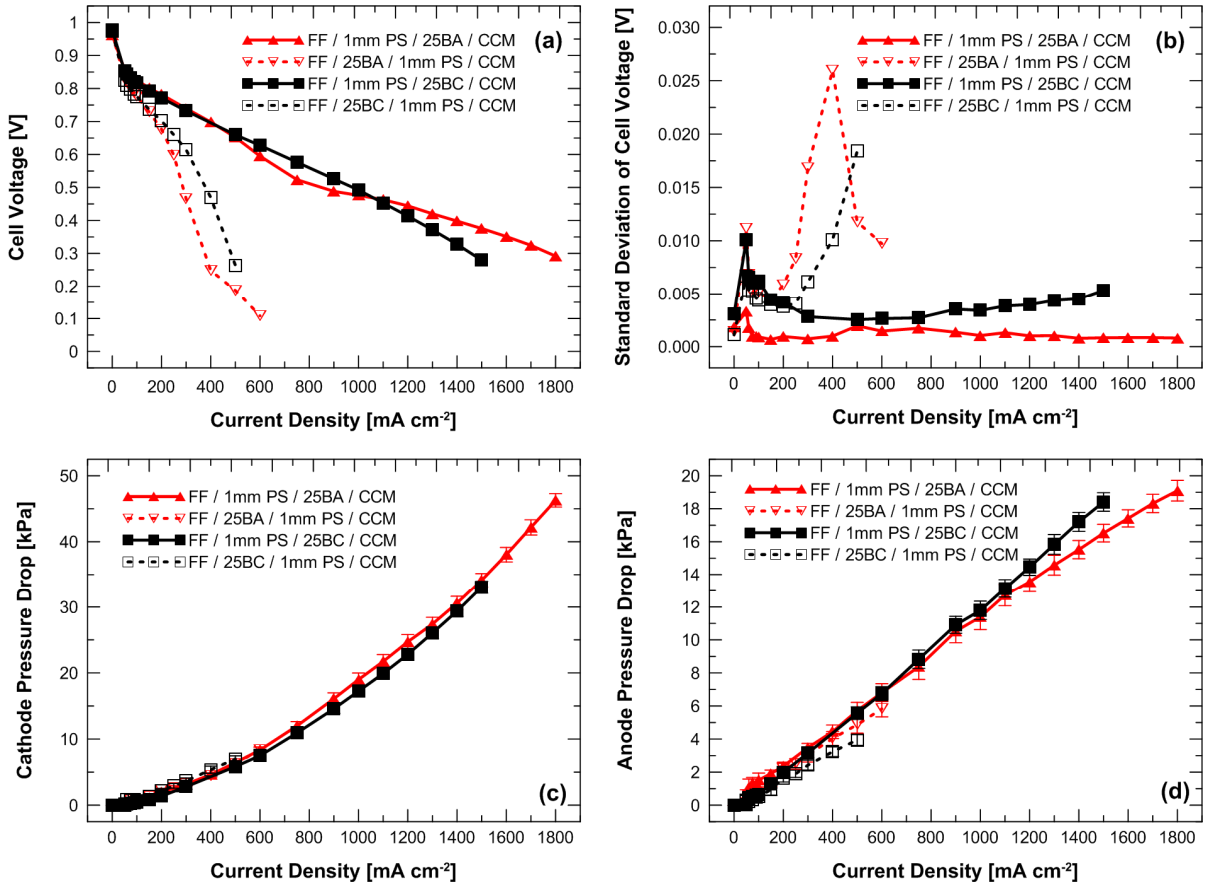

Figure 3.3 – Effect of perforation sheet location on the cathode side of the MEA: (a) cell voltage, (b) standard deviation of cell voltage, (c) cathode pressure drop, and (d) anode pressure drop versus current density. 1mm PS refers to a perforated sheet with 1 mm diameter holes. The thickness of the perforated sheets was 0.05 mm. FF, CCM, 25BA, and 25BC refer to flow field, catalyst coated membrane, SGL 25BA (GDL without MPL), and SGL 25BC (GDL with MPL), respectively. All tests were performed at low humidity conditions (25% RH).

On the other hand, with the 25BA paper, the larger pores help to improve the overall gas diffusion (and distribution) along the catalyst layer while still being able to remove some of the water accumulated in the regions corresponding to the landing areas of the perforated sheet. It is important to note that in the case of the baseline tests (see Section 3.2.1), at normal conditions the 25BA had similar performance at high current densities to that of 25BC paper. Differences in performance behaviour have been amplified once the perforated sheets were used with these carbon fiber

papers. Even though the 25BA paper does not have an MPL, it appears that at high current densities and flow rates it is capable of maintaining a better balance between water removal and humidification of the membrane than the 25BC paper. The combination of the greater thickness of the paper and the lower porosity MPL in the 25BC case causes the gas to flow over a longer path, which increases transport distance and resistance. In addition, it can be observed that at drying conditions the voltage stability (i.e., standard deviation) of the cell improves with the 25BA material compared to the 25BC (Figure 3.3b). This further implies that the PS/25BC combination has a less desirable water removal capability compared to the PS/25BA combination.

The pressure drops for the cathode and anode sides in these cases are similar at most current densities (see Figure 3.3c and 3.3d). At large flow rates, the case with the 25BC next to the CCM experiences greater anode pressure drop compared to the case with 25BA next to the CCM. This indicates that there is more water on the anode side when the CFP with MPL was used.

3.3.3 Effect of perforated sheet open area

The main function of the perforated sheets is to help with the water management inside the MEA at dry and low humidity (≤25% RH) conditions. Thus, it is important for the perforated sheets to act as a barrier and increase the amount of water saturation in the catalyst layer, and improve the membrane hydration. However, the effective porosity is smaller than the porosity of the GDLs and this directly affects the oxygen diffusion and overall fuel cell performance of the cell. Therefore, it is vital to use a perforated sheet that maintains water accumulation in the cell and simultaneously allows the cell to maintain an acceptable performance level.

Figure 3.4 shows how perforated sheets with different open areas affect the fuel cell performance with different GDLs. Please refer to Table 2.3 for the details of the different perforated sheets used. All the perforated sheets used in this chapter were 0.05 mm thick. The case with no open area is when the entire active area is covered, and the case with 100% open area corresponds to the situation where no

perforated sheets are used. At low current densities the performance difference between all open areas is lower, since water production is low and reactant transport requirements are not as limiting. However, as the open area decreases and the current density increases, the performance of the cell deteriorates because water saturation in the GDL and catalyst layers creates blockages that hinder the diffusion of oxidant gas. This performance drop becomes more predominant as the rate of water generation on the cathode side of the cell increases. In addition, perforated sheets with lower open area(s) have a greater negative effect when the GDL has an MPL because a greater amount of water accumulates inside the FF and GDL (see Figure 3.4a). The perforated sheets with 34.5 and 66.4% OA showed the least drop in performance. It is important to note that for the case with 100% OA (i.e., with no perforated sheets) the initial performance of the cell is better at all current densities. However, these values represent the cell voltages after just 15 minutes of fuel cell operation, which is not long enough to identify dehydration or degradation issues within the cell. Therefore, a better comparison of durability between commercially available GDLs with and without perforated sheets is presented in Section 3.2.5.

The difference in performance with and without a perforated sheet is not as severe when the CFP does not have an MPL (i.e., 25BA). In fact, with current densities greater than 1000 mA cm^{-2} the performance difference between the 100% OA case and the perforated sheet with 34.7% OA is relatively small (~65 mV). This indicates that there is an optimum open area where a balance between water accumulation at the cathode side and the water forced to the anode due to pressure gradients (greater hydraulic pressure on the cathode side) is achieved. Therefore, a perforated sheet with an open area of around 34.5% can be used for operation at low humidity conditions due to its acceptable performance and capability to enhance water saturation near the membrane.

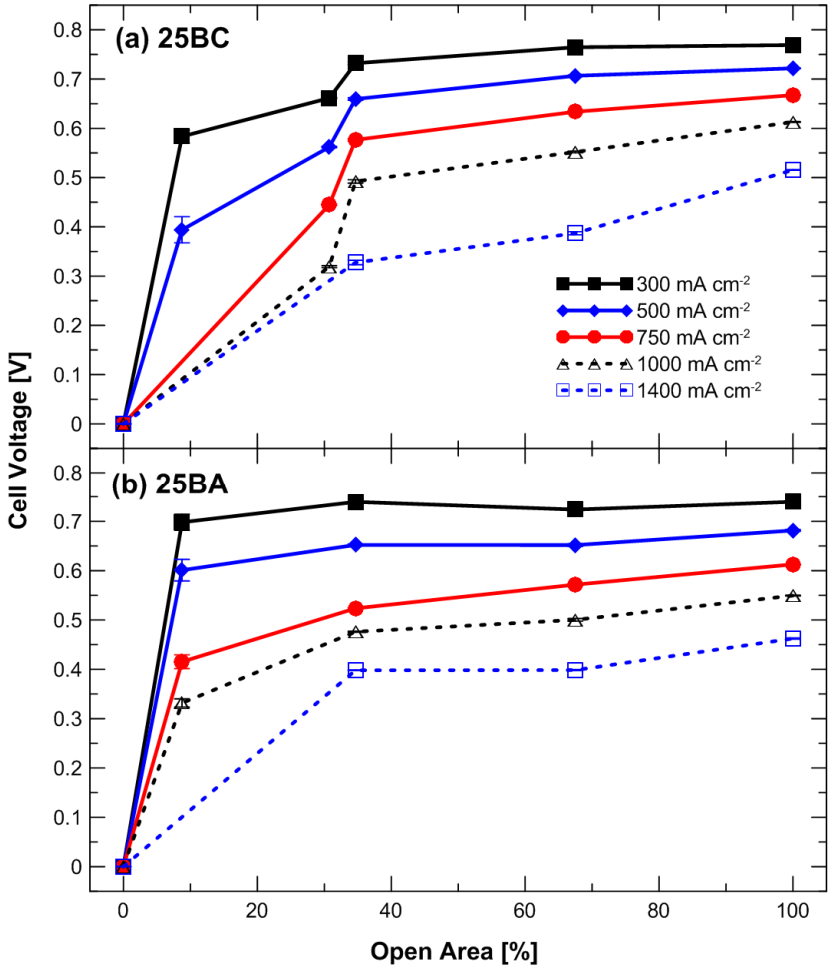

Figure 3.4 – Effect of perforated sheet open area on fuel cell performance at different current densities: (a) perforated sheets with 25BC GDL and (b) perforated sheets with 25BA GDL. 25BA and 25BC refer to SGL 25BA (GDL without MPL) and SGL 25BC (GDL with MPL), respectively. 100% Open area refers to CFP with no perforated sheet. All tests were performed at low humidity conditions (25% RH). The thickness of all the perforated sheets was 0.05 mm.

Figure 3.5 shows the cathode water transport rate for different perforated sheets when placed between the cathode flow field plate and GDL. The different air flow rates correspond to the flows for current densities between 300 and 1400 mA cm^{-2} (at an air stoichiometry of 2). This cathode water transport rate represents the maximum amount of water that can be transported through the cathode GDL configuration. Therefore, an adequate perforated sheet for dry and low humidity conditions should decrease this water flux in order to maintain the membrane hydrated without affecting the fuel cell performance significantly. As the open area of the perforated sheets decreases so does the capability of the cathode side to remove water, thus, more water accumulation is present in the catalyst layer. The

25BC (with MPL) experienced lower water fluxes through the GDL and perforated sheet as expected since the MPL prevents water from being transported across the carbon fiber paper [181]. This is due to the smaller pores that the MPL has compared to a GDL (20 to 200 nm pores for MPLs [157] versus 0.05-100 μm pores for typical CFP GDLs [158,159]), which increase the influence of capillary effects on water transport. In addition, Lu et al. [178] have shown that in GDLs with an MPL the water paths inside the CFP are not interconnected due to the blocking effect of the MPL, which reduces the water saturation inside the GDL and the amount of water breakthrough to the GDL/FF interface.

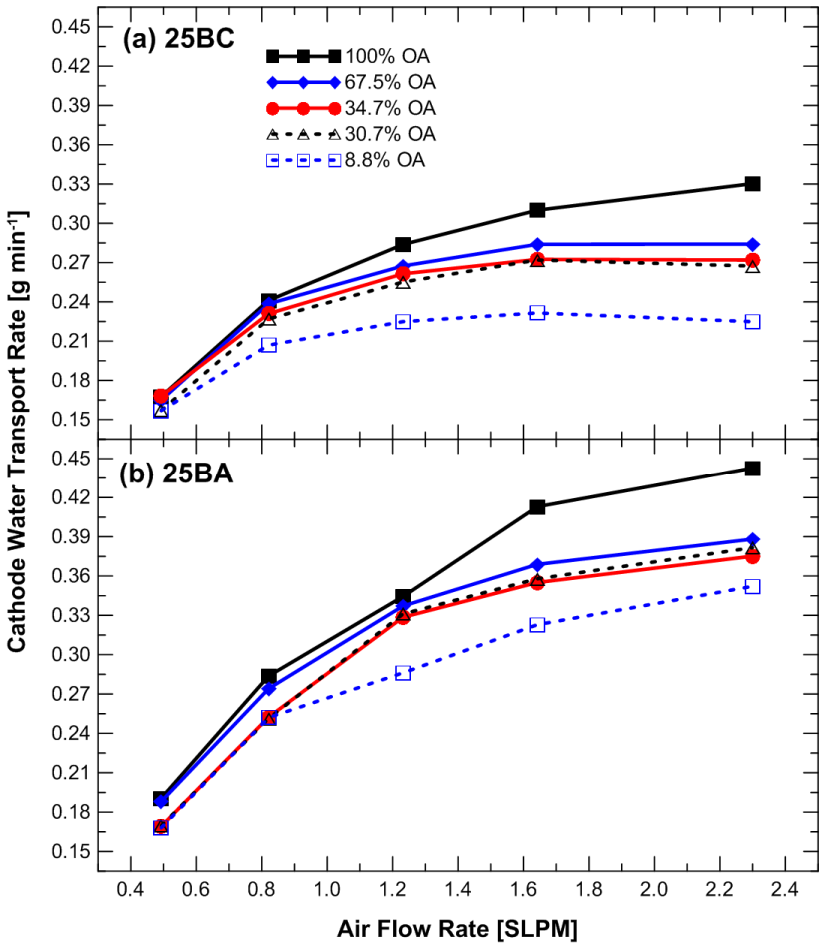

Figure 3.5 – Effect of perforated sheet open area on the cathode water transport rate through the GDL at different air flow rates: (a) perforated sheets with 25BC GDL and (b) perforated sheets with 25BA GDL. 25BA and 25BC refer to SGL 25BA (GDL without MPL) and SGL 25BC (GDL with MPL), respectively. 100% Open area refers to CFP with no perforated sheet. All tests were performed in non-active mode, at low humidity conditions (25% RH) and an air stoichiometry of 2.0. The thickness of all the perforated sheets was 0.05 mm.

With the 25BA paper (see Figure 3.5b) the water transport fluxes were greater than the 25BC paper since no additional MPL layer is present to impede water transport. In this figure it can also be observed that the difference of the water transport rates between the perforated sheets is not as significant as observed with the 25BC CFP. For example, when using 25BC CFPs (Figure 3.5a) the difference between the 67.5% OA and 8.8% OA sheets at a flow rate of 2.3 SLPM is around 0.06 g min^{-1}. On the other hand, this difference is just 0.035 g min^{-1} with the 25BA CFP and the same sheets (see Figure 3.5b). This is due to the water drainage mechanisms that GDLs without MPL have since these CFPs experience more interconnected water paths, which causes a larger number of water breakthrough points in the GDL/FF interface [178]. Thus, more water is transported towards the perforated sheets and flow field channels. It can also be observed that the perforated sheet with the lowest open area reduced the water transport rate across the GDL configuration the most. The perforated sheets with open areas between 30.7 and 67.5% experienced similar water transport rates at all air flow rates.

Based on these observations, perforated sheets with an open area of 34.7% (1 mm dia. holes) were chosen for the experiments discussed in the following sections. Perforated sheets with an OA of 34.7% showed both acceptable performance and a limited water flux towards the cathode outlet, which is important for long-term tests at dry conditions to limit performance loss.

3.3.4 Comparison between perforated metal sheets with 25BC and 25BA gas diffusion layers

Figure 3.6 compares fuel cell performance when a perforated stainless steel sheet is used with 25BC (with MPL) and 25BA (no MPL) GDLs. Figure 3.6a shows that at low current densities (less than 200 mA cm^{-2}) the performance for all cases was similar (±15 mV), with the 25BC GDL showing a slight improvement in performance. In the mid- to high current density range (>400 mA cm^{-2}) the two cases with only CFPs had better performance due to superior gas diffusion and limited water saturation in the catalyst layer. The metal sheets reduced the fuel cell performance; one reason for this is the difference in contact resistances between the stainless

steel sheets, CFPs and flow field plate (as also observed in the HFR values shown in Figure 3.6b). After correcting the cell voltages for ohmic losses, the performance difference between the cases with perforated sheets and without these sheets is reduced. However, there is still a performance difference, which indicates additional mass transport resistances for the cases with the metal sheets that affect the overall oxygen diffusion (see Figure 3.6c). Correcting for the ohmic resistance means that the concentration and mass transport are the main losses in performance, especially at mid- to high current densities. The lower open area with the perforated sheets has a direct impact on the gas diffusion through the GDL towards the catalyst sites.

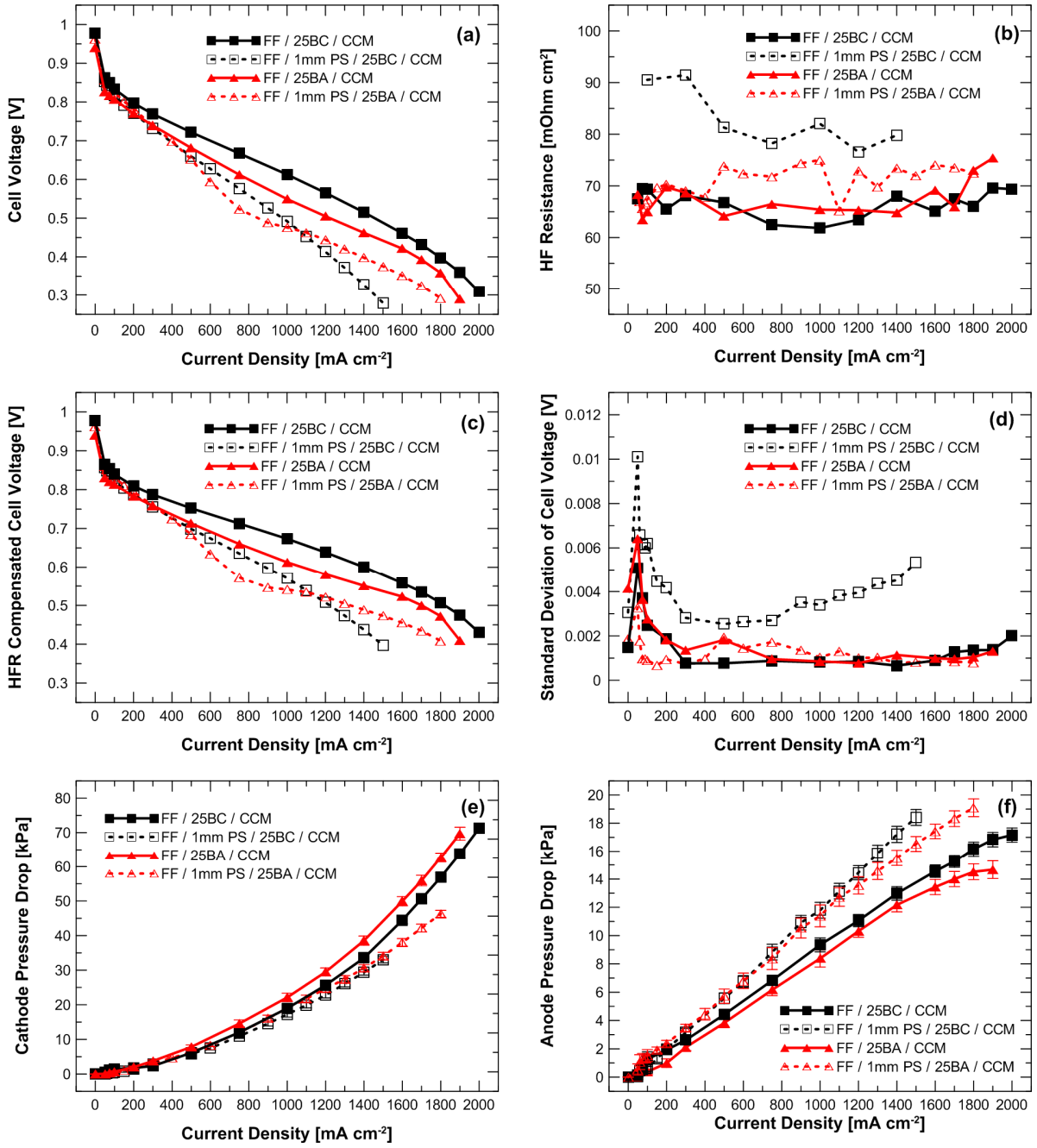

Figure 3.6 – Comparison of stainless steel perforated sheets with 25BC and 25BA GDLs at dry conditions: (a) cell voltage, (b) high frequency resistance, (c) resistance corrected cell voltage, (d) standard deviation of cell voltage, (e) cathode pressure drop, and (f) anode pressure drop versus current density. 1mm PS refers to a perforated sheet with 1 mm diameter holes. The thickness of the perforated sheet used was 0.05 mm. FF, CCM, 25BC, and 25BA refer to flow field, catalyst coated membrane, SGL 25BC (GDL with MPL), and SGL 25BA (GDL with MPL), respectively. All tests were performed at low humidity conditions (25% RH).

The standard deviations of the cell voltage (Figure 3.6d) are related to the voltage fluctuations of the cell and are a function of water accumulation in the catalyst layer,

GDL, and flow field channels. The standard deviations of the perforated sheet with the 25BA GDL are comparable to those of the 25BC and 25BA CFPs by themselves. However, for the case of the perforated sheet with the 25BC the voltage fluctuations were greater (0.004 V vs. 0.001 V at 1200 mA cm^{-2}), suggesting that for this case water accumulation inside the cathode side has increased. Normally, an increase in the voltage standard deviation is a sign of greater water accumulation in the cathode side and a greater cathode pressure drop (due to water in the flow field channels). However, the cathode pressure drop with the perforated sheet and the 25BC GDL decreased compared to the cases without additional layers (see Figure 3.6e). One reason for this observation is that the perforated metal sheets allow for greater water accumulation inside the catalyst layer affecting the voltage fluctuations, but decreasing the amount of water flux towards the flow field channels, thus, decreasing the cathode pressure drop. The cathode pressure drop of the stainless steel perforated sheet with the 25BA was also lower than when no sheet was used.

On the other hand, the anode pressure drops for both perforated sheet cases were around 20% larger compared to the cases with no metal sheets (see Figure 3.6f). This shows that greater amounts of water are being forced from the cathode towards the anode side when these additional layers are used. This effect is similar to the effect of the MPL described in section 3.1. The case with the 25BC CFP and the metal sheet had the greatest anode pressure drop since the water crossover to the anode side is increased when both MPL and metal sheet are used in the same cell. In fact, the anode pressure drop increased by around 32% (at 1400 mA cm^{-2}) compared to the case with the 25BC GDL by itself.

Another important observation is that when the perforated sheet is used with the 25BA GDL, the cell outperforms the case in which the perforated sheet is used with the 25BC GDL at high current densities (>1300 mA cm^{-2}). Even though this combination (1mm PS/25BA) does not have an MPL, it appears that at high flow rates it is capable of maintaining a better balance between water removal and membrane humidification than the other GDL configuration (1mm PS/25BC). The greater thickness of the paper and lower porosity of the MPL in the 25BC case results in a decrease of cell performance since the gas has to travel a longer

distance/path with liquid-water blockage along the way. Thus, the metal perforated sheet with the 25BA material has better water removal capability. However, for longer-term tests at dry or low humidity conditions greater water crossover (cathode to anode) will be more beneficial in keeping the membrane humidified.

3.3.5 Durability tests at dry conditions

Initial polarization tests do not provide enough insight regarding the durability characteristics of a fuel cell after extended periods of operation time. Therefore, long-term tests at a constant current of 1000 mA cm^{-2} were performed with the GDLs and the additional barrier layers (see Section 3.2). Severe dry operating conditions (no humidification, high temperature, low gas pressure, etc.) can accelerate the membrane dehydration and performance degradation even when additional layers used to increase water saturation are present. Temperature, pressure and gas flow rates (i.e., stoichiometries) in a flow field channel affect the ability of a gas stream to remove water vapor. In a cathode flow field channel the total pressure is expressed as:

$$P_{C,total} = P_{Air} + P_{H_2O,vap} \tag{3.1}$$

where $P_{C,total}$ is the total pressure (kPa) in the cathode gas stream (sum of all the partial pressures), P_{Air} is the partial pressure of air (or oxidant) (kPa), and $P_{H_2O,vap}$ is the partial pressure of the water vapor (kPa) in the air stream at a specific temperature. Based on thermodynamic principles, the partial pressures of the gas and water vapor inside the channel are related to the amount of air and water vapor present in the channel. This is shown in the following equation:

$$\frac{m_{H_2O,vap}}{m_{Air}} = \frac{P_{H_2O,vap}}{P_{Air}} \tag{3.2}$$

where $m_{H_2O,vap}$ is the molar flow rate of water vapor (mol s^{-1}), which represents the maximum amount of water that can be carried in a reactant gas stream at a given temperature and pressure, and m_{Air} is the molar flow rate of air (mol s^{-1}) in the flow

field. Equations (3.1) and (3.2) can be combined in order to give an expression for the molar flow rate of water vapor in a gas stream:

$$m_{H_2O,vap} = m_{Air} \frac{P_{H_2O,vap}}{P_{C,total} - P_{H_2O,vap}} \tag{3.3}$$

From this relationship, the average amount of water that can be carried in a gas stream can be calculated. The molar flow rate of air at the inlet is equal to the rate of supply air. At the outlet, this molar flow rate is equal to the rate of supply air minus the amount of oxidant consumed in the reaction. The use of the molar flow rate of water in a gas stream as a driving force in water removal inside fuel cells has also being discussed by St-Pierre [222].

For the rest of the chapter we use molar flux (mol s^{-1} cm^{-2}) instead of molar flow rate, since molar flux is the molar flow rate per unit area, and the specific area used here is the active area of the cell.

For the durability tests the cell was operated at a constant current density of 1000 mA cm^{-2} where the stainless steel sheets had an acceptable performance (17% lower than the 25BC case). Along with the analysis mentioned above, a number of different operating conditions (cell and gas temperature, gas pressure and air stoichiometry) were tested until the fuel cell was not able to hold the desired current and the output voltage was around 0.1 V. The maximum time, t_{max}, is referred to as the maximum time (in hr) that the cell was able to hold the current at the specific conditions and GDL configurations. Figure 3.7 presents how the average molar flux (molar flow rate per active area) of water vapor in the gas stream of the cathode flow field channel affects the difference between the maximum times of the fuel cell with just the 25BC GDL and with the perforated metal sheet and the GDL (i.e., $t_{max,1mmPS+25BC} - t_{max,25BC}$ (hr)). As the water vapor carrying capacity of the gas stream in the flow channels increases (due to the cathode pressure drop, air flow rate, temperature, and relative humidity) so does the dehydration rate in the membrane and catalyst layer ionomer, which in turn decreases the lifetime of the cell. In fact, when the gas stream can remove more than 0.020 µmol s^{-1} cm^{-2} of water vapor in

the flow field channels, the cathode pressure drop is so high that it causes severe membrane dehydration; thus, a desired current density of 1000 mA cm^{-2} cannot be maintained even if the perforated sheets are used. It is important to note that since the gases in these tests were dry, all the water vapor in the air stream that will be carried out originates from the fuel cell reaction (0.005 µmol s^{-1} cm^{-2} at 1000 mA cm^{-2}). The average molar flux shown in Figure 3.7 is based on the case without the perforated sheets since it represents the worse case scenario due to the increase in pressure drop without perforated sheet. However, the difference between the molar fluxes for each case is less than 3%, thus, the pattern observed with the $t_{max,1mmPS+25BC} - t_{max,25BC}$ term still applies with either molar flux.

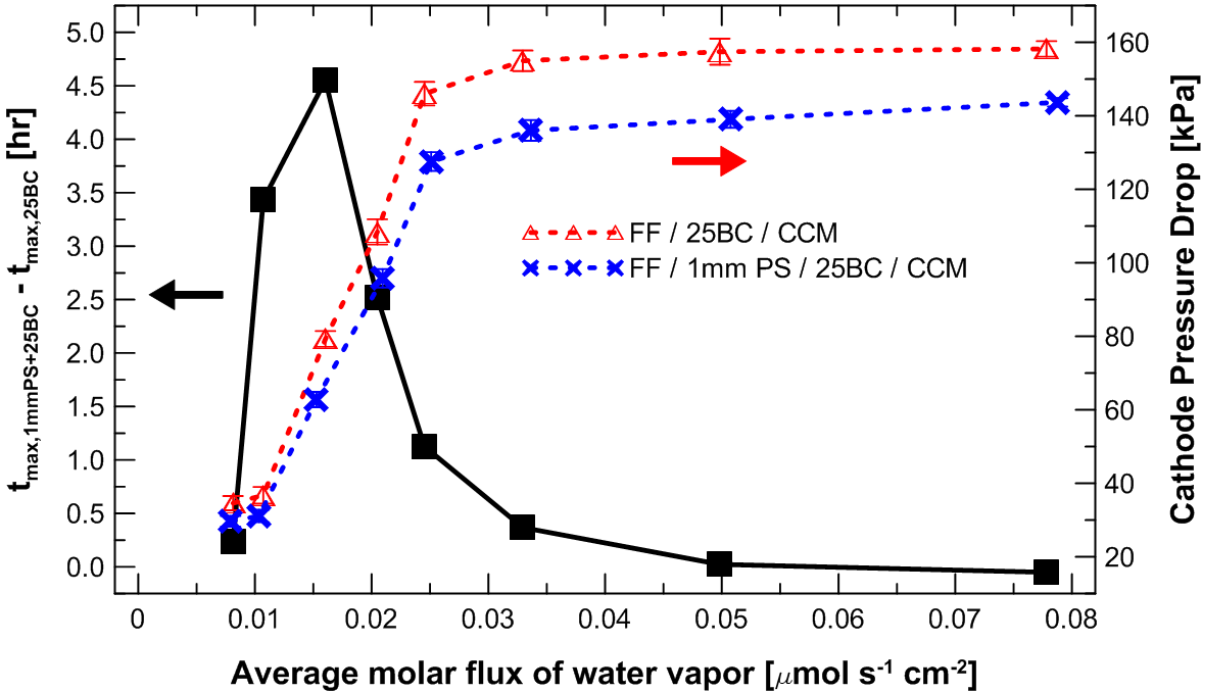

Figure 3.7 – Average molar flux of water vapor that can be removed by the gas stream of the cathode flow field channel versus the cathode pressure drop and the difference between the maximum times, $t_{max,1mmPS+25BC} - t_{max,25BC}$, that the fuel cell was able to hold the current loads at specific conditions and GDL configurations (25BC GDL and 1 mm perforated sheet placed near the 25BC). The average molar flow rate of water vapor is the average molar flow rate between the inlet and outlet streams of the flow field. The tests were performed with dry gases, a constant current (1000 mA cm^{-2}), and different air stoichiometries, gas pressures and temperatures. The anode stoichiometry was 1.5 for all the cases. 1mm PS refers to a perforated sheet with 1 mm diameter holes. The thickness of the perforated sheet was 0.05mm. 25BC refers to SGL 25BC GDL (with MPL).

As it can be observed in Figure 3.7, it is evident that there are conditions that are more favourable than others in order for the perforated sheet to improve the durability of the cell. For these specific tests, the largest difference between the two maximum times for two MEA configurations, $t_{max,1mmPS+25BC} - t_{max,25BC}$, was obtained when the average molar flux of water vapor in the gas stream was around 0.016 μmol s^{-1} cm^{-2}, which was achieved with a gas pressure of 90 kPag (13 psig), air/hydrogen stoichiometry ratio of 3.0/1.5, and gas/cell temperatures of 75 °C. These conditions would be less extreme with an optimized cell design (e.g., flow fields with lower pressure drops) and an optimized perforated sheet (e.g., perforation design based on the flow field channels). For example, in back-up power applications the oxidant stoichiometry is significantly larger (>30 vs. 2) due to the use of cooling fans in order to distribute the air in the stacks. Thus, the flow field used in these fuel cells must have low pressure drops for the cathode channels. Therefore, the optimized design of the perforated sheets should take these parameters and operating conditions into account in order to achieve improved fuel cell durability at dry conditions.

Figure 3.8 presents the durability tests at the above-mentioned conditions, for three cases: a perforated stainless steel sheet with the 25BC GDL, and the 25BA and 25BC GDLs by themselves. The 25BC and 25BA cases showed better initial performance, but both deteriorated quickly so that the current could not be maintained anymore. In addition, the high frequency resistance for both cases increases significantly indicating the decrease of water content in the membrane and catalyst layers (see Figure 3.8b). A decline in water accumulation in the GDL and flow field channels can also be observed with the cathode and anode pressure drops for the 25BC and 25BA cases. Both pressure drops decrease with time because of the lack of water in the MEA and flow field plates (see Figure 3.8c). Barbir et al. [223] also showed similar observations regarding the decrease in cathode pressure drop when reducing the gas temperature humidity. The 25BA had the worst durability since at extreme dry conditions water accumulation is limited inside this CFP and the catalyst layer. On the other hand, the 25BC GDL allowed a slight improvement in water accumulation inside this layer due to the use of the MPL, thus, keeping the membrane and catalyst layers hydrated for a longer time.

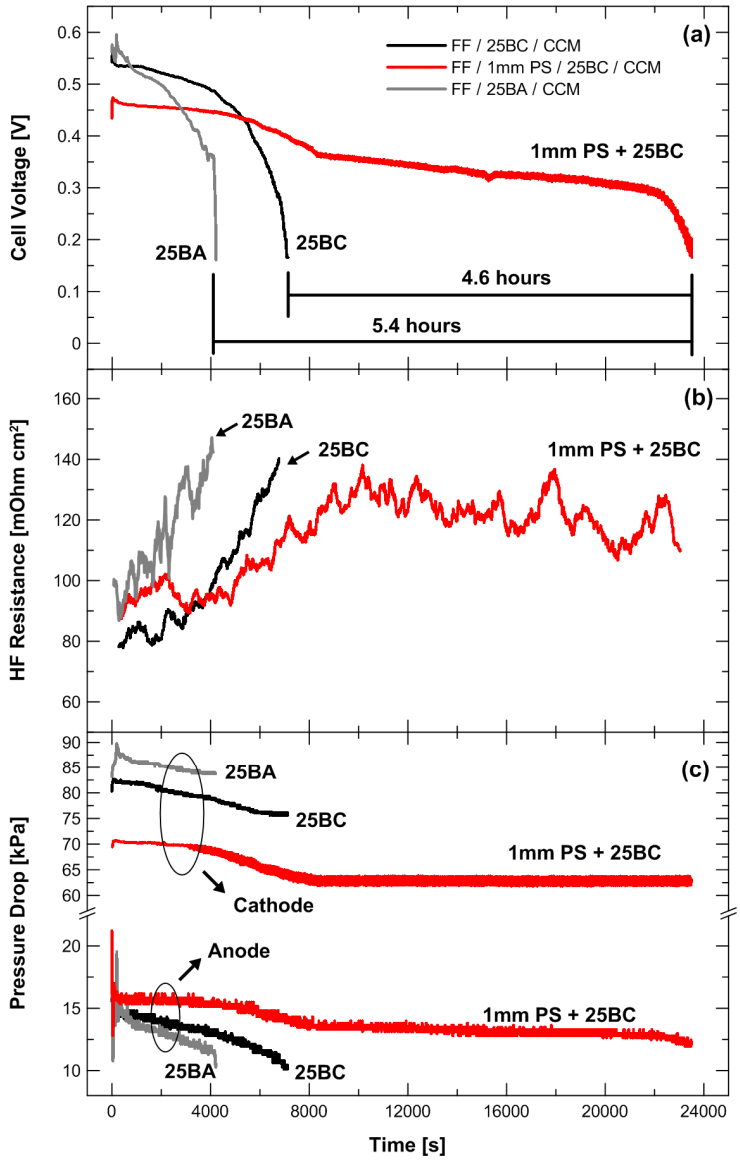

Figure 3.8 – Durability tests with the different GDL configurations at dry conditions: (a) cell voltage, (b) high frequency resistance (running average values), and (c) cathode and anode pressure drops versus time. For these tests the gases and cell temperatures were 75 °C, the pressure for both inlet reactant gases was 90 kPag (approx. 13 psig), the gases were dry (no humidification), the air/hydrogen stoichiometry ratio was 3.0/1.5, and the cell was kept at a constant current density of 1000 mA cm^{-2}. 1mm PS refers to a perforated sheet with 1 mm diameter holes. The thickness of the perforated sheet was 0.05mm. 25BC and 25BA refer to SGL 25BC GDL (with MPL) and SGL 25BA GDL (without MPL), respectively.

The case with the perforated sheet improved the durability of the fuel cell and maintained the set current for approx. 4.6 h and 5.4 h longer than the 25BC and 25BA CFPs, respectively (Figure 3.8a). Although the resistance for the metal sheets (Figure 3.8b) starts higher than for the 25BC case, it does not increase as much in

the first 2 h of the test. After this, the resistance values stay constant throughout the test, which is an indication that the humidity in the membrane and water content in the catalyst layers do not change substantially during most of the test. This can be corroborated with the lower cathode and higher anode pressure drops that the fuel cell experiences with the metal sheet (Figure 3.8c). Thus, less water is accumulated in the cathode flow field, and more is present in the anode flow field channels. In general, we attribute the better durability, when using the perforated sheets, to the greater accumulation of water between the cathode catalyst layer and the membrane, and to the better water cross-over to the anode side. This improvement in the durability (and water management in the cathode and anode sides) of the fuel cell, when an additional layer is placed between the cathode flow field and GDL, can be increased considerably with an optimized design of the cell and the perforated sheet.

3.4 Conclusions

In this chapter we studied the performance and durability capabilities of a PEM fuel cell operating at low humidity to dry conditions. Our results include an experimental comparison between MEAs with and without additional barrier layers used to improve the water management of the cell under these dry conditions. Perforated stainless sheets with different hole diameters, were used in order to understand in detail how each sheet affected the water accumulation inside the catalyst layer and flow field. The following conclusions were drawn:

1. Fuel cells at dry conditions experience a voltage drop due to dehydration of the membrane and ionomer in the catalyst layer. It was demonstrated that a cell at fully humidified conditions (100% relative humidity) has a better performance and lower high frequency resistance values than at low humidity conditions. In addition, the MPL in the cathode GDL improves water management and allows the cell to have a better performance at both normal and drying conditions than the GDL with no MPL.
2. The specific location of an additional barrier layer on the cathode side is important to effectively improve water management at low humidity

conditions. When the metal perforated sheet was located between the flow field channel and the GDL, the best performance, voltage stability, and water crossover from the cathode to the anode were obtained. When the metal sheet was placed between the GDL and the catalyst coated membrane, the water flooding increased significantly, so that current densities greater than 600 mA cm^{-2} could not be achieved.

3. An acceptable additional barrier layer used to improve durability at low humidity conditions must have an appropriate open area so there can be sufficient oxidant transport to the catalyst layer. In addition, it should enhance water accumulation in the GDL and water crossover towards the anode (i.e., reduce water flux from the GDL towards the flow field channels) in order for the membrane and catalyst layer to stay humidified.
4. A perforated metal sheet was tested with the 25BC (with MPL) and 25BA (no MPL) GDLs. In both cases, the fuel cell with the metal perforated sheets showed a lower initial performance mainly due to contact and mass transport resistances. These resistances can be reduced with improved surface treatment and an improved design of the perforations (e.g., shape, size and density) based on the operating conditions and the flow field design used. After all the tests, these metal sheets were still intact and were used a number of times without any mechanical or corrosion related problems.
5. The cell with the stainless steel perforated sheet performed about 5 h longer, at dry conditions and constant current, than the case with just the 25BC GDL. During this time, the perforated sheets were able to keep the humidity of the membrane relatively constant due to the accumulation of water in the cathode catalyst layer and the increase of water crossover to the anode side indicated by higher anode pressure drop.

These results presented are relevant for fuel cell applications in which low humidity or dry conditions are desired in order to reduce the balance of plant costs and parasitic losses, and improve system simplicity. However, it is still necessary to optimize the perforation design (e.g., size, hole density, cross-sectional shape, etc.) and surface treatment of these layers based on the particular application and the cathode flow field design. Although stainless steel was used in this study, other

materials should also be considered based on their electrical conductivities and their machinability and manufacturability.

4 EXPERIMENTAL INVESTIGATION OF THE EFFECT OF CATHODE AND ANODE MICROPOROUS LAYERS IN A PROTON EXCHANGE MEMBRANE FUEL CELL [4]

4.1 Introduction

Water management in PEM fuel cells is a critical parameter that determines the performance and durability of a fuel cell. At humidified conditions the water will accumulate over time in the catalyst layers, porous GDLs, and flow field channels. This accumulation of water causes flooding, which in turn, decreases the performance of the system and can result in critical failure modes [5]. As explained in Chapter 3, water management also requires maintaining the right water balance inside the cell in order to keep the membrane humidified at low to no gas humidification conditions. Microporous layers (MPLs) have been widely used for their capability to improve fuel cell performance and water management. In addition, these layers also enhance the contact resistance between the GDLs and the catalyst layer, and give mechanical support to the catalyst particles.

However, as important as the MPLs are, it is still unclear how exactly the MPL affects both the water and reactant gas transport mechanisms inside the catalyst layers and GDLs. There have been a significant number of studies in recent years focused on understanding and modelling how microporous layers affect mass transport losses and mechanisms inside the fuel cell. Figure 1.19 summarizes the main areas and theories that have been targeted by different research groups regarding the main functions of the MPL. A great emphasis has been given to the concept that the MPL enhances water back-diffusion (crossover) from the cathode to the anode side through the membrane [43,141,180-182]. Through modelling and experimental work, these studies concluded that one of the main methods of water removal when the cathode MPL is present is via the anode side by water back-diffusion. However, there are other studies that contradict this theory and give data

[4] Sections of this work have been submitted for publication:
Blanco M, Wilkinson DP, Wang H. Experimental investigation of the effect of cathode and anode microporous layers in a proton exchange membrane fuel cells.

showing that the overall water found in the anode side does not increase when cathode MPLs are used [46,183-185].

Other work postulates that the MPL increases the water removal from the cathode catalyst layer to the cathode GDL [174-176,185,224], yet others conclude that the MPL has no impact on this mechanism [43,150]. Additional work has been published stating that the MPL improves the water distribution over the active area enhancing the oxygen transport in the catalyst layer [177-179]. Recently, Owejan et al. [186] have identified that the thermal and vapor concentration gradients across the cathode GDL are sufficient for optimal water removal from the catalyst layer in the vapor phase at various current density ranges. In addition, the MPL acts a barrier that does not allow condensed water in the larger pores of the GDL to come back in contact with the cathode catalyst layer, thus, improving gas diffusion over the whole active area.

Most of these studies have concentrated on the effect of the cathode MPL because transport limitations due to gas diffusion and water accumulation are commonly present at the cathode side. However, it is also important to investigate how MPLs used on the anode side affect the fuel cell performance since it is a common practice in industry is to use anode MPLs [187] but only limited studies are found in the literature that discuss its influence [182,186,187].

In this chapter, a series of experimental studies are performed in order to better understand the role of the cathode microporous layer in water and gas transport mechanisms. Perforated metal sheets are used as a diagnostic tool to help understand the effect of liquid water accumulation in the cathode catalyst layer and GDL. Two main areas were investigated: i) the effect of the cathode MPL on water back-diffusion to the anode side and ii) the effect of the cathode MPL on water removal on the cathode side. These observations are achieved through polarization data (with air and heliox as oxidant gases), pressure drop measurements, high frequency resistance data, and the anode water removal (AWR) method. In addition, the effect that the anode MPL has on fuel cell performance and cell voltage stability is also investigated.

4.2 Experimental

The details of the fuel cell hardware, proton exchange membranes and catalyst layers, and testing equipment used can be found in Sections 2.1.1.1, 2.1.1.2, and 2.1.2, respectively. For this chapter, two anode GDLs, Sigracet® 25DC (with MPL) and 25DA (without MPL), were used. For the cathode side, two different GDLs were used: Sigracet® 25BC (with MPL) and 25BA (without MPL). Section 2.1.1.3 and Table 2.2 give more details regarding these GDLs. The description of the perforated metal sheets used is found in Section 2.1.1.4, Figure 2.4, and Table 2.3. All the perforated sheets used in this chapter were 0.05 mm thick in thickness.

The details of the polarization tests are given in Sections 2.1.3.1, 2.1.3, and Chapter 3. Three main operating conditions were tested: fully humidified (100% RH with T_{dp} and T_{gas} = 75 °C); flooding (T_{dp} = 95 °C and T_{gas} = 75°C); and low humidity conditions (25% RH with T_{dp} = 45.4 °C and T_{gas} = 75°C) (see Table 2.5). Polarization tests with heliox (21% O_2 and 79% He) as the oxidant gas were also performed. Heliox was used to give a better understanding of the mass transport effects (and losses) in the fuel cell (see Section 2.1.3.6).

In order to evaluate different GDL configurations without the influence of mass transport losses, the anode water removal (AWR) method was used. Section 2.1.5 explains in detail the steps followed in order to perform these tests. For the work presented in this chapter, all the AWR tests were performed at 1000 mA cm^{-2}.

4.3 Results and discussion

4.3.1 Effect of the microporous layer in the cathode gas diffusion layer

Two different cathode GDLs (with and without MPLs) were tested at three different operating conditions: fully humidified (100% RH), flooding, and low humidity (25% RH). The anode GDL used was a 25DC (with MPL) CFP and it was the same for both cases (and for all the tests presented in this section). Figure 4.1 shows the polarization and high frequency resistance (HFR) results for the two different cathode GDLs. For current densities below 400 mA cm^{-2}, the influence of the MPL is

insignificant for all the operating conditions. This indicates that at low flow rates the water removal capability of the cell is acceptable regardless of the operating condition. However, at current densities greater than 500 mA cm^{-2}, a significant performance difference between the GDLs with and without MPL is observed at all three operating conditions. In fact, under flooding conditions the GDL with MPL has cell voltage values that are 110-112 mV greater than the ones for the GDL without MPL at current densities between 1200 to 1600 mA cm^{-2}. This indicates that the MPL on the cathode side has a major role in the water removal process by reducing the liquid-water saturation in the catalyst layer and GDL, and enhancing oxygen diffusion.

At fully humidified conditions and high current densities (>2000 mA cm^{-2}), the GDL without MPL experiences an improvement in performance, thus, decreasing the performance difference between the two different GDLs. The inset in Figure 4.1 shows in more detail this reduction in performance difference at high current densities (and flow rates). For 25BC GDL this may be the result of membrane dehydration (increase in HFR) due to high flow rates and the use of the MPL for water removal. For the 25BA GDL, the high flow rates enhance the water removal capability, thus, improving the transport paths for the oxygen to diffuse and reach the catalyst layer. At low humidity conditions (25% RH) and high current densities (>1800 mA cm^{-2}), it can be observed that the resistance increases for the 25BA GDL due to membrane dehydration. On the other hand, the 25BC GDL is able to maintain a lower resistance (57 vs. 68 mOhm cm^{-2}) since the MPL allows for better water distribution within the catalyst layer, hydrating the membrane [177] (see Figure 4.1b).

Please note that error bars in the polarization data for Figure 4.1 were omitted for clarity. The largest standard deviation (i.e., error bar) was given by the case without MPL (25BA) at flooding conditions (in the range of 2 mV to 4 mV over the current density range of 1400 to 2100 mA cm^{-2}).

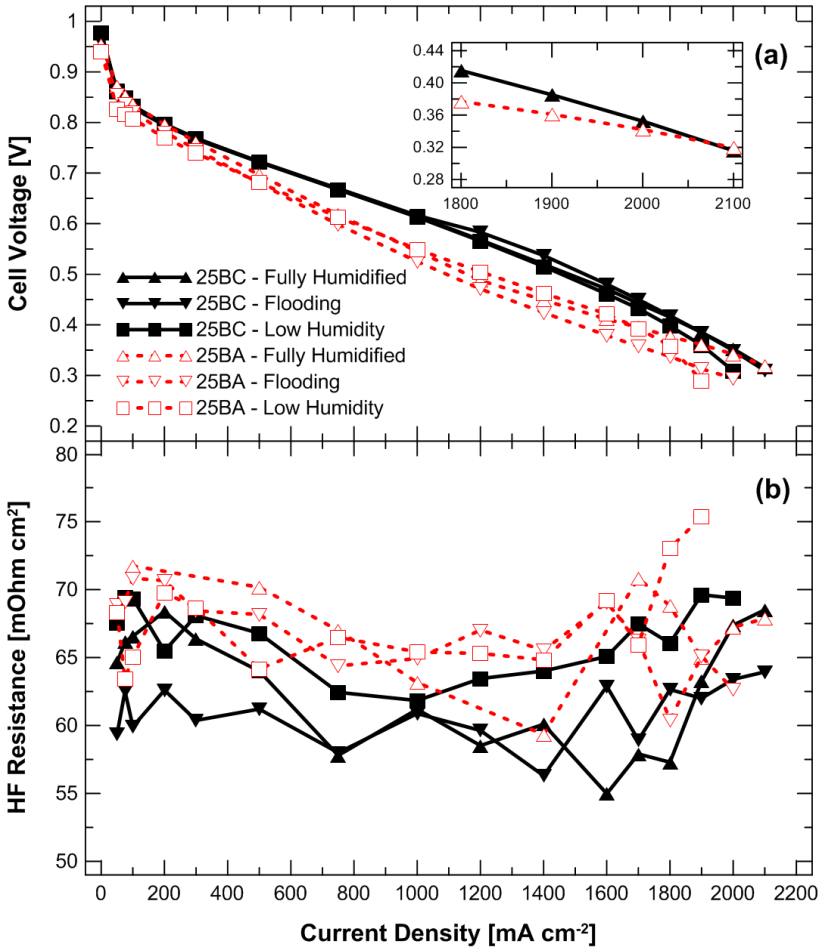

Figure 4.1 – (a) Cell voltage, and (b) high frequency resistance versus current density for PEM fuel cells with two different cathode GDLs at three different conditions: Fully humidified (100% RH with $T_{dp} = T_{gas} = 75$ °C), flooding ($T_{dp} = 95$ °C and $T_{gas} = 75$ °C), and low humidity (25% RH with $T_{dp} = 45.4$ °C and $T_{gas} = 75$ °C). 25BA and 25BC refer to SGL 25BA (GDL without MPL) and SGL 25BC (GDL with MPL), respectively. The anode GDL for all cases was 25DC (with MPL).

Voltage stability is another parameter that is affected when a cathode MPL is used. Figure 4.2 shows the cell voltage for the two GDLs at a constant current density of 1800 mA cm^{-2}. The cell voltage of the 25BA GDL (without MPL) is unstable due to water accumulation in the catalyst layer, thus, affecting the oxygen diffusion. The MPL enhances the oxygen diffusion in the catalyst layer by reducing the liquid water accumulation in this layer. Owejan et al. [186] proposed that the MPL acts as a barrier that prevents condensed water present in the larger pores of the GDL to be able to make contact with the catalyst layer. Thus, by reducing water pooling inside the catalyst layer, the MPL enhances voltage stability.

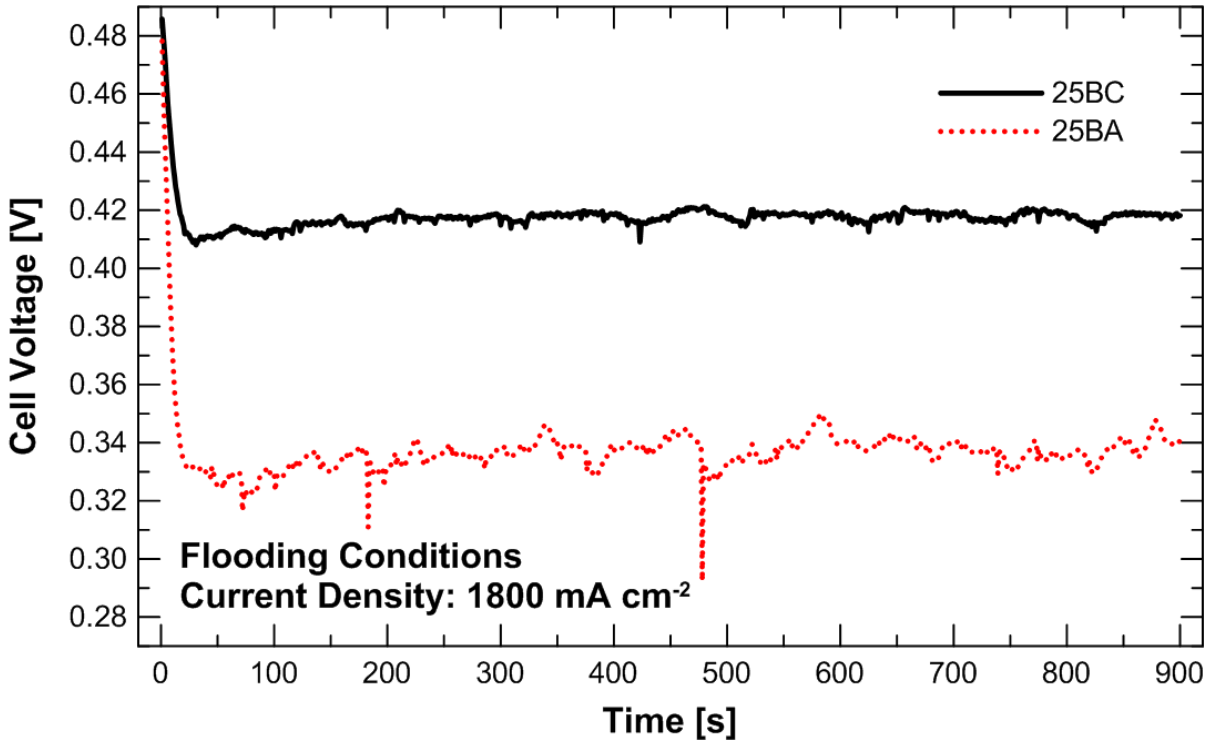

Figure 4.2 – Effect of cathode MPL on the voltage stability at a constant current density of 1800 mA cm^{-2} and at flooding conditions (T_{dp} = 95 °C and T_{gas} = 75 °C). 25BA and 25BC refer to SGL 25BA (GDL without MPL) and SGL 25BC (GDL with MPL), respectively. The anode GDL for all cases was 25DC (with MPL).

Figure 4.3 shows the subtraction of the pressure drops between the 25BC and 25BA cases for both the cathode and anode sides. The raw pressure drop data used for Figure 4.3 are shown in Appendix E. As shown in Chapter 3, the cathode MPL increases the anode pressure drop at all operating conditions, due to the positive impact that the MPL has on the water crossover from the cathode to anode side of the fuel cell (see Figure 4.3). For example, at flooding conditions and high current densities (>1400 mA cm^{-2}) the anode pressure drop for the 25BC GDL is 1 to 4 kPa (10 to 19%) greater than that for the 25BA GDL since the MPL increases the water back diffusion towards the anode side (see Figure 4.3b). The GDL without MPL shows greater cathode pressure drop at the different operating conditions due to water saturation in the GDL and flow field channels (see Figure 4.3a). Therefore, the MPL also has an effect on the reduction of water accumulation inside the GDL and flow field channels on the cathode side. In fact, Lu et al. [178] demonstrated that the

MPL stabilizes the water paths/morphology in GDLs lowering the water saturation in these layers.

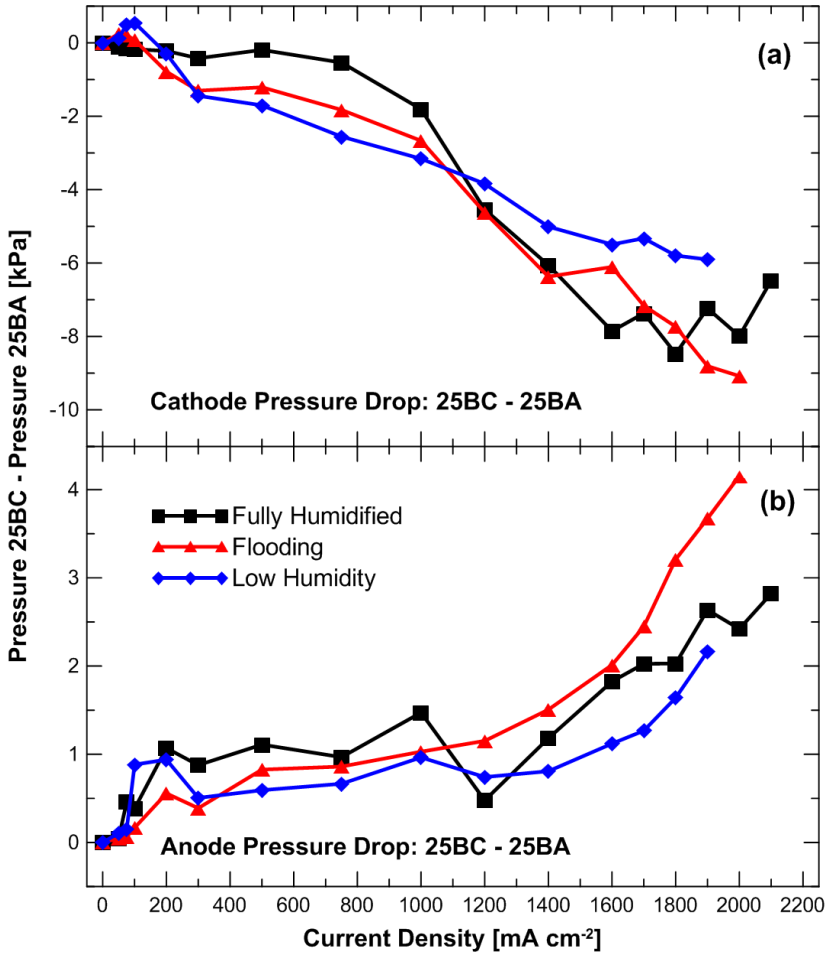

Figure 4.3 – Effect of the cathode MPL on (a) cathode and (b) anode pressure drops at three different operating conditions: Fully humidified (100% RH with T_{dp} = T_{gas} = 75 °C), flooding (T_{dp} = 95 °C and T_{gas} = 75 °C), and low humidity (25% RH with T_{dp} = 45.4 °C and T_{gas} = 75 °C). 25BA and 25BC refer to SGL 25BA (GDL without MPL) and SGL 25BC (GDL with MPL), respectively. The anode GDL for all cases was 25DC (with MPL).

To further investigate the MPL influence in the enhancement of oxygen diffusion in the cathode catalyst layer, polarization tests with heliox (21% O_2 and 79% air) as the oxidant gas were performed at flooding conditions. Heliox reduces mass transport losses inside a fuel cell due to the greater diffusion coefficient of oxygen in helium than in nitrogen (see Section 2.1.3.6). Flooding conditions were chosen since at these conditions greater water condensation occurs on the cathode side of the fuel cell, which creates mass transport issues. Thus, a better comparison between the two GDLs can be observed. Results shown in Figure 4.4 demonstrate that the 25BA

GDL has larger mass transport losses than the GDL with an MPL, especially at current densities higher than 1000 mA cm^{-2}. For example, the mass transport loss (cell voltage difference between heliox and air) for the 25BC case at 1600 mA cm^{-2} was 39 mV compared to 67 mV for the 25BA (see inset in Figure 4.4). Therefore, the MPL reduces the oxygen mass transport resistance by increasing water crossover to the anode side (i.e., greater anode pressure drops) and preventing water from getting to the catalyst layer from the cathode side.

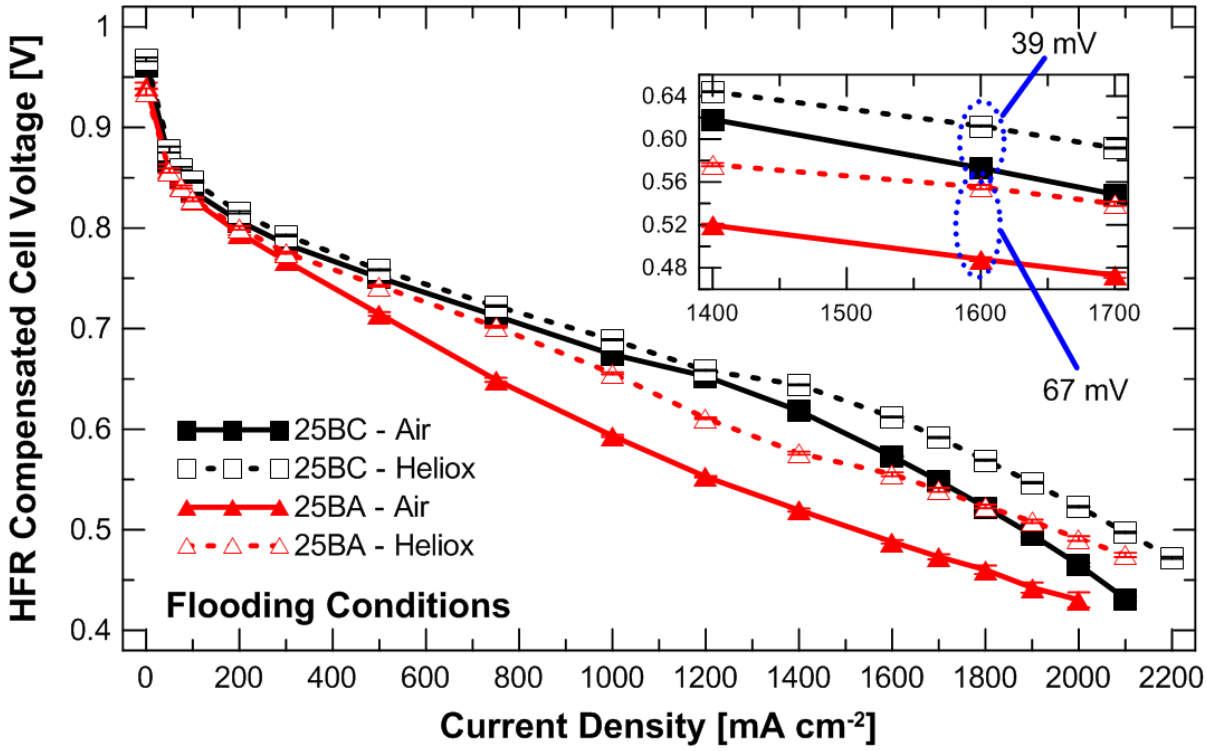

Figure 4.4 – Effect of heliox as the oxidant gas with two different cathode GDLs at flooding conditions (T_{dp} = 95 °C and T_{gas} = 75 °C). 25BA and 25BC refer to SGL 25BA (GDL without MPL) and SGL 25BC (GDL with MPL), respectively. The anode GDL for all cases was 25DC (with MPL).

All the observations mentioned above, demonstrate the ability of the cathode MPL to improve the overall fuel cell performance when used, and confirm the important role that the MPL plays in fuel cell performance. However, the observations do not explain in more detail how the MPL achieves these improvements. The MPL can improve the fuel cell performance if it increases the back-diffusion of water to facilitate its removal on the anode side [43,141] (see Figure 4.5). The MPL can also improve the water removal rate from the cathode catalyst layer to the cathode flow

field channels due to increased capillary pressure within the small pores of the MPL [174-176,185]. In addition, the MPL can act as a barrier to condensed water moving from the GDL/flow filed back to the catalyst layer [186]. In order to shed some light into the water transport inside the MEA, perforated metal sheets, similar to those presented in Chapter 3, were used. These perforated sheets, when placed on the cathode side between the flow field channels and the GDL, exacerbate the mass transport resistance and liquid water blockages inside the cell (see Figure 4.6). Thus, conclusions can be drawn regarding the liquid water transport mechanisms inside the fuel cell.

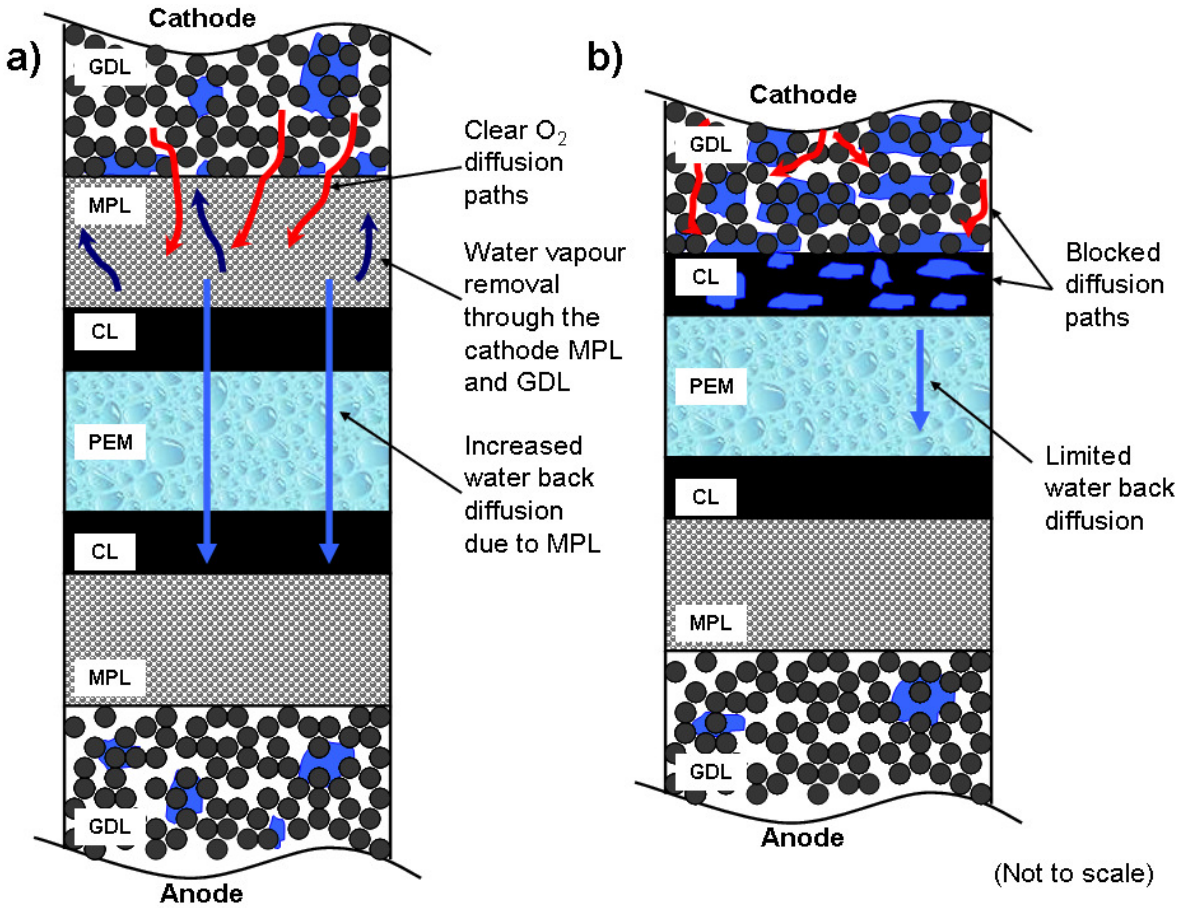

Figure 4.5 – Simplified schematic of water transport (a) with and (b) without a cathode MPL.

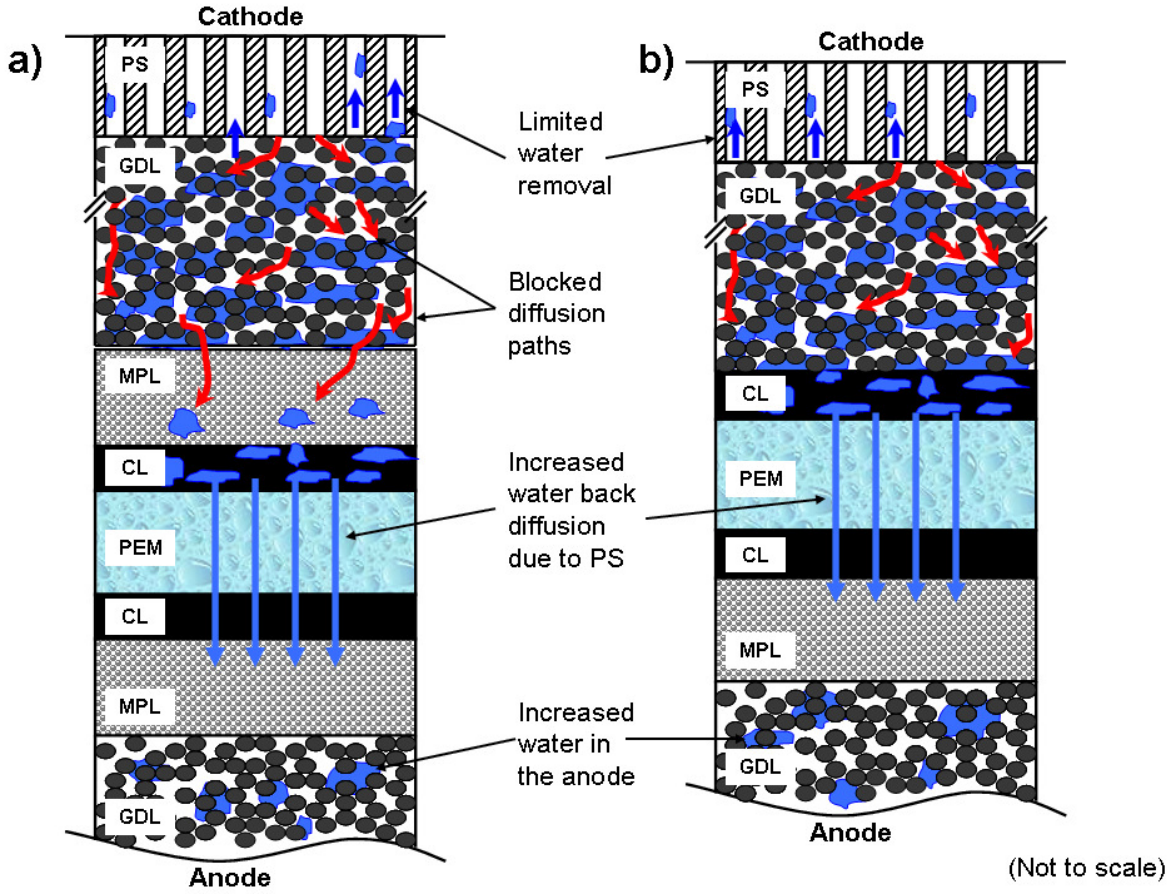

Figure 4.6 – Simplified schematic of water transport when a perforated sheet is placed between the GDL and flow field plate: (a) cathode GDL with MPL and (b) cathode GDL without MPL.

Figure 4.7 shows the effect of perforated sheet (PS) open area on cathode and anode pressure drops. 100% open area (OA) corresponds to a GDL without any additional PS. As mentioned earlier, for all the operating conditions, the 25BA has a greater cathode and lower anode pressure drop than the 25BC. These effects are attributed to the increase of water saturation in the cathode side due to poor water management and reduced water cross-over from the cathode to the anode side (see Figure 4.5). By using the PS, liquid water condensation and accumulation is promoted between the cathode catalyst layer and the GDL due to increased resistance (see Figure 4.6). At all conditions, the sheets are able to decrease the cathode pressure drops for both GDLs to similar values, indicating that for both 25BC and 25BA GDLs most of the water is accumulated in the catalyst layer and GDL. This result also illustrates that the perforated sheets decrease the amount of water breakthrough from the GDL to the flow field channels.

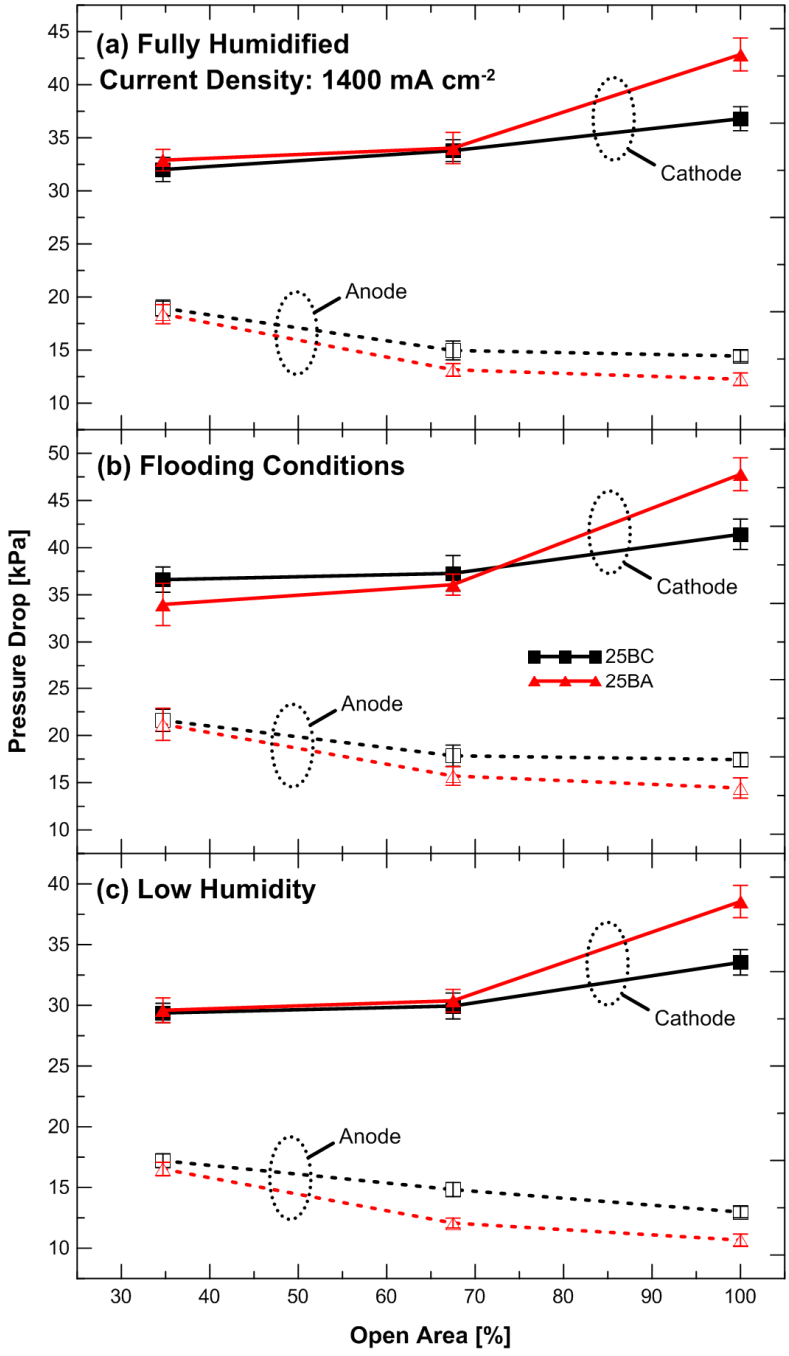

Figure 4.7 – Effect of perforated sheet open area on cathode and anode pressure drops for two different cathode GDLs at three operating conditions: (a) Fully humidified (100% RH with $T_{dp} = T_{gas} = 75$ °C), flooding ($T_{dp} = 95$ °C and $T_{gas} = 75$ °C), and low humidity (25% RH with $T_{dp} = 45.4$ °C and $T_{gas} = 75$ °C). The current density was 1400 mA cm^{-2}. 25BA and 25BC refer to SGL 25BA (GDL without MPL) and SGL 25BC (GDL with MPL), respectively. The anode GDL for all cases was 25DC (with MPL).

In addition, the anode pressure drops increase as the open area of the sheets decreases, thus, more water is forced from the cathode to the anode side due to the larger hydraulic pressures imposed by the sheets. For 25BA a lower open area of

the PS was required to match the anode pressure drop for 25BC. The reason for this is that the MPL in the 25BC GDL already enhances the water crossover; hence, for the 25BA GDL (without MPL) more water has to be accumulated in the catalyst layer in order to achieve similar water crossover rates to the case when an MPL is used. In addition, at low humidity conditions the 25BA GDL needs a lower open area sheet (i.e., more blocked area) in order to be capable of forcing water to the anode side. Without a PS, the 25BA CFP removes most of the water via the cathode side, which dehydrates the membrane.

These observations demonstrate that the MPL acts as barrier that forces water to the anode side. However, these results cannot determine whether this water removal mechanism is the main method of water management inside fuel cells when cathodes with an MPL are employed. Anode water removal (AWR) experiments were performed in an attempt to further identify if water removal through the cathode side is more dominant. Figure 4.8 shows the schematic of how the water concentration in a membrane changes when the AWR method is employed. The liquid water from the cathode catalyst layer is forced to the anode side due to a concentration gradient. Therefore, the larger the liquid water content accumulated in the cathode catalyst layer the greater the improvement in cell performance observed during these tests.

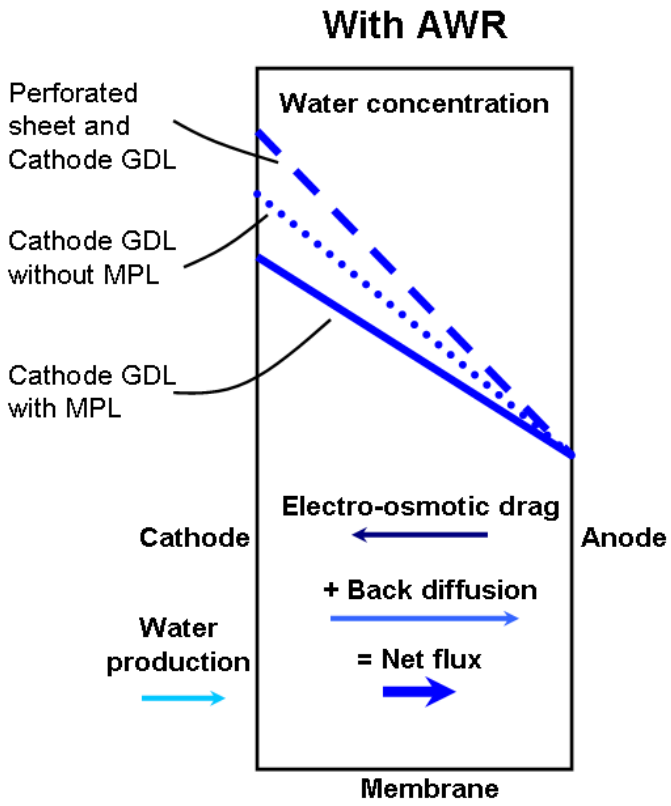

Figure 4.8 – Schematic of the water concentration through the membrane when the anode water removal (AWR). The water concentration changes depending on the cathode GDL configuration.

For the AWR tests, two main water transport mechanisms, hydraulic permeation and diffusion, dominate how the water can move from one side of the membrane to the other. Equations (1.32) and (1.31) describe each water transport mechanism, respectively. In order to have a better idea of which mechanism dominates the water transport, a quick analysis was performed using the mentioned equations. Figure 4.9 clearly shows that large hydraulic pressures are required in order for small amounts of water to be able to permeate through the membrane (Nafion 117). Through diffusion, on the other hand, more water can flow through the membrane. This indicates that diffusion, through concentration gradients, is the main transport mechanism through the membrane, especially with the AWR tests. For the calculations used in Figure 4.9, the following was assumed: a temperature of 75 °C; Nafion 117 membrane thickness, τ, of 25 µm; dynamic water viscosity, μ, of 0.3795 kg $m^{-1}s^{-1}$ [5]; water concentration, c_{H_2O}, of 55000 mol m^{-3}; hydraulic permeability, k_p,

of 3.5 x 10^{-19} m^2 [7]; and a water diffusion coefficient in the membrane, $D_{H_2O}(\lambda)$, of 5 x 10^{-10} m^2 s^{-1} [7].

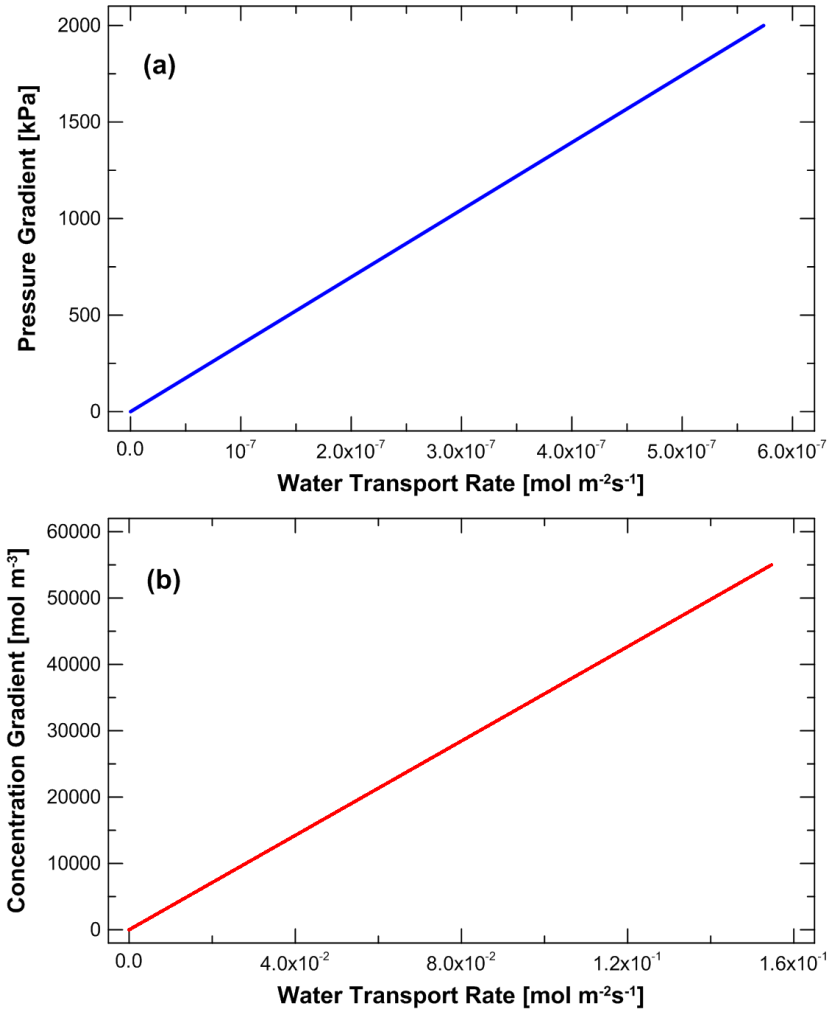

Figure 4.9 – Effect of (a) Pressure and (b) concentration gradients on the water transport rate inside a proton exchange membrane.

The results shown in Figure 4.10a demonstrate that the GDL without an MPL experiences a greater increase in performance improvement than the GDL with MPL. In addition, the peak cell voltage for the 25BA is achieved at a lower hydrogen stoichiometry than the 25BC (i.e., 9 vs. 11). This indicates that greater amounts of liquid water were accumulated in the cathode catalyst layer since the cell improvement was observed immediately after the water concentration gradient in the membrane started to increase. On the other hand, the cell voltage value for the 25BC GDL did not improve significantly, less than 6 mV, between hydrogen

stoichiometries values of 1.5 to 8. Once the concentration gradient increased substantially, the liquid water located in the cathode catalyst layer was forced across the membrane resulting in the peak voltage for the 25BC. Therefore, it can be concluded that the cathode MPL does in fact limit the water saturation inside the catalyst layer and enhances water removal through the cathode side, which confirms the work recently presented by Owejan et al. [186]. Although we have shown that the MPL also improves water crossover to the anode side, it is not the main mechanism for water removal, thus, this effect in Figure 4.5a is actually smaller than anticipated.

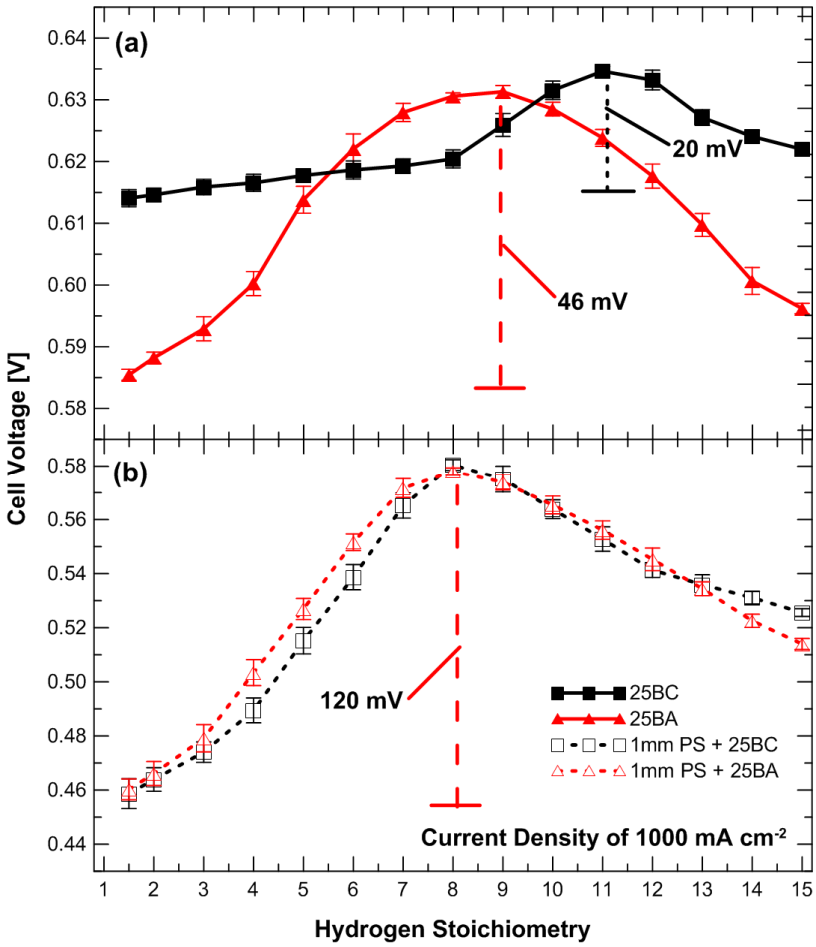

Figure 4.10 – Anode water removal tests for two different cathode GDLs (a) without and (b) with perforated sheets. The perforated sheet used for these tests had an open area of 34.7% and 1 mm diam. perforations. For these tests dry hydrogen gas was fed (no humidification) to the anode side while the oxidant gas was fully humidified (100% RH). The air stoichiometry was 2.0. 25BA and 25BC refer to SGL 25BA (GDL without MPL) and SGL 25BC (GDL with MPL), respectively. The anode GDL for all cases was 25DC (with MPL).

The AWR method was also performed with the two GDLs and a perforated sheet (1 mm diam. holes with 34.7% open area). Figure 4.10b confirms that the perforated sheet increases the liquid water accumulation in the cathode catalyst layer resulting in a large fuel cell performance improvement (around 120 mV for both cases). This behavior is similar to the one observed in Figure 4.10a with the 25BA GDL with no MPL, which again indicates that without an MPL on the cathode side the levels of water saturation in the catalyst layer are greater than with an MPL. It is interesting to note that the perforated sheet used here removes any benefit of the MPL with respect to removal of catalyst layer water.

4.3.2 Effect of the microporous layer in the anode gas diffusion layer

In this section we briefly considered the role of the anode MPL. Figure 4.11 shows the polarization and high frequency resistance data for two different anode GDLs: 25DC (with MPL) and 25DA (without MPL). The cathode GDL, 25BC (with MPL), was used in all the tests. It can be observed with these results that the anode MPL does not have a significant influence on the fuel cell performance at current densities below 1600 mA cm^{-2}. At high current densities, and fully humidified and flooding conditions, a performance difference between the two cases is observed possibly due to water saturation in the anode catalyst layer. This can be confirmed with the HFR data in which the 25DA case has lower resistance over the whole current density range, likely due to a more hydrated membrane. At low humidity conditions, the performance difference between the two anode GDLs is insignificant due to the decrease of water inside the MEA.

It is important to note that tests without anode and cathode MPLs were also performed at different conditions. However, low open circuit voltage (OCV) values (<0.92 V) and poor voltage stability at low and high current densities (<200 and >1000 mA cm^{-2}) were observed. Thus, it was decided to study the anode MPL effect when the cathode MPL is used since it is a common practice in industry to use this cathode GDL configuration [5].

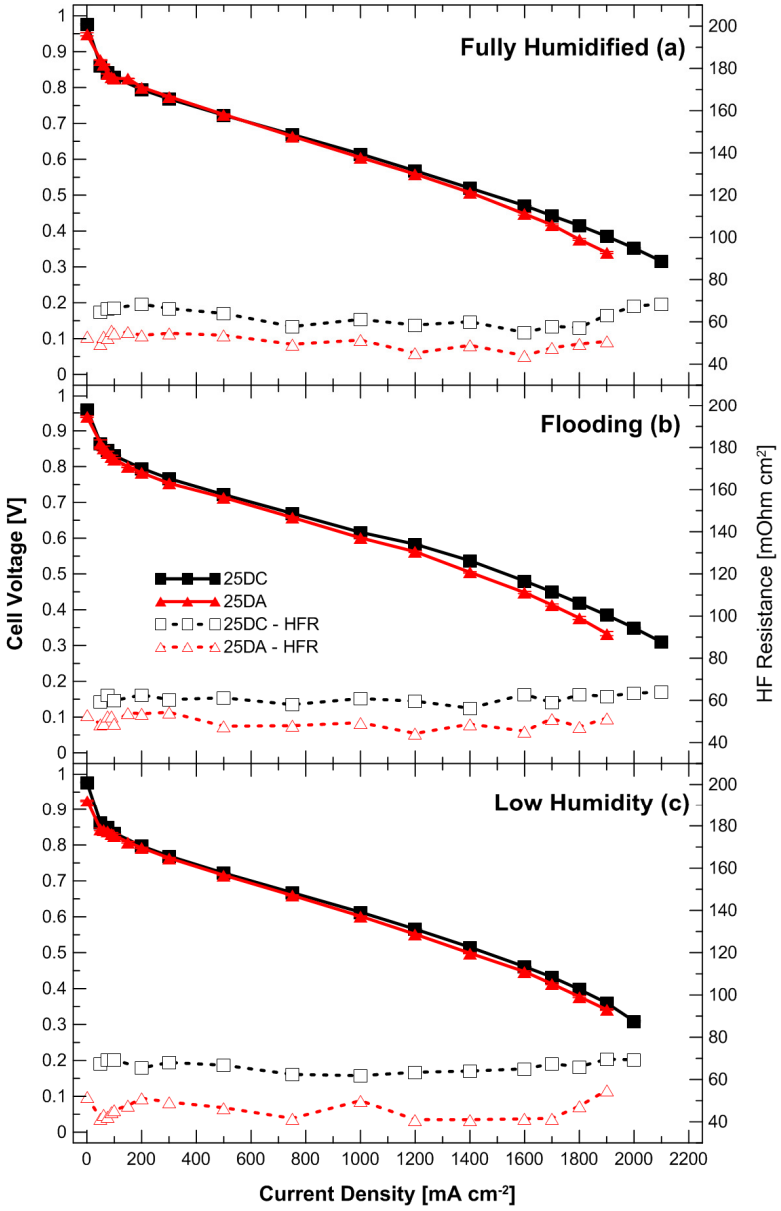

Figure 4.11 – Effect of anode MPL on polarization and high frequency resistance data for (a) fully humidified (100% RH), (b) flooding, and (c) low humidity (25%) conditions. 25DA and 25DC refer to SGL 25DA (GDL without MPL) and SGL 25DC (GDL with MPL), respectively. The cathode GDL for all cases was 25BC (with MPL).

Figure 4.12 shows that the 25DA GDL affects the water accumulation, pressure drops, and cell voltage stability. This confirms that the anode MPL enhances water removal towards the anode flow field channel resulting in a more stable cell voltage (and slightly higher anode pressure drop). In addition, it can be observed that without an anode MPL the cathode GDL experiences a higher pressure drop due to water accumulation in the flow field channels (see Figure 4.12b). Furthermore, this unstable voltage was also observed at low current densities (<200 mA cm^{-2}) for both

fully humidified and flooding conditions. Therefore, it is recommended to use an anode MPL since it reduces water accumulation in the anode catalyst layer due to the capillary forces within the small pores of the MPL.

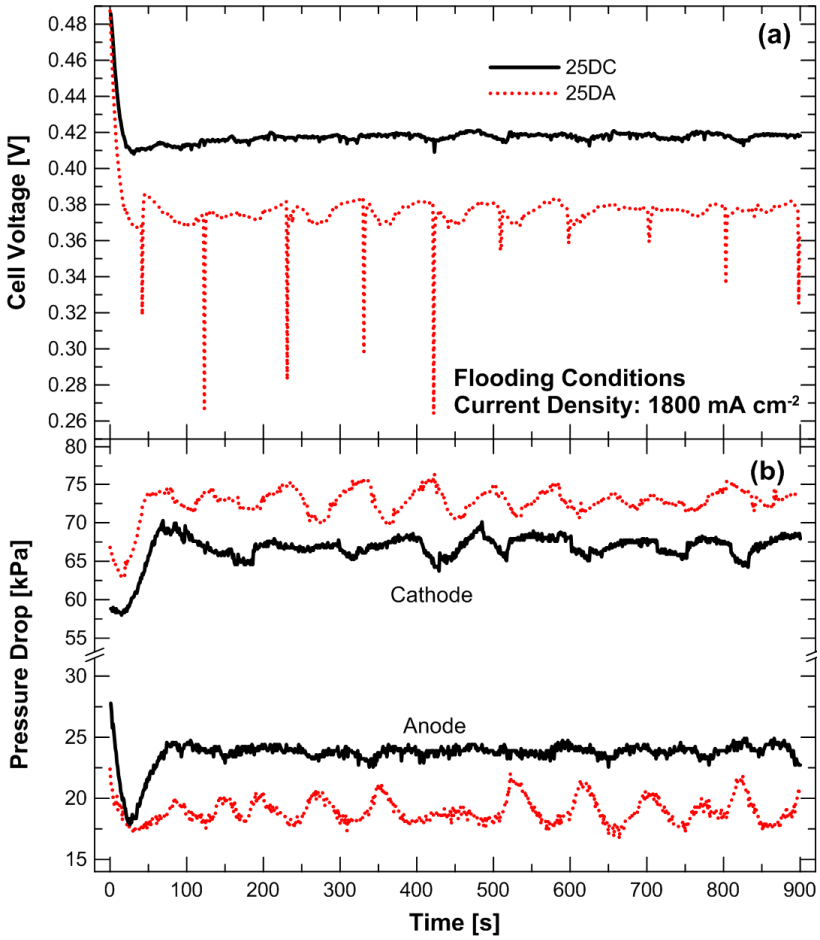

Figure 4.12 – Effect of anode MPL on the (a) voltage stability and (b) pressure drops at a constant current density of 1800 mA cm^{-2} and at flooding conditions (T_{dp} = 95 °C and T_{gas} = 75 °C). 25DA and 25DC refer to SGL 25DA (GDL without MPL) and SGL 25DC (GDL with MPL), respectively. The cathode GDL for all cases was 25BC (with MPL).

Perforated sheets were also used in order to analyze the effects of the anode MPL. Figure 4.13 shows that the pressure drops for 25DC and 25DA do not change significantly when reducing the open area of the perforated sheets. It is hypothesized that the anode MPL has a small role in enhancing water removal in the anode catalyst layer since it experiences a higher anode pressure drop than without an MPL. In addition, the 25DA case has greater cathode pressure drop in all the cases, indicating that the cathode GDL is removing even more water than when the anode MPL is used.

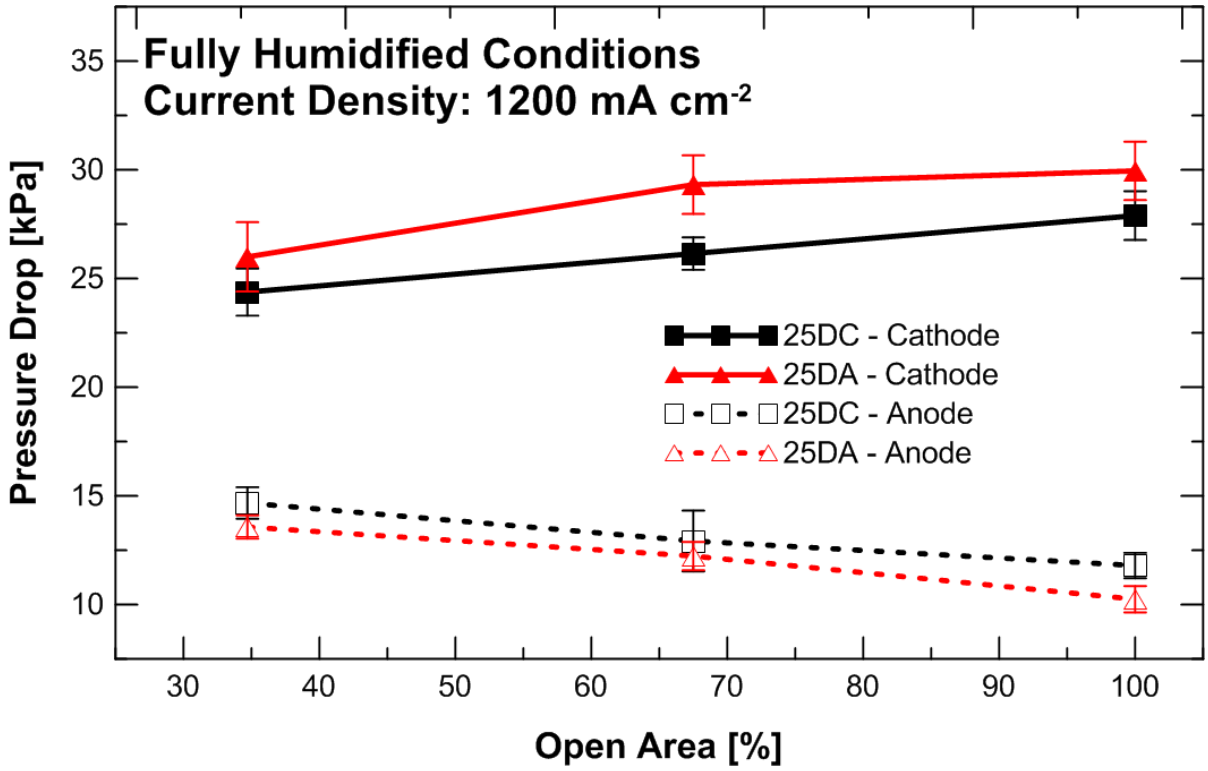

Figure 4.13 – Effect of perforated sheet open area on cathode and anode pressure drops for two different anode GDLs at fully humidified conditions - 100% RH ($T_{dp} = T_{gas} = 75$ °C). The current density was 1200 mA cm^{-2}. 25DA and 25DC refer to SGL 25DA (GDL without MPL) and SGL 25DC (GDL with MPL), respectively. The cathode GDL for all cases was 25BC (with MPL).

To further test the hypothesis that the anode MPL improves voltage stability and water removal, experiments with a perforated sheet with an open area of 8.8% (0.15 mm diam. perforations) were performed. This sheet was chosen since it increases significantly the liquid water blockages inside the cell due to its small open area. The perforated sheet was placed in the cathode side between the flow field plate and the 25BC GDL. Results shown in Figure 4.14 demonstrate the expected consequence of increased voltage instability due to flooding when the perforated sheets were added to the cathode side. It is observed that the anode MPL improves the voltage stability significantly, thus, confirming that it enhances the water removal towards the anode side due to the slightly higher anode pressure drop (see Figure 4.14b). The case without anode MPL experiences severe flooding due to water accumulation inside the MEA and flow field channels.

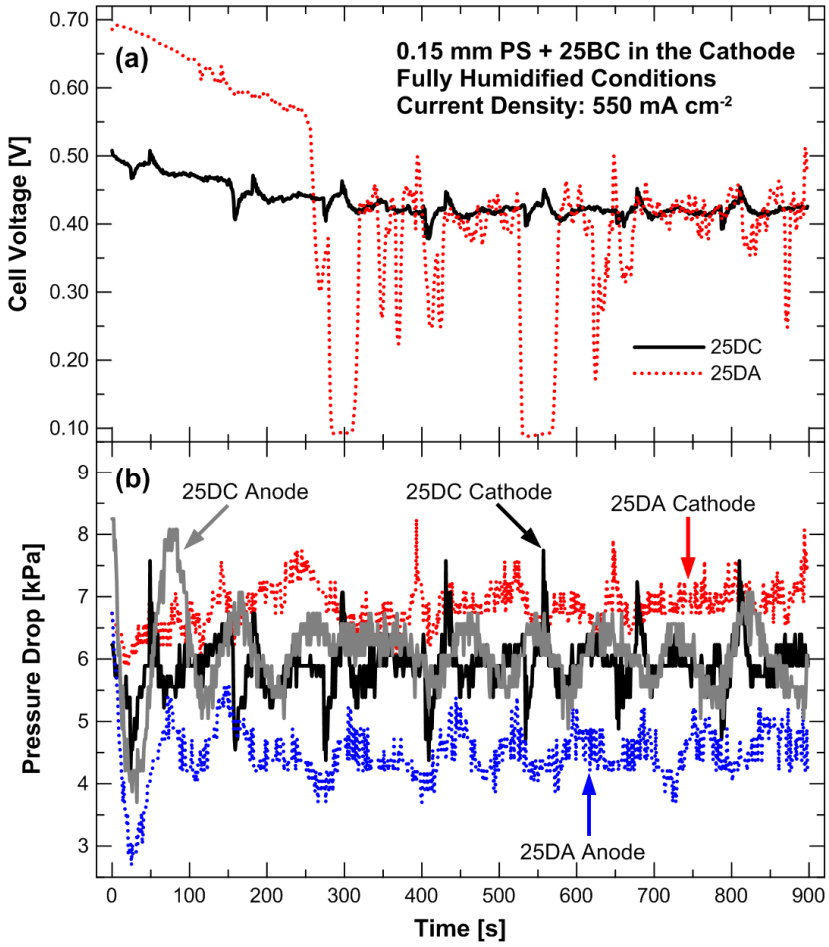

Figure 4.14 – Effect of a perforated sheet on (a) cell voltage stability and (b) pressure drops for two different anode GDLs The tests were performed at flooding conditions (T_{dp} = 95 °C and T_{gas} = 75 °C) and a current density of 550 mA cm^{-2}. The perforated sheet had 0.15 mm diam. holes and it was placed between the cathode flow field plate and GDL. 25DA and 25DC refer to SGL 25DA (GDL without MPL) and SGL 25DC (GDL with MPL), respectively. The cathode GDL for all cases was 25BC (with MPL).

The results shown in this section regarding the influence of the anode MPL contradict those found in the literature [182,186,187], since in this study a performance improvement was observed at high flow rates when the anode MPL was used. This difference in conclusions may be directly related to the materials (e.g., membrane, GDLs, catalyst layer, etc.) and flow field channels used, given that these components have an effect on water and gas transport inside the fuel cell. In addition, the work presented in this section gives detail to the influence of the anode MPL on voltage stability, which was not shown in the previous studies found in the literature.

In general, the use of an MPL on the anode side is also beneficial due to the mechanical support that it gives to the catalyst layer and membrane [186]. This is important especially from a durability point of view.

Additional data corresponding to the tests with different perforated sheets and carbon fiber papers can be found in Appendix E.

4.4 Conclusions

In this study, a detailed experimental investigation of the effect of microporous layers on both anode and cathode GDLs was performed. These experiments were focused on identifying the possible liquid water transport mechanisms inside the MEA when cathode and anode MPLs were used at different operating conditions. Perforated metal sheets with different open areas were used in order to understand in more detail the liquid water interaction in both the cathode and anode catalyst layers. In addition, the anode water removal (AWR) method was performed to study how each GDL modified the peak voltage value when no mass transport losses were present. The role of the anode MPL was also investigated. The following conclusions were drawn:

1. The cathode MPL improves fuel cell performance at all the three operating conditions (fully humidified, flooding, and low humidity). This is due to the water removal capability and enhancement of oxygen diffusion in the cathode catalyst layer. The MPL (for cathode and anode) also improves the cell voltage stability compared to the case without an MPL, indicating that the MPL reduces the water saturation inside the catalyst layer. In addition, experiments with heliox as the oxidant gas confirmed that the cathode MPL reduces the mass transport losses inside a MEA, especially at flooding conditions.
2. It was identified that the anode pressure drop when a cathode MPL is used increases compared to a cathode without an MPL. This is a result of the increase of water crossover from the cathode to the anode side across the membrane. This phenomenon was confirmed with the use of perforated

sheets that exacerbate the mass transport resistance and liquid water blockages inside the cell. With these sheets it was observed that the anode pressure drops for both cases (with and without MPL) were of similar magnitude resulting in more water crossover to the anode. This confirms that the cathode MPL acts as a barrier and enhances this water crossover.

3. The anode water removal method was used for the different GDLs in order to observe the peak cell voltage without mass transport issues related to liquid water in the catalyst layer. The GDL without an MPL experienced a greater increase in cell performance improvement since the water accumulated in the cathode catalyst layer was removed via the anode side. The cathode GDL with an MPL needed higher hydrogen flow rates in order to achieve the peak cell voltage since less liquid water was accumulated in the cathode catalyst layer. This confirms that the MPL improves the cell performance due to the reduction of water saturation in the cathode catalyst layer resulting in enhanced oxygen diffusion. With a cathode MPL the water removal occurs mostly on the cathode side, even though it also improves the water crossover to the anode.
4. The anode MPL influence on fuel cell performance is insignificant for current densities below 1600 mA cm^{-2}. However, it is recommended for an anode MPL to be used since it improves cell voltage stability and reduces water accumulation in the anode catalyst layer and in the cathode flow field channels.

The results presented in this work are important in order to have a better understanding of the main roles of both the cathode and anode MPLs. It is important to note that the observations and conclusions listed in this chapter reflect the performance of the specific fuel cell used here. These observations may change depending on fuel cell characteristics such as the cathode (and anode) flow field channel design, flow field configuration (e.g., co-flow, cross-flow, or counter-flow), and the thermal properties of different GDLs and MPLs. Therefore, more work still needs to be performed in order to take into account a full set of fuel cell parameters.

5 ENGINEERED PERFORATED SHEETS AS GAS DIFFUSION LAYERS[5]

5.1 Introduction

As mentioned in Section 1.4.2.1, the two materials used the most as GDLs in the fuel cell industry are carbon fiber papers and carbon cloths. However, they have a number of drawbacks, particularly with respect to their design and model complexity. One of the main issues with the carbon paper/cloth used as GDLs is the non-controlled variation in porosity (and other localized properties) since the porosity characteristics between carbon paper are not always repeatable [115]. Many of the water management and mass transport issues with GDLs could be improved considerably if the GDLs can be carefully tailored to specific fuel cell applications. Therefore, these issues have led researchers to study other possible materials in which the porosity and perforations used for liquid and gas transport are specifically designed in order to achieve the desired performance.

One approach to design these engineered GDLs is through the use of non-porous conductive materials that are perforated based on a detailed design. Research groups from Ballard Power Systems and Graftech Inc. presented designs of engineered GDLs based on graphitic foils [100,116]. A number of different designs (e.g., geometry, cross-sectional shape, hole density, etc.) were also proposed (see Section 1.4.2.1.4 for more details). Unfortunately, to the best of author's knowledge, there are limited published results from Graftech but none from Ballard that show complete studies of how these perforated graphitic foils perform inside the fuel cell with different operating conditions. Other groups have also proposed other non-porous materials as engineered GDLs, such as titanium [107] and copper [110] films. None of these studies attempted to understand in detail how the proposed GDLs affected the fuel cell performance.

[5] Sections of this work have been published in:
Blanco M, Wilkinson DP, Wang H, Liu SZS. Engineered gas diffusion layers for proton exchange membrane fuel cells. ECS Trans 2009;25(1):1507-18.
Sections of this work have been submitted for publication:
Blanco M, Wilkinson DP, Wang H. Structured perforated sheets as gas diffusion layers for proton exchange membrane fuel cells.

Another approach to develop engineered GDLs is through the use of perforations and grooves in carbon fiber papers and cloths. Based on the earlier work of Wilkinson et al. [39,128] the main idea behind the modification of CFPs with perforations is to improve liquid water transport at specific locations of the GDL. Gerteisen et al. [129,130,225] have shown that perforations (80 µm), made with a laser, in a CFP allow for lower levels of water accumulation, which improves the oxygen transport and overall fuel cell performance. However, at dry conditions these specific perforations (size and location) would increase membrane dehydration. Manahan et al. [131] have also used a laser to make perforations slightly larger than that of the previous group (300 µm vs 80 µm) that improve the cell performance at low to mid range current densities (<1600 mA cm^{-2}) and at 50% RH. It was concluded that these perforations acted as water pooling locations that collected and/or channelled water from the catalyst layer and GDL. It is important to note that at high relative humidities (>50% RH) the performance of the cell with these perforated CFPs deteriorated significantly due to mass transport losses. Similar conclusions were also drawn by Nishida et al. [133] and Lee et al. [134] regarding the use of grooves or engineered pore paths in conventional CFPs for enhanced water management.

In this study, *in-situ* experiments of perforated stainless steel sheets as GDLs were performed to study the effects of different sheet designs on the performance and transport characteristics inside a PEM fuel cell. An emphasis is given to the importance of in-plane diffusion in GDLs for gas transport and water removal. The use of free-standing microporous layers with the perforated sheets was also investigated in detail in order to understand how specific perforated sheet designs affect mass transport losses inside the MEA. Identification of key characteristics required to optimize gas and liquid transport with these perforated sheets are also established. Finally, this study offers observations regarding the viability of tailoring these sheets to specific parameters and conditions without deteriorating the overall cell performance.

5.2 Experimental

All the perforated sheets used for these tests were explained in detail in Section 2.1.1.4. These sheets were manufactured through photo-etching. This process is simple, cost effective, and is widely used in industry. Thus, it was chosen for making the perforations. In addition, the photo-etching process is already well developed and can easily be used for large-scale manufacturing. The spacing or landing between the perforations, and the width and depth of the channels connecting the perforations in each sheet were chosen based on the restrictions posed by the photo-etching manufacturing process (see Section 2.1.1.4 for more details regarding these restrictions). It was also important to not affect the flatness and structural properties of the sheets.

For all the tests, a 25 DC gas diffusion layer (SGL Carbon) was used as the anode GDL (refer to Table 2.2 for more details on this carbon fiber paper). A Primea® 5510 catalyst coated membrane (CCM) from W.L. Gore & Associates was used and conditioned based on the protocol explained in Section 2.1.3.1. For the various polarization tests performed in this chapter, the single fuel cell assembly was compressed to 792.9 kPa (100 psi), the gases were pressurized to 206.8 kPag (30 psig) at the inlet, and the air and hydrogen stoichiometries were kept constant at 2.0 and 1.5, respectively. For all the polarization performance tests, the temperatures of the gases, T_{gas}, and the fuel cell, T_{cell}, were kept constant at 75 °C. Three different conditions were tested: fully humidified conditions, 100% RH (T_{dp} and T_{gas} = 75 °C); flooding conditions (T_{dp} = 95 °C and T_{gas} = 75°C); and low humidity conditions, 25% RH (T_{dp} = 45.4 °C and T_{gas} = 75°C) (see Table 2.5). Polarization tests with heliox (21% O_2 and 79% He) as the oxidant gas were also performed. Heliox was used to give a better understanding of the mass transport effects (and losses) in the fuel cell (see Section 2.1.3.6).

In order to investigate the fuel cell and GDL performance potential in the absence of mass transport limitations due to water accumulation, the anode water removal (AWR) method was performed with various perforated sheets as GDLs. Section 2.1.5 explains in detail the steps followed in order to perform these tests. However, one step that was modified from the original protocol was the current density at

which the fuel cell performed. For most of the tests presented in this chapter the current density was kept constant at 200 mA cm^{-2}, unless specified otherwise. In general, the gases and cell temperatures were 75 °C, the dew point temperature for the cathode side was 75 °C, and no humidification was used in the anode side. The pressure for both inlet gases was 206.8 kPag (approx. 30 psig), the air stoichiometry was kept constant at 2.0, and the anode stoichiometry was increased stepwise.

For this chapter all polarization tests were conducted three times, as explained in Section 2.1.3.3.1, in order to obtain repeatable observations. However, due to the decrease of cell voltage stability with the perforated sheets in some of the tests, it was decided for the acceptable difference between each test to be between 15 to 20 mV.

5.3 Results and discussion

5.3.1 Effect of perforated sheet open area

A number of stainless steel sheets with different perforation diameters (and corresponding open areas) were first tested as GDLs in order to evaluate the effect that each design had on the fuel cell performance. Since it was desired to evaluate these sheets without the interference of associated mass transport resistances due to water accumulation in the catalyst layer, the anode water removal (AWR) method was executed at 200 mA cm^{-2}. This current density was chosen since the limiting current density for these perforated sheets during polarization tests was around 300 to 400 mA cm^{-2}. As it can be observed in Figure 5.1, the perforated sheet with the greatest open area (67.5%) and perforation diameter (10 mm) had the lowest peak voltage during the test. Since it is assumed that all the water inside the cell is removed through the anode side when performing these tests (see Section 2.1.5), one reason for the 10 mm PS to show the lowest peak cell voltage is the oxidant gas maldistribution along the catalyst layer. Due to the large perforations of this sheet, the catalyst layer itself becomes one of the main sources (along with the perforations) of gas diffusion along the active area. In addition, the high frequency resistance measured for the sheet with the 10 mm perforations was 26 to 32% greater than the resistances of the other sheets. Thus, indicating additional

resistances such as contact resistances between the catalyst layers, perforated sheets, and flow field plates that lower the performance. These resistances represent approximately 55 mV of losses at this current density (200 mA cm^{-2}). Although these losses are significant, mass transport limitations represent the dominant contributor of the large performance losses. Moreover, the sheets with large perforations cannot provide appropriate mechanical support to the CCM, which can cause failure related issues after long tests (i.e., membrane perforations).

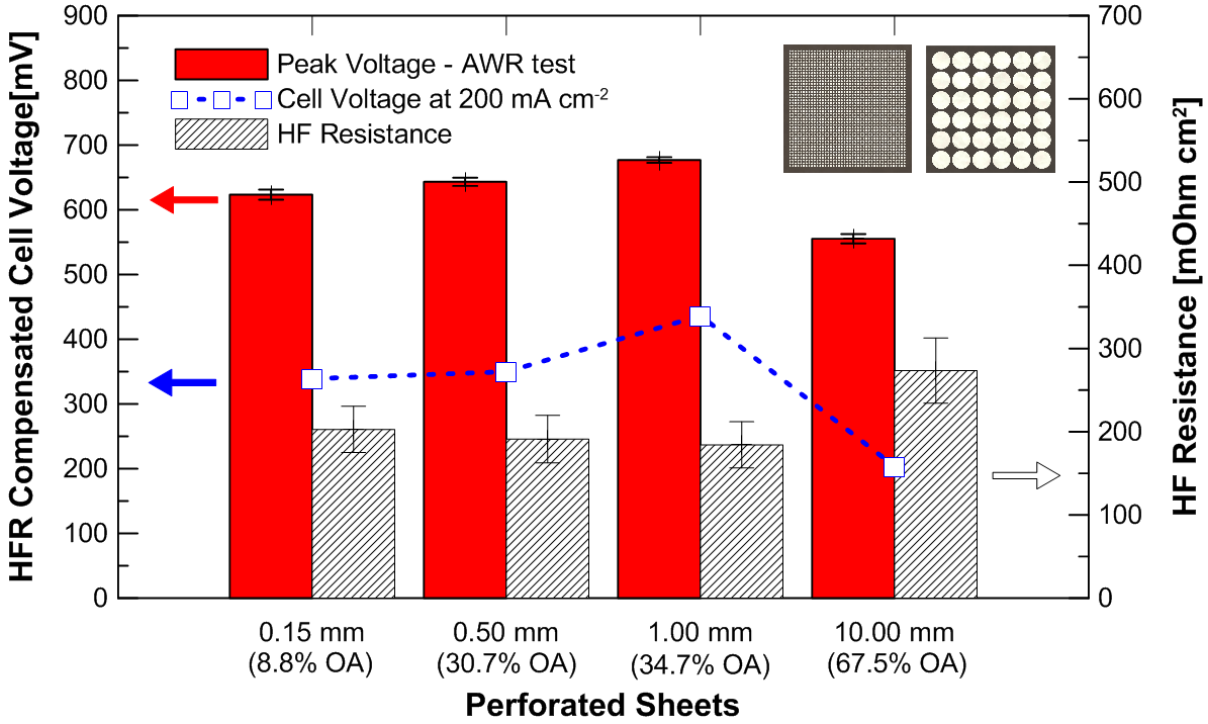

Figure 5.1 – Comparison of peak cell voltage in anode water removal (AWR) tests for metal perforated sheets with different perforation diameters. The voltage value for fully humidified conditions at 200 mA cm^{-2} is also shown for comparison. The HFR resistances shown correspond to the values observed in the AWR tests. All the cell voltage values presented have been HFR compensated. The perforated sheets were located on the cathode side between the flow field plate and the CCM. Schematics of some of these sheets are located in the top right-hand corner of this figure. The anode GDL for all cases was SGL 25DC (with MPL).

On the other hand, the peak cell voltage difference between the other three perforated sheets was not as great (54 mV between the 1 mm and the 0.15 mm PSs). The GDL with the 1 mm perforations (and 34.7 % open area) had the best performance and lowest resistance, resulting in the best balance between electrical

contact and gas transport. This sheet also gives enough mechanical support to the catalyst layer and membrane.

Unfortunately, the performance of these sheets was still poor (even after the anode water removal test) since the only diffusion mechanism for the gases (and liquid water) was through-plane diffusion. The very thin catalyst layers (12 to 15 μm) provided all of the in-plane diffusion, which was insufficient for uniform oxygen distribution throughout the active area. In order to prove that the limited in-plane diffusion in these GDL configurations was one of the dominant factors for poor performance, the perforated sheets were placed between the cathode flow field plate and a carbon fiber paper (CFP). Two CFPs with different in-plane characteristics were used: TGPH-030 (110 μm thick, 80% porous, and 20% PTFE) and 25BA (190 μm thick, 88% porous, and 5% PTFE). The results shown in Figure 5.2 confirm that limited in-plane diffusion is one of the main issues when perforated sheets are placed directly to the cathode catalyst layer.

Another dominant factor that decreases the cell performance was the lower open area of the perforated sheets compared to the porosity of carbon fiber papers, which limits the area that is accessible for the reactant gases.

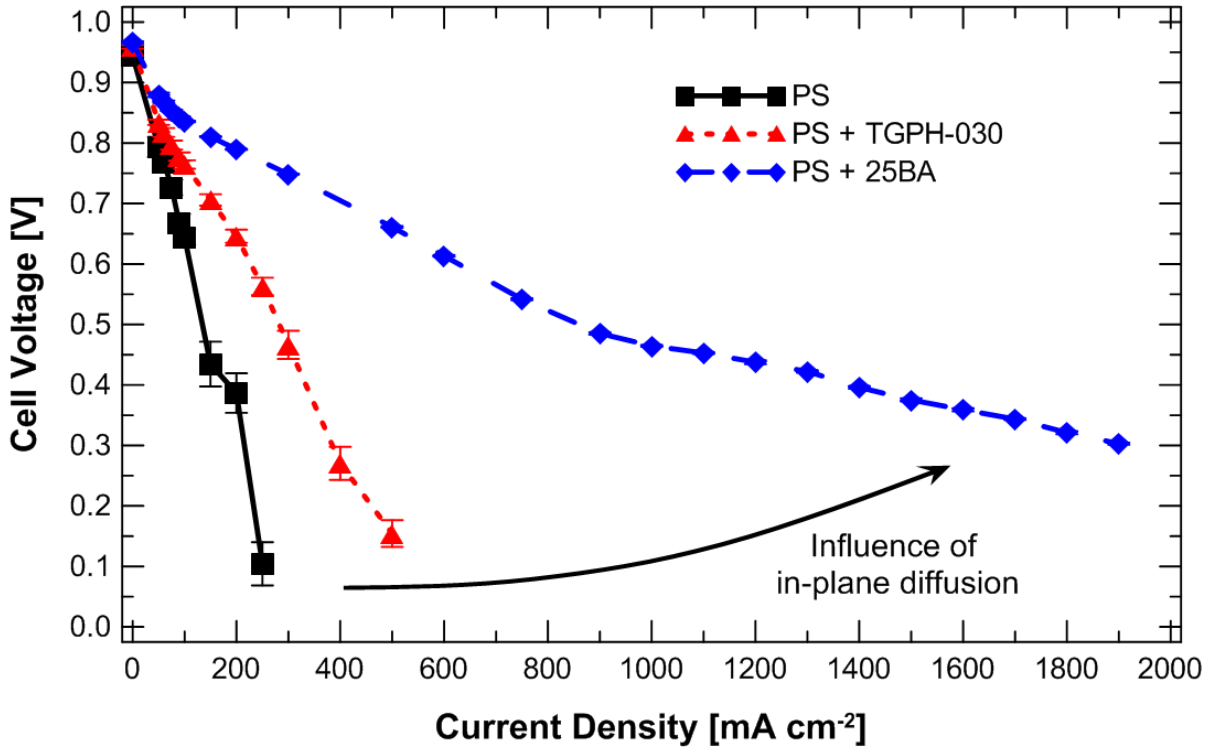

Figure 5.2 – Effect of in-plane diffusion when perforated sheets are used as GDLs. The tests were performed at fully humidified conditions (T_{dp} = 95 °C and T_{gas} = 75 °C). The perforated sheet used had 1 mm diam. holes and was 0.05 mm thick.

5.3.2 Effect of channels in perforated sheets for improvement of in-plane diffusion

The use of channels connecting the perforations on one side/surface of the perforated sheets was tested and investigated (see Figure 2.5). The reasoning behind the use of the channels is to improve the in-plane diffusion of the oxidant gases over the catalyst layer. In the previous section, it was shown that the sheets with 1 mm perforations had the best performance, thus, based on those observations, sheets with this perforation diameter were chosen for the new sheet designs with channels. Polarization tests were performed with a number of different perforated sheet designs used as GDLs. The main parameters changed were the material thickness, t, channel width, C_w, and channel depth, C_d. In general, the limiting current density was between 300 to 500 mA cm^{-2}. Anode water removal tests were also performed (at 200 mA cm^{-2}) with the different sheets. Table 5.1 and Figure 5.3 present the data of the mentioned tests. It is important to note that in the case of the sheets with channels, the side that has the channels is in contact with the CCM.

Table 5.1 – Cell voltage values at 200 mA cm^{-2} and peak cell voltage with anode water removal tests for perforated sheets with different thicknesses, channel widths, and depths. The diameter, *d*, for all the sheets was 1 mm. All the cell voltages are HFR compensated. The anode GDL for all cases was SGL 25DC (with MPL).

Name	*d* [mm]	*t* [mm]	C_w [mm]	C_d [mm]	Cell Voltage at 200 mA cm^{-2} [mV][a]	Peak Cell Voltage in Anode Water Removal Test [mV][b]
PS-A	1.00	0.05	0.00	0.00	423 ± 12	677 ± 4
PS-B	1.00	0.05	0.15	0.04	419 ± 7	655 ± 6
PS-C	***1.00***	***0.05***	***0.50***	***0.04***	***475 ± 9***	***656 ± 9***
PS-D	1.00	0.05	1.00	0.04	429 ± 11	593 ± 10
PS-E	1.00	0.10	0.00	0.00	359 ± 15	421 ± 12
PS-F	1.00	0.10	0.50	0.05	447 ± 12	517 ± 13
PS-G	***1.00***	***0.10***	***0.50***	***0.08***	***472 ± 10***	***595 ± 13***
PS-H	1.00	0.10	1.00	0.05	442 ± 13	535 ± 10
PS-I	1.00	0.10	1.00	0.08	461 ± 12	570 ± 10
PS-J	1.00	0.20	0.00	0.00	356 ± 20	423 ± 16
PS-K	1.00	0.20	0.50	0.10	307 ± 18	437 ± 16
PS-L	***1.00***	***0.20***	***0.50***	***0.15***	***577 ± 11***	***700 ± 9***
PS-M	1.00	0.20	1.00	0.10	376 ± 19	502 ± 15
PS-N	1.00	0.20	1.00	0.15	422 ± 16	550 ± 10

[a]The gases, dew point, and cell temperatures were 75 °C. The pressure for both gases was 206.8 kPag (approx. 30 psig) and the air/hydrogen stoichiometry ratio was 2.0/1.5.
[b]These tests were performed at a constant current density of 200 mA cm^{-2}.

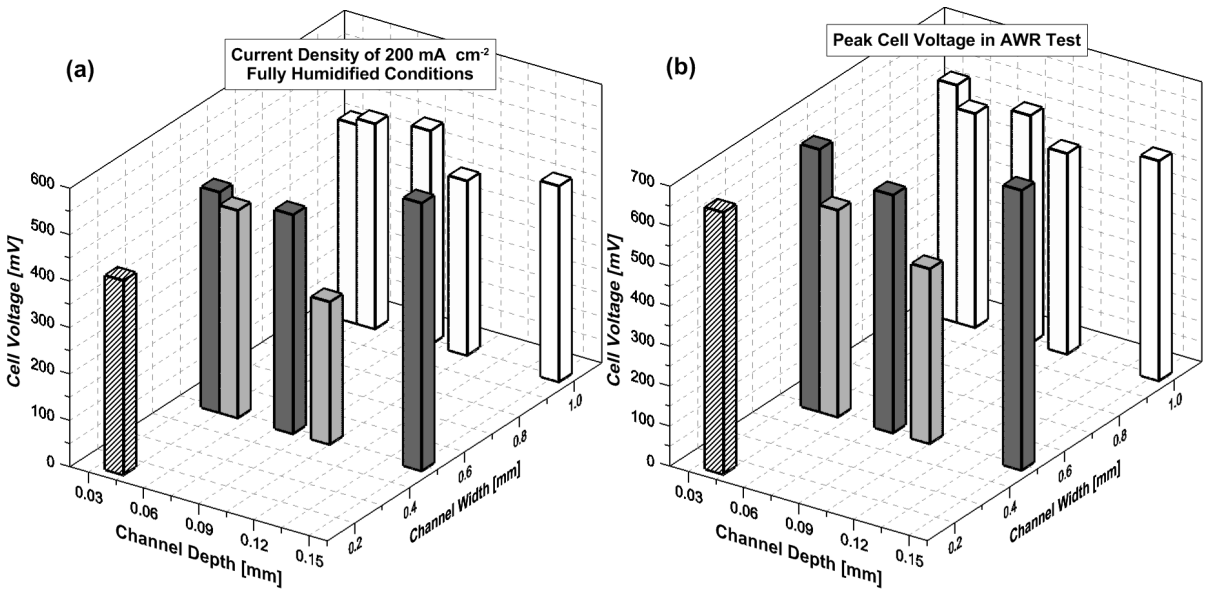

Figure 5.3 – (a) Cell voltage values at 200 mA cm^{-2} and (b) peak cell voltage with anode water removal tests for perforated sheets with different thicknesses, channel widths, and depths. The perforated sheets without channels are not shown in these plots. All the cell voltages are HFR compensated. The anode GDL for all cases was SGL 25DC (with MPL).

For the first two perforated sheets (0.05 mm thickness), the use of a thin channel (0.15 mm) did not translate into better performance at a current density of 200 mA cm^{-2}. In fact, the PS-A and PS-B cases showed similar performances. On the other hand, when wider channels are used the performance increases, especially in the case of the 0.5 mm wide channel (PS-C) as highlighted in the Table 5.1 and Figure 5.3 (dark grey). An interesting point is that with the AWR test, the sheet without channels showed the greatest peak voltage (677 mV) out of the first four sheets (see Table 5.1). This indicates that without significant amounts of water inside the catalyst layer, the channels do not improve the gas diffusion significantly.

Since the use of the channels did not show major improvements with thin metal sheets, it was decided to test thicker sheets. In addition, narrow channels (0.15 mm) were not used for thicker sheets since they did not show cell improvement with a 0.05 mm thick sheet. Out of the five 0.1 mm thick perforated sheets, the sheet with the 0.5 mm channel (0.08 mm deep), PS-G, showed the best performance under fully humidified conditions (highlighted in Table 5.1 and Figure 5.3). However, the anode water removal tests show that this sheet does not enhance the peak voltage value as much compared to the thinner sheets. Thus, the deeper channels do not improve oxidant gas diffusion further, but instead allow for better water transport since this sheet can achieve greater limiting current densities (400 mA cm^{-2} vs. 250 mA cm^{-2} for the case without channels at fully humidified conditions) (see Table 5.2).

The overall best performance and peak voltage (during the anode water removal tests) was shown by the 0.2 mm thick sheet with 0.5 mm wide and 0.15 mm deep channels (PS-L – highlighted in Table 5.1 and Figure 5.3). This is a surprising result since thicker materials represent a longer path for the oxidant gas to travel. This may be due to the deeper channels that allow for enhanced gas diffusion and water removal. However, the sheet with wider channels but same depth (PS-N) does not show a significant improvement in gas and water transport. Thus, there has to be a balance between channel width and depth that allows for enhanced gas diffusion and liquid water removal.

Ideally, the perforations should be interconnected in a way in which the oxygen and water transport are enhanced due to in-plane diffusion. These connections could be tailored for specific transport mechanisms (i.e., some channels meant for oxygen transport and other meant for just water). However, current manufacturing capabilities limit the parameters (size, length, depth, etc.) of such connections without damaging the sheets. Other manufacturing and machining methods used for microelectromechanical systems (MEMS) can be considered. However, these methods are commonly used with materials that have poor electrical conductivity (e.g., silicon), which makes them difficult to be used in fuel cell systems.

Table 5.2 – Limiting current densities at three different operating conditions for perforated sheets with different thicknesses, channel widths, and depths. The diameter, *d*, for all the sheets was 1 mm. The anode GDL for all cases was SGL 25DC (with MPL).

Name	*d* [mm]	*t* [mm]	C_w [mm]	C_d [mm]	Limiting Current Density at Three Operating Conditions [mA cm^{-2}]		
					Fully Humidified	Flooding	Low Humidity
PS-A	1.00	0.05	0.00	0.00	250	200	250
PS-B	1.00	0.05	0.15	0.03	300	300	300
PS-C	***1.00***	***0.05***	***0.50***	***0.04***	***300***	***300***	***300***
PS-D	1.00	0.05	1.00	0.04	300	300	300
PS-E	1.00	0.10	0.00	0.00	250	250	250
PS-F	1.00	0.10	0.50	0.05	300	300	300
PS-G	***1.00***	***0.10***	***0.50***	***0.08***	***400***	***300***	***300***
PS-H	1.00	0.10	1.00	0.05	300	300	300
PS-I	1.00	0.10	1.00	0.08	300	300	300
PS-J	1.00	0.20	0.00	0.00	250	250	250
PS-K	1.00	0.20	0.50	0.10	300	250	250
PS-L	***1.00***	***0.20***	***0.50***	***0.15***	***400***	***300***	***400***
PS-M	1.00	0.20	1.00	0.10	300	250	250
PS-N	1.00	0.20	1.00	0.15	300	250	250

5.3.3 Effect of MPL film in perforated sheets and reactant transport

Although the addition of channels did improve the perforated sheet performance, it was not sufficient to meet the necessary in-plane diffusion required by the cathode side. Therefore, the use of a freestanding microporous layer (MPL) between the perforated sheets and the CCM was investigated. The MPLs used were 50 µm thick Gore Carbel (MP30Z) expanded PTFE layers that were impregnated with carbon black powder. These layers have similar characteristics to those MPLs presented in

typical PEMFC designs (e.g., mean pore diameter is 30 nm) [186]. The perforated sheets chosen for these experiments were the ones that showed the best performance in the previous section, mainly: PS-A, PS-C, PS-G, and PS-L (see Table 5.1). All the perforated sheets had 1 mm perforations. For the sheets with channels, the side that had the channels was placed facing the MPL.

Figure 5.4 shows HFR compensated polarization data for the four different GDL configurations with and without MPL. All the tests were performed at fully humidified conditions (100% RH). The results for the cases without MPL show similar patterns as those observed in Table 5.1 and Figure 5.3. Without an MPL, up to a current density of 100 mA cm^{-2}, all the perforated sheets have comparable performance; however, at higher current densities the perforated sheets without channels experienced greater water accumulation and corresponding mass transport losses. In addition, the sheets with channels (PS-C, PS-G, and PS-L) showed better voltage stability (indicated by the error bars) due to improved water removal capabilities. The PS-L sheet displayed the best overall performance.

The performance of all the perforated sheets with MPL is reasonably similar for the low current density range (0 to 400 mA cm^{-2}) since the cell voltages are within 20 mV of each other. Above 400 mA cm^{-2}, however, the PS-L sheet (0.2 mm thick, channels 0.5 mm wide, and 0.15 mm deep) is observed to exhibit an average of 72 mV greater potential for current densities from 500 to 1000 mA cm^{-2}. This behaviour indicates decreased mass transport losses compared to the other perforated sheets. At low current densities, the perforated sheets with additional MPL appeared to experience similar gas diffusion and water removal capabilities. While at high current densities, the PS-L sheet avoids severe flooding as a result of improved water removal capability due to the greater in-plane diffusion spaces given by the deeper channels connecting the perforations.

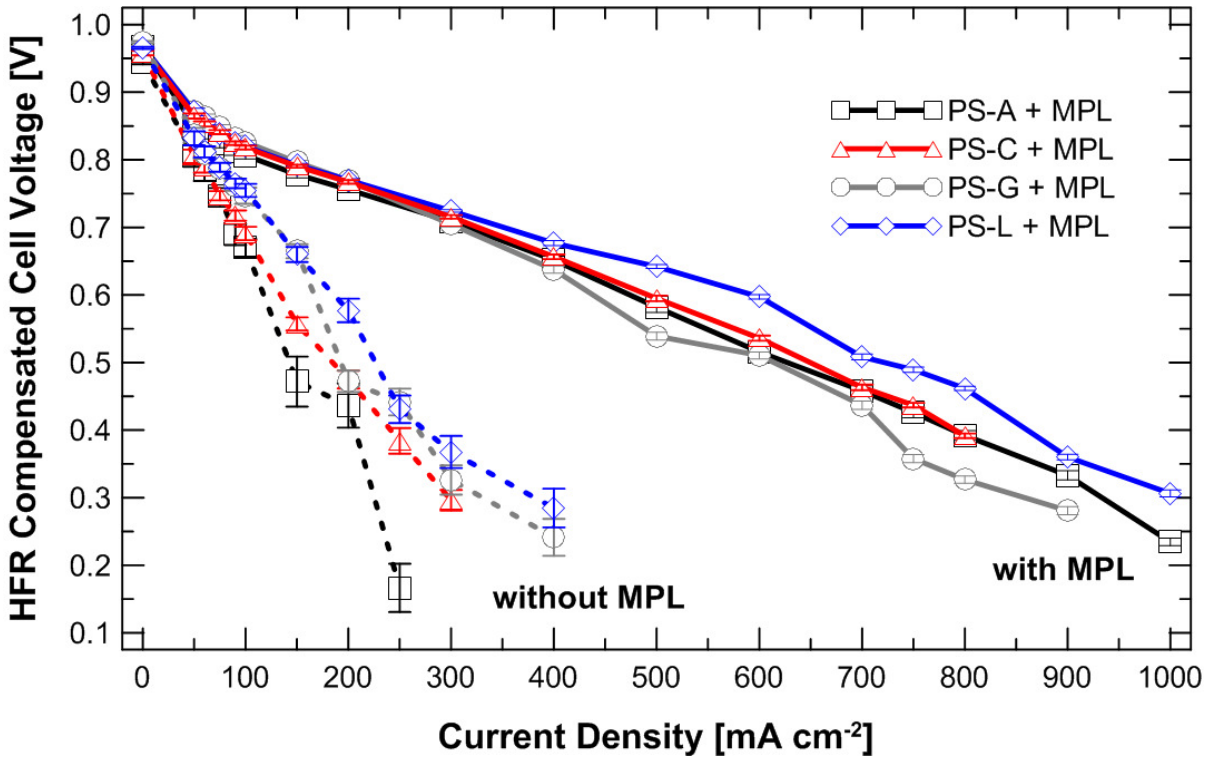

Figure 5.4 – Fuel cell performance with different perforated sheets. All the perforated sheets had 1 mm diam. perforations. The specifics of each PS are listed in Table 5.1. For all the cases the MPL films were used between the CCM and the PS. The side of the PS with channels is in contact with the MPL. All the tests were performed at fully humidified conditions (100% RH).

In terms of voltage stability, the GDL configurations with channels in the perforated sheets experienced a drop in voltage fluctuations over all current densities but especially in the high current density. Figure 5.5 shows the voltage of three GDL configurations over a time period of 900 s (15 min) at a constant current density of 800 mA cm^{-2}. As can be observed, the voltage stability achieved with the sheets with channels is significantly better than the sheets without channels. In fact, these reduced fluctuations correspond to voltage standard deviations comparable to those observed in Chapter 3 (Figure 3.1) with a conventional carbon fiber paper (25BC with MPL) as the GDL (2.5 mV for PS-L vs. 1.7 mV for 25BC CFP).

In general, voltage fluctuations are a function of water accumulation in the catalyst layer, GDL, and flow field channels. Thus, the case without channels (PS-A) experiences more water build up in these regions of the cell (likely more in the catalyst layer). However, for the case of the PS-B sheet, the decrease in voltage

fluctuations does not translate into an improvement in performance. This is possibly an indication that these channels in this sheet (0.5mm wide and 0.03mm deep) create a capillary or wicking effect in the sheet's surface that improves the water removal. However, the channels do not appear to improve gas transport significantly since there is no significant variation in performance (1.5 mV difference).

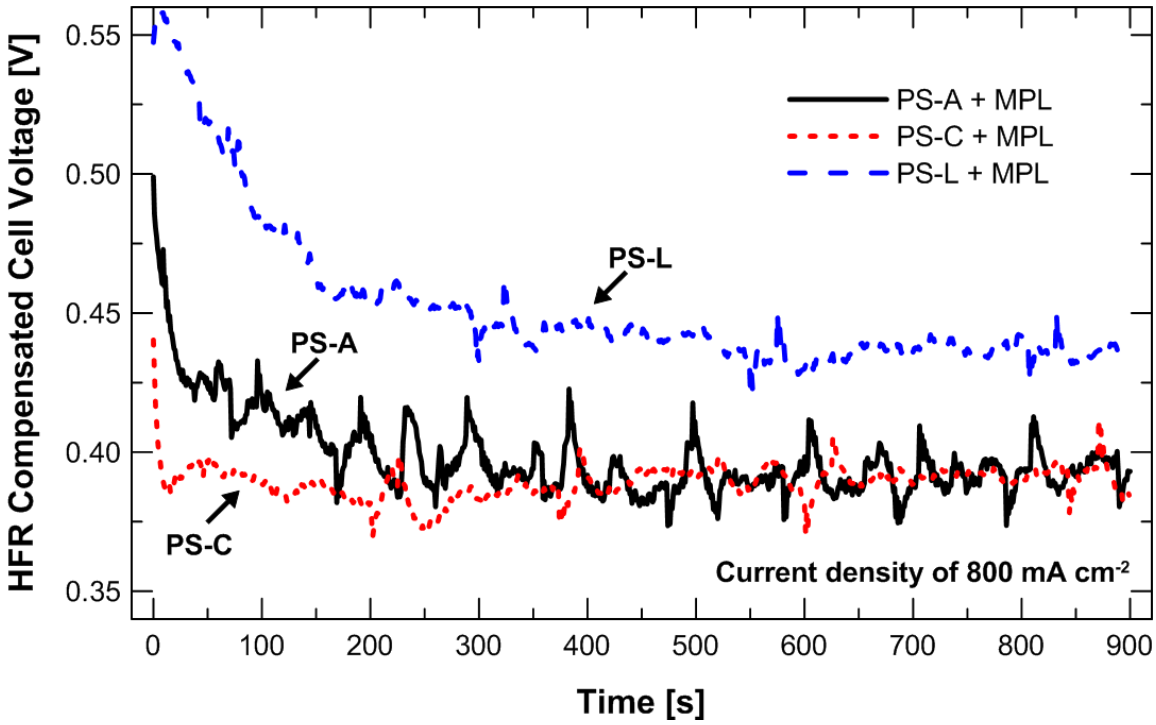

Figure 5.5 – Comparison between perforated sheets with and without channels. The specifics of each PS are listed in Table 5.1. All perforated sheets had MPL films located between the CCM and the PS. All tests were performed at fully humidified conditions (100% RH).

5.3.4 Effect of oxidant gas in reactant transport

In order to understand in more detail how the perforated sheets with channels affect the gas and liquid water transport inside the MEA, two different oxidant gases were used: air and heliox (see Section 2.1.3.6). Figure 5.6 compares the HFR compensated polarization results of the perforated sheet that showed the best performance in the previous sections, PS-L, with and without an MPL. Three different conditions were tested: fully humidified conditions, flooding conditions, and low humidity conditions. Tests with baseline GDLs (25BC CFP on the cathode side) are also shown in Figure 5.6 for comparison. The perforated sheet (PS-L) without

the MPL had poor performance for all three operating conditions with both air and heliox as oxidant gases. This observation is a deviation from the expected results since oxygen diffuses better in helium than in nitrogen. In theory, it was anticipated that heliox would improve the oxygen diffusion and the overall performance of the cell for the PSs without MPLs. However, the lack of in-plane diffusion coupled with the water accumulation inside the cathode catalyst layer (as observed by the greater error bars for these cases) affects the mass transport losses significantly. In addition, for the case of flooding conditions, it achieved the lowest limiting current density, 300 vs. 400 mA cm^{-2} (see Figure 5.6b).

In contrast with the previous observations, the perforated sheets with microporous layers showed improved performance for all three operating conditions with heliox as the reactant gas. The greatest improvement was for flooding conditions, in which the heliox improved the current density at 0.4 V by 32%. Therefore, it can be hypothesized that with these perforated sheets water accumulation is a key factor for mass transport losses. This can be proven at dry conditions in which the heliox case improves the current density at 0.4V by only 18% due to the lower water accumulation that is present at these conditions (see Figure 5.6c). This leads to the conclusion that these engineered perforated sheets are better suited to be used as GDLs at low humidity conditions.

It is important to note that the performance of these sheets is still well below baseline; however, they have the potential to be used as GDLs with more detailed optimization.

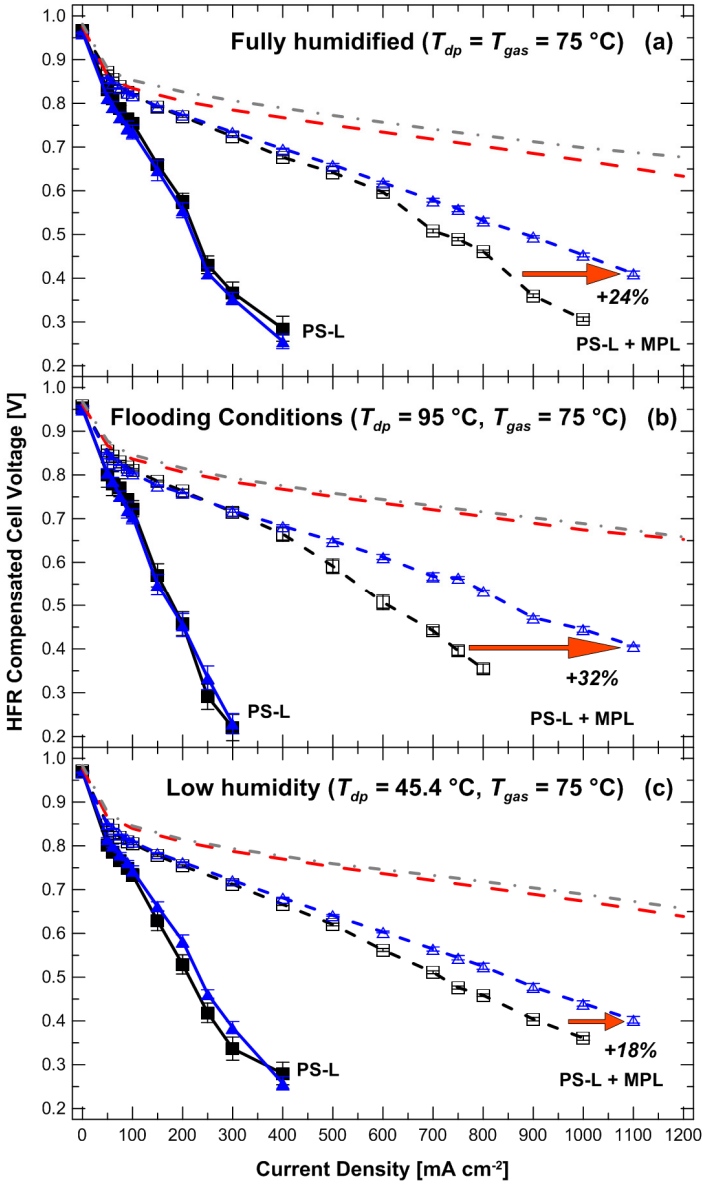

Figure 5.6 – Effect of heliox as the oxidant gas when using a perforated sheet (PS-L) with and without an additional MPL (MP30Z), at three different operating conditions. (a) Fully humidified, (b) flooding conditions, and (c) low humidity. (—■—) PS-L without MPL and air, (--⊡--) PS-L with MPL and air, (—▲—) PS-L without MPL and heliox, (--△--) PS-L with MPL and heliox, (- - - -) baseline and air, and (·-·-·-·) baseline and heliox. The baseline MEA used a 25BC GDL for the cathode. All tests had 25DC GDLs in the anode side.

5.4 Conclusions

This chapter presents the investigation of *in-situ* performance characteristics of structured perforated sheets used as gas diffusion layers. Different parameters such as diameters (and open areas), thicknesses, and in-plane diffusion capabilities through the use of channels were investigated. Microporous layers were also used in

order to observe the effect of improved in-plane diffusion when coupled with perforated sheets. The following conclusions resulted from the study:

1. Perforated sheets with just perforations (no channels) showed low performance due to the lack of in-plane diffusion. Performance decreases when thicker materials are used due to the increase in the transport travel path.
2. Although the use of channels that connect perforations on one side of the sheets was expected to allow for enhanced oxygen diffusion towards the catalyst layer, it is observed that these channels have a greater effect on the improvement of water transport. A balance between channel width and depth is important in order to achieve better performance. From Table 5.1, it can be concluded that for these specific perforated sheets the optimal channel width (C_w) is approximately 0.5 mm, and the performance improves with greater channel depth.
3. Perforated sheets with channels (with and without a microporous layer) improve voltage stability and water removal capabilities compared to cases of perforated sheets without channels.
4. Structured GDLs show promise for applications in which dry (no humidification) to fully humidified conditions are used due to their lower open area (compared to CFPs).

These results, along with the other investigations found in the literature [110,124], suggest that engineered GDLs have the potential to be used for specific applications and operating conditions. Proper design and tailoring of these materials (e.g., perforation geometry, density, location, etc.) could result in a reduction of overall fuel cell costs and an improvement in performance, particularly for more challenging operating conditions. As mentioned previously, the major issues with these materials are the lack of open area and in-plane diffusion. Unfortunately, these issues are closely connected to the manufacturing capabilities/methods of materials that meet the restrictions set in fuel cell industry (e.g., electrical and thermal conductivities, thickness, mechanical strength, corrosion resistance, etc.). However, as the field of manufacturing keeps evolving so will the opportunities of tailoring new materials that

can work properly in fuel cell applications. It is important to note that the perforated stainless steel sheets did not puncture or damage any CCM or MPL during testing. However, for durability purposes softer and more corrosion-resistant materials, such as graphitic foils or conductive polymers, could be considered instead of stainless steel sheets.

6 FLOW CONTROL IN A FUEL CELL FLOW FIELD FOR IMPROVED PERFORMANCE AND RELIABILTY[6]

6.1 Introduction

Normally, proton exchange membrane fuel cells and, particularly, the flow fields are designed around their maximum power operating point in order to maximize the overall performance. For applications with a wide range of operating conditions, this means that the fuel cell and flow fields are not optimally designed for the lower power regime. This is particularly true for automotive fuel cell applications where the turndown ratio can be very significant (>100). For example, in a typical dynamic testing profile (DTP), reported by the U.S. Fuel Cell Council, it is shown that a normal fuel cell stack used in transportation applications experiences a number of instant changes in power levels (e.g., from 100 to 60% and from 60 to 20%) [226]. These sudden changes in power significantly affect the performance of the fuel cell stack, especially in the low power range. This is a result of water accumulation in the bipolar plate flow field channels (after the stack performed at high power levels where more water is generated) that can no longer be removed because of the significantly reduced gas flow rates [227] and corresponding lower pressure drops. This can result in poor cell water management and cell-to-cell reactant distribution in the whole stack, which in turn can cause temperature gradients across the cell active area (damaging the membrane), loss of efficiency, and even operating failure. In fact, this erratic performance can lead to a low cell voltage condition and, in the worst-case, cell reversal in a fuel cell stack with inherent failure mode issues [203].

In fuel cell stacks, the gas mal-distribution and water management issues that each cell experiences are increased since each cell is located in parallel with respect to each other in terms of flow distribution (they are in series in terms of electrical connection) with one common inlet manifold and one common outlet manifold (usually both located inside the stack) [73]. In general, it is critical that each cell in

[6] Sections of this work have been published in:
M. Blanco, D.P. Wilkinson, G. Yan, H. Zhao, H. Wang. Flow control in a fuel cell flow field for improved performance and reliability. ECS Transactions 2006;1:355-66.
D.P. Wilkinson, M. Blanco, H. Zhao, J. Wu, H. Wang. Dynamic flow field for fuel cells. Electrochemistry and Solid State Letters 2007;10:B155-60.

the stack can receive an adequate amount of reactant gases; however, this can be difficult to accomplish with parallel manifolding and cell water management issues, such as water accumulation, in the inlet region of the cells [228]. Numerous studies of flow distribution in stacks (cell-to-cell distribution) can be found in the literature [229-233].

As stated in Chapter 1 (Section 1.4.1.2), some of the common approaches to improve the water management in a cell/stack include performing systematic purges and/or increasing the reactant flow rate. However, both of these solutions increase the parasitic loads significantly. Section 1.4.1.2.4 describes a number of proposed systems that have been attempted in order to improve the overall fuel cell stack performance without increasing the parasitic energy demand. In this chapter, we discuss in detail, an approach for changing the flow field active area within a cell with changing operating conditions. It is shown that the voltage instability and water management issues that occur in a fuel cell, particularly at low power levels, can be mitigated by changing the effective active area inside the cell.

6.2 Experimental

The details regarding the fuel cell hardware and fuel cell test station are given in Section 2.2. The modified flow field plates for single cell and stack testing are explained in Sections 2.2.1.1 and 2.2.1.2. The membrane electrode assemblies used for all the tests were conditioned following the protocols explained in Section 2.1.3. The experiments used to test the voltage stability of a fuel cell at low gas stoichiometries and low power densities are explained in detail in Section 2.2.3. For all the tests, the gases were pressurized to 206.8 kPag (30 psig) and both the single cell fuel cell and stack were compressed to 689.5 kPa (100 psia).

6.3 Results and discussion

6.3.1 Comparison performance of standard and modified flow field plates

Figure 6.1 shows the single cell polarization curves (based on current density) and associated pressure drop curves for both the modified interdigitated and serpentine

flow field plates. For comparison, a polarization curve of a Mk 5 standard cathode serpentine flow field (six path) is also shown. All the polarization curves were performed following the protocol explained in Section 2.1.3. For the interdigitated flow field, for a typical minimum voltage efficiency design point of 0.6 V the current density is approximately 1130 mA cm^{-2}, the areal power density is 0.68 W cm^{-2}, and the pressure drop is 17.1 kPa (2.48 psi). However, at low power (e.g., 0.083 W cm^{-2} at 100 mA cm^{-2}) the pressure drop is 1.6 kPa (0.23 psi), about an order of magnitude lower. Similarly, for the serpentine flow field the current density at 0.6 V is approximately 800 mA cm^{-2}, the areal power density is 0.48 W cm^{-2}, and the pressure drop is 18 kPa (2.61 psi). At the low power (100 mA cm^{-2}) the pressure drop is around 2.0 kPa (0.29 psi), again about an order of magnitude lower. At this low power end there can be insufficient flow and pressure drop to remove liquid water, and to ensure uniform reactant flow over the cell active area and cell-to-cell in a fuel cell stack.

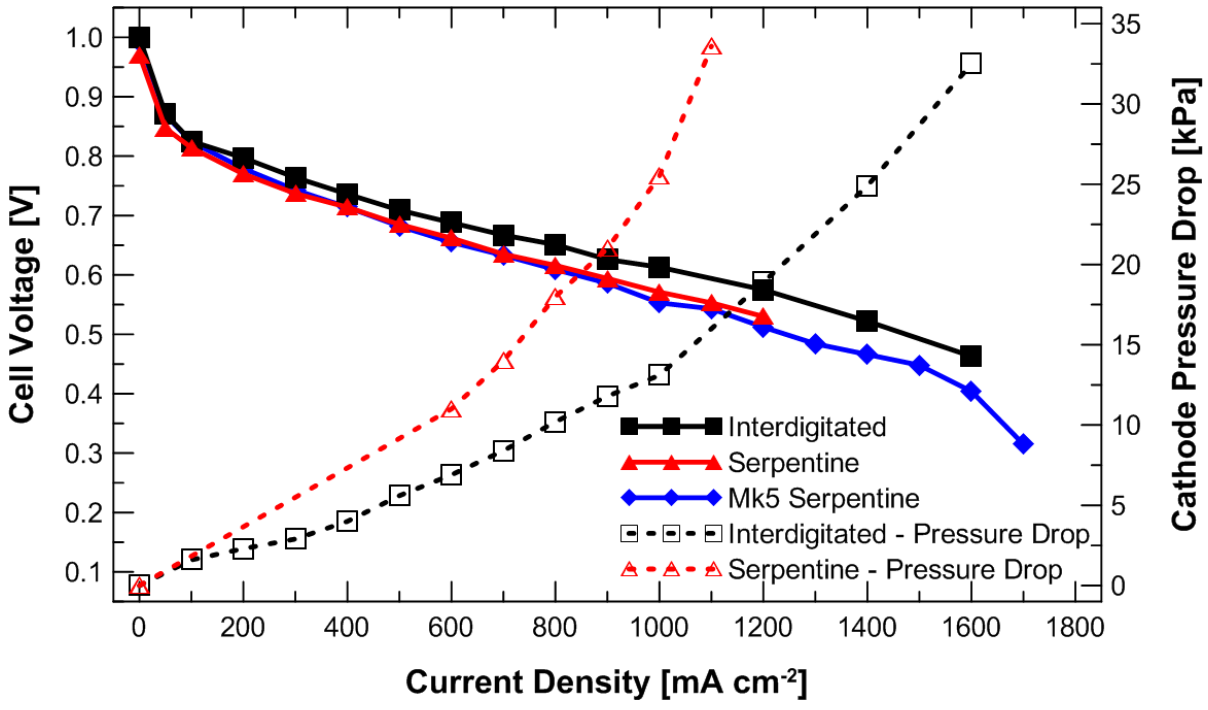

Figure 6.1 – Polarization and pressure drop data for the single cell with the interdigitated (all valves open), serpentine flow field plate (all valves open), and standard serpentine flow field plate (no pressure drop for this case). The cell, gas, and dew point temperatures were 75°C. The gases were pressurized to 206.8 kPag (30 psig) and the cell was compressed to 689 kPa (100 psia). The air/H_2 stoichiometric ratio was 2/1.5.

Figure 6.2 shows the polarization curves of the modified serpentine flow field for each cell of the fuel cell stack with all valves opened. It is evident that there are no significant differences between the performances of each cell, indicating good reproducibility.

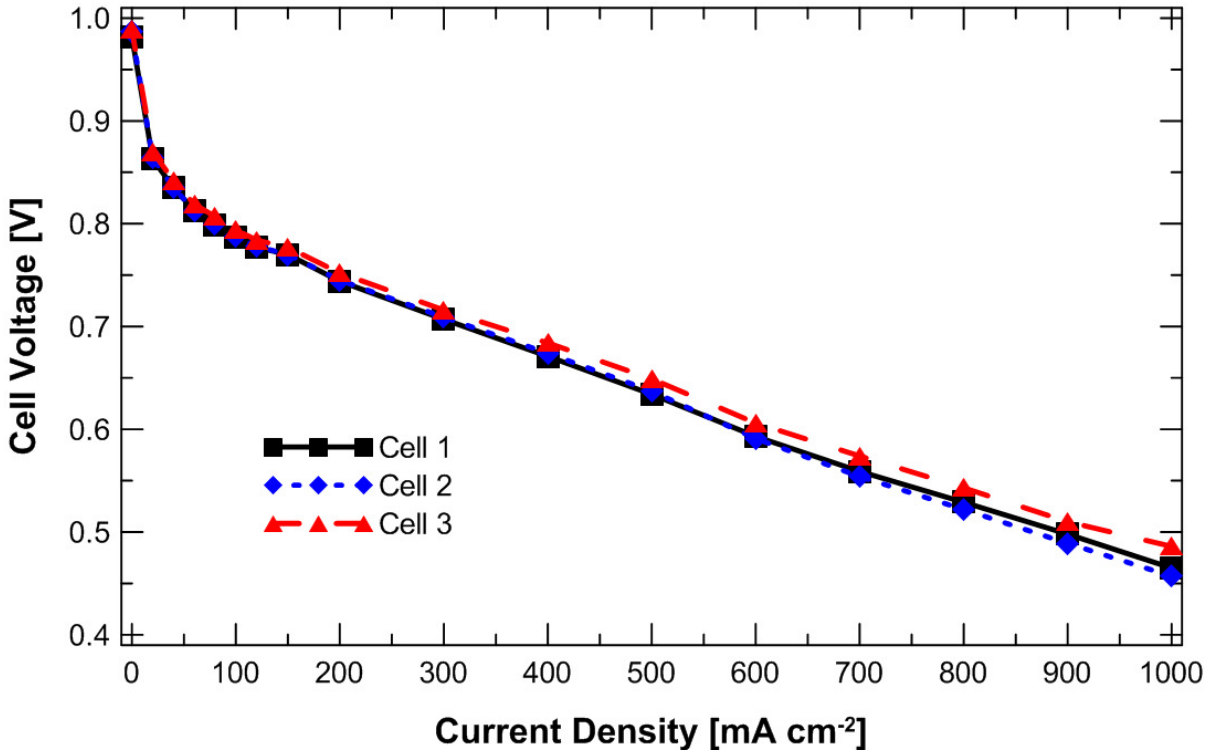

Figure 6.2 – Polarization curves for the three cells of the fuel cell stack (serpentine flow field plates with all valves open). The cell and gas temperatures were 75°C and the dew point temperature was 80°C. The gases were pressurized to 206.8 kPag (30 psig) and the cell was compressed to 689 kPa (100 psia). The air/H_2 stoichiometric ratio was 3/1.5.

For the single cell tests, Figure 6.3 shows that the cell performance (with the interdigitated flow field) is similar on a current density basis for the full active area (all valves open) and for a partial active area (four valves closed in this case). Basically, for the case shown here, the combined active cell area of sections 3 and 4 (total area 78.8 cm^2) gives similar polarization results to the full active area of 260 cm^2 (sections 3 and 4 are located in the middle of the active area – see Figure 6.3). This result indicates that each partial active section of the cell is performing similarly, which is critical in any approach that involves changing the active area. Figure 6.4 compares polarization curves on an absolute current basis for the full active area (all valves open) and for a partial active area (four valves closed) with the interdigitated

flow field in the single cell fuel cell. In the case of the partial active area, the voltage is lower because of the higher effective current densities. However, the associated higher effective reactant flow over the reduced area is the main factor that improves the performance stability in the low power range.

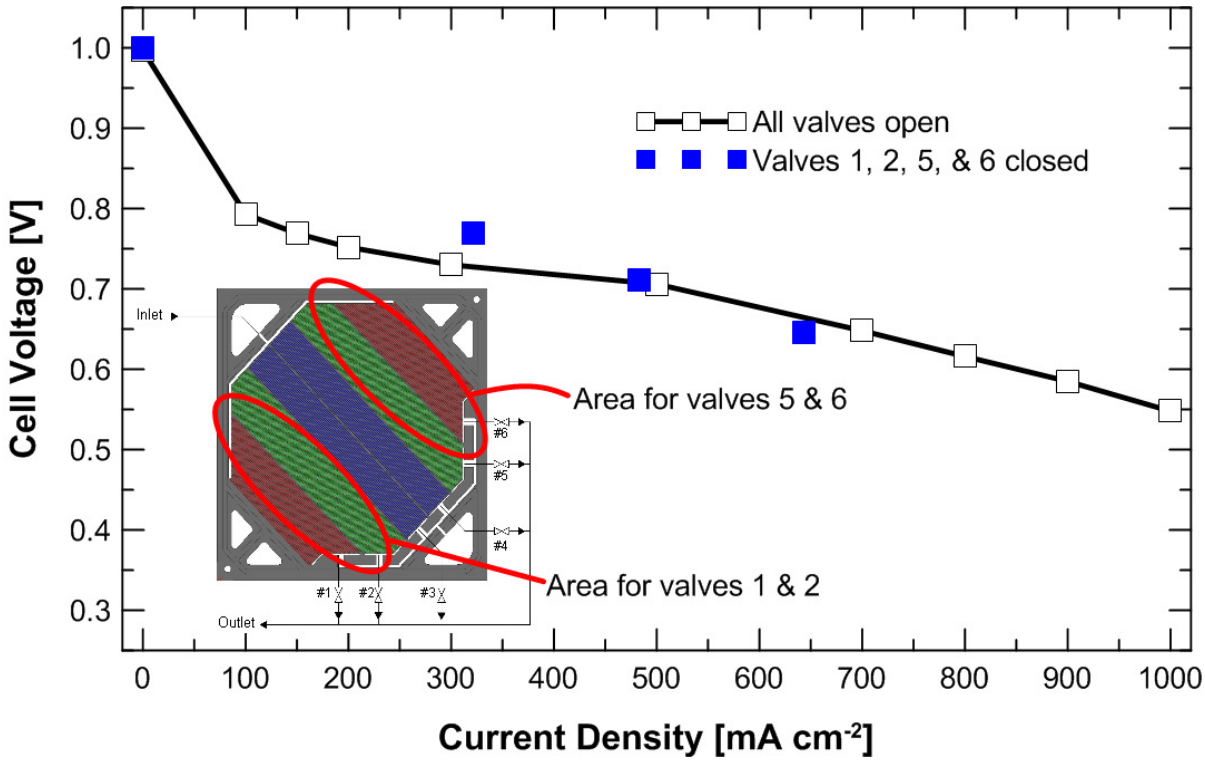

Figure 6.3 – Voltage vs. current density for all valves open and four valves closed. The cell, gas, and dew point temperatures were 75°C. The gases were pressurized to 206.8 kPag (30 psig) and the air/H_2 stoichiometric ratio was 1.5/1.5.

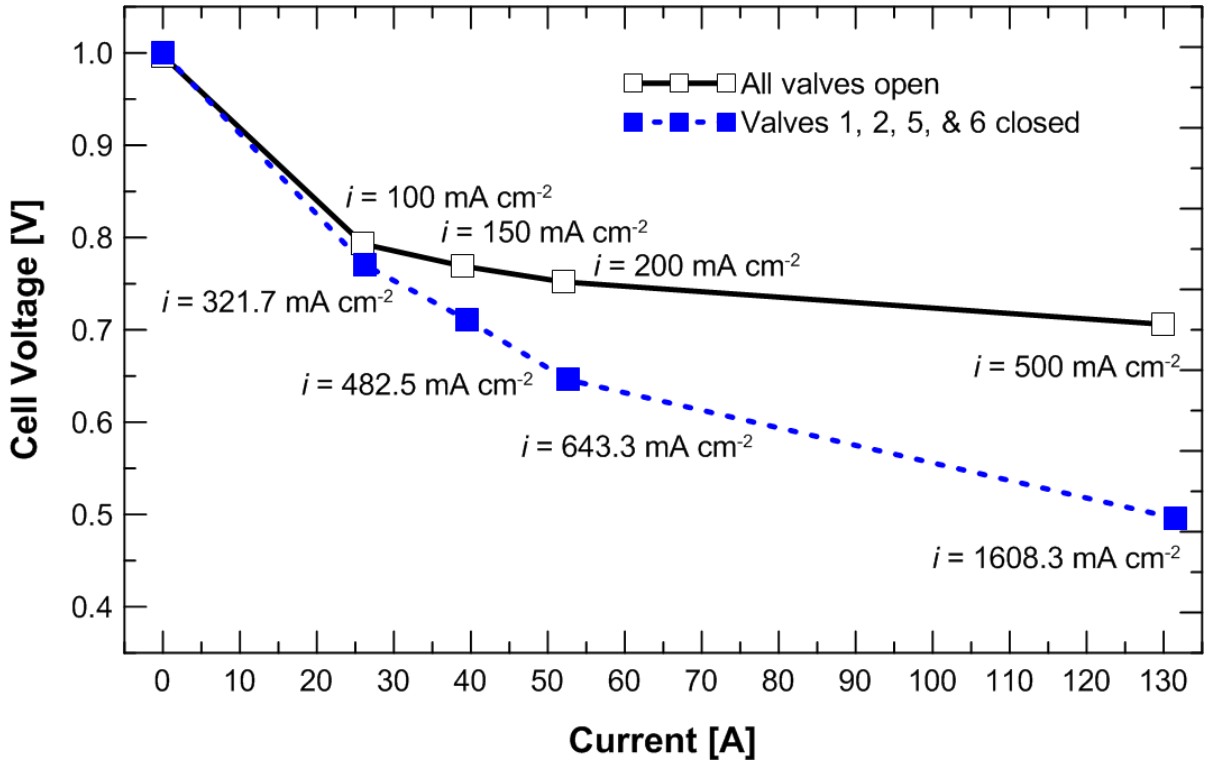

Figure 6.4 – Voltage vs. current for all valves open and four valves closed. The cell, gas, and dew point temperatures were 75°C. The gases were pressurized to 206.8 kPag (30 psig) and the air/H_2 stoichiometric ratio was 1.5/1.5.

The similar polarization results, analyzed on a current density basis, for partial active areas versus the full active area indicate that the blocked area provides essentially no current. Any initial reactant in the blocked area would be consumed rapidly and lateral reactant transport through the diffusion layers is slow. The electrode potential experienced by the blocked area is largely determined by the partial active area, which is supplying the current since both areas are in electrical contact. For the blocked stagnant area the electrode potential is not expected to be in a range that causes water electrolysis or material decomposition. Future work will involve current mapping of the active and blocked regions to further elucidate the effects of changing the active area.

6.3.2 Impact of low air stoichiometry on voltage stability

Figure 6.5 shows the impact of decreasing air stoichiometry on voltage stability at a fixed low power current density of 100 mA cm^2 with the interdigitated flow field in the single cell fuel cell. Clearly, as the air stoichiometry is decreased below 1.3 the

voltage oscillations increase significantly indicating an unstable performance condition. This is often an indication of liquid water blockage in the channel(s) and/or in the gas diffusion layer (GDL) with insufficient gas flow or pressure drop for water removal. As mentioned previously, this erratic performance can lead to a low cell voltage condition and, in the worst-case, cell reversal in a fuel cell stack with inherent failure mode issues [203].

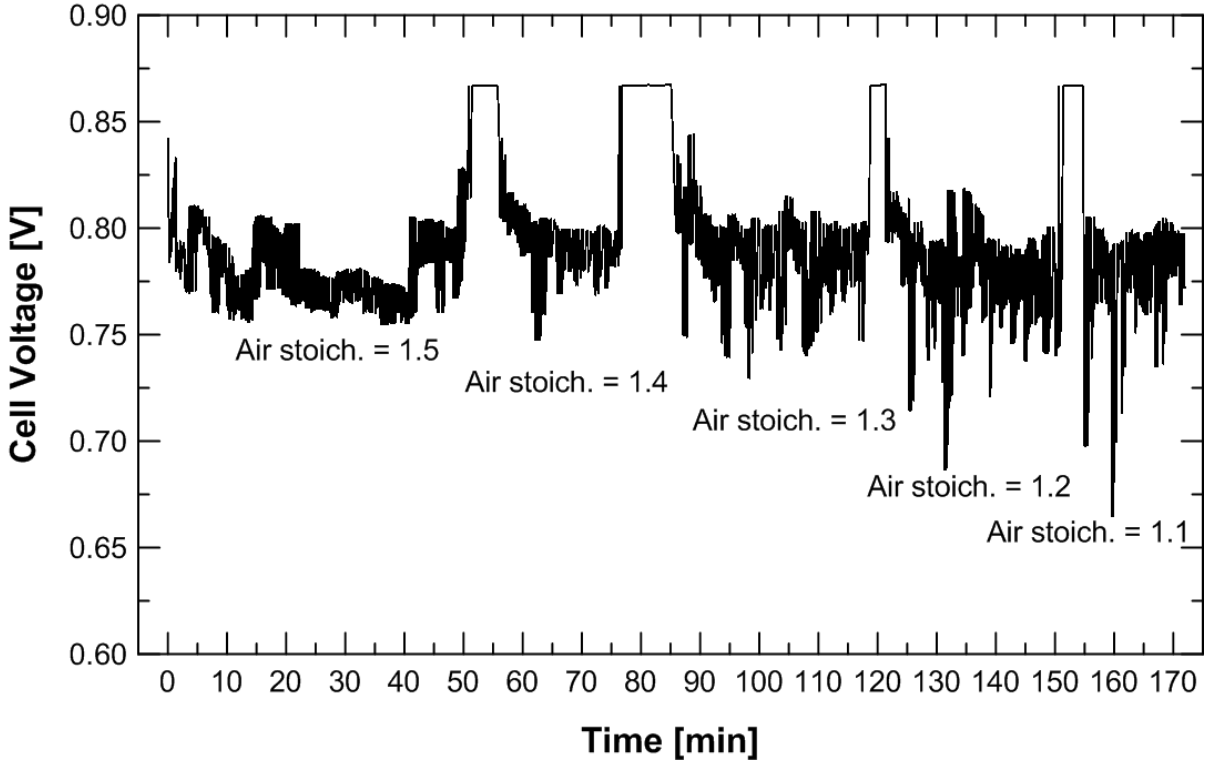

Figure 6.5 – Voltage oscillations for decreasing air stoichiometry (all valves open). For this case the single cell with interdigitated flow field was operated under a load of 100 mA cm^{-2}, H_2 stoichiometry of 1.5, and cell temperature of 75°C. The gases were pressurized to 206.8 kPag (30 psig).

6.3.3 Improvement of voltage stability in a single cell fuel cell

By decreasing the active area of the interdigitated flow field in the fuel cell, stable performance was recovered at low power conditions (e.g., 80 mA cm^{-2}) and at low reactant stoichiometry (see Figure 6.6). In this case, decreasing the active area by around 70% (from 260 to 78.8 cm^2) increases the effective current density (from 80 mA cm^{-2} for the full active area to 264 mA cm^{-2} for the reduced active area) and reactant flow (from 0.38 to 1.27 SLPM) by about 330%, stabilizing the cell voltage

and removing the large voltage oscillations and spikes. It is important to note that there are still small voltage oscillations, which are likely a result of residual water in the channels. More studies on the relationship between voltage stability, voltage oscillations, and water management can be found in the literature [71,234-236].

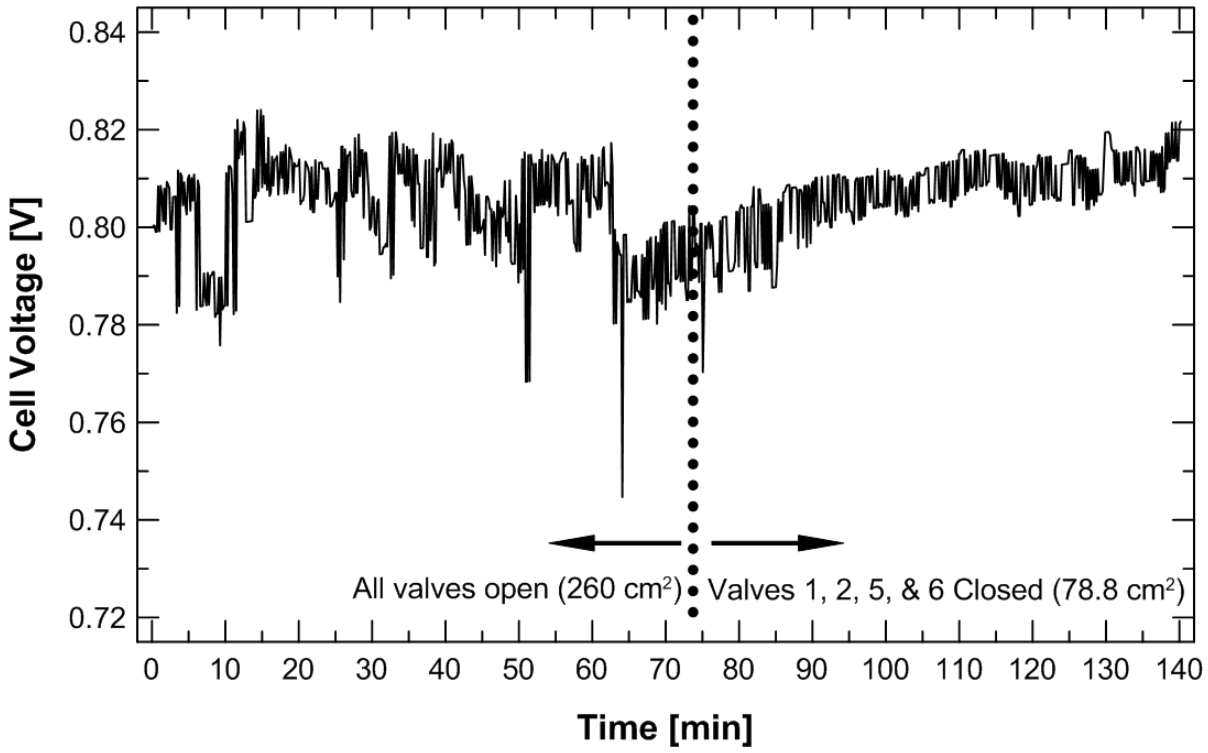

Figure 6.6 – Voltage traces showing recovery of unstable performance with active area sections closed (valves 1, 2, 5, and 6 closed). For this case the single cell with the interdigitated flow field was operated under a load of 80 mA cm^{-2}, air/H_2 stoichiometries of 1.1/1.5, and cell temperature of 75°C. The gases were pressurized to 206.8 kPag (30 psig).

When a serpentine flow field was used, the cell's voltage instabilities were not as visible and obvious at low currents (<100 mA cm^{-2}), as with the interdigitated flow fields. This is due to the differences between each flow field design for water management control. The serpentine flow field has better water management control at low power but the interdigitated flow field performs substantially better at high power. In order to be able to observe the voltage instability of the serpentine flow field it was necessary to run the single cell at more severe operating conditions than for the interdigitated flow field, mainly at lower air/H_2 stoichiometries of approximately 1.2/1.1, respectively. Figure 6.7 shows a voltage trace of the single cell fuel cell with serpentine flow field with all valves open and with two valves

closed. Closing the two valves located at the edges of the flow field (i.e., valves 1 and 6) reduces the voltage oscillations observed when all the valves are open. However, the effects are not as pronounced as for the interdigitated flow field. Further tests with a lower cell temperature (60°C) were performed in order to achieve more distinct voltage oscillations at the low power end (<0.08 W cm^{-2}) but the cell's performance did not deteriorate significantly more with these changes. These results indicate that the effect of controlling the performance by manipulating the active area is more effective for flow fields that have more erratic performance at low power.

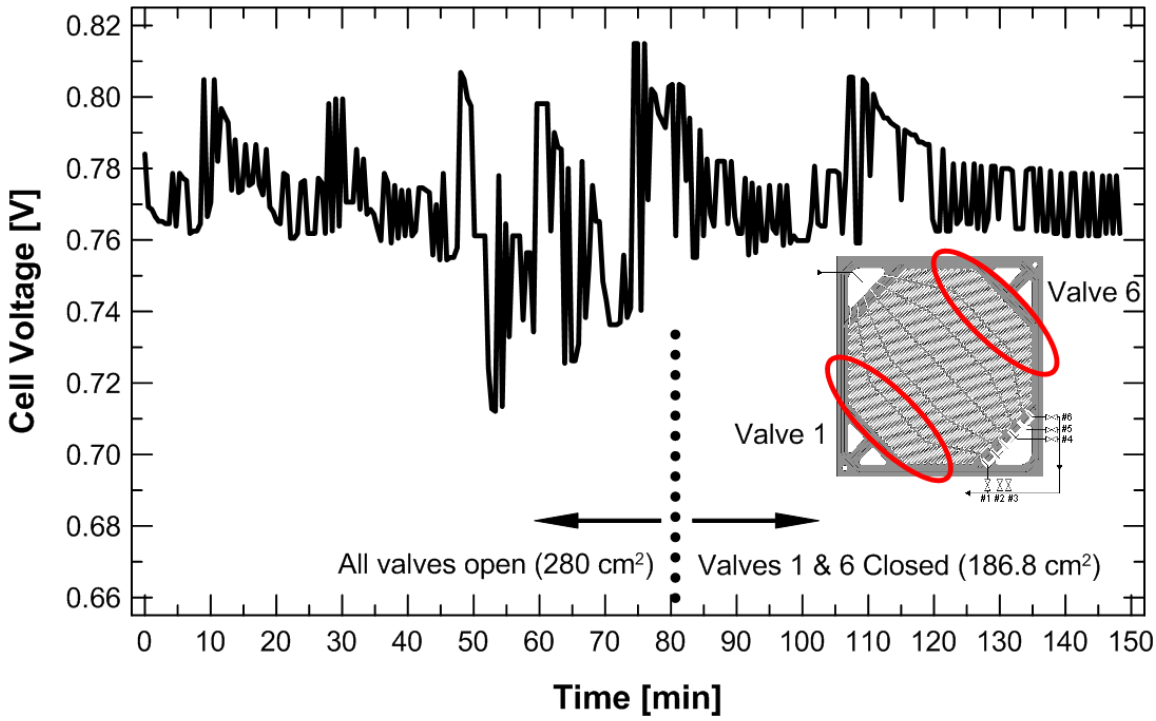

Figure 6.7 – Voltage traces showing recovery of unstable performance with active area sections closed (valves 1 and 6). For this case the single cell with serpentine flow field was operated under a load of 100 mA cm^{-2}, air/H_2 stoichiometries of 1.2/1.1, and a cell temperature of 75°C. The gases were pressurized to 206.8 kPag (30 psig).

6.3.4 Improvement of voltage stability in a fuel cell stack

Operating conditions can be chosen to enhance the flooding process on the cathode side of the cell, thus, making the voltage instabilities more apparent, especially when reducing from high to low power densities. For this reason, the three-cell fuel cell stack with serpentine flow fields used in this study was over humidified. Figure 6.8

shows both the voltage instability of the fuel cell stack when running at low power (current density of 107 mA cm^{-2}) and the impact of decreasing the active flow field area of all the cathode plates (serpentine flow field) in the stack by closing just two valves (valves 1 and 2 in this specific case; 169 cm^2 active area for each cell). For these measurements the gases were humidified at 75°C and the cell and gas temperatures were kept at 60°C. This temperature difference was used in order to accelerate the flooding process on the cathode flow fields and promote unstable performance. As a result, it can be observed that cell 2 is unstable since its voltage is lower and shows significant oscillations. Given that the other two cells within the stack seem to be performing well without major difficulties, it can be concluded that at these operating conditions there is an unequal cell-to-cell reactant distribution within the stack. Basically, there is insufficient flow rate and pressure drop inside cell 2 to remove the liquid water located in the GDL and flow channels, resulting in major performance issues (e.g., limited gas permeability, inactivity of certain areas of the catalyst layer, etc.). Once valves 1 and 2 are closed it can be observed that cell 2 recovers and the performance difference between the cells in the stack is decreased dramatically. The average voltage of each cell is decreased once the active areas are reduced due to an increase in the effective current density. Through this mechanism the overall cell-to-cell flow distribution in the stack has been improved and potential major failure modes have been mitigated. It was observed that the low performing cell(s) can move around in the stack for a given set of operating conditions. In all cases the approach of changing the effective cell active area or increasing the absolute reactant flow to the cell recovers performance and stability.

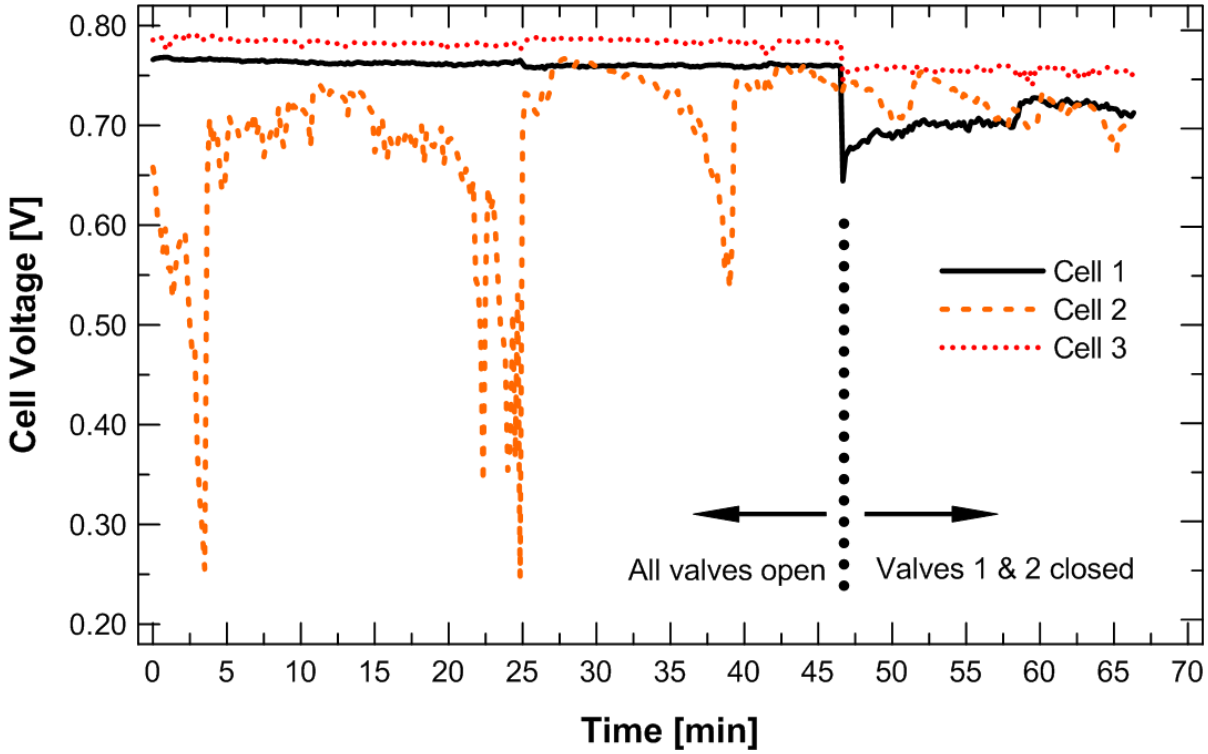

Figure 6.8 – Individual cell voltages at low load without and with valves closed. For these tests the cell and gases temperatures were kept constant at 60°C, the humidification temperature was 75°C, the current load was 107 mA cm^{-2} (30 A) and the air/H_2 stoichiometries were 2.8/1.5. The gases were pressurized to 206.8 kPag (30 psig),

In general, reducing the active area in the low power region increases the effective current density, and increases the effective reactant flow and associated pressure drop. However, the absolute current and flow do not change from the normal situation for the full active area. Thus, improved fuel cell stack performance stability is achieved without increasing the parasitic load significantly (only a small increase for the increase in pressure drop). In fact, the overall system's parasitic load may be significantly reduced because increased absolute reactant flow and purges are not required (optimized usage of reactant gases). The suppressed voltage curve at low power as a result of higher current density may also have benefits in terms of reduced corrosion issues (and other failure modes).

6.4 Conclusions

In this work we studied the cell voltage stability of a proton exchange membrane fuel cell at low power densities and low reactant stroichiometries. A new approach used

to improve the cell's performance and stability at these conditions was demonstrated. The following are the conclusions that were drawn:

1. It was observed that fuel cells at low current densities (<100 mA cm^{-2}) and low reactant stoichiometries (<1.5 for the oxidant gas) experience increased cell voltage oscillations indicating an unstable performance. This is due water blockage in the channel(s) and/or in the GDL.
2. Our research has demonstrated that fuel cell performance stability can be achieved at low power and low reactant stoichiometry by using the novel approach of changing the cathode flow field active area with changing operating conditions.
3. By reducing the active area of the flow fields, the effective current density and effective reactant flow and associated pressure drop are increased. However, the absolute current and flow do not change from the normal situation for the full active area. Thus, the higher effective reactant flow over the reduced area is the main factor that improves the performance stability at low power densities.
4. This method was verified in a single cell fuel cell and in a three-cell fuel cell stack. In each case, the fuel cells were able to reach voltage stability after the active areas were modified, thus improving the water management, and the cell-to-cell reactant distribution within the stack, and reducing the potential for low power failure modes.
5. This approach maintains high and stable performance in the fuel cell system without significantly increasing the parasitic load. In addition, the optimized usage of reactant gases is improved with this method since the need of using high reactant flow rates and purges is reduced significantly.

Changing the active area in a fuel cell flow field (for both anode and cathode flow fields) with respect to its operating conditions is a very new approach and could provide significant benefits for future fuel cell designs, particularly for applications with a wide range of operating conditions such as transportation applications. However, one drawback of this approach is the addition of more parts and valves to the overall fuel cell system. Thus, more work must be done in order to use smaller

valves that could be placed inside the flow field plates. This could be accomplished by using microelectromechanical (MEMS) valves.

7 CONCLUSIONS AND RECOMMENDATIONS

7.1 Conclusions

This thesis focused on the understanding of water management issues inside PEM fuel cells and on the development of methods that can reduce the negative effects of these issues. Emphasis was given to water management at low to no gas humidification conditions, voltage and power instability at low power levels, and further clarification of the role of the cathode and anode microporous layers. The use of perforated sheets as engineered gas diffusion layers was also investigated. The following conclusions were drawn from each chapter of this thesis.

Application of water barrier layers in PEM fuel cells:

- The performance of fuel cells deteriorates significantly when low to no gas humidification is used.
- Adding a non-porous material with perforations between the cathode flow field plate and the GDL improves water saturation in the cathode GDL and catalyst layer, increases water content in the anode, and keeps the membrane hydrated.
- The slight voltage drop in the performance as a result of transport limitations brought by the use of the perforated sheets is justifiable since the overall durability of the cell at these extreme conditions is enhanced.
- The perforated layer(s) enhanced the operational life of the PEM fuel cell under completely dry conditions by 3.5 times compared to a fuel cell without the additional water barrier layers.

Experimental study of the role of the microporous layer:

- The cathode MPL improves the fuel cell performance at three different operating conditions: fully humidified (100% RH), flooding, and low humidity (25% RH).
- The cathode MPL improves the voltage stability of the cell compared to a GDL without an MPL.

- The MPL increases the water back-diffusion from the cathode to the anode through the membrane. However, it was shown with the use of perforated sheets and the anode water removal (AWR) method that this method of water removal is not the main mechanism that the MPL uses to improve water management on the cathode side.
- The cathode GDL without an MPL allows for greater water accumulation inside the catalyst layer, thus, resulting in flooding issues.
- The main mechanism of water removal that is used when a cathode MPL is present is through the cathode side of the fuel cell (not the anode as previously proposed in the literature). The MPL does not allow water accumulation in the catalyst layer, thus, it improves the water removal from the catalyst layer to the flow field channels. It is postulated that the water is rejected by the MPL in vapor form at the catalyst layer and it then condenses in the GDL. This is a similar conclusion to that proposed by Owejan et al. [186].
- The influence of the anode MPL on fuel cell performance is insignificant for current densities below 1600 mA cm^{-2}; however, it decreases the voltage stability especially at higher current densities.
- It is recommended for the anode MPL to be used in PEM fuel cells due to its ability to remove water accumulated on the anode side. This was proven by a decrease in voltage fluctuations when an anode MPL was used.

<u>Use of perforated sheets as engineered GDLs:</u>

- In-plane diffusion is an important parameter in order to achieve a better distribution of oxygen along the catalyst layer.
- The use of narrow channels connecting the perforations improves the water removal capabilities of the perforated sheets but not the oxygen diffusion. Wider and deeper channels allow both enhanced water and oxygen transport.
- The implementation of a free-standing MPL along with the perforated sheets improves the performance of the fuel cell substantially, compared to the cases without the MPL. This is a further indication of the importance of in-plane diffusion.

- The use of channels in perforated sheets with an MPL improves the voltage stability of the cell at all current densities. This is an indication that the channels allow the liquid water to be removed more efficiently, compared to the cases without channels.
- Deeper channels improve oxygen diffusion due to the increase in paths that the gas can travel.
- Perforated sheets as GDLs perform well below baseline GDLs (with an MPL), but show promise to be a viable possibility as a GDL in the future due to their ability to be tailored and modified (i.e., perforation size and shape, interconnections, etc.).

Flow control in a fuel cell flow field:

- This work showed that fuel cells designed around their maximum power operating point can experience voltage and power stability issues at low power levels. This results in cell water management issues and poor cell-to-cell reactant distribution in a fuel cell stack.
- An approach in which the cathode flow field active area is changed with changing operating conditions was investigated and it showed that it maintains high and stable performance in the fuel cell system without increasing the parasitic load significantly.
- Reducing the active area with these flow fields in the low power region increases the effective current density and the effective reactant flow and associated pressure drop. However, the absolute current and flow do not change from the normal conditions for the full active area.
- This dynamic flow field is beneficial for applications with a range of operating conditions since it improves cell-to-cell reactant distribution and reduced low current density failure modes.

7.2 Recommendations for future work

This thesis investigated different water management issues at different operating conditions within the fuel cell. Throughout this work, various areas were identified as potential topics that should be investigated even further to build upon this PhD work.

The following are the proposed research directions for future work. They primarily involve the optimization of the different approaches and experimental techniques discussed in Chapters 3, 4, 5 and 6.

Perforated sheets as water barrier layers:

- Study the effect of the perforated sheets when located between the anode flow field channels and GDL. These sheets may improve water management inside the cell while not affecting the performance as significantly as when used on the cathode side.
- Optimization of the perforated sheets and corresponding flow field design in order to improve the performance while still allowing the membrane to stay hydrated at low to no gas humidification conditions:
    - Consider a new fuel cell design closer to that used in back-up power applications in which the oxygen stoichiometries are significantly larger (>30) due to the use of cooling fans.
    - Design perforated sheets to match the open area of the flow field channels, thus, maximizing the area for oxygen diffusion.
    - Investigate the use of perforations with different cross-sections that could improve oxygen diffusion and water removal, while still maintaining a balanced distribution of water content in the cathode catalyst layer.
    - Examine various flow field designs (e.g., parallel and multiple-path serpentine).
- Consider other possible electrical and thermal conductive materials that could be used as water barrier layers based on their machinability and manufacturability.
    - Investigate possible surface treatments (or modifications) that enhance water and gas transport with these perforated sheets.
- Perform different durability tests to observe possible issues with the water barrier layers
    - Long-term testing at dry gases and room temperature conditions.
    - Testing at low to freezing temperatures with no gas humidification.
- Develop mathematical models that will help the development of new designs:

- Study the relationship between perforation size, shape, and location in order to understand the effect on oxygen diffusion and liquid water saturation.
- Predict long-term failure modes with these water barrier layers. These results will help the development of new designs.

Perforated sheets as engineered gas diffusion layers:

- Further development is required for engineered GDLs based on non-porous materials with perforations (see Figure 7.1):
  - Identify the best fuel cell application for these type of GDLs since each application represents a different set of requirements to be met and achieved.
  - Investigate the application of a sprayed MPL on one of the surfaces of the perforated sheet. This layer enhances in-plane diffusion and water removal capabilities.
  - Use mathematical modelling to investigate the gas and liquid water interaction with different perforation designs (i.e., size, shape, density).
  - Develop perforations that are specifically designed for liquid water transport. Different cross sectional shapes of the perforations can be taken into account. Coating of hydrophobic (or/and hydrophilic) layers should also be implemented and tested
  - Investigate the interaction between different cathode flow field channel designs and the perforated GDLs. These GDLs could be tailored depending on the flow field channel used.
  - Investigation of softer and corrosion resistant materials is a critical step in order for this engineered GDL approach to achieve acceptable performance. An emphasis on machinability and manufacturability has to be given.
  - Investigate the possibility of designing and developing an engineered GDL and flow field channel plate into one component. This can possibly reduce the overall costs of the fuel cell system.
- Another approach to achieve engineered gas diffusion layers with improved fuel cell performance is through the use of porous materials (see Figure 7.1):

These GDLs that use porous materials as the substrates that are then perforated and mechanically modified have been shown to have similar performance to unmodified carbon fiber paper (CFP) GDLs [39,128-131,225].

- Investigate different methods to perforate CFPs taking into account the feasibility of expanding such method for large-scale production.
- Identify how different sizes of perforations modify the water and gas transport mechanisms inside the cathode catalyst layer.

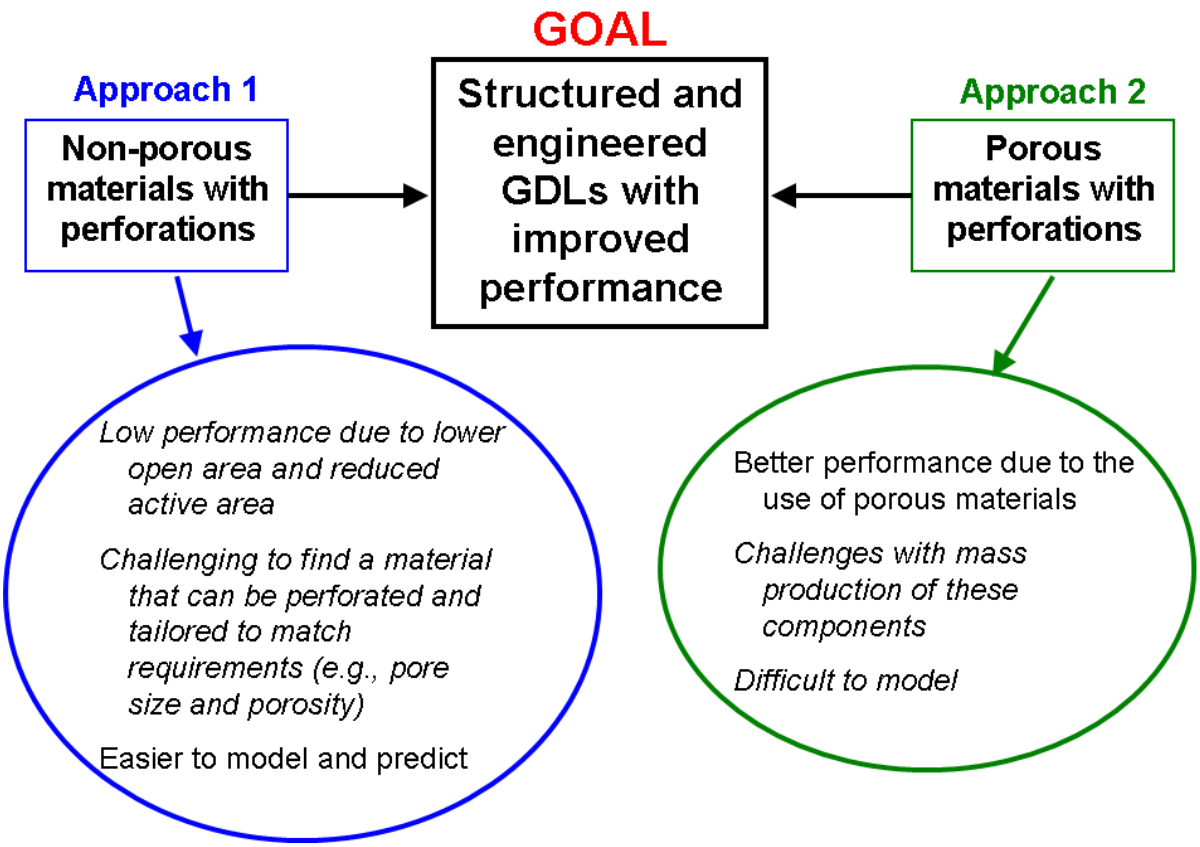

Figure 7.1 – Two main approaches for development of structured and engineered gas diffusion layers for PEM fuel cells.

Understanding of water transport inside a fuel cell – the role of the MPL:

- The fact that many competing hypothesis can be found in literature regarding how the MPL works inside a fuel cell is a sign that there is not a standard in the investigation of this component. Each fuel cell, flow field channel design, material, membrane, catalyst layer, and operating condition changes the

overall gas and water transport inside the fuel cell. Therefore, a thorough study of the MPL taking into account different parameters is needed:

- Investigate different carbon fiber papers and carbon cloths GDLs with different thermal properties in order to observe their effect on the MPL.
- Develop a study of the effect of the MPL with different flow field channels that are designed for optimal performance:
  - Interdigitated
  - Serpentine, single and multiple path
  - Parallel with adequate aspect ratio

  Ideally, these flow field designs should resemble those used by the state-of-the-art fuel cells found in industry.
- Perform water balance measurements to observe the effect of the MPL in water back-diffusion to the anode side.
- Study different catalyst layers and membranes since they affect oxygen and water transport, thus, affecting the MPL's role.

<u>Dynamic flow field for flow control inside a PEM fuel cell:</u>

- Perform further experiments with the interdigitated flow field in order to observe how these dynamic flow fields can improve the power stability in a fuel cell stack. Long-term tests with different loading cycles should be performed to understand the long-term effects of using this system.
- Investigate the possibility of using microelectromechanical (MEMS) valves that can be placed inside the flow field channels in order to control the areas in which the reactant gases are flow through. Conductive polymers can be possible candidates since they have the ability of changing shape (i.e., closing and opening certain areas) when exposed to specific potentials.
- Develop a current mapping technique coupled with the dynamic flow field to further elucidate the effects of changing the active area at different operating conditions.
- Develop MEAs that use different types of GDLs that match the area of the flow field that can be closed or open. Different carbon fiber papers and carbon cloths should be tested in order to have the best combination of materials that are better suited to the flow field (when open and closed).

- Use the dynamic flow fields as diagnostic tools in fuel cell stack testing. Different sections of the channels can be blocked in order to investigate cell-to-cell oxygen and water distribution.

REFERENCES

[1] Schoenbein CF. On the voltaic polarization of certain solid and fluid substances. Philosophical Magazine 1839;14:43-5.

[2] Grove WR. On voltaic series and the combination of gases by platinum. Philosophical Magazine 1839;14:127-30.

[3] Grove WR. On a gaseous voltaic battery. Philosophical Magazine 1842;21:417-20.

[4] Chen E. History. In: Hoogers G, editor. Fuel cell technology handbook, Boca Raton, FL: CRC; 2003.

[5] Barbir F. PEM fuel cells: Theory and practice. Burlington, MA: Elsevier Academic Press; 2005.

[6] Li X. Principles of fuel cells. New York: Taylor & Francis; 2006.

[7] Gyenge EL. CHBE 477: Fuel cells & Electrochemical systems course notes; 2004.

[8] Larminie J, Dicks A. Fuel cell systems explained. Toronto: John Wiley & Sons; 2003.

[9] Li H, Tang Y, Wang Z, Shi Z, Wu S, Song D, et al. A review of water flooding issues in the proton exchange membrane fuel cell. Journal of Power Sources 2008;178:103-17.

[10] Yousfi-Steiner N, Moçotéguy P, Candusso D, Hissel D, Hernandez A, Aslanides A. A review on PEM voltage degradation associated with water management: Impacts, influent factors and characterization. Journal of Power Sources 2008;183:260-74.

[11] Dai W, Wang H, Yuan XZ, Martin JJ, Yang D, Qiao J, et al. A review on water balance in the membrane electrode assembly of proton exchange membrane fuel cells. International Journal of Hydrogen Energy 2009;34:9461-78.

[12] O'Hayre R, Cha SW, Colella W, Prinz FB. Fuel cell fundamentals. New York: John Wiley & Sons; 2006.

[13] Kulikovsky AA. Analytical modelling of fuel cells. Amsterdam: Elsevier; 2010.

[14] Wilkinson DP, Voss HH, Prater K. Water management and stack design for solid polymer fuel cells. Journal of Power Sources 1994;49:117-27.

[15] Natarajan D, Nguyen TV. Current distribution in PEM fuel cells. Part 1: Oxygen and fuel flow rate effects. AIChE Journal 2005;51:2587-98.

[16] St-Pierre J, Roberts J, Colbow KM, Campbell S, Nelson A. PEMFC operational and design strategies for Sub zero environments. Journal of New Materials for Electrochemical Systems 2005;8:163-76.

[17] Fletcher NJ, Boehm GA, Pow EG. Method and apparatus for commencing operation of a fuel cell electric power generation system below the freezing temperature of water. US5,798,186; 1998.

[18] Roberts J, St-Pierre J, Van Der Guesst ME, Atbi A, Fletcher NJ. Method for improving the cold starting capability of an electrochemical fuel cell. US6,479,177;. 2002.

[19] Tajiri K, Wang CY, Tabuchi Y. Water removal from a PEFC during gas purge. Electrochimica Acta 2008;53:6337-43.

[20] Cho KT, Turhan A, Lee JH, Brenizer JS, Heller AK, Shi L, et al. Probing water transport in polymer electrolyte fuel cells with neutron radiography. Nuclear Instruments and Methods in Physics Research Section A: Accelerators, Spectrometers, Detectors and Associated Equipment 2009;605:119-22.

[21] Hou J, Yu H, Zhang S, Sun S, Wang H, Yi B, Ming P. Analysis of PEMFC freeze degradation at -20 ℃ after gas purging. Journal of Power Sources 2006;162:513-20.

[22] Hou J, Yu H, Yi B, Xiao Y, Wang H, Sun S, Ming P. Comparative study of PEM fuel cell storage at -20 ℃ after gas purging. Electrochemical and Solid-State Letters 2007;10:B11-15.

[23] Yu X, Pingwen M, Ming H, Baolian Y, Shao ZG. The critical pressure drop for the purge process in the anode of a fuel cell. Journal of Power Sources 2009;188:163-9.

[24] Owejan JP, Gagliardo JJ, Falta SR, Trabold TA. Accumulation and removal of liquid water in proton exchange membrane fuel cells. Journal of the Electrochemical Society 2009;156:B1475-83.

[25] Owejan JP, Gagliardo JJ, Sergi JM, Kandlikar SG, Trabold TA. Water management studies in PEM fuel cells, Part I: Fuel cell design and in situ water distributions. International Journal of Hydrogen Energy 2009;34:3436-44.

[26] Cho EA, Ko JJHHY, Hong SA, Lee KY, Lim TWOIH. Effects of water removal on the performance degradation of PEMFCs repetitively brought to <0℃. Journal of the Electrochemical Society 2004;151:A661-65.

[27] Wilkinson DP, Voss HH, Watkins DS, Prater KB. Solid polymer fuel cell systems incorporating water removal at the anode. US5366818; 1994.

[28] Voss HH, Wilkinson DP, Pickup PG, Johnson MC, Basura V. Anode water removal: A water management and diagnostic technique for solid polymer fuel cells. Electrochimica Acta 1995;40:321-8.

[29] Voss HH, Wilkinson DP, Watkins DS. Method and apparatus for removing water from electrochemical fuel cells by controlling the temperature and pressure of the reactant streams. US5441819; 1995.

[30] Liu X, Guo H, Ma CF. Water flooding and two-phase flow in cathode channels of proton exchange membrane fuel cells. Journal of Power Sources 2006;156:267-80.

[31] He W, Lin GY, Nguyen TV. Diagnostic tool to detect electrode flooding in proton-exchange-membrane fuel cells. AIChE Journal 2003;49:3221-8.

[32] Chuang PA, Turhan A, Keller AK, Brenizer JS, Trabold TA, Mench MM. The nature of flooding and drying in polymer electrolyte fuel cells. Proceedings of 3rd International Conference of Fuel Cell Science, Engineering and Technology; 2005 May 23-25; Ypsilanti, MI, USA. p. 31-7.

[33] Wilkinson DP, Voss HH, Fletcher NJ, Johnson MC, Pow EG. Electrochemical fuel cell stack with concurrent flow of coolant and oxidant streams and countercurrent flow of fuel and oxidant streams. US5773160; 1998.

[34] Zaffou R, Yi JS, Kunz R, Fenton JM. Temperature-Driven Water Transport Through Membrane Electrode Assembly of Proton Exchange Membrane Fuel Cells. Electrochemical and Solid-State Letters 2006;9:A418-22.

[35] Villaluenga JPG, Seoane B, Barragán VM, Ruiz- Bauzá C. Thermo-osmosis of mixtures of water and methanol through a Nafion membrane. Journal of Membrane Science 2006;274:116-22.

[36] Bernardi DM. Water-balance calculations for solid-polymer-electrolyte fuel cells. Journal of the Electrochemical Society 1990;137:3344-50.

[37] Buchi FN, Srinivasan S. Operating proton exchange membrane fuel cells without external humidification of the reactant gases. Journal of the Electrochemical Society 1997;144:2767-72.

[38] Anderson R, Zhang L, Ding Y, Blanco M, Bi X, Wilkinson DP. A critical review of two-phase flow in gas flow channels of proton exchange membrane fuel cells. Journal of Power Sources 2010;195:4531-53.

[39] Wilkinson DP, St-Pierre J. In-plane gradients in fuel cell structure and conditions for higher performance. Journal of Power Sources 2003;113:101-8.

[40] Nguyen TV. Water Management by Material Design and Engineering for PEM Fuel Cells. ECS Transactions 2006;3:1171-80.

[41] Watanabe M, Satoh Y, Shimura C. Management of the water content in polymer electrolyte membranes with porous fiber wicks. Journal of the Electrochemical Society 1993;140:3190-3.

[42] Nguyen TV, Natarajan D, Jain R. Optimized catalyst layer structure for PEM fuel cells. ECS Transactions 2005;1:501-8.

[43] Lin GY, Nguyen TV. Effect of thickness and hydrophobic polymer content of the gas diffusion layer on electrode flooding level in a PEMFC. Journal of the Electrochemical Society 2005;152:A1942-48.

[44] Watanabe M, Uchida H, Seki Y, Emori M, Stonehart P. Self-humidifying polymer electrolyte membranes for fuel cells. Journal of the Electrochemical Society 1996;143:3847-52.

[45] Watanabe M, Uchida H, Emori M. Analyses of self-humidification and suppression of gas crossover in Pt-dispersed polymer electrolyte membranes for fuel cells. Journal of the Electrochemical Society 1998;145:1137-41.

[46] Atiyeh HK, Karan K, Peppley B, Phoenix A, Halliop E, Pharoah J. Experimental investigation of the role of a microporous layer on the water transport and performance of a PEM fuel cell. Journal of Power Sources 2007;170:111-21.

[47] GrafTech International [Internet]. Lakewood: GrafTech [cited 2011 April 9]. Gas Diffusion Barrier Specification Sheet; [about 1 screen]. Available from: http://www.graftechaet.com/GRAFCELL/GRAFCELL-Products/Gas-Diffusion-Barrier-%28GDB%29.aspx.

[48] Lam A. Novel direct liquid fuel cell - membraneless architecture and simple power and fuel crossover control; Ph.D thesis. University of British Columbia; 2009.

[49] Spiegel CS. Designing & building fuel cells. New York: The McGraw-Hill Companies; 2007.

[50] Wilkinson DP, Vanderleeden O. Serpentine flow field design. In: Vielstich W, Gasteiger HA, Lamm A, editors. Handbook of fuel cells - Fundamentals, technology and applications - Vol. 3, New York: John Wiley & Sons; 2003, p 316-24.

[51] Nguyen TV, He W. Interdigitated Flow Field Design. In: Vielstich W, Gasteiger HA, Lamm A, editors. Handbook of fuel cells - Fundamentals, technology and applications - Vol. 3, New York: John Wiley & Sons; 2003, p 325-36.

[52] Gibb P. Fuel cell fluid flow field plate and methods of making fuel cell flow field plates. US2002064702; 2002.

[53] Fox R, McDonald A. Introduction to Fluid Mechanics. New York: John Wiley and Sons; 1992.

[54] Li X, Sabir I, Park J. A flow channel design procedure for PEM fuel cells with effective water removal. Journal of Power Sources 2007;163:933-42.

[55] Perry RH, Green DW. Perry's Chemical Engineers Handbook. 7th ed. NY: McGraw-Hill; 1997.

[56] Trabold TA, Owejan JP. Flow field geometries for improved water management. US7087337; 2005.

[57] Owejan JP, Trabold TA, Jacobson DL, Arif M, Kandlikar SG. Effects of flow field and diffusion layer properties on water accumulation in a PEM fuel cell. International Journal of Hydrogen Energy 2007;32:4489-502.

[58] Montie G, Redlich RB, Leger DE. Fuel cell cathode flow field. US20080213648; 2008.

[59] Johnson MC, Wilkinson DP, Tabatabaian M. Differential pressure fluid flow fields for fuel cells. US6586128; 2003.

[60] Quan P, Lai MC. Numerical study of water management in the air flow channel of a PEM fuel cell cathode. Journal of Power Sources 2007;164:222-37.

[61] Akhtar N, Qureshi A, Scholta J, Hartnig C, Messerschmidt M, Lehnert W. Investigation of water droplet kinetics and optimization of channel geometry for PEM fuel cell cathodes. International Journal of Hydrogen Energy 2009;34:3104-11.

[62] Litster S, Santiago JG. Dry gas operation of proton exchange membrane fuel cells with parallel channels: Non-porous versus porous plates. Journal of Power Sources 2009;188:82-8.

[63] Yi JS, Yang JD, King C. Water management along the flow channels of PEM fuel cells. AIChE Journal 2004;50:2594-603.

[64] Meyer AP, Scheffler GW, Margiott PR. Water management system for solid polymer electrolyte fuel cell power plants. US5503944; 1996.

[65] Reiser CA. Proton exchange membrane fuel cell device with water transfer separator plates. WO9415377; 1994.

[66] Reiser CA. Ion exchange membrane fuel cell power plant with water management pressure differentials. US5700595; 1997.

[67] Miachon S, Aldebert P. Internal hydration H_2/O_2 100 cm^2 polymer electrolyte membrane fuel cell. Journal of Power Sources 1995;56:31-6.

[68] Ge SH, Li XG, Hsing IM. Water management in PEMFCs ssing absorbent wicks. Journal of the Electrochemical Society 2004;151:B523-28.

[69] Ge SH, Li XG, Hsing IM. Internally humidified polymer electrolyte fuel cells using water absorbing sponge. Electrochimica Acta 2005;50:1909-16.

[70] Fabian T, O'Hayre R, Litster S, Prinz FB, Santiago JG. Passive water management at the cathode of a planar air-breathing proton exchange membrane fuel cell. Journal of Power Sources 2010;195:3201-6.

[71] Sugiura K, Nakata M, Yodo T, Nishiguchi Y, Yamauchi M, Itoh Y. Evaluation of a cathode gas channel with a water absorption layer/waste channel in a PEFC by using visualization technique. Journal of Power Sources 2005;145:526-33.

[72] Nguyen TV. Methodology and apparatus for supply of reactant fluids to and purging of product and inert fluids from cells of fuel cell stack. US6503651; 2003.

[73] Nguyen TV, Knobbe MW. A liquid water management strategy for PEM fuel cell stacks. Journal of Power Sources 2003;114:70-9.

[74] Knobbe MW, He W, Chong PY, Nguyen TV. Active gas management for PEM fuel cell stacks. Journal of Power Sources 2004;138:94-100.

[75] Matsumoto T, Tomizawa T, Kokawa K, Kanbara T, Kobayashi S, Hatoh K, et al. Polymer electrolyte fuel cell. US2004224206; 2004.

[76] Hensel JP, Gemmen RS, Thornton JD, Vipperman JS, Clark WW, Bucci BA. Effects of cell-to-cell fuel mal-distribution on fuel cell performance and a means to reduce mal-distribution using MEMS micro-valves. Journal of Power Sources 2007;164:115-25.

[77] Gemmen R, Thornton J, Vipperman J, Clark WW. Piezoelectric axial flow microvalve. US7159841; 2007.

[78] Santiago JG, Posner JD, Prinz FB, Fabian T, Eaton JK, Cha SW, et al. Fuel cell with electroosmotic pump. US2006029851; 2006.

[79] Fabian T, Litster S, Santiago JG, Buie CR, Tsuru H, Sasahra J, et al. Fuel cell water management. US2007284253; 2007.

[80] Buie CR, Posner JD, Fabian T, Cha SW, Kim D, Prinz FB, et al. Water management in proton exchange membrane fuel cells using integrated electroosmotic pumping. Journal of Power Sources 2006;161:191-202.

[81] Litster S, Buie CR, Fabian T, Eaton JK, Santiago JG. Active Water Management for PEM Fuel Cells. Journal of the Electrochemical Society 2007;154:B1049-58.

[82] Strickland DG, Litster S, Santiago JG. Current distribution in polymer electrolyte membrane fuel cell with active water management. Journal of Power Sources 2007;174:272-81.

[83] Kim YH, Han HS, Kim SY, Rhee GH. Influence of cathode flow pulsation on performance of proton-exchange membrane fuel cell. Journal of Power Sources 2008;185:112-7.

[84] Palan V, Shepard WS, Williams KA. Removal of excess product water in a PEM fuel cell stack by vibrational and acoustical methods. Journal of Power Sources 2006;161:1116-25.

[85] Palan V, Shepard WS. Enhanced water removal in a fuel cell stack by droplet atomization using structural and acoustic excitation. Journal of Power Sources 2006;159:1061-70.

[86] Mathias M, Roth J, Sompalli B, Schoeneweiss M, Wood D. Diffusion media, fuel cells, and fuel cell powered systems. US2004137311; 2004.

[87] Kinoshita K. Carbon - Electrochemical and physicochemical properties. New York, NY: John Wiley & Sons, Inc.; 1988.

[88] Decrecente MA, Layden GK, Pike RA. Fibrillar carbon fuel cell electrode substrates and method of manufacture. US4064207; 1997.

[89] Mathias M, Roth J, Fleming J, Qi Z. Diffusion media materials and characterization. In: Vielstich W, Gasteiger HA, Lamm A, editors. Handbook of fuel cells - Fundamentals, technology and applications - Vol. 3, New York: John Wiley & Sons; 2003, p 517-37.

[90] Tawfik H, Hung Y, Mahajan D. Metal bipolar plates for PEM fuel cell-A review. Journal of Power Sources 2007;163:755-67.

[91] Lee WK, Ho CH, Van Zee JW, Murthy M. The effects of compression and gas diffusion layers on the performance of a PEM fuel cell. Journal of Power Sources 1999;84:45-51.

[92] Allen RG, Lim C, Yang LX, Scott K, Roy S. Novel anode structure for the direct methanol fuel cell. Journal of Power Sources 2005;143:142-9.

[93] Nidola A. Water electrolysis in alkaline solutions. New electrode materials. International Journal of Hydrogen Energy 1984;9:367-75.

[94] Lipp L, Pletcher D. Extended area electrodes based on stacked expanded titanium meshes. Electrochimica Acta 1997;42:1101-11.

[95] Brown CJ, Pletcher D, Walsh FC, Hammond JK, Robinson D. Studies of three-dimensional electrodes in the FMO1-LC laboratory electrolyser. Journal of Applied Electrochemistry 1994;24:95-106.

[96] Walsh FC. A First Course in Electrochemical Engineering. Romsey, U.K.: The Electrochemical Consultancy; 1993.

[97] Levine DG, Worsham CH, Tarmy BL. Fuel cell comprising metal screen electrodes. US3281275; 1966.

[98] Argyropoulos P, Scott K, Taama WM. Carbon dioxide evolution patterns in direct methanol fuel cells. Electrochimica Acta 1999;44:3575-84.

[99] Shao ZG, Lin WF, Zhu F, Christensen PA, Li M, Zhang H. Novel electrode structure for DMFC operated with liquid methanol. Electrochemistry Communications 2006;8:5-8.

[100] Wilkinson DP, Stumper J, Campbell SA, David MT, Lamont GJ. Electrochemical cell with fluid distribution layer having integral sealing capability. US5976726; 1999.

[101] Knights SD, Wilkinson DP, Beattie P. Electrochemical fuel cell with fluid distribution layer having non-uniform perforations. US2003039876; 2003.

[102] Hamada A, Nakato K. Gas diffusion layer for fuel cell and manufacturing method of the same. US2002068215; 2002.

[103] Dexmet Corporation [Internet]. Wallingford, CT: Dexmet; [cited 2011 April 9]. Available from: http://www.dexmet.com/.

[104] Hottinen T, Mikkola M, Mennola T, Lund P. Titanium sinter as gas diffusion backing in PEMFC. Journal of Power Sources 2003;118:183-8.

[105] Hottinen T, Himanen O, Lund P. Effect of cathode structure on planar free-breathing PEMFC. Journal of Power Sources 2004;138:205-10.

[106] Cisar AJ, Murphy OJ, Jeng KT, Salinas C, Simpson S, Weng D, et al. Unitized barrier and flow control device for electrochemical reactors. US6232010; 2001.

[107] Fushinobu K, Takahashi D, Okazaki K. Micromachined metallic thin films for the gas diffusion layer of PEFCs. Journal of Power Sources 2006;158:1240-5.

[108] Wan N, Wang C, Mao Z. Titanium substrate based micro-PEMFC operating under ambient conditions. Electrochemistry Communications 2007;9:511-6.

[109] Zhang FY, Prasad AK, Advani SG. Investigation of a copper etching technique to fabricate metallic gas diffusion media. Journal of Micromechanical Microengineering 2006;16:N23-7.

[110] Zhang FY, Advani SG, Prasad AK. Performance of a metallic gas diffusion layer for PEM fuel cells. Journal of Power Sources 2008;176:293-8.

[111] Lee CY, Lee SJ, Hu YC, Lin CH, Lee YM, Fan WY. Integration of micro temperature sensor and metal foil as gas diffusion layer for micro fuel cell. Proceedings of the 4th IEEE International Conference on Nano/Micro Engineered and Molecular Systems. 2009 Jan 5-8, Shenzhen, China. IEEE; 2009, p. 168-71.

[112] Lee CY, Lee SJ, Lee YM, Chu KY. Integration of micro flow sensor and flexible substrate as GDL in micro fuel cell. Proceedings of the 4th IEEE International Conference on Nano/Micro Engineered and Molecular Systems. 2009 Jan 5-8, Shenzhen, China. IEEE; 2009, p. 637-640. 2009.

[113] Gamburzev S, Appleby AJ. Recent progress in performance improvement of the proton exchange membrane fuel cell (PEMFC). Journal of Power Sources 2002;107:5-12.

[114] Fly GW, Brady BK. Fuel cell with variable porosity gas distribution layers. US6566004; 2003.

[115] Qi Z, Kaufman A. Improvement of water management by a microporous sublayer for PEM fuel cells. Journal of Power Sources 2002;109:38-46.

[116] Mercuri RA. Fluid permeable flexible graphite fuel cell electrode. US6413663; 2002.

[117] Mercuri RA, Krassowski DW. Flooding-reducing fuel cell electrode. US6521369; 2003.

[118] Mercuri RA, Weber TW. Hydrophobic fuel cell electrode. US6902841; 2005.

[119] Reynolds RA, Mercuri RA. Fuel cell assembly method with selective catalyst loading. US20020022570; 2002.

[120] Mercuri RA, Weber TW, Warddrip ML. Flexible graphite article and fuel cell electrode with enhanced electrical and thermal conductivity. WO0178179; 2001.

[121] Yazici MS. Mass transfer layer for liquid fuel cells. Journal of Power Sources 2007;166:424-9.

[122] Yazici MS. Passive air management for cylindrical cartridge fuel cells. Journal of Power Sources 2007;166:137-42.

[123] Yazici MS, Mercuri RA, Reynolds RA, Calarco P. Perforated cylindrical fuel cells. US2004001986; 2004.

[124] Gurau V, Zawodzinski T, Wayne R. In-situ characterization of GRAFCELL® flexible graphite film as gas diffusion layers for PEMFCs. ECS Transactions 2008;16:1651-9.

[125] Jiao K, Zhou B. Innovative gas diffusion layers and their water removal characteristics in PEM fuel cell cathode. Journal of Power Sources 2007;169:296-314.

[126] Jiao K, Zhou B. Effects of electrode wettabilities on liquid water behaviours in PEM fuel cell cathode. Journal of Power Sources 2008;175:106-19.

[127] Lee CY, Chuang CW. A novel integration approach for combining the components to minimize a micro-fuel cell. Journal of Power Sources 2007;172:115-20.

[128] Johnson MC, Wilkinson DP, Asman CP, Bos ML, Potter RJ. Electrochemical fuel cell with an electrode substrate having an in-plane nonuniform structure for control of reactant and product transport. US5840438; 1998.

[129] Gerteisen D, Heilmann T, Ziegler C. Enhancing liquid water transport by laser perforation of a GDL in a PEM fuel cell. Journal of Power Sources 2008;177:348-54.

[130] Gerteisen D, Sadeler C. Stability and performance improvement of a polymer electrolyte membrane fuel cell stack by laser perforation of gas diffusion layers. Journal of Power Sources 2010;195:5252-7.

[131] Manahan MP, Hatzell MC, Kumbur EC, Mench MM. Laser perforated fuel cell diffusion media, Part I: Related changes in performance and water content. Journal of Power Sources 2011;196:5573-82.

[132] Nishida K, Murakami T, Tsushima S, Shuichiro H. Microscopic visualization of state and behavior of liquid water in a gas diffusion layer of PEFC. Electrochemistry 2006;75:149-51.

[133] Nishida K, Murakami T, Tsushima S, Hirai S. Measurement of liquid water content in cathode gas diffusion electrode of polymer electrolyte fuel cell. Journal of Power Sources 2010;195:3365-73.

[134] Lee KJ, Kang JH, Nam JH, Kim CJ. Steady liquid water saturation distribution in hydrophobic gas-diffusion layers with engineered pore paths: An invasion-percolation pore-network analysis. Journal of Power Sources 2010;195:3508-12.

[135] Chen-Yang YW, Hung TF, Huang J, Yang FL. Novel single-layer gas diffusion layer based on PTFE/carbon black composite for proton exchange membrane fuel cell. Journal of Power Sources 2007;173:183-8.

[136] Koschany P. Electrodes with adjustable gas permeability, and method of producing such electrodes. US2003138689; 2003.

[137] Voss S, Kollmann H, Kollmann W. New innovative materials for advanced electrochemical applications in battery and fuel cell systems. Journal of Power Sources 2004;127:93-7.

[138] Campbell SA, Stumper J, Wilkinson DP, Davis MT. Porous electrode substrate for an electrochemical fuel cell. US5863673; 1999.

[139] Beattie PD, Wilkinson DP, Kozak P, Wang H, Neumann S, Gordon JB, et al. Fluid diffusion layers for fuel cells. US6667127; 2003.

[140] Ralph TR, Hards GA, Keating JE, Campbell SA, Wilkinson DP, Davis M, et al. Low cost electrodes for proton exchange membrane fuel cells. Journal of the Electrochemical Society 1997;144:3845-57.

[141] Spernjak D, Prasad AK, Advani SG. Experimental investigation of liquid water formation and transport in a transparent single-serpentine PEM fuel cell. Journal of Power Sources 2007;170:334-44.

[142] Moreira J, Sebastian PJ, Ocampo AL, Castellanos RH, Cano U, Salazar MD. Dependence of PEM fuel cell performance on the configuration of the gas diffusion electrodes. Journal of New Materials for Electrochemical Systems 2002;173-5.

[143] Williams MV, Kunz HR, Fenton JM. Operation of Nafion(R)-based PEM fuel cells with no external humidification: influence of operating conditions and gas diffusion layers. Journal of Power Sources 2004;135:122-34.

[144] Williams MV, Begg R, Bonville L, Kunz HR, Fenton JM. Characterization of gas diffusion layers for PEMFC. Journal of the Electrochemical Society 2004;151:A1173-80.

[145] Antolini E. Recent developments in polymer electrolyte fuel cell electrodes. Journal of Applied Electrochemistry 2004;34:563-76.

[146] Akyalçin L, Kaytakoglu S. Optimization of structural combinations on the performance of a PEMFC's MEA. Journal of Power Sources 2008;180:767-72.

[147] Wang Y, Wang CY, Chen KS. Elucidating differences between carbon paper and carbon cloth in polymer electrolyte fuel cells. Electrochimica Acta 2007;52:3965-75.

[148] Frey T, Linardi M. Effects of membrane electrode assembly preparation on the polymer electrolyte membrane fuel cell performance. Electrochimica Acta 2004;50:99-105.

[149] Holmstrom N, Ihonen J, Lundblad A, Lindbergh G. The influence of the gas diffusion layer on water management in polymer electrolyte fuel cells. Fuel Cells 2007;7:306-13.

[150] Park GG, Sohn YJ, Yang TH, Yoon YG, Lee WY, Kim CS. Effect of PTFE contents in the gas diffusion media on the performance of PEMFC. Journal of Power Sources 2004;131:182-7.

[151] Velayutham G, Kaushik J, Rajalakshmi N, Dhathathreyan KS. Effect of PTFE content in gas diffusion media and microlayer on the performance of PEMFC tested under ambient pressure. Fuel Cells 2007;7:314-8.

[152] Tuber K, Pocza D, Hebling C. Visualization of water buildup in the cathode of a transparent PEM fuel cell. Journal of Power Sources 2003;124:403-14.

[153] Khandelwal M, Mench MM. Direct measurement of through-plane thermal conductivity and contact resistance in fuel cell materials. Journal of Power Sources 2006;161:1106-15.

[154] Ismail MS, Damjanovic T, Ingham DB, Pourkashanian M, Westwood A. Effect of polytetrafluoroethylene-treatment and microporous layer-coating on the electrical conductivity of gas diffusion layers used in proton exchange membrane fuel cells. Journal of Power Sources 2010;195:2700-8.

[155] Campbell SA, Chisham JE, Wilkinson DP. Carbon-supported catalysts for fuel cells. US6548202; 2003.

[156] Jung UH, Park KT, Park EH, Kim SH. Improvement of low-humidity performance of PEMFC by addition of hydrophilic SiO2 particles to catalyst layer. Journal of Power Sources 2006;159:529-32.

[157] Gurau V, Bluemle MJ, De Castro ES, Tsou YM, Zawodzinski J, Mann J. Characterization of transport properties in gas diffusion layers for proton exchange membrane fuel cells: 2. Absolute permeability. Journal of Power Sources 2007;165:793-802.

[158] Wilson MS, Valerio JA, Gottesfeld S. Low platinum loading electrodes for polymer electrolyte fuel cells fabricated using thermoplastic ionomers. Electrochimica Acta 1995;40:355-63.

[159] Wang X, Zhang H, Zhang J, Xu H, Zhu X, Chen J, et al. A bi-functional micro-porous layer with composite carbon black for PEM fuel cells. Journal of Power Sources 2006;162:474-9.

[160] Litster S, McLean G. PEM fuel cell electrodes. Journal of Power Sources 2004;130:61-76.

[161] Song JM, Cha SY, Lee WM. Optimal composition of polymer electrolyte fuel cell electrodes determined by the AC impedance method. Journal of Power Sources 2001;94:78-84.

[162] Park S, Lee JW, Popov BN. Effect of PTFE content in microporous layer on water management in PEM fuel cells. Journal Power Sources 2008;177:457-63.

[163] Jian-hua T, Zhao-yuan S, Jin-song S, Zhong-qiang S. Preparation of water management layer and effects of its composition on performance of PEMFCs. Energy Conversion and Management 2008;49:1500-5.

[164] Park S, Lee JW, Popov BN. Effect of carbon loading in microporous layer on PEM fuel cell performance. Journal of Power Sources 2006;163:357-63.

[165] Park S, Lee JW, Popov B. Effect of PTFE content in microporous layer on water management. ECS Transactions 2007;11:623-8.

[166] Shi J, Tian J, Zhang C, Shan Z. A novel method for the preparation of a PEMFC water management layer. Journal of Power Sources 2007;164:284-6.

[167] Mench MM. Fuel cell engines. Hoboken, NJ: John Wiley & Sons; 2008.

[168] Koyama T, Miyashita M, Matsui Y. Methods of producing composite material, filter and diffusion layer of fuel cell. US2007231470; 2007.

[169] E.Passalacqua, F.Lufrano, G.Squadrito, A.Patti, L.Giorgi. Influence of the structure in low-Pt loading electrodes for polymer electrolyte fuel cells. Electrochimica Acta 1998;43:3665-73.

[170] Song JM, Uchida H, Watanabe M. Effect of wet-proofing treatment of carbon backing layer in gas diffusion electrodes on the PEFC performance. Electrochemistry 2005;73:189-93.

[171] Nakajima H, Konomi T, Kitahara T. Direct water balance analysis on a polymer electrolyte fuel cell (PEFC): Effects of hydrophobic treatment and micro-porous layer addition to the gas diffusion layer of a PEFC on its performance during a simulated start-up operation. Journal of Power Sources 2007;171:457-63.

[172] Mirzazadeh J, Saievar-Iranizad E, Nahavandi L. An analytical approach on effect of diffusion layer on ORR for PEMFCs. Journal of Power Sources 2004;131:194-9.

[173] Williams MV, Kunz HR, Fenton JM. Influence of convection through gas-diffusion layers on limiting current in PEM FCs using a serpentine flow field. Journal of the Electrochemical Society 2004;151:A1617-27.

[174] Nam JH, Kaviany M. Effective diffusivity and water-saturation distribution in single- and two-layer PEMFC diffusion medium. International Journal of Heat and Mass Transfer 2003;46:4595-611.

[175] Pasaogullari U, Wang CY. Two-phase transport and the role of micro-porous layer in polymer electrolyte fuel cells. Electrochimica Acta 2004;49:4359-69.

[176] Kitahara T, Konomi T, Murata M, Berg N, Wilde P. Influences of gas diffusion layer design parameters on the performance of polymer electrolyte fuel cells. ECS Transactions 2007;5:27-36.

[177] Owejan JP, Trabold TA, Jacobson DL, Arif M, Kandlikar SG. Effects of flow field and diffusion layer properties on water accumulation in a PEM fuel cell. Int J Hydrogen Energy 2007;32:4489-502.

[178] Lu Z, Daino MM, Rath C, Kandlikar SG. Water management studies in PEM fuel cells, part III: Dynamic breakthrough and intermittent drainage characteristics from GDLs with and without MPLs. International Journal of Hydrogen Energy 2010;35:4222-33.

[179] Nam JH, Lee KJ, Hwang GS, Kim CJ, Kaviany M. Microporous layer for water morphology control in PEMFC. International Journal of Heat and Mass Transfer 2009;52:2779-91.

[180] Weber AZ, Newman J. Effects of microporous layers in polymer electrolyte fuel cells. Journal of the Electrochemical Society 2005;152:A677-88.

[181] Pasaogullari U., Wang C.Y., Chen K.S. Two-Phase transport in polymer electrolyte fuel cells with bilayer cathode gas diffusion media. Journal of the Electrochemical Society 2005;152:A1574-82.

[182] Kim T, Lee S, Park H. A study of water transport as a function of the micro-porous layer arrangement in PEMFCs. International Journal of Hydrogen Energy 2010;35:8631-43.

[183] Pharoah JG, Peppley B, Atiyeh HK, Halliop E, Karan K. Investigating the role of a microporous layer on the water transport and performance of a PEMFC. ECS Transactions 2006;3:1227-37.

[184] Karan K., Atiyeh H., Phoenix A., Halliop E., Pharoah J., Peppley B. An experimental investigation of water transport in PEMFCs - The role of microporous layers. Electrochemistry and Solid State Letters 2007;10:B34-B38.

[185] Malevich D, Halliop E, Peppley B, Pharoah JG, Karan K. Investigation of Charge-Transfer and Mass-Transport Resistances in PEMFCs with Microporous Layer Using Electrochemical Impedance Spectroscopy. Journal of the Electrochemical Society 2009;156:B216-B224.

[186] Owejan JP, Owejan JE, Gu W, Trabold TA, Tighe TW, Mathias MF. Water Transport Mechanisms in PEMFC Gas Diffusion Layers. Journal of the Electrochemical Society 2010;157:B1456-B1464.

[187] Kitahara T., Konomi T., Nakajima H., Tateishi Y., Murata M., Haak N., Wilde P. Best Combination of Gas Diffusion Layers for Polymer Electrolyte Fuel Cell under Cathode Condition of Very Low Humidity. ECS Transactions 2008;16:1603-13.

[188] Ge SH, Yi BL. A mathematical model for PEMFC in different flow modes. Journal of Power Sources 2003;124:1-11.

[189] Single cell test protocol. US Fuel Cell Council's Single Cell Testing Task Force. US Fuel Cell Council; 2006 July 13. Document No. 05-014B.2

[190] Procedure for performing PEM single cell testing. Cocoa (FL): Florida Solar Energy Center; 2009 April 8. Report, Contract No. DOE # DE-FC36-06G016028

[191] Xie Z, Zhao Z, Adachi M, Shi Z, Machio T, Ohma T, et al. Fuel cell cathode catalyst layers from "green" catalyst inks. Energy and Environmental Science 2008;1:184-93.

[192] Yuan X, Wang H, Colin SJ, Zhang J. AC impedance technique in PEM fuel cell diagnosis – A review. International Journal of Hydrogen Energy 2007;32:4365-80.

[193] Gomadam PM, Weidner JW. Analysis of electrochemical impedance spectroscopy in proton exchange membrane fuel cells. International Journal of Energy Resources 2005;29:1133-51.

[194] Mérida W. Diagnosis of PEMFC stack failures via electrochemical impedance spectroscopy; Ph.D thesis. University of Victoria; 2002.

[195] Hussaini IS, Wang CY. Visualization and quantification of cathode channel flooding in PEM fuel cells. Journal of Power Sources 2009;187:444-51.

[196] Lu Z, Kandlikar SG, Rath C, Grimm M, Domigan W, White AD, Hardbarger M, et al. Water management studies in PEM fuel cells, Part II: Ex situ investigation of flow maldistribution, pressure drop and two-phase flow pattern in gas channels. International Journal of Hydrogen Energy 2009;34:3445-56.

[197] Rho YW, Velev OA, Srinivasan S, Kho YT. Mass Transport phenomena in proton exchange membrane fuel cells using O_2/He, O_2/Ar, and O_2/N_2 mixtures – I. Experimental analysis. Journal of the Electrochemical Society 1994;141:2084-9.

[198] Rho YW, Srinivasan S, Kho YT. Mass transport phenomena in proton exchange membrane fuel cells using O_2/He, O_2/Ar, and O_2/N_2 mixtures – II. Theoretical analysis. Journal of the Electrochemical Society 1994;141:2089-96.

[199] Ralph TR, Hogarth MP. Catalysis for low temperature fuel cells - Part I: The cathode challenges. Platinum Metals Review 2002;46:3-14.

[200] Dai W, Wang H, Yuan XZ, Martin JJ, Luo Z, Pan M. Measurement of the water transport rate in a proton exchange membrane fuel cell and the influence of the gas diffusion layer. Journal of Power Sources 2008;185:1267-71.

[201] Dai W, Wang H, Yuan XZ, Martin J, Shen J, Pan M, Luo Z. Measurement of water transport rates across the gas diffusion layer in a proton exchange

membrane fuel cell, and the influence of polytetrafluoroethylene content and micro-porous layer. Journal of Power Sources 2009;188:122-6.

[202] Hoogers G. Fuel Cell Technology Handbook. Boca Raton: CRC Press; 2003.

[203] Wilkinson DP, St-Pierre J. Durability. In: Vielstich W, Gasteiger HA, Lamm A, editors. Handbook of fuel cells - Fundamentals, technology and applications - Vol. 3, New York: John Wiley & Sons; 2003, p 611-26.

[204] Rama P, Chen R, Andrews J. A review of performance degradation and failure modes for hydrogen-fuelled polymer electrolyte fuel cells. Proceedings of the Institution of Mechanical Engineers, Part A: Journal of Power and Energy 2008;222:2041-967.

[205] Kim HT, Song KY, Reshetenko TV, Han SI, Kim TY, Cho SY, et al. Electrochemical analysis of polymer electrolyte membrane fuel cell operated with dry-air feed. Journal of Power Sources 2009;193:515-22.

[206] Zawodzinski TA, Derouin C, Radzinski S, Sherman RJ, Smith VT, Springer TE, et al. Water uptake by and transport through Nafion® 117 membranes. Journal of the Electrochemical Society 1993;140:1041-7.

[207] Zhang J, Tang Y, Song C, Cheng X, Zhang J, Wang H. PEM fuel cells operated at 0% relative humidity in the temperature range of 23-120 ℃. Electrochimica Acta 2007;52:5095-101.

[208] Herrera O, Mérida W, Wilkinson DP. Sensing electrodes for failure diagnostics in fuel cells. Journal of Power Sources 2009;190:103-9.

[209] Westerlain S, Candusso D, Harel F. Durability test results of a polymer electrolyte membrane fuel cell operated at overnominal temperature with low humidified reactants. Journal of Fuel Cell Science and Technology 2010;7:024502-1-4.

[210] Yan Q, Toghiani H, Wu J. Investigation of water transport through membrane in a PEM fuel cell by water balance experiments. Journal of Power Sources 2006;158:316-25.

[211] Cai Y, Hu J, Ma H, Yi B, Zhang H. Effect of water transport properties on a PEM fuel cell operating with dry hydrogen. Electrochimica Acta 2006;51:6361-6.

[212] Colinart T, Chenu A, Didierjean S, Lottin O, Besse S. Experimental study on water transport coefficient in proton exchange membrane fuel cell. Journal of Power Sources 2009;190:230-40.

[213] Hogarth WHJ, Benziger JB. Operation of polymer electrolyte membrane fuel cells with dry feeds: Design and operating strategies. Journal of Power Sources 2006;159:968-78.

[214] Rajalakshmi N, Jayanth TT, Thangamuthu R, Sasikumar G, Sridhar P, Dhathathreyan KS. Water transport characteristics of polymer electrolyte membrane fuel cell. International Journal of Hydrogen Energy 2004;29:1009-14.

[215] Yoshikawa Y, Matsuura T, Kato M, Hori M. Design of low-humidification PEMFC by using cell simulator and its power generation verification test. Journal of Power Sources 2006;158:143-7.

[216] Qi Z, Kaufman A. PEM fuel cell stacks operated under dry-reactant conditions. Journal of Power Sources 2002;109:469-76.

[217] Sinha PK, Wang CY, Beuscher U. Effect of flow field design on the performance of elevated-temperature polymer electrolyte fuel cells. International Journal of Energy Resources 2007;31:390-411.

[218] St-Pierre J., Wilkinson D.P., Knights S., Bos M. Relationships between water management, contamination and lifetime degradation in PEFC. Journal of New Materials for Electrochemical Systems 2000;3:99-106.

[219] Nakagawa N, Abdelkareem MA, Sekimoto K. Control of methanol transport and separation in a DMFC with a porous support. Journal of Power Sources 2006;160:105-15.

[220] Abdelkareem MA, Morohashi N, Nakagawa N. Factors affecting methanol transport in a passive DMFC employing a porous carbon plate. Journal of Power Sources 2007;172:659-65.

[221] Mossman A, Wells B, Barton B, Voss H. Passive recovery of liquid water produced by fuel cells. US2008241623; 2008.

[222] St-Pierre J. Simple mathematical model for water diffusion in Nafion membranes. Journal of the Electrochemical Society 2007;154:B88-B95.

[223] Barbir F, Gorgun H, Wang X. Relationship between pressure drop and cell resistance as a diagnostic tool for PEM fuel cells. Journal of Power Sources 2005;141:96-101.

[224] Kitahara T, Konomi T, Nakajima H. Microporous layer coated gas diffusion layers for enhanced performance of polymer electrolyte fuel cells. Journal of Power Sources 2010;195:2202-11.

[225] Alink R, Gerteisen D, Mérida W. Investigating the water transport in porous media for PEMFCs by liquid water visualization in ESEM. Fuel Cells 2011;In Press. DOI: 10.1002/fuce.201000110.

[226] Protocol on fuel cell component testing: suggested dynamic testing profile (DTP). Joint Hydrogen Quality Task Force. US Fuel Cell Council; 2006. Document No. USFCC 04-068A.

[227] Turhan A, Heller K, Brenizer JS, Mench MM. Quantification of liquid water accumulation and distribution in a polymer electrolyte fuel cell using neutron imaging. Journal of Power Sources 2006;160:1195-203.

[228] Rodatz P, Büchi F, Onder C, Guzzella L. Operational aspects of a large PEFC stack under practical conditions. Journal of Power Sources 2004;128:208-17.

[229] Barreras F, Lozano A, Valino L, Marin C, Pascau A. Flow distribution in a bipolar plate of a proton exchange membrane fuel cell: experiments and numerical simulation studies. Journal of Power Sources 2005;144:54-66.

[230] Kee RJ, Korada P, Walters K, Pavol M. A generalized model of the flow distribution in channel networks of planar fuel cells. Journal of Power Sources 2002;109:148-59.

[231] Chang PAC, St-Pierre J, Stumper J, Wetton B. Flow distribution in proton exchange membrane fuel cell stacks. Journal of Power Sources 2006;162:340-55.

[232] Park J, Li X. Effect of flow and temperature distribution on the performance of a PEM fuel cell stack. Journal of Power Sources 2006;162:444-59.

[233] Koh JH, Seo HK, Lee CG, Yoo YS, Lim HC. Pressure and flow distribution in internal gas manifolds of a fuel-cell stack. Journal of Power Sources 2003;115:54-65.

[234] Trabold TA. Minichannels in Polymer Electrolyte Membrane Fuel Cells. Heat Transfer Engineering 2005;26:3-12.

[235] Hickner MA, Siegel NP, Chen KS, McBrayer DN, Hussey DS, Jacobson DL, et al. Real-time imaging of liquid water in an operating proton exchange membrane fuel cell. Journal of the Electrochemical Society 2006;153:A902-8.

[236] Owejan JP, Trabold TA, Jacobson DL, Baker DR, Hussey DS, Arif M. In situ investigation of water transport in an operating PEM fuel cell using neutron radiography: Part 2 - Transient water accumulation in an interdigitated cathode flow field. International Journal of Heat and Mass Transfer 2006;49:4721-31.

APPENDIX A – PUBLICATIONS AND INTELLECTUAL PROPERTY

Book Chapters:

- Blanco M, Wilkinson DP. Diffusion Layers. In: Wilkinson DP, Zhang JJ, Fergus JW, Hui R, Li X, editors. Proton Exchange Membrane Fuel Cells: Materials Properties and Performance, Green Chemistry and Chemical Engineering Series, Boca Raton, FL: CRC Press; 2009. p. 191-303.

Journal and Conference Proceedings:

- Blanco M, Wilkinson DP, Wang W. Application of water barrier layers in a proton exchange membrane fuel cell for improved water management at low humidity operating conditions. Int J Hydrogen Energy 2011;36:3635-48.

- Anderson R, Zhang L, Ding Y, Blanco M, Bi X, Wilkinson DP. A Critical Review of Two-phase Flow in Gas Flow Channels of PEM Fuel Cells. J Power Sources 2010;195:4531-53.

- Blanco M, Wilkinson DP, Wang H, Liu SZS. Engineered gas diffusion layers for proton exchange membrane fuel cells. ECS Trans 2009;25:1507-18.

- Wu J, Yuan XZ, Wang H, Blanco M, Martin JJ, Zhang J. Diagnostic Tools in PEM Fuel Cell Research: Part I Electrochemical Techniques. Int J Hydrogen Energy 2008;33:1725-46.

- Wu J, Yuan XZ, Wang H, Blanco M, Martin JJ, Zhang J. Diagnostic Tools in PEM Fuel Cell Research: Part II Physical/Chemical Methods. Int J Hydrogen Energy 2008;33:1747-57.

- Wilkinson DP, Blanco M, Zhao H, Wu J, Wang H. Dynamic flow field for fuel cells. Electrochem Solid-State Lett 2007;10:B155-60.

- Blanco M, Wilkinson DP, Yan G, Zhao H, Wang H. Flow control in a fuel cell flow field for improved performance and reliability. ECS Trans 2006;1:355-66.

- Yuan X, Sun JC, Blanco M, Wang H, Zhang JJ, Wilkinson DP. AC Impedance Diagnosis of a 500W PEM Fuel Cell Stack – Part I: Stack Impedance. J Power Sources 2006;161:920-28.

- Wilkinson M, Blanco M, Gu E, Martin JJ, Wilkinson DP, Zhang JJ, et al. In-Situ Experimental Technique for Measurement of Temperature and Current Distribution in PEM Fuel Cells. Electrochem Solid-State Lett 2006;9:A507-11.

- Blanco M, Wilkinson DP, Rahbari R, Zimmerman J. Active Flow Control in a Fuel Cell Flow Field. In: Ghosh D, editor. 44th Annual Conference of Metallurgists (COM2005): Proceedings of the First International Symposium on Fuel Cell and Hydrogen Technologies; 2005 Aug 21-24; Calgary, Canada. p. 203-214.

- Gu C, Blanco M, Martin JJ, Shen J, Zhang J, Wang H, Wilkinson DP. Measurement of Reactant Distribution in Flow Field Channels. In: Ghosh D, editor. 44th Annual Conference of Metallurgists (COM2005): Proceedings of the First International Symposium on Fuel Cell and Hydrogen Technologies; 2005 Aug 21-24; Calgary, Canada. p 193–202.

Intellectual property:

- Wilkinson DP, Rahbari R, Zimmerman J, Blanco M, inventors; National Research Council, assignee. Flow control apparatus and method of fuel cell flow field. US2008248365, WO02005121917, CA2569859.

APPENDIX B – FABRICATION PROCEDURES FOR MEMBRANE ELECTRODE ASSEMBLIES

The following are the steps used to assemble a membrane electrode assemble (MEA) with catalyst coated membranes (CCM):

1. Cut two square pieces of the polyimide film to be used as sub-gaskets (see figure B.1). These pieces should be slightly smaller than the stainless steel brackets/frames.

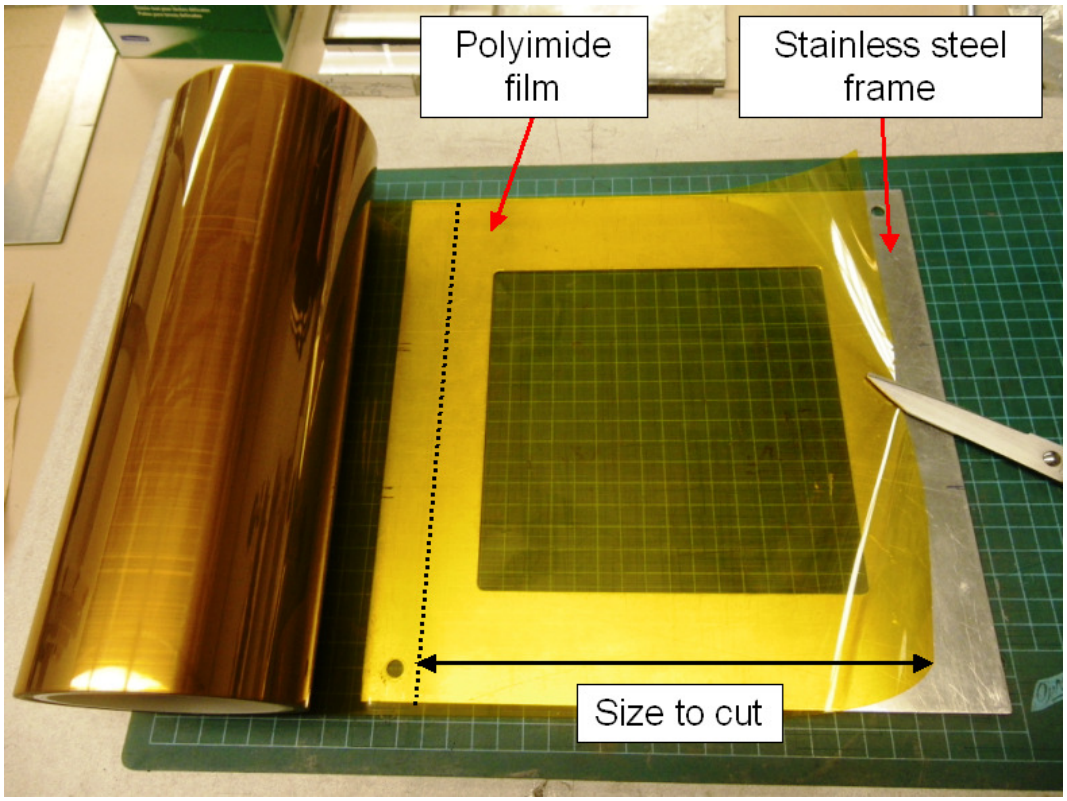

Figure B.1 – Picture corresponding to step 1 of the MEA assembly process. Note that the size of the films should be smaller than that of the stainless steel frame.

2. Remove the liner (or transparent film that protects the adhesive in the polyimide film) and carefully glue the polyimide film to the metal brackets making sure that there is enough tension around the whole sheet (see figure B.2). Repeat this step with the other film.

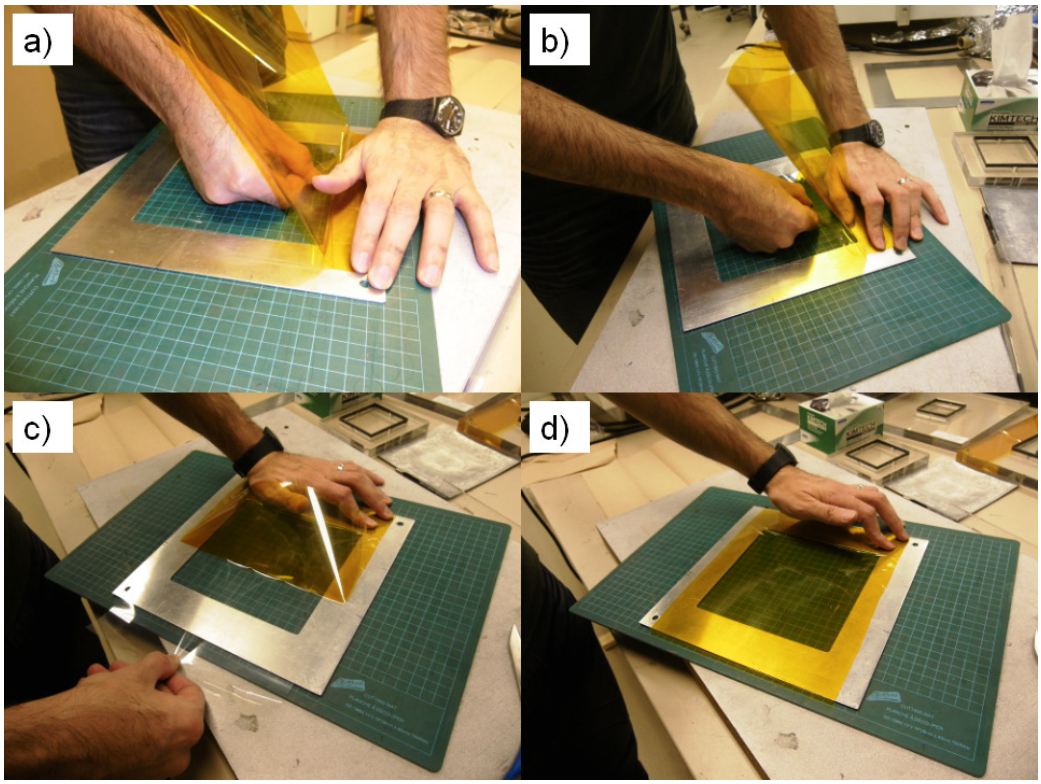

Figure B.2 – Picture corresponding to step 2 of the MEA assembly process. Peel the liner from the polyimide film carefully and glue it to the stainless steel frame (a and b). Then maintain constant tension while removing the liner (c) until the film is glued completely to the frame (d).

3. Use the rule die labelled “GDL” to cut a hole corresponding to the size of the GDL in both polyimide films. Use alignment pins (or ¼ inch bolts) in order to align the rule die with the metal brackets (see figure B.3). Use a rubber mallet to hit the rule die. A press (or hot press) can also be used here instead of the rubber mallet.

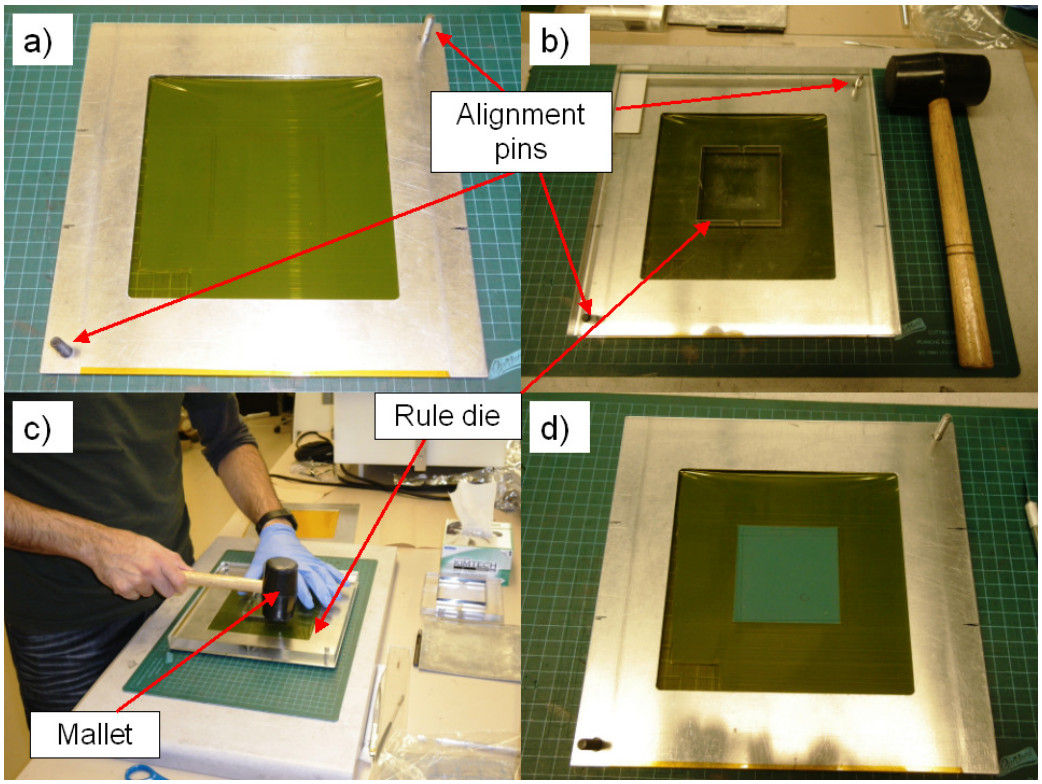

Figure B.3 – Align the metal bracket with the GDL rule die with the help of the aligning pins (a and b), and use the mallet (c) to carefully cut the corresponding hole in the polyimide film (d).

4. Cut a piece of the CCM with the rule die labelled “CCM” (see figure B.4). Use a rubber mallet to cut this piece. Use gloves when dealing with the membrane. This CCM sheet will be around 7.4 cm by 7.4 cm in size, which is larger than the actual active area, in order to stick to the polyimide films.

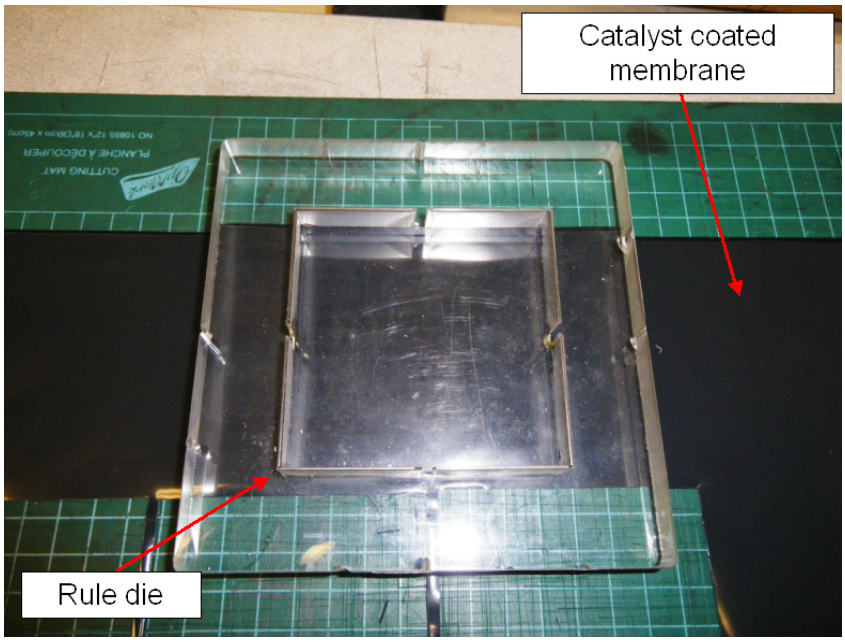

Figure B.4 – Picture of the rule die used to cut a piece of the catalyst coated membrane.

5. Remove the protective layers of the CCM and carefully place it on top of one of the polyimide films (in the side that has the adhesive). With a fingertip or with the help of a small spatula glue the edges of the CCM onto the polyimide film (see figure B.5).

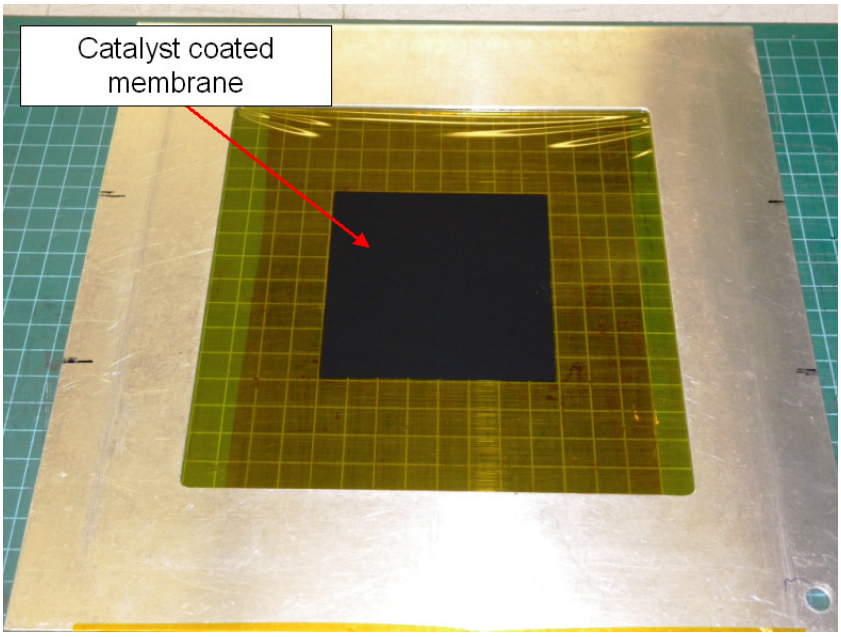

Figure B.5 – Picture of the CCM placed on top of the polyimide film.

6. Place the alignment pins (or bolts) in the metal bracket and put the other metal bracket (the one without the CCM) on top of it (see figure B.6). Make sure that both adhesive layers are facing each other.

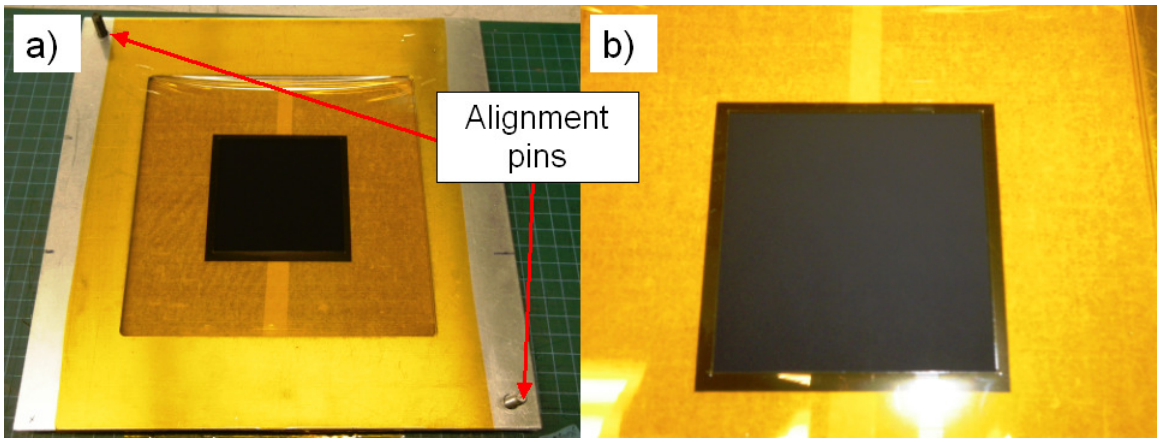

Figure B.6 – (a) Picture of both metal brackets placed on top of each other using the alignment pins. (b) Zoom-in picture of the top polyimide film ready to be attached to the CCM. Note the KimWipes® placed underneath the brackets in order to protect the CCM.

7. With the help of a spatula, stick both polyimide films together without leaving any bubbles between the two layers (see figure B.7).

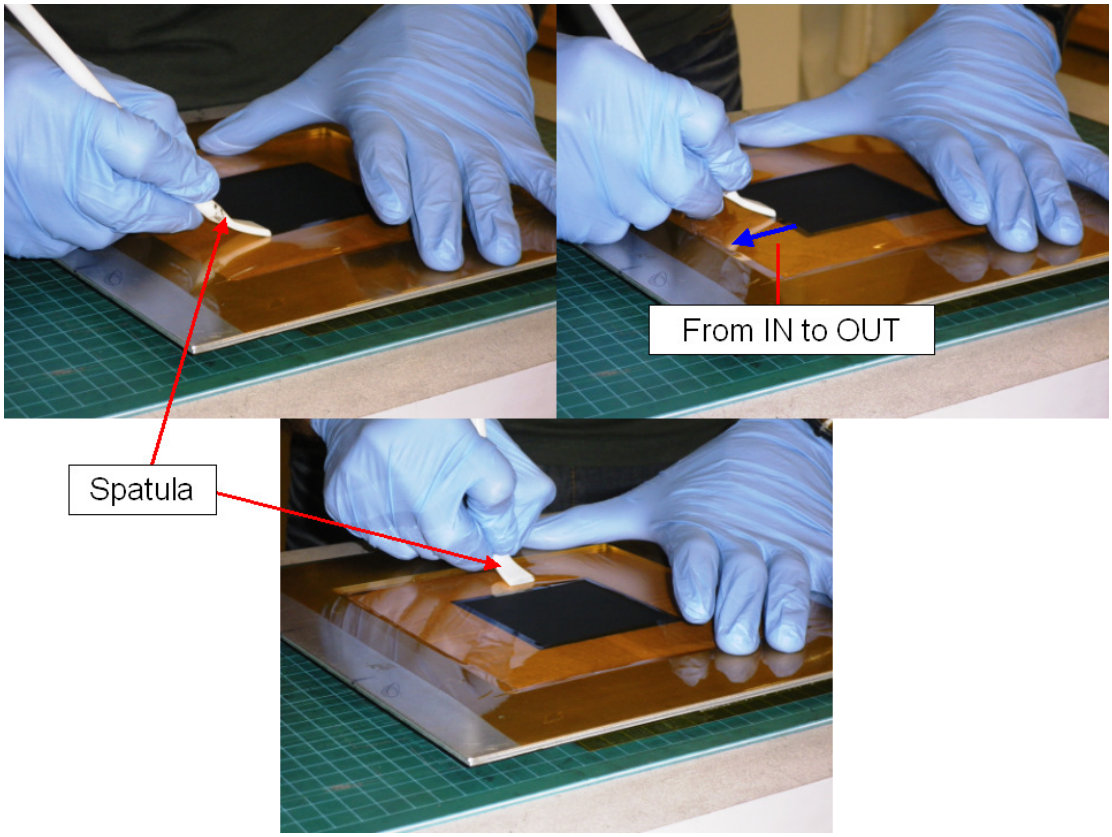

Figure B.7 – Picture corresponding to step 7 of the MEA assembly process. Note that the spatula should be moved from inwards (near CCM) to outwards.

8. Once the CCM and the two polyimide films are put together, use the alignment pins (or bolts) and the rule die labelled “MEA” in order to make the inlet and outlet holes for the reactant gases and coolant line (see figure B.8). When hitting the rule die with the rubber mallet be careful to not damage the die. If any of the wholes are not cut completely, then use a hole punch to finish the holes.

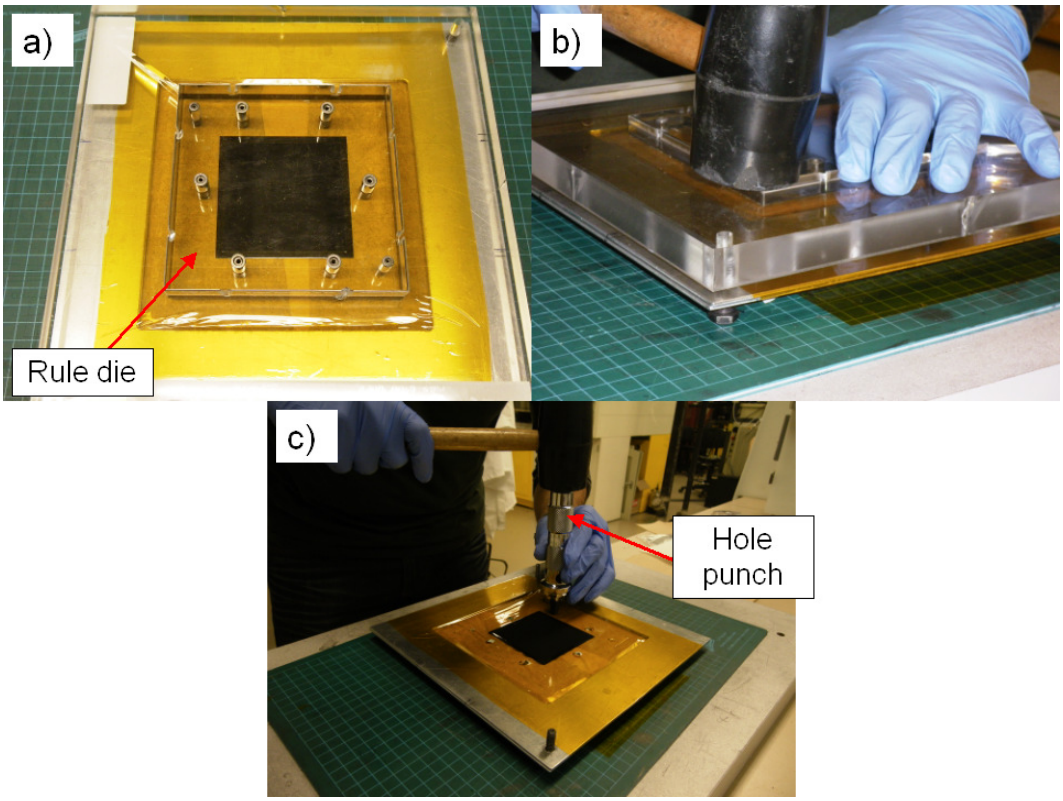

Figure B.8 – (a) Rule die on top of the polyimide film and CCM; (b) Using the rule die with a rubber mallet; and (c) Hole punch used to finalize holes that were not cut with the rule die.

9. Clean any pieces of the polyimide film and with a scalpel cut the edges of the polyimide film (see figure B9).

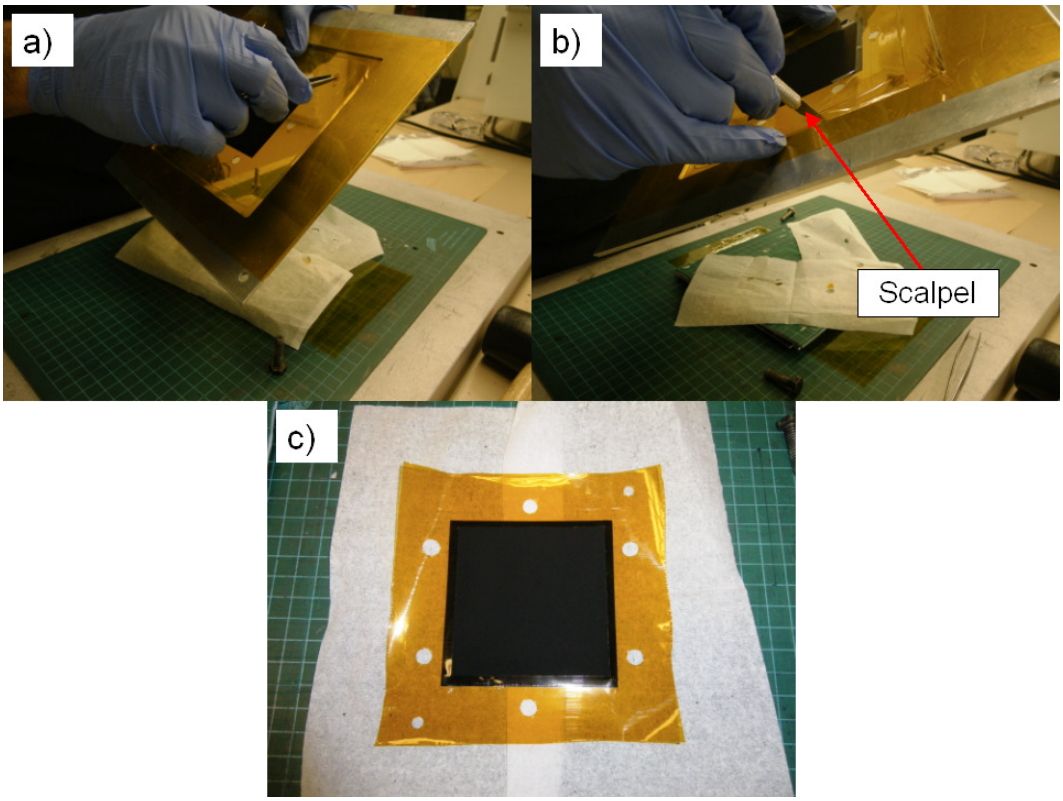

Figure B.9 – (a) Cleaning any leftover pieces of the polyimide film; (b) Cutting the outside edges of the polyimide film; and (c) final CCM and sub-gasket assembly.

10. Cut the carbon fiber papers (CFP) with the rule die labelled “GDL”, similarly to step 3.
11. Place the CFP corresponding to the anode side on top of the anode flow field plate.
12. Place the CCM/polyimide film assembly on top of the anode plate.
13. Place the cathode GDL on top of the CCM (see figure C.13).

Notes:

- Always use gloves when dealing with the CCMs
- Make sure that the surface of the CCM is always clean

APPENDIX C – DETAILED PROCEDURES FOR POLARIZATION TESTS

C.1 Conditioning of the membrane electrode assembly

The following protocol is for the fuel cells and membrane electrode assemblies (MEA) described in Chapter 2. If any of these components changes then this protocol should be taken just as a guide. The steps for the MEA conditioning are:

1. Set the test station to the following typical pressure and flow conditions:
    a. Air/hydrogen stoichiometry ratio of 2.0/1.5 (flow corresponding to a 500 mA/cm^2)
    b. Pressurise gases stepwise to 206.8 kPag (30 psig) in 50 kPa increments.
2. Set the current density to 500 mA cm^{-2} (a fairly low current so the voltage output is not lower than 0.5V)
3. Set the test station to the following typical temperature conditions:
    a. T_{cell} = 75ºC
    b. T_{gas} = 75ºC
    c. T_{dp} = 75ºC (100% RH for both sides)
4. While the station heats the gases and the humidifiers, continue increasing the current density around every 5 minutes (*e.g.,* 600, 700, 800, 900 mA cm^{-2}).
5. Once the temperature conditions are achieved, operate the fuel cell at a current density in which the cell's voltage output is approximately 0.6V (e.g., for the 49 cm^2 fuel cell with a Primea® 5510 Gore CCM and SGL Carbon 25BC (cathode) and 25DC (anode) GDLs try a current density of 1000 mA cm^{-2})
6. Operate the cell at the above load until the cell's voltage has stabilized for more than an hour, this usually takes between 6 to 8 hours. By stabilized voltage is meant that the variations in the cell voltage are smaller than ±10 mV for at least one hour.

These steps can also be used when conditioning an MEA that is old and has not been used for more than 3 days. In general, the total time for MEA re-conditioning for an old MEA is shorter than with a new MEA.

C.2 Polarization curve protocols

The following protocol is for the fuel cells and membrane electrode assemblies (MEA) described in Chapter 2. If any of these components changes then this protocol should be taken just as a guide. This protocol is meant for polarization curve tests with standard materials (i.e, commercially available). For example, SGL Carbon GDLs, Toray carbon fiber papers, and Primea® Gore CCMs. Depending on the flow field channels used in both anode and cathode flow field plates the cell's overall performance may change substantially. Therefore, certain stages of this protocol may change accordingly (e.g., the amount of current density points). The minimum rate of data acquisition is 1 point every 2 seconds. The recommended rate is 1 point per second (in some cases an even faster rate is preferable). The steps for a polarization curve are:

1. Set the desired operating conditions (pressure and temperatures)
2. Once the operating conditions are ready, operate the fuel cell at the following current densities (in mA cm^{-2}) and leave the cell at each point for at least 15 minutes (i.e., at constant current):

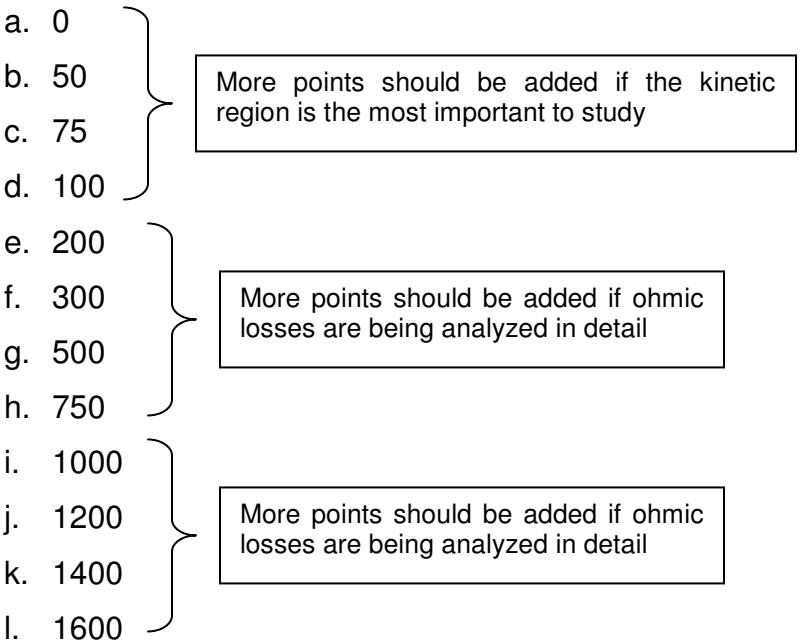

m. 1700
n. 1800
o. 1900
p. 2000
q. 2100
r. 2200
s. 2300

More points should be added if mass transport losses are being are being analyzed in detail

The lowest cell voltage should be 0.3V, unless the limiting current density is desired.

The cell voltage recorded at each current measurement is averaged over a time period of at last 3 minutes corresponding to the steady state condition of the cell. Depending on the MEA and flow fields that are used the amount of points will change, therefore, the current densities shown here are just examples of the typical points that are necessary in order to cover the most important areas of the polarization curve. In addition, in some tests it is desired to study the limiting current density of the fuel cell, thus, it may be necessary to run the cell at very high current densities in which the cell's voltage would be less than 0.3 V. However, the load bank of the test station also limits the minimum voltage since for most load banks need a voltage of around 0.2 V in order to work, thus, an additional power supply would be necessary.

The value for the open circuit voltage should be recorded after the highest current density point is completed. After this, the fuel cell has to be tested at least at six more current densities, in a descending order from high to low current values, for at least 15 to 20 minutes at each point. This was performed to compare the hysteresis associated with increasing or decreasing current densities. This is especially important when testing at low humidity conditions since the cell could be degrading. If the difference between the increasing and decreasing cases is less than or equal to 10 mV at a given current value then the polarization curve is completed. If the difference between the cases is greater than 10 mV then the polarization curve should be repeated. The most common current densities tested in a descending order are 2000, 1700, 1400, 1000, 500, and 100 mA cm^{-2}.

At flooding conditions (dew point temperature greater than the temperature of the gases) it is necessary to purge the cell after each current density, thus, the water accumulated in the previous point does not affect the future current loads. In addition, these purging steps may also have to be used when materials more susceptible to water flooding are used (e.g., CFPs with no PTFE treatment) even at conditions in which the temperature of the gases are greater than the dew point temperatures.

APPENDIX D – TESTS WITH PERFORATED GRAPHITIC FOILS AS WATER BARRIERS

Perforated graphite foils manufactured by Graftech International Ltd. were used as additional layers to improve fuel cell performance at low to no gas humidification. The purpose of these layers was to be similar to that of the stainless steel sheets mentioned in Chapter 3 and to prove the claims published by Graftech International [47]. However, severe issues related to the mechanical properties of the graphite foils were found and did not allow for a clear understanding of the effect of using this specific material. This appendix briefly explains the results and findings when these materials were tested in a fuel cell.

The perforated flexible graphitic foils (GF) manufactured by Graftech International Ltd. These sheets, also called Grafcell®, were composed of compressed expanded graphite particles, which were then reinforced with resins and perforated by a mechanical impact process. For this work, graphite sheets with a hole density of 1200 tpi (tips per square inch) (186 tips per square centimetre), 21% open area, and 0.171 mm thick were used. The hole density is directly related to the size of the perforations, i.e., high hole density results in smaller-sized holes and low hole density results in larger-sized holes. Due to the manufacturing process used to perforate the laminated graphite sheets, the shape of the holes is trapezoidal and their cross-sectional shape has a tapered shape along the thickness of the sheet. Therefore, the area of each hole on one face of the sheet is 0.47 mm^2 and the area of each hole on the other face of the sheet is 0.11 mm^2. Figure D.1 shows images of these graphitic foil materials. Due to this cross-sectional shape of the perforations, the transport mechanisms of gases and liquids through this material can vary significantly depending on the sheet's orientation. After performing fuel cell testing with these materials it was concluded that the best performance was achieved when the smaller openings were placed next to the GDL (i.e., Figure D.1b), and the larger openings faced the cathode flow field channels (i.e., Figure D.1a). Fuel cell performance was significantly reduced in the other orientation.

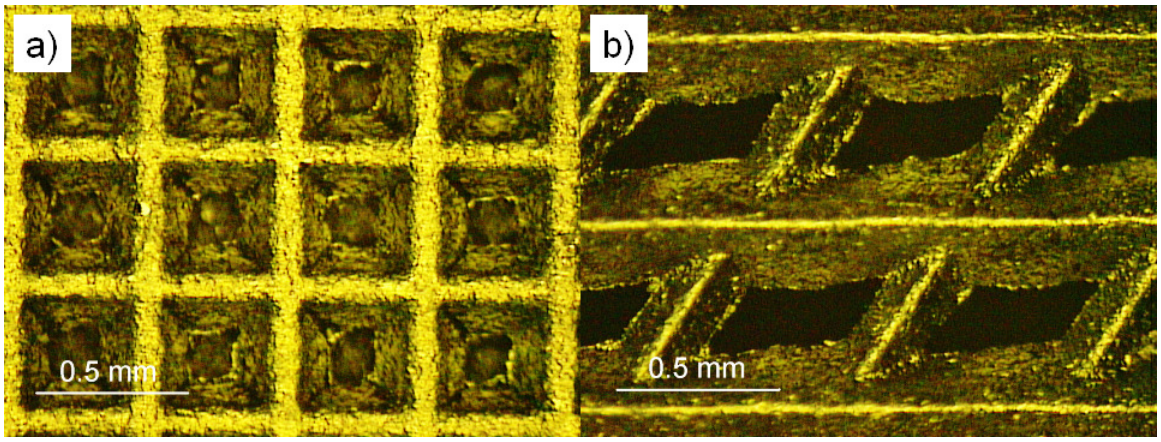

Figure D.1 – Images of the two sides of the graphitic foil (GF): (a) large and (b) small opening.

Figure D.2 shows the fuel cell performance when perforated stainless steel or flexible graphitic sheets are placed between the cathode flow field and the GDL (with MPL). Figure D.2a shows that the cell with only a GDL and no additional layers has better performance due to better gas diffusion and limited water saturation in the catalyst layer. The metal sheets reduced the fuel cell performance more than the graphitic film. One reason for this is the difference in contact resistances (as also observed in the HFR values shown in Figure D.2b). After correcting the cell voltages for ohmic losses the performance difference between the two different types of perforated sheets is less. There is still a performance difference, which indicates there are still additional mass transport resistances in the case with the metal sheets that affect the overall oxygen diffusion (see Figure D.2c). Correcting for the ohmic resistance means that the concentration and mass transport are the main losses in performance, especially at mid- to high current densities. The lower open area with the perforated sheets has a direct impact on the gas diffusion through the GDL towards the catalyst sites.

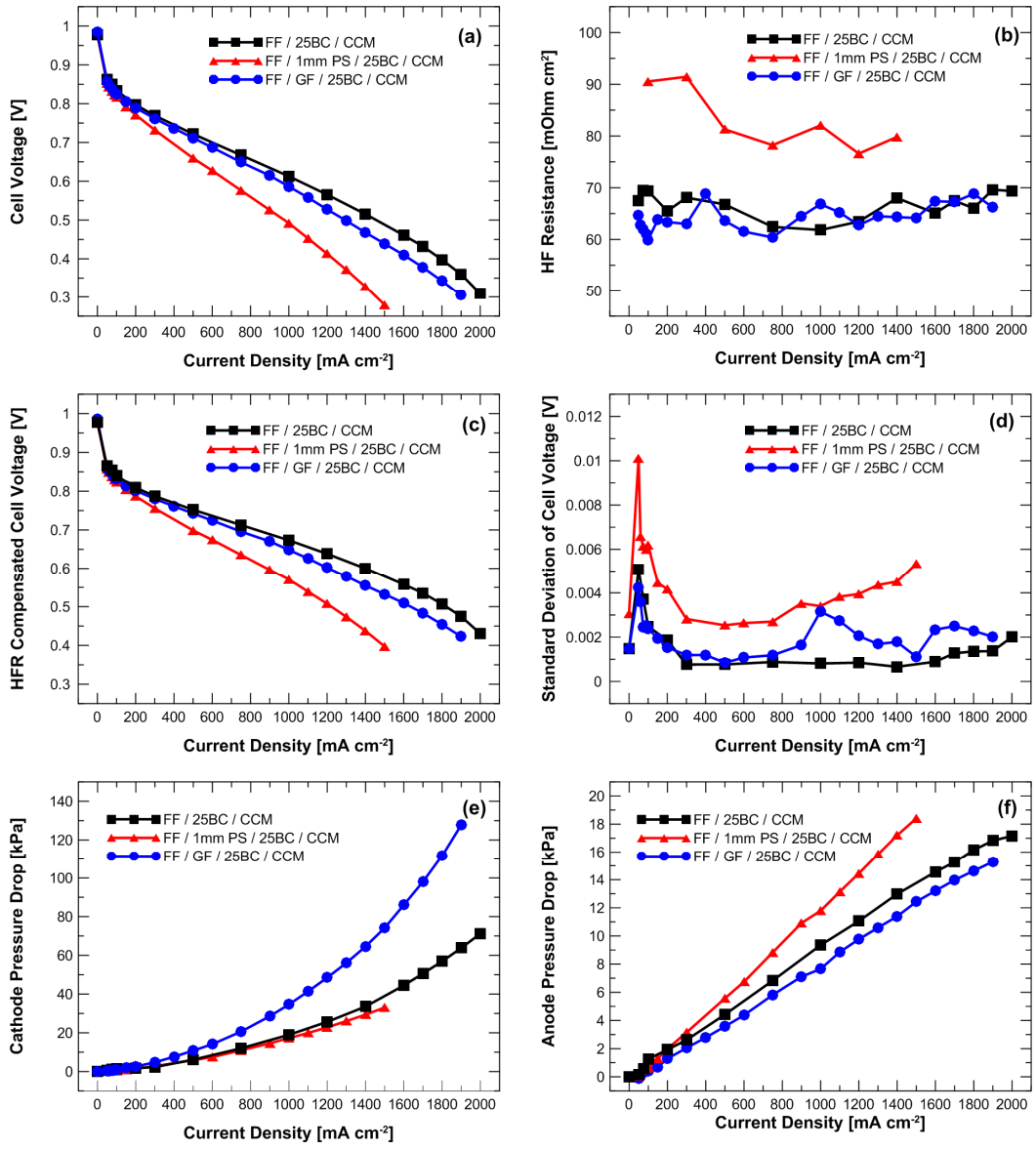

Figure D.2 – Comparison between graphitic foil and stainless steel perforated sheets with 25BC GDL at dry conditions: (a) cell voltage, (b) high frequency resistance, (c) resistance corrected cell voltage, (d) standard deviation of cell voltage, (e) cathode pressure drop, and (f) anode pressure drop versus current density. 1mm PS refers to a perforated sheet with 1 mm diameter holes. FF, CCM, 25BC, and GF refer to flow field, catalyst coated membrane, SGL 25BC (GDL with MPL), and graphitic foil, respectively. All tests were performed at dry conditions (25% RH).

As mentioned previously, the graphitic foil material has smaller mass transport losses compared to the metal sheet as a result of the tapered cross-sectional shape of the perforations that may cause an enhanced gas distribution in the catalyst layer compared to the metal sheets. In addition, the voltage fluctuations (Figure D.2d), which are a function of water accumulation in the catalyst layer, GDL and flow field

channels, of the graphitic foils are comparable to those of the 25BC by itself, and lower than when the perforated SS sheet is used. Normally, a decrease in the voltage standard deviation is a sign of less water accumulation in cathode side and a lower cathode pressure drop. However, the cathode pressure drop with the graphite sheets increases significantly, almost by a factor of two at high current densities compared to the other two cases (see Figure D.2e). These tests were repeated three times in order to confirm repeatability. Mechanical deformation of these materials, which occurs because of the compressive forces exerted inside the cell, can result in partial obstruction of the channels and increase air flow resistance. Figure D.3 shows an SEM picture of the deformations caused by the flow field landing widths of the channels to a graphitic sheet after compression and fuel cell testing. Analysis of the graphitic foils after fuel cell operation indicated that there was a reduction of approximately 19% in the cross-sectional area of the channel due to intrusion. This reduction in the channel area can increase the pressure drop of the channels up to 60% (at 1000 mA cm^{-2} and assuming laminar flow). If turbulent flow is present or if water accumulation is taken into account then the pressure drop should increase even more, which justifies the large cathode pressure drops observed in Figure D.2e.

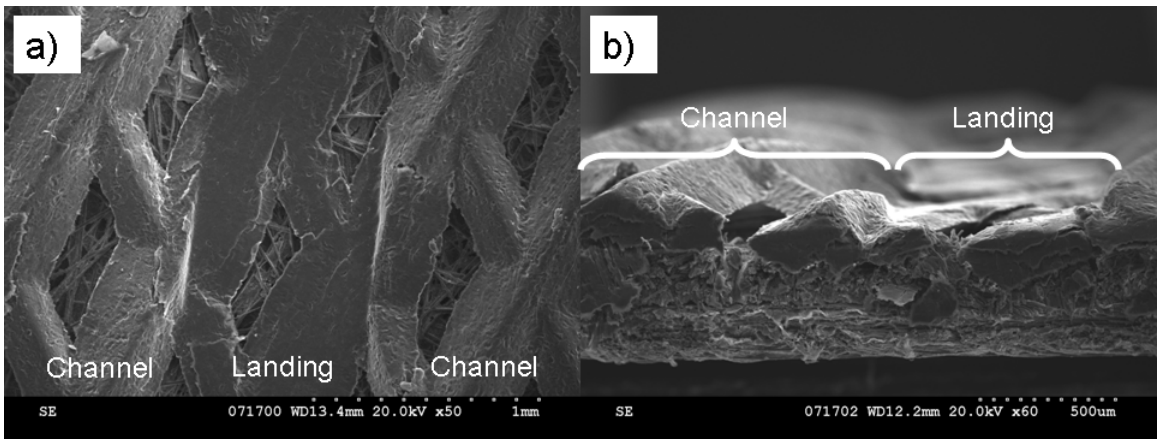

Figure D.3 – Scanning electrode microscope (SEM) micrographs of the graphitic foil after fuel cell testing. (a) Top view and (b) side view of the graphitic foil with a 25BC GDL. The region that has been flattened and compressed corresponds to the area of the flow field landing widths.

In addition, the graphitic foils were nearly always damaged after testing. These mechanical failures were not observed with the metal sheets and we were able to use them a number of times.

When stainless steel sheets were used, higher anode pressure drops were observed compared to cases where the graphitic sheets and 25BC GDLs (with no additional layers) were used (see Figure D.2f). This shows that greater amounts of water are being forced from the cathode towards the anode side when stainless steel sheets are used. In fact, the anode pressure drops between the other two cases are similar, thus, the graphitic foils do not seem to influence the water crossover to the anode even though they have smaller open areas than the metal sheets. However, reasons for this could be that the open area may increase due to cracks formed in the graphitic foil under compression, and the high cathode pressure drop changing the water balance inside the MEA.

When 25BA CFP was used, the case with just the GDL did not significantly outperform the other two cases (with additional barrier layers). Figure D.4a shows that at low current densities (less than 400 mA cm^{-2}) the performance of all three cases was similar, with the graphitic sheet showing a slight improvement the performance. Both polarization curves, uncorrected and corrected, for the graphitic foil material present an unusual reproducible improvement in the performance at a current density range of 1200 to 2100 mA cm^{-2}. The standard deviation of the cell voltage increases prior to the mentioned current density range (i.e., at 1000 mA cm^{-2}), but it quickly decreases indicating removal of water inside the cathode side of the fuel cell. However, there are no other indicators that could explain this unusual behaviour. Certainly the increased pressure due to intrusion would improve the water management and gas diffusion in this current density range.

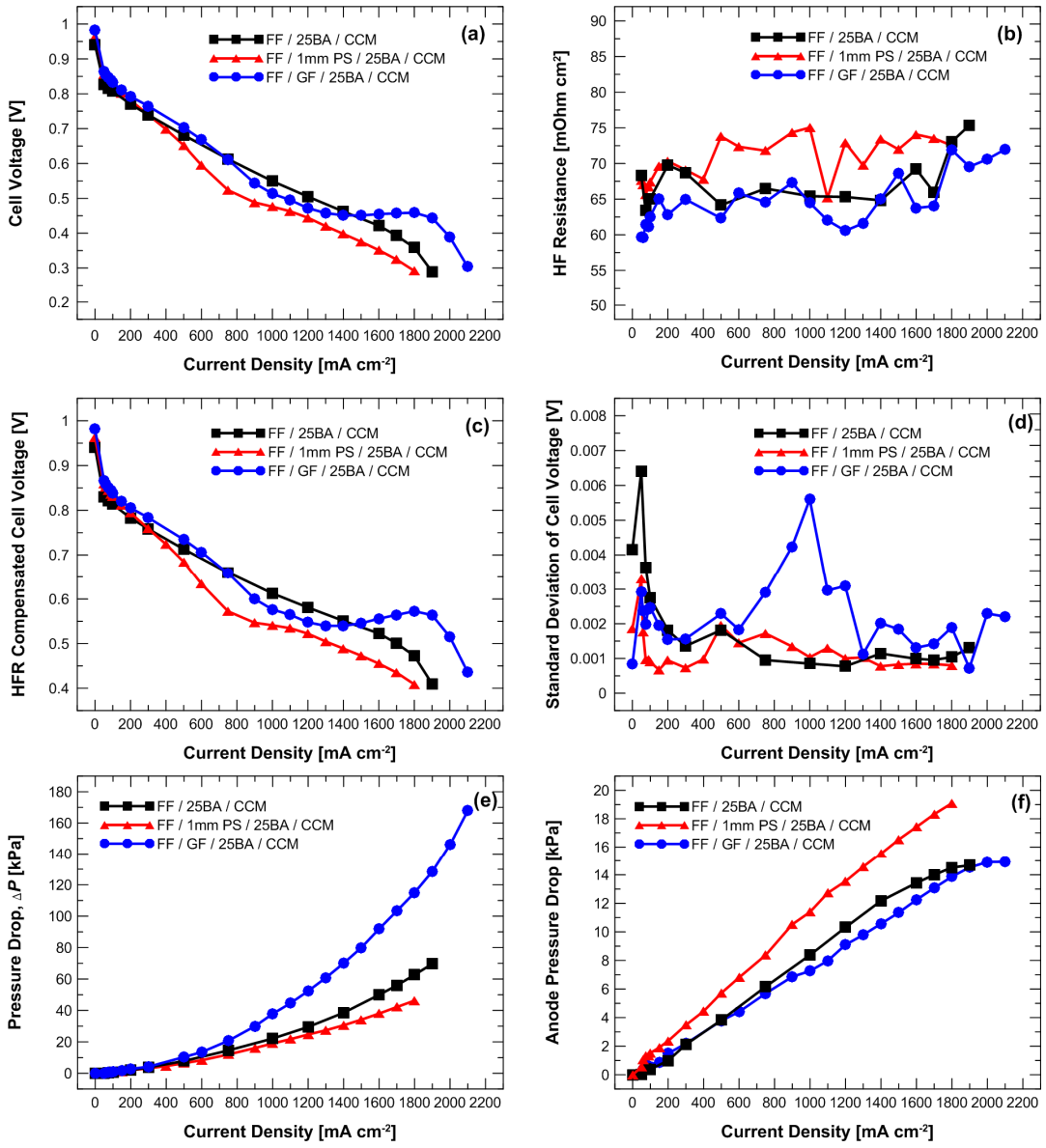

Figure D.4 – Comparison between graphitic foil and stainless steel perforated sheets with 25BA GDL at dry conditions: (a) cell voltage, (b) high frequency resistance, (c) resistance corrected cell voltage, (d) standard deviation of cell voltage, and (e) pressure drop versus current density. 1mm PS refers to a perforated sheet with 1 mm diameter holes. FF, CCM, 25BA, and GF refer to flow field, catalyst coated membrane, SGL 25BA (GDL with no MPL), and graphitic foil, respectively. All tests were performed at dry conditions (25% RH).

The cathode pressure drop (Figure D4e) behaviour for the 1 mm metal and graphitic sheets with the 25BA is similar to the 25BC GDLs (Figure D.2e). For the graphitic foil, it is unclear if it allows the same level of water accumulation with both GDLs, or if the similar cathode pressure drops are just the results of the air flow resistance in the flow field channels due to the deformation of the sheet. Based on the SEM

image of the foil (see Figure D3) it appears that the intrusion of the foil into the channels is the dominant factor for the increase in the pressure drop.

Due to the mechanical issues of the graphite foils and their intrusion to the flow field channels, all the results with the graphite foil are unclear and not fully understood. Therefore, it was decided to remove this portion of the work presented in Chapter 3. It is important to note that these findings do show that these graphite sheets may not be ready as gas diffusion barriers for low to no gas humidification systems, as stated by Graftech [47], since they have critical issues that still have to be dealt with.

APPENDIX E – ADDITIONAL SUPPORTING DATA

E.1 Pressure drop data for 25BC and 25BA cathode GDLs

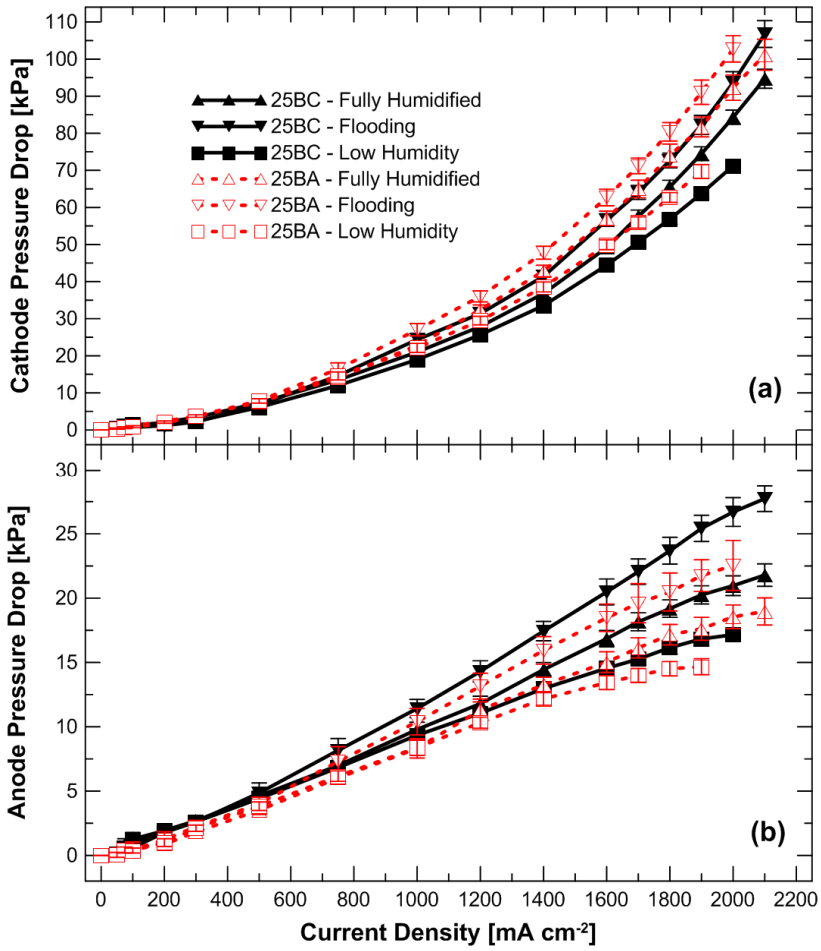

Figure E.1 – Effect of the cathode MPL on (a) cathode and (b) anode pressure drops at three different operating conditions: Fully humidified (100% RH with T_{dp} = T_{gas} = 75 °C), flooding (T_{dp} = 95 °C and T_{gas} = 75 °C), and low humidity (25% RH with T_{dp} = 45.4 °C and T_{gas} = 75 °C). 25BA and 25BC refer to SGL 25BA (GDL without MPL) and SGL 25BC (GDL with MPL), respectively. The anode GDL for all cases was 25DC (with MPL).

E.2 Perforated sheets with different carbon fiber papers

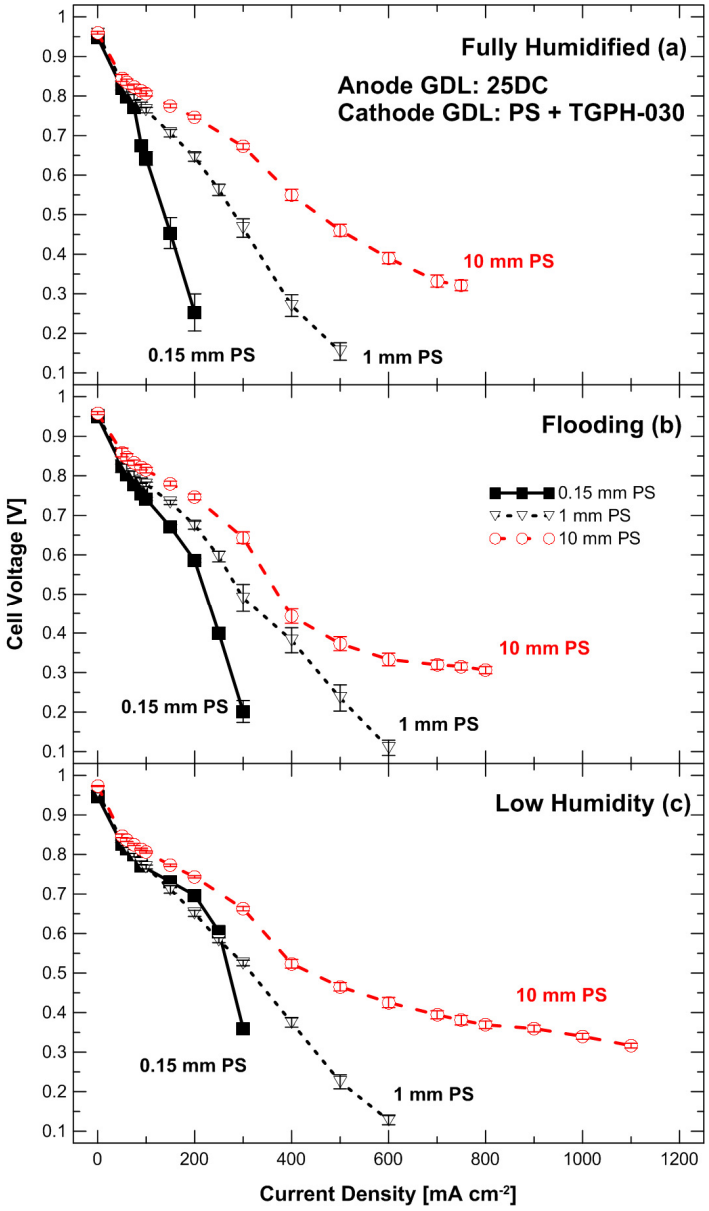

Figure E.2 – Polarization data of three different perforated sheets with a TGPH-030 CFP at three different operating conditions: (a) fully humidified, (b) flooding, and (c) low humidity. The sheets were placed between the cathode flow field plate and CFP. The three perforated sheets had different diam. holes: 0.15, 1.0, and 10.0 mm.

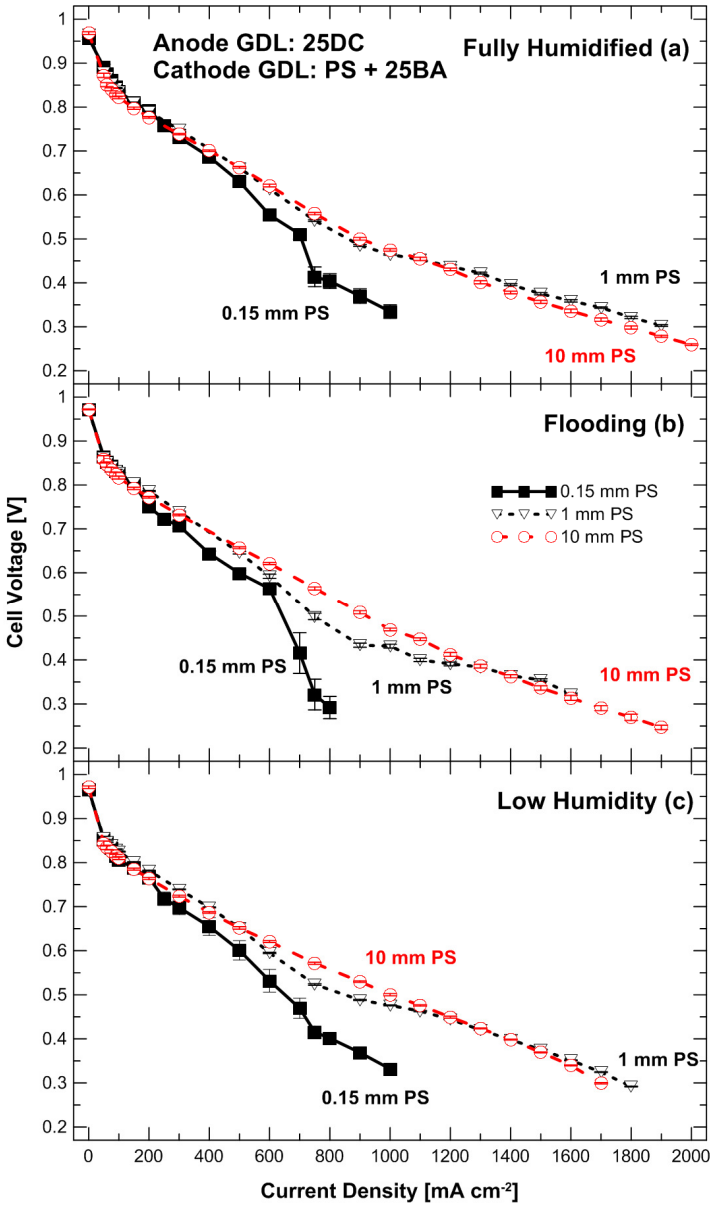

Figure E.3 – Polarization data of three different perforated sheets with a 25BA CFP at three different operating conditions: (a) fully humidified, (b) flooding, and (c) low humidity. The sheets were placed between the cathode flow field plate and CFP. The three perforated sheets had different diam. holes: 0.15, 1.0, and 10.0 mm.

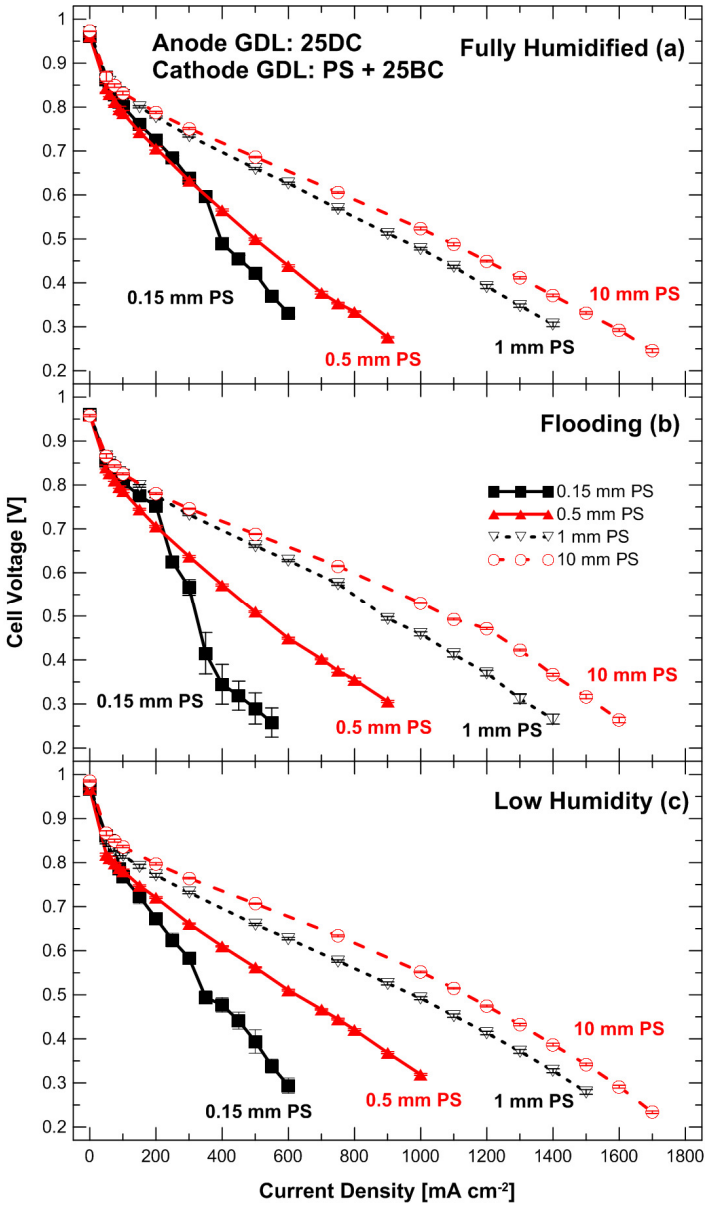

Figure E.4 – Polarization data of four different perforated sheets with a 25BA CFP at three different operating conditions: (a) fully humidified, (b) flooding, and (c) low humidity. The sheets were placed between the cathode flow field plate and CFP. The three perforated sheets had different diam. holes: 0.15, 0.5, 1.0, and 10.0 mm.

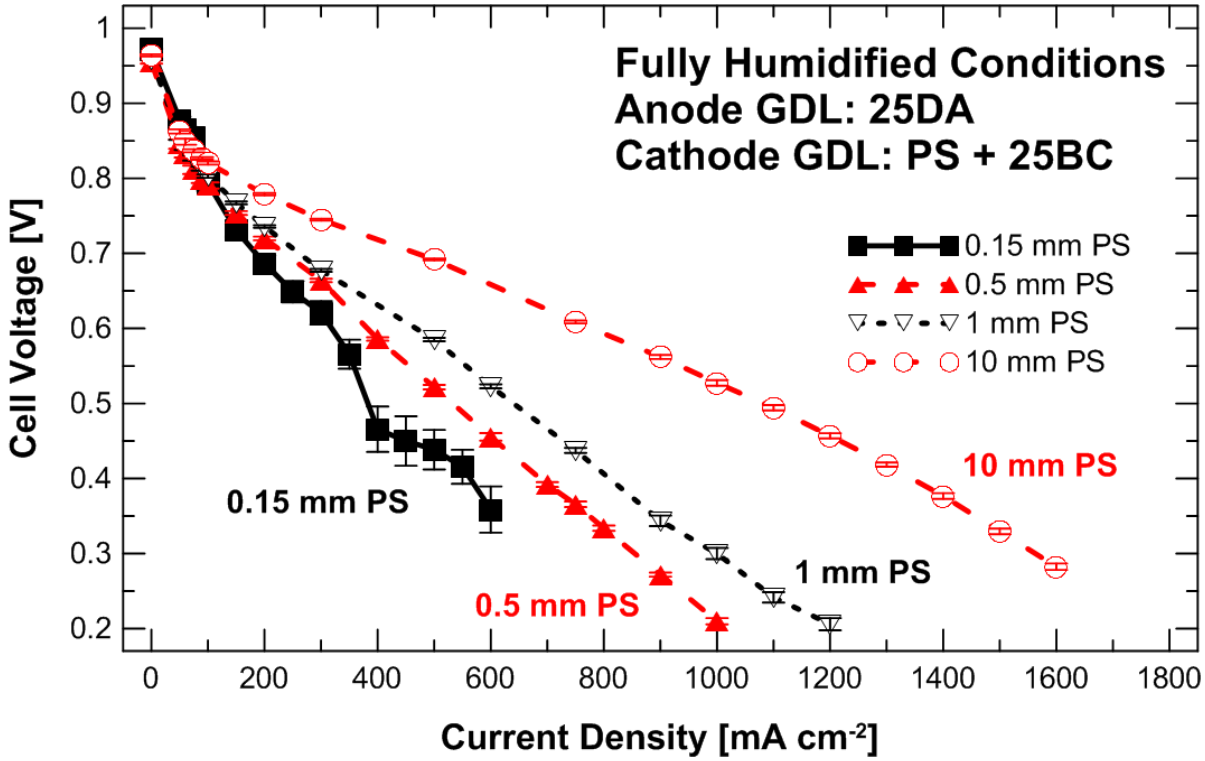

Figure E.5 – Polarization data of four different perforated sheets with a 25BA CFP at fully humidified conditions. The sheets were placed between the cathode flow field plate and CFP. The three perforated sheets had different diam. holes: 0.15, 0.5, 1.0, and 10.0 mm.